# REMOTE SENSING OF THE PACIFIC NORTHWEST BUNCHGRASS PRAIRIE FOR LANDSCAPE SCALE MONITORING AND MANAGEMENT

A Dissertation

Presented in Partial Fulfillment of the Requirements for the

Degree of Doctorate of Philosophy

with a

Major in Natural Resources

in the

College of Graduate Studies

University of Idaho

by

Vincent S. Jansen

Major Professor: Crystal Kolden, Ph.D.

Committee Members: John Abatzoglou, Ph.D.; Jan Eitel, Ph.D.; Eva Strand, Ph.D.; Robert V. Taylor, Ph.D.

Department Administrator: P. Charles Goebel, Ph.D.

December 2018

# Authorization to Submit Dissertation

This dissertation of Vincent S. Jansen, submitted for the degree of Degree of Doctorate of Philosophy with a Major in Natural Resources and titled "**Remote Sensing of the Pacific Northwest Bunchgrass Prairie for Landscape Scale Monitoring and Management**," has been reviewed in final form. Permission, as indicated by the signatures and dates given below, is now granted to submit final copies to the College of Graduate Studies for approval.

Major Professor _____Date_____
Crystal Kolden, Ph.D.

Committee Members _____Date_____
John Abatzoglou, Ph.D.

_____Date_____
Jan Eitel, Ph.D.

_____Date_____
Eva Strand, Ph.D.

_____Date_____
Robert V. Taylor, Ph.D.

Department Administrator _____Date_____
P. Charles Goebel, Ph.D.

# Abstract

Temperate grassland ecosystems are an at-risk biome type due to large amounts of conversion to other land use types as well as the mismanagement of livestock grazing. Livestock grazing is the largest human modified land use type across the globe and can have both positive and negative feedbacks on an ecosystem. There is scientific and management interest in quantifying management feedbacks on grazed lands, and particularly, resolving the ability to quantify and monitor habitat heterogeneity due to its positive link to biodiversity. Monitoring meaningful grassland ecosystem indicators at relevant spatial scales, and how they respond to management and environmental drivers has proven difficult with small plot scale research projects as well as in-field point based monitoring. Remote sensing technologies provide a different way to quantify grassland landscapes at various scales and can provide information on important and needed ecological patterns and management relevant grassland attributes such as biomass.

In this dissertation I build upon the previous remote sensing science, by developing an empirical model that estimates vegetation cover and biomass using Landsat products. These linear models were significantly correlated to vegetation cover and biomass ($R^2 > 0.70$) across varying phenological states enabling them to be used to monitor and analyze vegetation amounts across the grazing season for adaptive management.

Next, I tested the ability of airborne lidar to provide estimates of grassland biomass at the landscape scale. Airborne lidar showed reasonable correlation for modeling grassland biomass using a Random Forest modeling approach (pseudo $R^2$ =0.59; Root Mean Squared Difference =139.4 g $m^{-2}$). The estimated biomass from the airborne data then allowed us to answer three of our research questions 1) how does increasing spatial resolution (i.e. grain size) impact measures of spatial heterogeneity, 2) what measures of spatial heterogeneity are most sensitive to grazing intensity and 3) how does this sensitivity change with increasing spatial resolution of remotely sensed data? To answer these questions, I aggregated this biomass data to coarser cell sizes and compute geo-statistics on each of the resulting resolutions to determine the effect grazing has on vegetation heterogeneity. Results showed that statistically different measures of heterogeneity were produced from the variogram models using the biomass estimates from the varying grid cell sizes. When relating the pasture

level variogram statistics to stocking rate across the 23 pasture areas, we observed that the range statistic (a proxy for patch size) was only variogram metric sensitive to grazing and this was only significant across the 1m through 8m cell sizes tested. This research successfully quantifies spatial heterogeneity and finds that within the Zumwalt Prairie (a section of the Pacific Northwest Bunchgrass Prairie), May through July grazing decreases spatial heterogeneity of vegetation amount.

Lastly, I tested the relationships between the Landsat-derived biomass algorithm tuned for the Pacific Northwest bunchgrass prairie with short-term monitoring data on stocking rate and end of year utilization. We found significant but weak to moderate correlations between the short-term monitoring indicators at both the pasture and plot scales and the biomass metrics including end of year residual biomass, and the relative difference in biomass between summer and fall. The ability to track biologically relevant thresholds of vegetation amount and change in vegetation between summer and fall using satellite-based measures provides a new way for land managers and rancher to monitor their management actions across the landscape.

# Acknowledgements

This research was completed with support from The Nature Conservancy (TNC), the Priscilla Bullitt Collins Trust; USDA Climate Hub grant 17-JV-11261944-073, and an Oren Pollack Student Research Grant.

Vital support also came in the form of volunteer labor and vegetation storage. I would like to thank all the many field technicians who help collect data for this analysis.

I am greatly appreciative for all the support, encouragement and mentoring from Dr. Crystal Kolden. Without her help, consistent effort and science expertise this document and achievement would not be possible. Thank you Crystal!. Acknowledgements also must go out to all the faculty, staff and students at the University of Idaho and employees of The Nature Conservancy who assisted in the completion of this research. I would like to thank my committee; John Abatzoglou, Jan Eitel, Eva Strand, Robert V. Taylor, for providing guidance, feedback, and support at U of I. I am also thankful to Heidi Schmalz, for her interest in this research and all her help from the field to the publishing of manuscripts. Thanks to Jeff Fields and Derek Johnson from TNC for all the encouragement, patience and funding support on and off the Zumwalt Prairie Preserve.

## Dedication

To my parents, my family and friends. To the vegetation, water and soil that supports my life.

Thank you!

# Table of Contents

# List of Figures

# List of Tables

# Chapter 1: Setting the Scene: Pushing the boundaries of using remotely sensed data to quantify grassland vegetation, vegetation pattern, and the vegetation that has been removed.

The world's temperate grassland ecosystems are of high conservation importance, as nearly half the historic area has been converted to different land use types and less than 5% of what remains falls under conservation protection (Henwood, 2010; Hoekstra et al., 2005). Grasslands provide important ecosystem services (Svoray et al., 2013), forage for the livestock industry, and vital habitat for native wildlife (Chapin et al. 1995; Conner et al. 2002). The current state and condition of grassland systems are dynamic and ever changing, determined by interacting biophysical and human drivers (Galvin et al., 2006; Reynolds et al., 2007). This dynamic process happens across multiple scales, from the plant to the landscape and overtime, which makes it difficult to quantify vegetation amounts and ecosystem processes for adaptive management, and in-turn monitor the impacts of the prescribed management.

Understanding how management practices impact vegetation quantity, heterogeneity and ecosystem function across large spatial scales has proved elusive using traditional monitoring approaches. Remote sensing has the ability to overcome many of the monitoring obstacles associated with in-field data and provides a way to make inferences of vegetation quantity and vigor across large landscapes. Many previous studies have explored using satellite data to indirectly measure biophysical vegetation variables such as above ground biomass and foliar cover. One of the most widely used satellite dataset for vegetation monitoring comes from the National Aeronautics and Space Administration's (NASA) Landsat mission, which provides free moderate-resolution satellite data. One can use the rich record of Landsat, to go back in time, to understand how vegetation amounts have changed over the last 30 years (Bastin et al., 2012; Pickup et al., 1998).

In grassland systems across the globe, remotely sensed data is increasingly being used to quantify vegetation amounts and how these amounts change with grazing (Jansen et al., 2016; Numata et al., 2007; Todd et al., 1998), change with management/ownership (Washington-Allen et al., 2006), or shifts in governmental regimes (Sankey et al., 2009). Researchers are also using remote sensing data to help monitor grassland conservation easement compliance (Ford et al., 2017; Tsalyuk et al., 2015) and how grazing impacts

vegetation pattern or heterogeneity (Virk and Mitchell, 2015). While these previous remote sensing studies lay the foundation for using remote sensing data to quantify and study grassland ecosystems at landscape scales, important extensions of this science are vital to help fill knowledge gaps moving forward.

<u>The existing knowledge gaps addressed in this dissertation:</u>

- Vegetation models and or vegetation indices used to explain vegetation metrics are often quantified for a single point in time of year , typically peak greenness, using the normalized difference vegetation index (NDVI) (Jansen et al., 2016). This often limits the ability to understand how grazing impacts the current years vegetation amounts after the grass has senesced at the end of the grazing season.
- Currently rangeland managers and scientists are pushing for a new conservation management paradigm where process and pattern is promoted over uniform grazing amounts (Fuhlendorf and Brown, 2016; Fuhlendorf et al., 2012) yet, very few studies have used remotely sensed data to analyze the effect of grazing on spatial patterns of vegetation heterogeneity (Virk and Mitchell, 2015). Therefore, there is a large gap in our ability to monitor rangeland vegetation pattern with remotely sensed data, to better align with management paradigms focused on process and pattern.
- Lidar is a commonly used remote sensing technique which offers the ability to map vegetation structure and biomass across landscapes, but very little research has been published on using airborne lidar to quantify herbaceous vegetation amounts (Kulawardhana et al., 2014). There are good examples of lidar use to quantify biomass from other small statured ecosystems, but very few studies attempt to use lidar data to create high resolution maps of above ground grassland biomass in native grassland systems.
- There is a lack of integration of remotely sensed data with rangeland management decision-making and monitoring (Butterfield and Malmstrom, 2006). This is largely due to most vegetation monitoring products not being made easily available to end users (Jansen et al., 2018), as well as researchers

> continued effort to find better ways to model the relationship between vegetation and remotely sensed data, rather than in testing how these products can be used for management and monitoring.

This dissertation fills the knowledge gaps outlined above in three chapters written in manuscript form. The first manuscript (chapter 2) is titled "*The Development of Near Real-Time Biomass and Cover Estimates for Adaptive Rangeland Management Using Landsat 7 and Landsat 8 Surface Reflectance Products"* and has been published in the journal Remote Sensing. In this chapter I developed automated algorithms driven by vegetation phenology which compute vegetation biomass and cover using the Landsat surface reflectance products. This algorithm is unique in that it produces estimates of vegetation amount no matter the phenological state of the vegetation, creating the ability to monitor vegetation cover or biomass across the grazing season. The second manuscript (chapter 3) is titled "*Using airborne lidar to estimate above-ground grassland biomass and the effects of grazing and pixel size on spatial heterogeneity in a native bunchgrass ecosystem".* In this chapter I use airborne lidar to map above ground grassland biomass at the 1 meter scale using a workflow previously developed to map small statured Arctic shrub biomass. These fine scale (1m resolution) biomass maps then allowed me to explore measures of spatial heterogeneity across pasture areas, as well as scale up (by aggregation) the resolution of this data, to determine the suitable resolutions to monitor how grazing impacts spatial heterogeneity of biomass. The final chapter (chapter 4) is titled "*Short term rangeland vegetation monitoring from space: Exploring the relationships between in-field stocking rates and end of year utilization with Landsat-derived biomass data for management and monitoring purposes",* and tests the sensitivity of the biomass algorithm from chapter 2 (Jansen et al., 2018) by correlating biomass metrics with two short-term field monitoring indicators, stocking rate and end of year utilization, which are currently used for adaptive management across the study area. The remotely sensed biomass metrics quantifying end of year residual biomass, and the relative difference in biomass between summer and fall were significantly correlated ($\alpha$=0.05) to short-term monitoring indicators at both the pasture and plot scales. We then created maps using breakpoints to classify our biomass raster metrics guided by in-field utilization monitoring data, to highlight the year to year variability in end of season biomass due to

climate variability, as well as areas that have greater amounts of change relative to other areas across the landscape. These results highlight the potential to integrate remote sensing tools into existing monitoring and management data to improve adaptive management and conservation outcomes on a grassland prairie.

In performing this research one of the biggest lessons learned is having a respect and understanding of the interrelationship between the ecology and diversity of habitat, and the science being produced from it. In my opinion place matters, and the ecology, phenology and local management and climate drivers are vitally important to both the questions asked, and the methods used to pursue new knowledge. It really does behoove the researcher using remotely sensed data to have a good understanding of both, the ecologically of the study area, and how the components and phenology of the habitat are spatially and temporally observed by the satellite's specific resolutions (spatial, temporal, radiometric, spectral). This is often referred to as the scene model (Phinn et al., 2003; Woodcock and Strahler, 1987). It cannot be stressed enough that the researcher has field data from the ground, or expert knowledge to help explain patterns and results from the remote sensing analysis.

This dissertation took place on the Zumwalt prairie which is of the largest remaining sections Pacific Northwest Bunchgrass Prairie. This grassland is highly threatened and understudied (Kimoto et al., 2012; Tisdale, 1982) and once extended over eight million hectares across Northwest United States, and British Columbia and Alberta Canada (Tisdale, 1982). The Zumwalt Prairie is a highly heterogeneous landscape dominated by C3 grasses that include Idaho fescue (*Festuca idahoensis* Elmer), bluebunch wheatgrass (*Pseudoroegneria spicata* (Pursh) A. Love) and Sandberg's bluegrass (*Poa secunda* J Presl). Elevations range across the Zumwalt Prairie from 1000 meters to 1600 meters. Summer time (June – August) average temperatures range from 11.8 – 17.5˚C with the annual precipitation totals averaging around 350 mm (2006-2012 Zumwalt Weather Station). While this grassland system is unique and much of the research and products are specifically created for this grassland system, it is hoped that the methodological approaches and research findings can be used to advance remote sensing studies in rangeland and grassland ecosystems across the globe. That said, in the end, the greatest driving factor behind this work, is that the information and data products created from this dissertation are useful to promote the

conservation of the Pacific Northwest Bunchgrass Prairie, an endangered and often overlooked ecosystem.

**References**

Bastin, G., Scarth, P., Chewings, V., Sparrow, a., Denham, R., Schmidt, M., O'Reagain, P., Shepherd, R., Abbott, B., 2012. Separating grazing and rainfall effects at regional scale using remote sensing imagery: A dynamic reference-cover method. Remote Sens. Environ. 121, 443–457. doi:10.1016/j.rse.2012.02.021

Butterfield, H.S., Malmstrom, C.M., 2006. Experimental Use of Remote Sensing by Private Range Managers and Its Influence on Management Decisions. Rangel. Ecol. Manag. 59, 541–548.

Chapin, F.S., Allen-Diaz, B., Diaz, S., M. Howden, J.P., Smith, M.S., 1995. Rangelands in a Changing Climate: Impacts, Adaptations, and Mitigation. Clim. Chang. 1995—Impacts, Adapt. Mitigation, W. T. Watson, M. C. Zinyowera, R. H. Moss, D. J. Dokken, (eds.), pp. 131–158.

Conner, R., Seidl, A., VanTassell, L., Wilkins, N., 2002. United States Grasslands and Related Resources: An Economic and Biological Trends Assessment. Natl. Cattlemen's Beef Assoc. Nat. Conserv. Ducks Unltd.

Ford, L.D., Butterfield, H.S., Van Hoorn, P.A., Allen, K.B., Inlander, E., Schloss, C., Schuetzenmeister, F., Tsalyuk, M., 2017. Testing a Remote Sensing-Based Interactive System for Monitoring Grazed Conservation Lands. Rangelands 39, 123–132. doi:10.1016/j.rala.2017.06.005

Fuhlendorf, B.S.D., Brown, J.R., 2016. Communities to Landscapes. RALA 38, 75–78. doi:10.1016/j.rala.2016.01.005

Fuhlendorf, S.D., Engle, D.M., Elmore, R.D., Limb, R.F., Bidwell, T.G., 2012. Conservation of Pattern and Process: Developing an Alternative Paradigm of Rangeland Management. Rangel. Ecol. Manag. 65, 579–589. doi:10.2111/REM-D-11-00109.1

Galvin, K.A., Thornton, P.K., de Pinho, J.R., Sunderland, J., Boone, R.B., 2006. Integrated Modeling and its Potential for Resolving Conflicts between Conservation and People in the Rangelands of East Africa. Hum. Ecol. 34, 155–183. doi:10.1007/s10745-006-9012-6

Henwood, W.D., 2010. Toward a Strategy for the Conservation and Protection of the World's Temperate Grasslands. Gt. Plains Res. 20, 121–34.

Hoekstra, J.M., Boucher, T.M., Ricketts, T.H., Roberts, C., 2005. Confronting a biome crisis: global disparities of habitat loss and protection. Ecol. Lett. 8, 23–29. doi:10.1111/j.1461-0248.2004.00686.x

Jansen, V., Kolden, C., Schmalz, H., 2018. The Development of Near Real-Time Biomass and Cover Estimates for Adaptive Rangeland Management Using Landsat 7 and Landsat 8 Surface Reflectance Products. Remote Sens. 10, 1057. doi:10.3390/rs10071057

Jansen, V.S., Kolden, C.A., Taylor, R. V., A. Newingham, B., 2016. Quantifying livestock effects on bunchgrass vegetation with Landsat ETM+ data across a single growing season. Int. J. Remote Sens. 37, 150–175. doi:10.1080/01431161.2015.1117681

Kimoto, C., DeBano, S., Thorp, R., 2012. Investigating temporal patterns of a native bee community in a remnant North American bunchgrass prairie using blue vane traps. J. Insect Sci. 12, 1–23.

Kulawardhana, R.W., Popescu, S.C., Feagin, R. a., 2014. Fusion of lidar and multispectral data to quantify salt marsh carbon stocks. Remote Sens. Environ. 154, 345–357. doi:10.1016/j.rse.2013.10.036

Numata, I., Roberts, D.A., Chadwick, O.A., Schimel, J., Sampaio, F.R., Leonidas, F.C., Soares, J. V., 2007. Characterization of pasture biophysical properties and the impact of grazing intensity using remotely sensed data. Remote Sens. Environ. 109, 314–327. doi:10.1016/j.rse.2007.01.013

Phinn, S.R., Stow, D.A., Franklin, J., Mertes, L.A.K., Michaelsen, J., 2003. Remotely Sensed Data for Ecosystem Analyses : Combining Hierarchy Theory and Scene Models 31, 429–441. doi:10.1007/s00267-002-2837-x

Pickup, G., Bastin, G.N., Chewings, V.H., 1998. Identifying trends in land degradation in non-equilibrium rangelands. J. Appl. Ecol. 35, 365–377. doi:10.1046/j.1365-2664.1998.00319.x

Reynolds, J.F., Smith, D.M.S., Lambin, E.F., Turner, B.L., Mortimore, M., Batterbury, S.P.J., Downing, T.E., Dowlatabadi, H., Fernández, R.J., Herrick, J.E., Huber-Sannwald, E., Jiang, H., Leemans, R., Lynam, T., Maestre, F.T., Ayarza, M., Walker, B., 2007. Global desertification: building a science for dryland development. Science 316, 847–851. doi:10.1126/science.1131634

Sankey, T.T., Sankey, J.B., Weber, K.T., Montagne, C., 2009. Geospatial Assessment of Grazing Regime Shifts and Sociopolitical Changes in a Mongolian Rangeland. Rangel. Ecol. Manag. 62, 522–530. doi:10.2111/.1/REM-D-09-00014.1

Svoray, T., Perevolotsky, A., Atkinson, P.M., 2013. Ecological sustainability in rangelands: the contribution of remote sensing. Int. J. Remote Sens. 34, 6216–6242. doi:10.1080/01431161.2013.793867

Tisdale, E.W., 1982. Grasslands of western North America, In A. C. N. ed.

Todd, S.W., Hoffer, R.M., Milchunas, D.G., 1998. Biomass estimation on grazed and ungrazed rangelands using spectral indices. Int. J. Remote Sens. 19, 427–438.

Tsalyuk, M., Kelly, M., Koy, K., Getz, W.M., Butterfield, H.S., 2015. Monitoring the Impact of Grazing on Rangeland Conservation Easements Using MODIS Vegetation Indices. Rangel. Ecol. Manag. 68, 173–185. doi:10.1016/j.rama.2015.01.006

Virk, R., Mitchell, S.W., 2015. Effect of Different Grazing Intensities on the Spatial-Temporal Variability in Above-Ground Live Plant Biomass in North American Mixed Grasslands. Can. J. Remote Sens. 40, 423–439. doi:10.1080/07038992.2014.1009882

Washington-Allen, R.A., West, N.E., Ramsey, R.D., Efroymson, R.A., 2006. A Protocol for Retrospective Remote Sensing – Based Ecological Monitoring of. Rangel. Ecol. Manag. 59, 19–29.

Woodcock, C. E., & Strahler, A. H. (1987). The Factor of Scale in Remote Sensing, 332, 311–332.

# Chapter 2: The Development of Near Real-Time Biomass and Cover Estimates for Adaptive Rangeland Management Using Landsat 7 and Landsat 8 Surface Reflectance Products

"The Development of Near Real-Time Biomass and Cover Estimates for Adaptive Rangeland Management Using Landsat 7 and Landsat 8 Surface Reflectance Products." Remote Sensing, 10,1059, 2018.

## Abstract

Rangelands are critical working landscapes and are the focus of considerable conservation planning efforts globally. A key conservation challenge in these landscapes is that high interannual variability in both climatic conditions and land use greatly limits the utility of outdated or static vegetation maps for management decision-making. One potential solution to this problem lies in remote sensing-derived information; however, prospective users must have continuous and timely access to vegetation products tailored to their needs. Google Earth Engine (GEE) can overcome the many storage, processing, and visualization barriers associated with creating ready-to-use remote sensing products for the public. While GEE provides a platform for building tools to analyze data and share results with users in near real-time for adaptive management, monitoring products need to (1) provide accurate and stable estimates over time and (2) align with management goals and the ecology of the rangeland system in question. Here, we assess estimates of vegetation cover and above-ground biomass at two dominant phenological time periods (summer/green and fall/brown), as modeled from the Landsat 7 and Landsat 8 Climatic Data Record (CDR) product. Using a best-subset regression modeling approach, we modeled vegetation cover and biomass, finding that the best predictors vary by season, corresponding to vegetation phenology. We also found that sensor-specific models decreased the relative differences between mapped cover and biomass estimates when comparing Landsat 7 and Landsat 8 scenes one day apart in the summer and fall. Ultimately, we developed an automated model selection process driven by sensor and vegetation greenness that can run in GEE to monitor and analyze vegetation amounts across the grazing season for adaptive management.

## 1.0 Introduction

Rangelands are estimated to cover more than 30–40% of Earth's ice-free land and 70% of the western United States (Asner et al., 2004; Fleishchner, 1994). Today, rangelands continue to be at high risk of conversion and fragmentation (Brunson and Huntsinger, 2008; Sullins et al., 2002) due to their marginality for income production for land owners (Sayre et al., 2013) compared to the high value of the land (Huntsinger and Sayre, 2007). Many rangelands have been degraded by overgrazing and continue to be threatened by poor grazing management and invasive species (Huntsinger and Sayre, 2007; Sayre et al., 2013). Rangelands are described as working landscapes and are being included in conservation planning because of their value for protecting and enhancing existing ecosystem services (Huntsinger and Sayre, 2007) while maintaining livelihoods. Management decisions (e.g., setting stocking rates, herd size, rotations) aimed at balancing economic profitability and ecosystem services are challenging in rangelands due to interannual climate variability as well as the changes in social systems, such as commodity prices or governmental policies (Mckeon et al., 1990; Stafford Smith et al., 2007). These challenges will likely grow as anthropogenic climate change amplifies variability in coupled socioecological systems characteristic of working rangelands (Joyce et al., 2013). To support socioecological resilience and conservation of ecosystem services, there is a need to monitor short- and long-term ecological indicators that respond to management actions at relevant conservation and management scales (Stafford Smith et al., 2007).

Providing relevant data to ranchers and land managers to improve management outcomes has proved difficult using traditional in-field monitoring approaches (Bestelmeyer and Briske, 2012; Sayre et al., 2012; Washington-Allen et al., 2006). Qualitative methods are highly subjective and cannot robustly be compared over time and between areas or observers (Briske et al., 2005; Pyke et al., 2002). In-field quantitative methods have been critiqued because data acquisition is expensive, data may not be representative of conditions outside of sampling sites, and the scale of data collection seldom matches the spatial and temporal scales of management (Briske et al., 2010; Weltz et al., 2003; West, 2003). By contrast, remotely sensed data are spatiotemporally consistent and objective, overcoming these critiques, and can provide valuable information on rangeland condition when coupled with field data (Hagen et al., 2012; Herrick et al., 2010).

In rangeland systems, data from Landsat and the moderate resolution imaging spectroradiometer (MODIS) are commonly used to analyze vegetation amounts because they are free and provide long-term continuous datasets. Tradeoffs between the two sensors such as spatial scale (30 m versus 250–1000 m), temporal scale (16 day versus daily), and the spectral bands desired for analysis are important considerations. Landsat data is often preferred over MODIS because it provides a longer continuous dataset and the 30-m resolution is more appropriate for mapping heterogenous rangeland vegetation (Ikeda et al., 1999) and assessing distinct management areas (Jansen et al., 2016). Also, timely processing of this data to at-surface reflectance is now made possible by the Landsat Climate Data Record (CDR). One of Landsat's known drawbacks is the 16-day acquisition interval, but this interval is reduced when there are multiple Landsat platforms in orbit (currently Landsat 7 and Landsat 8) and overlapping scenes at higher latitudes (Roy D. P. et al., 2015).

Using any remotely sensed dataset to provide accurate vegetation monitoring data across the year (or years) presents challenges. Specific to the Landsat CDR record, the multiple sensors have different spectral response functions, sensor configurations (Roy D. P. et al., 2015), and data processing algorithms (Holden and Woodcock, 2016). Sensor differences are highlighted by Holden and Woodcock (Holden and Woodcock, 2016), who suggest several methods to integrate data from the two current Landsat sensors for time-series analysis, including image normalization, modeling attribute data such as vegetation cover separately for each sensor, or using a dummy variable within the time-series model.

Spatial and temporal variation in phenology make it difficult to assess vegetation amounts with only one vegetation index across the year (Butterfield and Malmström, 2009; Jansen et al., 2016). For example, the amount of senescent early season growth or standing dead material (prior year's growth) impacts the ability of spectral data to accurately quantify vegetation amounts (Huete and Jackson, 1987; Todd et al., 1998; Van Leeuwen and Huete, 1996; Xu et al., 2014). This is especially important in heterogenous rangeland landscapes because green vegetation canopies often include senesced plant material (Elvidge, 1990; Van Leeuwen and Huete, 1996), particularly in areas far from water or rested from grazing the prior year (Hagen et al., 2012; Todd et al., 1998). Jacques et al. (Jacques et al., 2014) suggest that a dry-season forage index should be able to resolve the difference between soil and dry vegetation, vegetation structure, biochemical state, and disturbance such as fire. This rationale

can be extended to the entire growing season, especially in rangeland systems, where residual dry vegetation remains standing from previous years. To address the difficulties of monitoring vegetation amounts irrespective of phenology, Marsett et al. (Marsett et al., 2006) found the soil-adjusted total vegetation index (SATVI) represented vegetation cover, and the near-infrared red (NIR) represented plant height and biomass. This study focused on the arid southwestern U.S., and when modeling biomass and plant height, eliminated field sites with >30% forb cover. Hagen et al. (Hagen et al., 2012) extended this research to the MODIS sensor across western U.S. rangelands, but only analyzed total vegetation cover. While both studies demonstrate the ability of remotely sensed data to monitor vegetation cover across the year, neither created robust models for biomass across grasslands, which can often include forb cover greater than 30%. Jansen et al. (Jansen et al., 2016) analyzed the ability of Landsat 7 Enhanced Thematic Mapper Plus (ETM+) to monitor vegetation biomass and cover across the grazing season and demonstrated that the best spectral predictors changed as vegetation senesced; however, this study was limited to only one year and a limited sample size ($N = 32$).

An adaptive management framework that incorporates remote sensing products will be most effective when vegetation estimates are readily available in near real-time. While previous research in rangeland systems highlights the ability of remotely sensed data to assess vegetation over time or monitor grazing effects, ranchers and others who must adapt their management to changing conditions still need easily accessible, spatiotemporally consistent data products. For example, management decisions may depend on multiple estimates of vegetation across the grazing season (Jansen et al., 2016) or on residual vegetation amounts after vegetation has senesced (e.g., (Guerschman et al., 2015; Jacques et al., 2014)). New developments in the automatic post-processing of raw remote sensing data (e.g., Landsat CDR surface reflectance products) and cloud computing and storage makes this increasingly achievable. This is demonstrated by Google Earth Engine (GEE), which was developed to help overcome many of the challenges of making remote sensing products available to a broad range of end users.

Google Earth Engine is a broad platform with diverse uses, from simple downloads of satellite data to an all-in-one platform to gather, analyze, and visualize remotely sensed data. The GEE image catalog is continuously updated with new Landsat CDR products, negating the need to download, process, store, and disseminate large amounts of data on local servers

(Gorelick et al., 2017). GEE-based tools can be configured to produce and visualize near real-time monitoring data to end users by applying algorithms that process new images as soon as they become available. The GEE platform also allows users to upload personal data (such as management units) via Google fusion tables, tailoring the analysis to their own property. Google Earth Engine is uniquely suited for users to utilize the platform at various steps in a project workflow. For example, it can be used to analyze changes in global forest cover (Hansen et al., 2013) or facilitate sharing of near real-time remotely sensed data in a streamlined and cost-effective way (see ClimateEngine.org (Huntington et al., 2017)). However, the powerful benefits of leveraging GEE for rangeland management decision-making can only be realized if the underlying algorithms (1) provide accurate and stable estimates of vegetation metrics over time and (2) align with management goals and the ecology of the rangeland system in question.

Our ongoing goal is to develop a GEE-based rangeland monitoring tool that uses Landsat 7 and Landsat 8 CDR surface reflectance products to estimate vegetation cover and biomass across the grazing season. To meet this goal, the specific objective of this study is to assess the accuracy and stability of these cover and biomass metrics between Landsat 7 and Landsat 8 as phenology changes across the grazing season. Here, we first create and compare Landsat 7- and Landsat 8-derived models of vegetation cover and biomass at three phenological (temporal) periods: (1) peak vegetation biomass (summer), (2) senescent vegetation (fall), and (3) a combined dataset (summer and fall data). Next, over the study area, we assess the stability of these models across both Landsat sensors by calculating the relative differences between the modeled vegetation using paired scenes one day apart. We then identify sensor-specific greenness (Normalized Difference Vegetation Index (NDVI)) thresholds to align the appropriate models with plant phenology. Lastly, we explore what biophysical, sensor, and sample design variables most influence model accuracy. The resulting algorithms from this research are encoded in GEE to deliver analysis products to land managers and ranchers in a new tool under development which leverages the ClimateEngine (Huntington et al., 2017).

## 2.0 Materials and Methods

### 2.1. Study Area

The study area covers approximately 26,300 hectares across six different private land holdings on the Zumwalt Prairie in northeastern Oregon (Figure 2.1). The Zumwalt Prairie is a grassland dominated by C3 grasses including Idaho fescue (*Festuca idahoensis* Elmer), bluebunch wheatgrass (*Pseudoroegneria spicata* (Pursh) A. Love), and Sandberg's bluegrass (*Poa secunda* J. Presl). Average yearly rainfall is 352 mm, with 42% coming between 1 April and 1 July; average monthly temperatures range from −3.3 °C in January to 17.8 °C in July (Zumwalt Weather Station 2006–2017 data, https://www.conservationgateway.org). Most soils are classified as xerolls, with parent material coming from basalt, loess, and colluvium (Schmalz, 2011) .

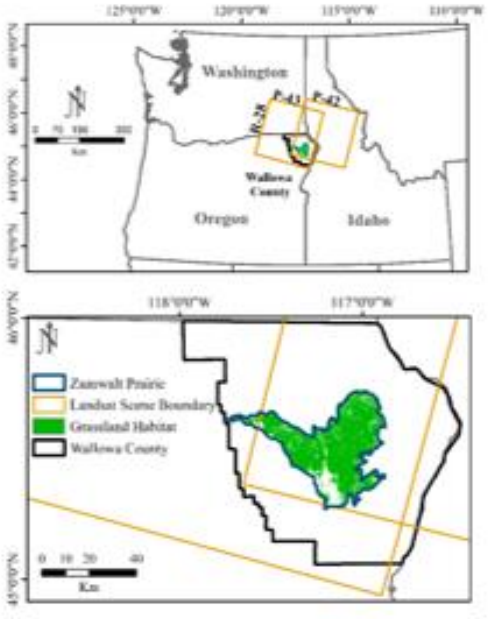


Figure 2.1 Study area map of the grassland habitat across the Zumwalt Prairie in Wallowa County, OR, USA. The study area intersects two Landsat scenes falling on row 28 (R-28) and paths 42 and 43 (P-42 and P-43).

## 2.2. Sampling Design

Field data was collected over three years (2014 to 2016) across a suitable habitat sampling area on the Zumwalt prairie. The suitable habitat area was delineated by excluding (1) non-grassland habitat types (developed, agriculture, rock, or forest) as defined by the ReGap Ecological Systems data (Kagan et al., 2006); (2) slopes greater than 45%; and (3) any area falling within 50 m of stock ponds, roads, and fence lines. Sample sites were located at least 200 m away from other sites for each field campaign, and for efficiency purposes, sites were located within 1.1 km of access roads. The sample site locations were located using a stratified random sampling approach generated iteratively for each season and year. Sampling strata were divided by quartiles of predicted biomass amounts derived initially using vegetation models created for this study area (Jansen et al., 2016) and then subsequently updated as new data were collected and analyzed for each season. This stratification was performed for more informed and efficient sampling across a gradient of vegetation amounts. Sites were located within relatively homogenous areas of vegetation and in pastures with various levels of stocking, timing of grazing, and grazing rotation strategies. Sampling was performed at two dominant phenological time periods: during peak biomass (i.e., summer, when green vegetation is dominant) in 2015 and 2016, and during full senescence (i.e., autumn, when brown vegetation is dominant) in 2014, 2015, and 2016.

## 2.3. Data

### 2.3.1. Field Data

During the study period (2014–2016), data on standing crop biomass, vegetation cover, soil surface, and utilization were collected at total of 272 sample sites. Field data was collected across three parallel 60-m transects located 30 m apart and oriented east to west with the middle 60-m transect intersecting the site center (Figure A1.1). Vegetation cover, color/ condition (i.e., green/photosynthetically active, brown/senesced, and grey/standing dead) and soil surface data were collected every meter across all transects using line–point intercept (Herrick et al., 2005), providing 180 measures per site. Total above-ground biomass was collected using an adapted photo-enhanced comparative yield method described by Friedel and Bastin (Friedel and Bastin, 1988). Our method involved field observers estimating dry vegetation weight using photographic standards obtained across the Zumwalt Prairie. Biomass

collection at each sample site was performed using the photo standards to estimate the weight of standing crop within 39 1.0 × 0.4 m quadrats located every 5 m along each transect. We corrected the field estimated biomass by creating individual observer calibration equations for each year and seasonal data collection bout. This was done by clipping standing crops at four quadrats (at 30 m along the northern and southern transect and 20 m and 40 m along the middle transect) to 0.5 cm above ground surface, and oven drying at 60 °C for 48 h to obtain a dry weight. For each observer, calibration equations were then created using the estimated plot weight and the actual clipped weight. The resulting equations were then applied to each observer's estimate. Utilization was also assessed at each 1 × 0.4 m quadrat in unison with biomass estimates by visually estimating the amount of vegetation removed by grazing animals. The methods followed double-weight sampling described by Parsons et al. (Parsons et al., 2003).

2.3.2. Remotely Sensed Data

The climate data record (CDR) Collection 1 Level 2 products for Landsat 7 ETM+ and Landsat 8 Operational Land Imager (OLI) were downloaded from USGS Earth Explorer (https://earthexplorer.usgs.gov/, accessed 5 December 2017). Each scene is terrain-corrected and processed to at-surface reflectance based on the sensor type; Landsat 7 ETM+ data is processed with the Landsat Ecosystem Disturbance Adaptive Processing System (LEDAPS) algorithm (Masek et al., 2006) and Landsat 8 OLI with the Landsat 8 Surface Reflectance Code (LaSRC) (Vermote et al., 2016). This data product also includes a pixel quality assurance (pixel_qa) band derived largely from the CFMask algorithm (Zhu and Woodcock, 2012), which was used to filter pixels containing clouds or shadows over the study site. The location of this study area falls on swath edge paths, enabling each Landsat sensor to pass over every 8 days, and providing Landsat 7 and Landsat 8 scene acquisitions one day apart (e.g., (Roy D. P. et al., 2015)). We selected images that were mostly cloud-free and closest in date to the field campaigns which also had a one-day paired sensor scene (Table A1.1). The paired scenes facilitated a comparison of modeled biomass and cover between sensors. For each of the selected scenes, we masked out bad data by applying the pixel_qa mask. This included the no-data pixels associated with the permanent failure of the Landsat 7 ETM+ scan line corrector in 2006, as well as clouds and shadows across both Landsat 7 and Landsat 8 datasets. For one scene, imaged on 17 October 2015 from Landsat 8, we further applied a

manual cloud mask due to error of omission with the pixel_qa mask. Next, we obtained the common spectral bands, and computed 12 vegetation indices and the wetness, greenness, and brightness tasseled cap transformation (Kauth and Thomas, 1976) using the coefficients for reflectance data (Crist, 1985) (Table A1.2) based on previous studies across grassland and dryland systems. For each field sample site, we averaged pixel values across a 2 × 2 pixel window surrounding the sample site to fully capture the field site extent, as the field sites did not fall directly within individual pixels.

## 2.4. Statistical Analysis

### 2.4.1. Variable Selection

Using a best-subset regression modeling approach (Hudak et al., 2006; Jansen et al., 2016), we determined which spectral indices (Table A1.2) were most commonly selected for a defined number of variables (Hudak et al., 2006) when estimating vegetation biomass and cover for nine different data combinations based on the sensor and time of year (sensor-time). The best-subset approach exhaustively searches all possible single and multiple variable linear models (with model size defined by the user) and selects the models with the best fit (Hudak et al., 2006). The sensor–time data combinations consisted of three sensor groupings (Landsat 7, Landsat 8, and Landsat 7/8 combined) and three-time groupings that aligned with the dominant phenological periods: peak biomass (i.e., summer, when green vegetation is dominant), full senescence (i.e., autumn, when brown vegetation is dominant), and the combined dataset (i.e., all year). To limit the influence that outlier observations can have on variable selection for each of the nine sensor–time combinations, we ran 1000 iterations, guided by Crowley (Crowley, 1992), of a random selection with replacement of two-thirds of the data and performed a best-subset regression (regsubsets in the leaps package in R) (R Development Core Team, 2016; Thomas, 2017) for each run. We then summed the predictor variables selected as “best” across the 1000 runs to guide the creation of candidate models for each combination.

### 2.4.2. Model Creation

For each of the nine sensor–time data groups, we divided the valid sample sites into training and testing sets by selecting 75% of the data for training and leaving 25% out for testing. Using the variables selected as “best” from the previous variable selection step (see

Section 2.4.1), coefficients for each candidate model were obtained by averaging the coefficient values from 1000 linear models built by randomly selecting two-thirds of the training data for each model run. Using these coefficients, we then created linear models and computed measures of model performance (i.e., relative root mean squared error (rRMSD) and root mean squared deviation (RMSD) (Pineiro et al., 2008)) for both the training and testing datasets. Linear model residuals were tested for normality using the Lilliefors test (Lilliefors, 1967) and visually inspected for homoscedasticity. When candidate models had more than one predictor variable, the variance inflation factor (VIF) was calculated. Guided by Graham (Graham, 2003), only candidate models with a VIF of less than 2 were considered for further analysis. From the candidate models, we selected the "best" model as the ones that most consistently had the lowest model errors, while giving priority to vegetation models that contained the same spectral variables across the three sensor data groups for each dominant phenological time period.

2.4.3. Model Comparison across Landsat 7 and Landsat 8 Scenes for Summer and Fall

Once the best model was selected for each of the 9 sensor–time data groups, we compared modeled vegetation amounts between models by applying each model to the paired Landsat 7 and Landsat 8 scenes. We did this for the summer and fall time periods separately due to notable increases in accuracy when modeling the summer vegetation data separately from the fall data. By separating the data in this way, there are nine comparisons when applying each model to each scene (Figure A1.2, step 4: all combinations explored). Across the study area for each scene and model combination, a relative difference raster was calculated as:

$$\% \text{ RelDif} = ((x - y)/((x + y)*0.5)*100) \quad (1)$$

where x represents the modeled vegetation amount derived from Landsat 8 scene data and y represents the modeled vegetation amount derived from Landsat 7 data. Next, to minimize the effect of forward and back-scatter, we combined all paired scene pixel differences for the summer and fall periods for a total dataset comparison. We computed the median and mean percent relative differences for each of the six scene date comparisons for each temporal period as well as averages across the six scenes for both the summer and fall periods.

### 2.4.4. Exploring Pixel-Wise Phenology-Driven Model Application

Due to the impact that vegetation phenology has on accurately estimating vegetation amounts with remotely sensed data (Jansen et al., 2016; Malmstrom et al., 2009; Vescovo and Gianelle, 2008) and the desire to automate the application of the appropriate phenological models across the grazing season, we estimated vegetation amounts using an 'if-else' statement, whereby if the sampling site value of the NDVI is greater than x, apply the summer model, else apply the fall model. To determine the threshold for each metric (biomass or cover) and sensor, we created a sequential range of NDVI values from 0.25 to 0.60 with a 0.01 step and applied our 'if-else' statement to predict a vegetation amount for each site. This sequential range of NDVI values was based on the overlapping span of NDVI values from the summer and fall sampling (Figure A1.5h). For each sensor and vegetation (cover and biomass) dataset and NDVI value between 0.25 and 0.60, we randomly selected 75% of the data and computed measures of model performance (rRMSE and RMSD) on the estimated versus the observed data, with 500 iterations. We averaged measures of model performance across all 500 runs and selected the thresholds that minimized the RMSD. We then compared the three ways to model vegetation across the year with (1) the nonautomated application of summer and fall models based on season; (2) the automated application of models based on phenology (i.e., NDVI threshold); and (3) the consistent application of the all-year models, with the full datasets of Landsat 8 and Landsat 7 separately for each vegetation metric (i.e cover and biomass).

### 2.4.5. Analysis of Model Residuals

To understand what physical, environmental, or sampling components most likely influence model error in the cover and biomass threshold algorithms, we correlated the algorithm residuals to ancillary environmental, topographic, in-field, and sensor data using the Spearman's rank method. Variables related to the sensor and sampling included: in-field sample date (i.e., Julian day), sensor date, number of days between field data collection date and scene acquisition date (days off), and number of days since last measured rainfall prior to overpass. Ecological variables collected at the site included percent foliar cover by plant functional group (perennial grass, perennial forb, annual grass, annual forb) and litter cover. Other data included soil surface variables when no canopy was observed, such as percent soil, moss and lichen cover, and rock. We also further explored the impacts of vegetation color

(green, brown, standing dead (grey)) as well as an estimate of percent utilization collected at each sample site. The topographic variables, slope and aspect, were derived from the 30-m national elevation dataset (NED) and averaged across a 2 × 2-pixel window to match the scale of the remotely sensed data (Table A1.3).

## 3.0 Results

### 3.1. Biomass and Cover Field Data

Across the 272 field sites visited during the study period, the average biomass was 133.23 g/m$^2$ and the average percent foliar cover was 0.56%. Biomass and cover data collected in summer exhibited greater average vegetation amounts when compared to data collected in the fall (Table 2.1). Our sampling design captured a gradient of vegetation amounts exhibited by the high range in biomass and cover amounts for both the summer and fall datasets.

Table 2.1. Summary statistics of in-field measures of biomass and cover collected across the study sites and sampling period.

| | **Biomass (g/m$^2$)** | | | **Cover (%)** | | |
|---|---|---|---|---|---|---|
| | **Summer** | **Fall** | **Total** | **Summer** | **Fall** | **Total** |
| ***N*** | 124 | 148 | 272 | 124 | 148 | 272 |
| **Mean** | 162.61 | 108.61 | 133.23 | 0.61 | 0.52 | 0.56 |
| **Min** | 39.59 | 12.19 | 12.19 | 0.21 | 0.13 | 0.13 |
| **Max** | 366.10 | 302.97 | 366.10 | 0.94 | 0.94 | 0.94 |
| **SD** | 71.25 | 59.59 | 70.40 | 0.19 | 0.21 | 0.21 |
| **Median** | 158.36 | 94.50 | 120.67 | 0.63 | 0.52 | 0.57 |

### 3.2. Variable Selection

The “best” predictor variables selected from the bootstrapped best-subset regression were relatively consistent between Landsat 7 and Landsat 8 across the three time data groupings. For the summer datasets, across all sensor groupings, the variables selected most for cover and biomass were the normalized difference infrared index 7 (NDII7) and the normalized difference water index (NDWI). When exploring the summer datasets with two-variable models, the NDII7 variable was most often selected, but the second variable varied

between the sensor groups and the vegetation metric (Tables A1.4 and A1.7). For both the fall and all-year (summer + fall) data, across all sensor groupings, the normalized difference tillage index (NDTI) was selected as the best predictor variable, while the NDII7 was selected as the second-best predictor (see Figures A1.3– A1.5 for scatterplots). The variables selected most for the two-variable models differed between the fall and the all-year datasets. The two-variable fall models contained the NDTI variable within each model, with the second variable again varying across the vegetation metric and sensor group. The all-year two-variable models for cover and biomass relied most heavily on the NDTI, NDII7, and to a lesser extent the NDWI (Tables A1.4– A1.9).

### 3.3. Candidate Model Comparisons and Model Selection

Across all three time periods analyzed, the two-variable models with variance inflation factors (VIF) under two did not consistently (across training and testing datasets) outperform the one-variable models by more than 1.5% rRMSE, or more than 1% for cover, or 1 g for biomass RMSD (Tables A1.10 and A1.11). The highest-ranked one-variable models for each time and sensor combination were all significant, with coefficients of determination ($r^2$) ranging from 0.65 to 0.81, and with rRMSE ranging from 13.00% to 30.88%.

Since the NDII7-based models had the lowest predictor error across the majority of the summer cover and biomass modeling datasets, we selected the NDII7 models for further analysis. The NDII7 models for cover had rRMSE values less than 18% and RMSD values less than 11% ($r^2 > 0.70$), with similar model evaluation statistics observed between the training and testing datasets. For biomass, model evaluation statistics for the training data had rRMSE values less than 23% and RMSD values less than 40 g/m$^2$ ($r^2 > 0.69$), while the testing dataset had lower rRMSE values (<21.5%) and RMSD values (<35 g/m$^2$) and higher $r^2$ coefficients (>0.8) (Table 2.2).

Table 2.2. Model evaluation statistics for final linear models to estimate biomass and cover, for both the training and testing datasets. LS7: Landsat 7, LS8: Landsat 8, NDII7: Normalized Difference Infrared Index 7, NDTI: Normalized Difference Tillage Index, Veg: vegetation, $r^2$: correlation of determination, rRMSE; relative root mean squared error, RMSD: root mean squared deviation.

| Metric | Time | Sensor | Veg Index | Training | | | | | | Validation | | | |
|---|---|---|---|---|---|---|---|---|---|---|---|---|---|
| | | | | N | Int | Slope | $r^2$ | rRMSE | RMSD | N | $r^2$ | rRMSE | RMSD |
| Biomass | Summer | LS7 | NDII7 | 60 | 104.06 | 343.18 | 0.69 | 22.84 | 39.27 | 20 | 0.81 | 21.25 | 34.87 |
| | Summer | LS8 | NDII7 | 93 | 101.09 | 330.25 | 0.80 | 20.07 | 32.08 | 30 | 0.81 | 16.86 | 28.96 |
| | Summer | LS78 | NDII7 | 153 | 102.18 | 335.95 | 0.76 | 21.38 | 35.07 | 50 | 0.81 | 18.50 | 30.89 |
| | Fall | LS7 | NDTI | 78 | −56.45 | 1042.00 | 0.71 | 30.46 | 32.67 | 25 | 0.77 | 24.19 | 26.43 |
| | Fall | LS8 | NDTI | 99 | −58.04 | 1070.64 | 0.67 | 30.88 | 31.20 | 32 | 0.70 | 26.69 | 32.02 |
| | Fall | LS78 | NDTI | 177 | −55.30 | 1044.67 | 0.69 | 30.73 | 31.80 | 57 | 0.73 | 25.86 | 29.54 |
| | All-year | LS7 | NDTI | 120 | −36.53 | 944.63 | 0.67 | 29.32 | 40.52 | 40 | 0.76 | 25.94 | 37.26 |
| | All-year | LS8 | NDTI | 184 | −41.74 | 1028.00 | 0.74 | 26.34 | 35.38 | 62 | 0.77 | 27.22 | 35.32 |
| | All-year | LS78 | NDTI | 304 | −38.08 | 984.32 | 0.70 | 27.88 | 37.82 | 102 | 0.76 | 26.10 | 35.11 |
| Cover | Summer | LS7 | NDII7 | 60 | 0.44 | 0.95 | 0.70 | 16.89 | 0.11 | 20 | 0.70 | 17.39 | 0.11 |
| | Summer | LS8 | NDII7 | 93 | 0.43 | 0.94 | 0.78 | 16.07 | 0.10 | 30 | 0.75 | 13.00 | 0.08 |
| | Summer | LS78 | NDII7 | 153 | 0.44 | 0.94 | 0.75 | 16.44 | 0.10 | 50 | 0.72 | 14.84 | 0.09 |
| | Fall | LS7 | NDTI | 78 | −0.09 | 3.88 | 0.78 | 19.87 | 0.10 | 26 | 0.81 | 17.07 | 0.09 |
| | Fall | LS8 | NDTI | 99 | −0.10 | 3.97 | 0.72 | 21.73 | 0.11 | 32 | 0.72 | 22.71 | 0.13 |
| | Fall | LS78 | NDTI | 177 | −0.09 | 3.91 | 0.75 | 20.92 | 0.11 | 58 | 0.73 | 20.69 | 0.11 |
| | All-year | LS7 | NDTI | 120 | 0.07 | 2.70 | 0.65 | 22.85 | 0.13 | 40 | 0.72 | 21.00 | 0.12 |
| | All-year | LS8 | NDTI | 184 | 0.06 | 2.95 | 0.69 | 20.55 | 0.12 | 62 | 0.70 | 21.02 | 0.12 |
| | All-year | LS78 | NDTI | 304 | 0.07 | 2.82 | 0.67 | 21.71 | 0.12 | 102 | 0.70 | 20.74 | 0.12 |

Across the fall and all-year datasets, the NDTI-based models were selected because this predictor minimized errors across every sensor group for both cover and biomass when compared to the other one-variable models. For fall cover data, the NDTI-based models had $r^2$ values greater than 0.72, with rRMSE values less than 23% and RMSD values less than 13%. For fall biomass data, the NDTI based models had $r^2$ values greater than 0.67, with rRMSE under 31% and RMSD under 33 g/m$^2$. Including both the summer and fall data together for the all-year datasets, the NDTI biomass models had $r^2$ values ranging from 0.67 to 0.77, with rRMSE less than 30% and RMSD ranging from 35.11 to 40.52 g/m$^2$. Cover NDTI models had $r^2$ values ranging from 0.65 to 0.72, with rRMSE less than 23% and RMSD ranging from 0.12 to 0.13%.

The relative root mean squared errors (rRMSE) were smaller on average when modeling summer vegetation datasets as compared to modeling the fall vegetation data, and the vegetation cover metric had lower rRMSE values compared to the biomass metric. While the rRMSE values were lower for the summer dataset, this pattern was not observed with the RMSD statistic for the biomass metric, which showed improvements in prediction accuracy for the fall data versus the summer data across all sensor groups and testing and training datasets, except the LS8 testing dataset.

When removing all sampling locations which were only valid for one sensor, so that we could compare model accuracy between sensors using an identical dataset of field data, we observed that for vegetation cover, the Landsat 7 and Landsat 8 data products provide very similar model fit estimates (i.e., within 1.5% rRMSE of each other) across all three temporal datasets (summer, fall, all year). When modeling summer biomass, the Landsat 8 sensor-based model was more accurate than the Landsat 7 biomass model, having a lower rRMSE of 3% and 2% with the training and testing data, respectively. When modeling the fall biomass data, the Landsat 7 biomass model reduced errors when compared to the Landsat 8-based model, with a 0.5% and 3% reduction of the rRMSE with the training and testing data, respectively (Tables A1.12 and A1.13).

### 3.4. Relative Differences in Modeled Vegetation across Paired Landsat 7 and Landsat 8 Scenes

The cover and biomass vegetation models that aligned to each sensor (sensor-aligned models; i.e., applying the Landsat 8 model to Landsat 8 data) had the smallest differences between estimated vegetation across the scene pairs for both summer and fall (Figures 2.2 and 2.3). For biomass, applying the sensor-aligned models across the six summer scene pairs resulted in a range of median percent relative differences from −2.73% (Landsat 7 bias) to 2.63% (Landsat 8 bias) with an average median percent relative difference of 0.33%. Across the six fall scenes, using the sensor-aligned biomass models, the median percent relative differences ranged from −4.54% to 3.55% with an average median percent relative difference of −0.39% (Table A1.14). These results are similar to the sensor-aligned cover models for both summer (median range = −1.62% to 2.00%, average median = 0.49%) and fall (median range = −3.87% to 2.21%, average median = −0.58%) (Table A1.15).

Across the six summer scene pairs, we observed a positive bias (average median percent relative difference of +2.22%) in NDII7 values from Landsat 8 as compared to Landsat 7. Across the six fall scene pairs, we observed a small negative bias (average median percent relative difference of −1.16%) in NDTI values with Landsat 8 data as compared to Landsat 7. Applying the sensor-data aligned models to the Landsat 7 and Landsat 8 data decreased sensor bias for the resulting vegetation amounts in both the summer and fall time periods (Tables A1.14 and A1.15).

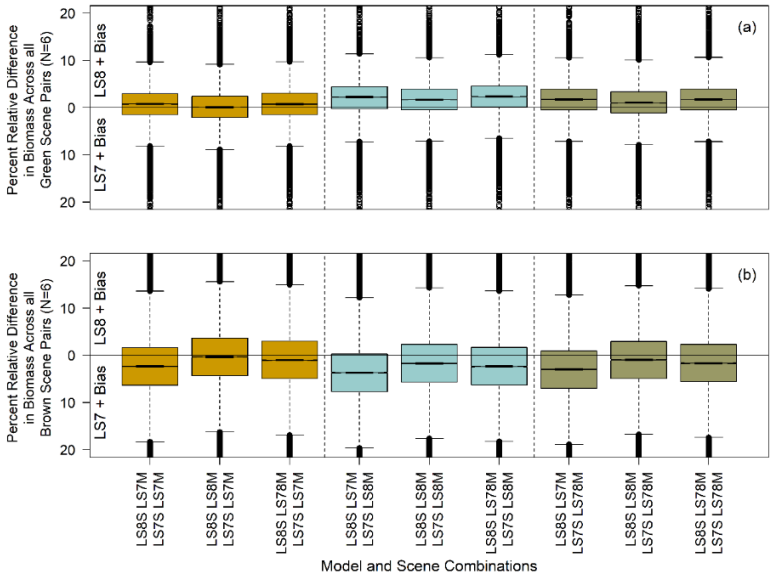


Figure 2.2. Boxplots of pixel-by-pixel comparison of estimated biomass for all paired Landsat 7 and Landsat 8 scenes using all model/scene combinations for the summer (green (a)) and fall (brown (b)) Landsat 7 and Landsat 8 scenes. LS7S: Landsat 7 scene, LS8S: Landsat 8 scene, LS7M: Landsat 7 data model, LS8M: Landsat 8 data model, LS78M: combined Landsat 7 and Landsat 8 data model.

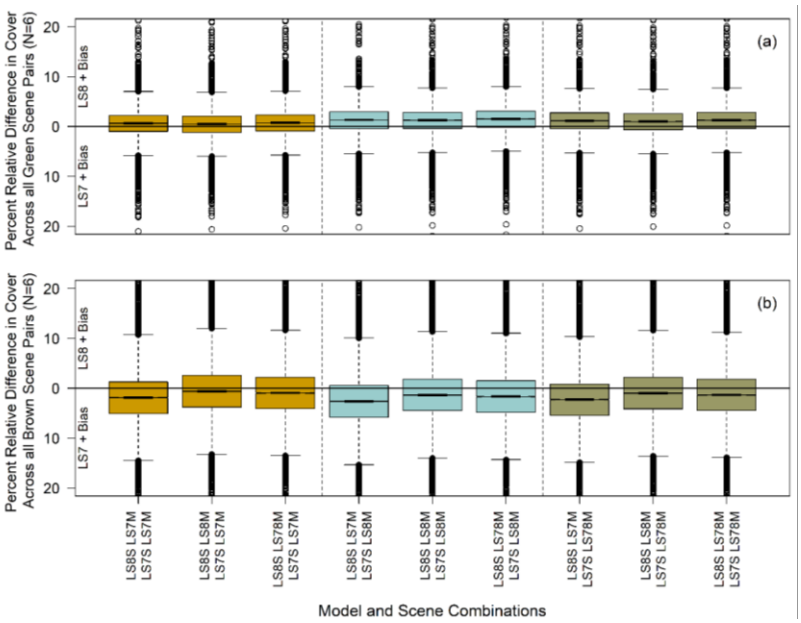


Figure 2.3. Boxplots of pixel-by-pixel comparison of estimated cover for all paired Landsat 7 and Landsat 8 scenes using all model/scene combinations for the summer (green (a)) and fall (brown (b)) Landsat 7 and Landsat 8 scenes. LS7S: Landsat 7 scene, LS8S: Landsat 8 scene, LS7M: Landsat 7 data model, LS8M: Landsat 8 data model, LS78M: combined Landsat 7 and Landsat 8 data model.

### 3.5. Assessing a Pixel-Wise Phenologically (NDVI) Driven Model Application across the Grazing Season

The NDVI threshold values that guide application of season-specific models for biomass were 0.38 and 0.32 for Landsat 8 and Landsat 7 data, respectively. Cover thresholds were very similar to that of biomass, with the RMSD minimized at NDVI values of 0.37 for Landsat 8 data and 0.31 for Landsat 7 data (Figure 2.4).

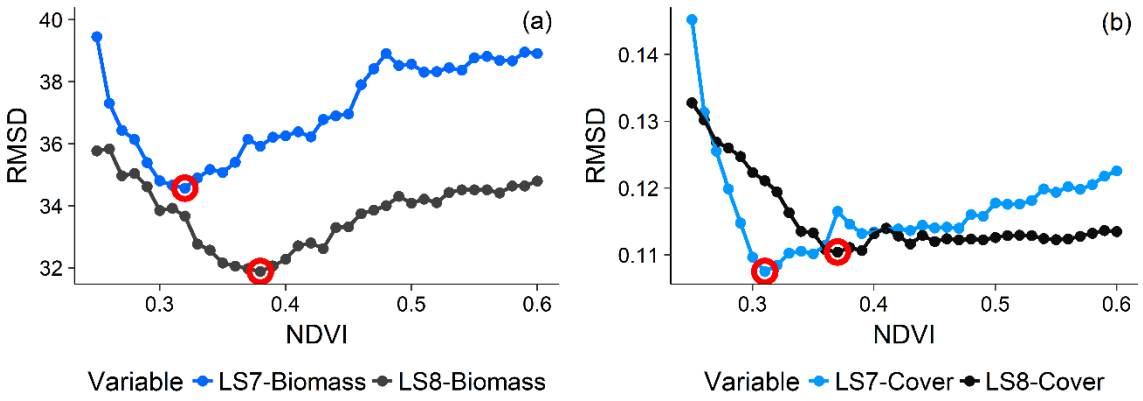


Figure 2.4. The Normalized Difference Vegetation Index (NDVI) threshold value that minimizes the relative root mean squared difference (RMSD) when applying the summer and fall models to a balanced summer and fall dataset for Landsat 7 (LS7) and Landsat 8 (LS8) data separately to predict (**a**) biomass and (**b**) cover across the grazing season. The minimum RMSD values are highlighted with red circles.

The RMSD varied less than 1.5 g/m$^2$ for biomass (Figure 2.5) and less than 1% for cover (Figure 2.6) when comparing the season-specific model (Figures 2.5 a, b and 2.6 a, b) to the NDVI-threshold algorithm method (Figures 2.5 c, d and 2.6 c, d). The all-year NDTI-based models (Figures 2.5 e, f and 2.6 e, f) also performed well, but had the largest RMSD across both sensors and vegetation metrics when compared to the other two methods of applying the models' Landsat data.

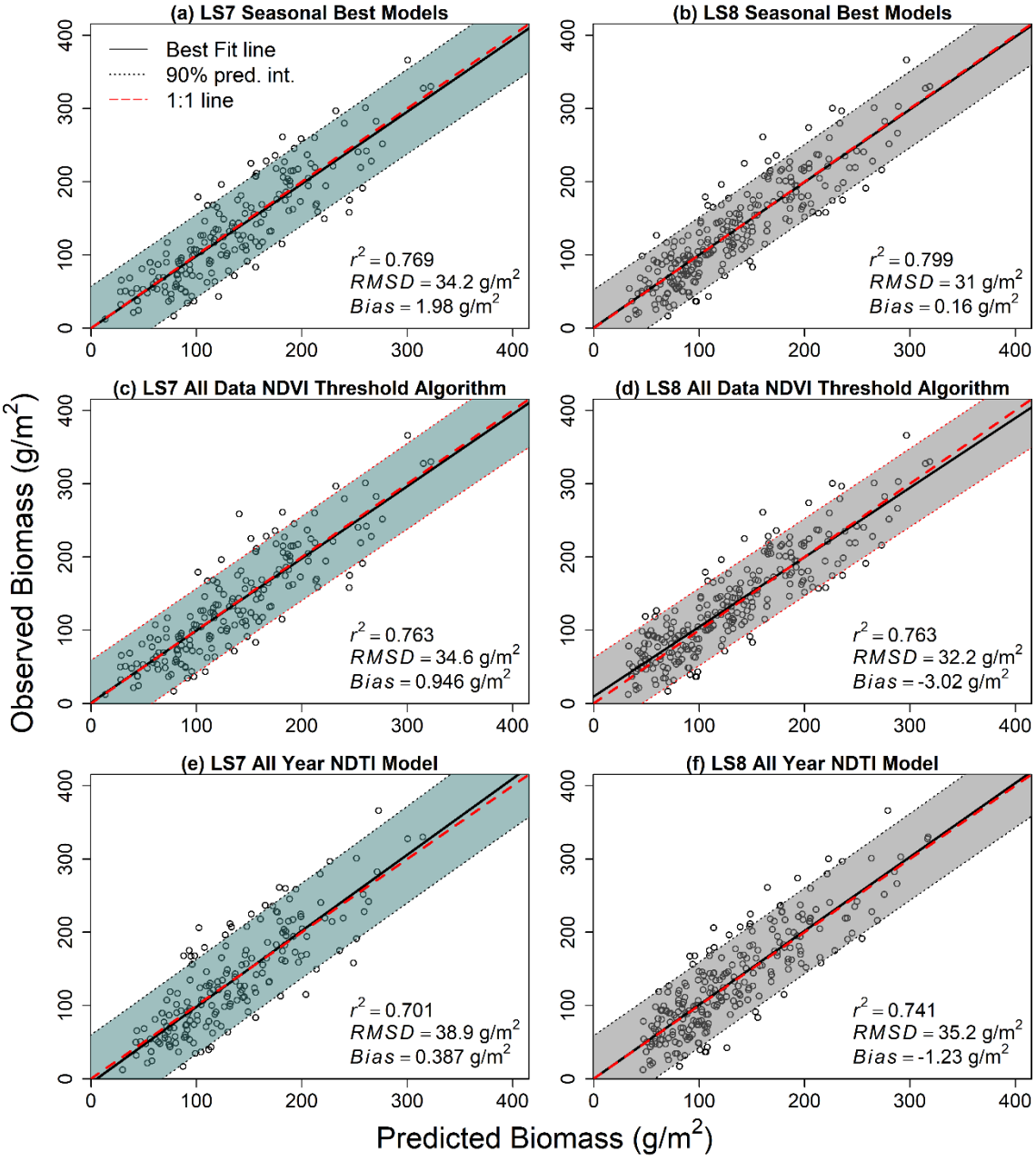


Figure 2.5. Observed versus predicted biomass using three approaches to model vegetation biomass using all the sampling data: (1) applying the seasonal best models (Table 2.3 summer/fall models) to (**a**) Landsat 7 (LS7) and (**b**) Landsat 8 (LS8) data based on a calendar date; (2) applying the seasonal best models based on the NDVI threshold by sensor (**c**,**d**) and (3) applying single all-year models (Table 2.3) to (**e**) LS7 and (**f**) LS8 data. The shaded area represents the 90% prediction interval, the black line represents the best fit line, and the dashed red line represents the one-to-one line.

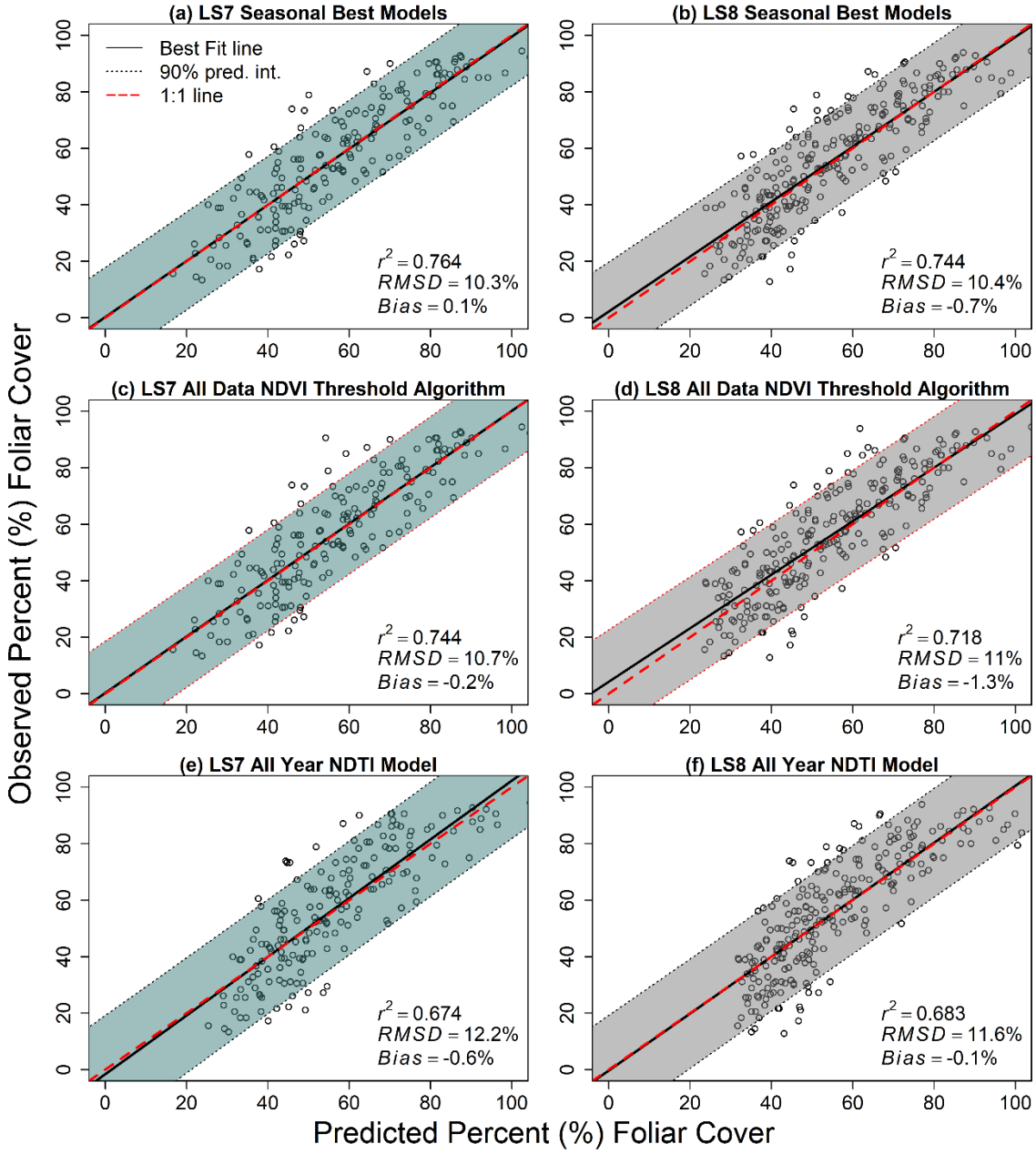


Figure 2.6. Observed versus predicted cover using three approaches to model vegetation cover using all the sampling data: (1) applying the seasonal best models (Table 2.3 summer/fall models) to (**a**) Landsat 7 (LS7) and (**b**) Landsat 8 (LS8) data based on a calendar date; (2) applying the seasonal best models based on the NDVI threshold by sensor (**c**,**d**) and (3) applying single all-year models (Table 2.3) to (**e**) LS7 and (**f**) LS8 data. The shaded area represents the 90% prediction interval, the black line represents the best fit line, and the dashed red line represents the one-to-one line.

### 3.6. Correlation of NDVI Threshold Model Error with Sensor, Sampling, and Field Variables

For both the cover and biomass metrics, the maximum significant correlation had an absolute correlation coefficient (*r*) of 0.41. Only percent perennial grass, percent litter, prior rain events, and percent moss and lichen had *r* values over 0.30 for any sensor/vegetation metric (Table 2.3).

Table 2.3. Sensor, sampling, and ecological variables significantly correlated (Spearman rank) to NDVI threshold algorithm residuals used to model vegetation amounts across the grazing season. LPI: line point intercept, r: correlation coefficient, SD: standing dead vegetation (last years growth), NS: not significant at the 0.05 p-value.

| Metric | Variable | Variable Source | Landsat 7 | | Landsat 8 | |
|---|---|---|---|---|---|---|
| | | | ***r*-val** | ***p*-val** | ***r*-val** | ***p*-val** |
| Biomass | % Perennial Grass | LPI (canopy) | −0.21 | 0.001 | −0.15 | 0.006 |
| Biomass | % Litter | LPI (canopy) | 0.2 | 0.013 | 0.18 | 0.006 |
| Biomass | Rain Lag (days) | Sensor (Field) | 0.36 | 0.027 | 0.24 | 0.006 |
| Biomass | % Moss/Lichen | LPI (soil surface) | 0.13 | 0.014 | 0.004 | NS |
| Biomass | % Rock | LPI (soil surface) | 0.01 | 0.046 | −0.0578 | NS |
| Biomass | % Mean Utilization | Utilization | NS | NS | 0.1 | 0.003 |
| Cover | % Perennial Grass | LPI (canopy) | −0.407 | 0 | −0.3546 | 0 |
| Cover | % Annual Grass | LPI (canopy) | −0.174 | 0.018 | −0.2150 | 0 |
| Cover | % Annual Forb | LPI (canopy) | −0.264 | 0 | −0.1981 | 0.0322 |
| Cover | Field Data Lag (Days) | Sensor (Field) | −0.178 | 0.016 | −0.1800 | 0.0233 |
| Cover | % Brown and SD Color | LPI (color) | −0.178 | 0.016 | −0.1700 | NS |
| Cover | % Litter | LPI (canopy) | 0.315 | 0 | 0.2379 | 0 |
| Cover | Rain Lag (days) | Sensor (Weather Station) | 0.327 | 0 | 0.1815 | 0 |
| Cover | % Rock | LPI (soil surface) | 0.277 | 0 | 0.18317 | 0 |
| Cover | % Soil | LPI (soil surface) | 0.162 | 0.029 | 0.211 | 0.001 |
| Cover | % Moss/Lichen | LPI (soil surface) | 0.381 | 0 | 0.304 | 0 |
| Cover | % Green Color | LPI (color) | 0.178 | 0.016 | 0.17 | NS |

## 4.0 Discussion

To provide near real-time data for adaptive management, we developed and tested an approach to automate the quantification and mapping of vegetation cover and biomass using Landsat 7 and Landsat 8 CDR products across the grazing season (i.e., changing phenological conditions) by relying on NDVI thresholds to guide season-specific model application. We showed that using NDVI to select from seasonal models for application increased accuracies when modeling vegetation amounts at varying growth stages compared to the single variable all-year NDTI models. Our finding that Landsat 8 has a larger NDVI threshold value as compared to Landsat 7 aligns with previous literature that found that Landsat 8-derived NDVI values are greater than those of Landsat 7 (Holden and Woodcock, 2016; Roy D. P. et al., 2015). These sensor-specific algorithms enable efficient mapping, analysis, and accessibility of biomass and cover estimates throughout the grazing season as vegetation changes due to phenology and management. This is a substantial improvement over point-based quantitative observations or plot-based qualitative assessments. The vegetation maps provide a richer, more complete representation of vegetation amounts for land managers and ranchers to use in assessing the outcomes of their management actions. One example application of this model at the pasture scale reveals the differences in biomass corresponding to various management strategies (Figure 2.7).

Our results from season-specific modeling, using data from the summer sampling period, determined that NDII7 was the most accurate spectral predictor of biomass and cover; this is in contrast to the wide use of NDVI as a proxy for rangeland vegetation (Svoray et al., 2013). We attribute this result to the fact that over one-third of our summer sampling sites had more than 30% brown or standing dead vegetation cover, since the relationship between total biomass and NDVI is affected by the amount of standing dead (prior year's growth) or senescent (current year's growth that is no longer photosynthetically active) vegetation (Xu et al., 2014). Furthermore, in rangelands where species diversity and heterogenous soil conditions create high phenological variability within a single pixel as well as over the study area, the impact of nonphotosynthetically active vegetation is especially important to take into account when modeling vegetation metrics for rangeland monitoring (Marsett et al., 2006; Todd et al., 1998).

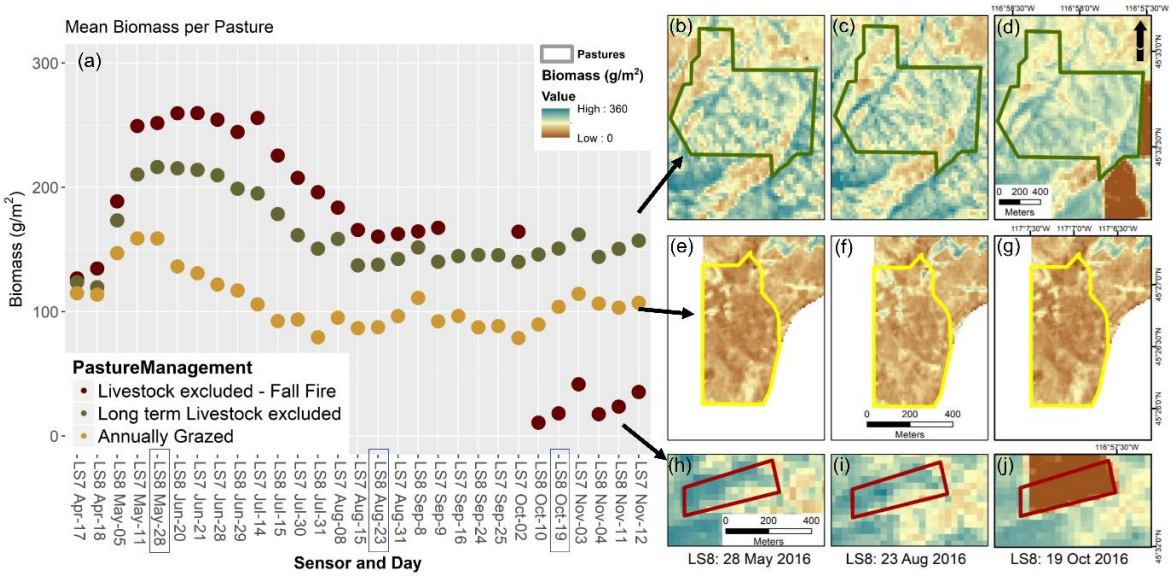


Figure 2.7. (**a**) Estimating the mean biomass (g/m$^2$) with the Landsat 7 and 8 Climate Data Record (CDR) products across three selected pastures with different management actions for the 2016 grazing season (17 April to 12 November). Mapping biomass (**b**–**j**) using three 2016 scenes (28 May, 23 August, 19 October) across the three selected pastures with different management action ((**b**–**d**) long-term livestock excluded, (**e**–**g**) annually grazed, (**h**,**i**) livestock excluded: fall fire).

For the fall sampling period, the best predictor (NDTI) contained the two shortwave infrared bands, which correlate to cellulose and lignin in vegetation (Elvidge, 1990; Jacques et al., 2014; Roberts et al., 1993). Vegetation indices such as the soil tillage index (STI), the normalized difference tillage index (NDTI), and the soil adjusted total vegetation index (SATVI), which rely in part on the shortwave infrared (SWIR) bands, have been used to estimate dry vegetation and total vegetation in semiarid rangelands across the African Sahel (Jacques et al., 2014), the southwest USA (Hagen et al., 2012; Marsett et al., 2006), and photosynthetic and nonphotosynthetic vegetation across the Australian savanna (Guerschman et al., 2009). Our ability to explain the variance of dry vegetation amounts in both cover and biomass is comparable and slightly better than that of Jacques et al. (Jacques et al., 2014), who found an $r^2$ of 0.67 when linearly relating biomass and STI across the year, an $r^2$ of 0.59 when using only the dry season measures, and an $r^2$ of 0.66 during the wet season. We attribute this slight improvement to our dataset containing fewer years' data, being collected across a smaller, more similar habitat type, and the higher spatial resolution of Landsat compared to MODIS. Furthermore, compared to Jansen et al. (Jansen et al., 2016), we

observed improved model accuracy as well as simplified models (one-variable models compared to multivariable models). Model improvement is especially evident for the fall biomass models, exhibited by an increase of the $r^2$ from 0.35 in Jansen et al. (Jansen et al., 2016) to 0.67 in this study. This is likely due to our larger in-field plot size, improved in-field biomass estimates, as well as the fact that we sampled a greater range of vegetation amounts and had a much larger sample size. Similar to Jacques et al. (Jacques et al., 2014), NDTI also performed quite well across both the summer and fall periods of this study. These findings support the idea that SWIR vegetation indices are sensitive to both green and brown vegetation (Renier et al., 2015) in grassland systems with darker soil. The parent material that makes up the Zumwalt Prairie soils comes from basalt and loess, creating dark soils in contrast to the bright soils of the Sahel (Jacques et al., 2014).

Comparing the relative differences between paired scenes showed that sensor-specific models decreased differences in predicted vegetation amounts between Landsat 7 and Landsat 8 scenes. Across the Zumwalt study area, we observed a small positive bias with the Landsat 8 summer time NDII7 (also known as the Normalized Burn Ratio (NBR)) and a small negative bias with the Landsat 8 fall NDTI (Tables A1.14 and A1.15). Using sensor-specific models for vegetation biomass and cover eliminates the need to normalize images across the image analysis stack (Holden and Woodcock, 2016). While we observed reduced bias between scenes with sensor-specific models, the individual scene pair comparisons did vary, with bias not always trending in the same direction for each Landsat 7/Landsat 8 scene pair. This is likely due to differences in atmospheric effects and pixels missed by the pixel quality assurance (pixel_qa) mask that contained clouds, shadows, and aerosols. For example, we had to apply a manual cloud mask to the 17 October 2015 scene, due to errors of omission of the pixel_qa mask with high cirrus clouds and shadows. Such errors can lead to spurious results, necessitating the collection of field data across many years (Jansen et al., 2016) and careful screening of scenes to effectively remove spurious data due to clouds, shadows, and aerosol effects (Roy D. P. et al., 2015) for more accurate models and their associated vegetation products.

Another important aspect of understanding the accuracy of these models for decision-making tools is assessing where or when they may produce unreliable estimates. Places where the model tended to underestimate vegetation amounts were in highly productive areas of

deep soil with dense, multi-layered vegetation canopies (potentially due to shadowing), areas where annual grass has filled interspaces between bunchgrasses, and areas of dense, continuous annual grass cover (Figure 2.8). Further evidence of this underestimation is our finding that both perennial and annual grass cover were negatively correlated to model residuals.


Figure 2.8. Sites with high underestimation of cover data as estimated by Landsat 8 cover models: (**a**) Homogenous deep soiled meadow area. Remotely Sensed (RS) estimate = 59%; Field estimate = 85%; (**b**) Homogenous annual grass dominated with rock. RS estimate = 55%; Field estimate = 78%; (**c**) Heterogenous perennial grass/annual grass. RS estimate = 64%; Field estimate = 87%.

Overestimation seemed to be associated with several different factors. Sites where the models tended to overpredict vegetation amounts, especially vegetation cover, were in areas with high vegetation heterogeneity, such as on mima mounds (Cramer and Barger, 2014) or areas with greater rock cover (Figure 2.9).

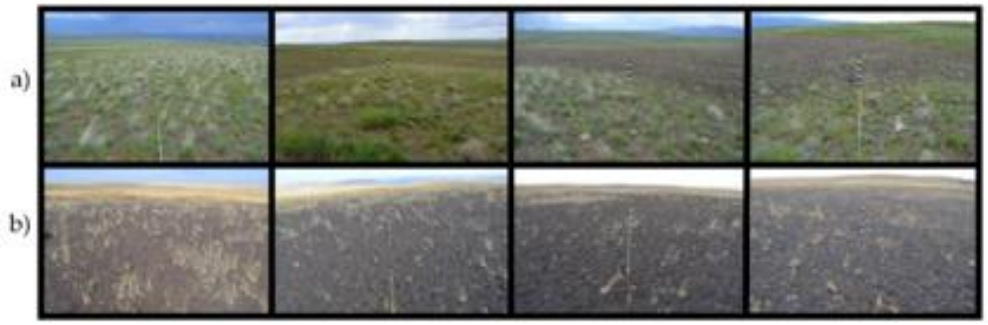


Figure 2.9. Sites with high overestimation of cover data as estimated by Landsat 8 cover models: (**a**) Highly heterogenous on big mima mounds. Remotely Sensed (RS) estimated cover = 49%; LPI field estimated cover 27%; (**b**) Homogenous rock cover. RS estimate = 40%; LPI field estimated cover = 22%.

Cover and biomass on sites with a greater percentage of moss/lichen cover also tended to be overestimated. This aligns with Rodriquez-Caballero et al. (Rodríguez-caballero et al., 2015), who found that NDVI and the enhanced vegetation index (EVI) were impacted by biological crust cover, resulting in higher vegetation index values. Litter cover was another factor contributing to overestimation, which is likely due to the models and associated vegetation indices not being sensitive to the difference between attached and unattached plant material. Litter has been cited as a source of error when estimating biophysical parameters in grassland systems (Van Leeuwen and Huete, 1996). The NDII7 and NDTI vegetation indices used to model cover and biomass are sensitive to both green and brown plant material (McNairn and Protz, 1993; Renier et al., 2015; Zheng et al., 2013), such as crop residue, because the SWIR band (around 2100 nm) effectively differentiates plant material (cellulose and lignin) from soil (Daughtry, 2001; Daughtry et al., 2005; Elvidge, 1990). Overestimation observed with rain lag is likely due to the SWIR bands also being sensitive to water content (Daughtry, 2001; Daughtry and Hunt, 2008), with greater reflectance occurring with drier conditions as opposed to greater absorption with more moisture (Daughtry and Hunt, 2008; Knipling, 1970; Tucker, 1980).

This study revealed challenges and tested the feasibility of using Landsat's surface reflectance products to model vegetation amounts that are applicable to rangeland management across the grazing season. Improvements can be made with more technical and automated cloud and shadow filtering. For example, Roy et al. [22] used the blue-band filter

to remove pixels with significant surface change from the image pair. Exploring different modeling methods such as random forests (L. Breiman, 2001), artificial neural networks (e.g., (Yang et al., 2018)), or support vector machines (Wang et al., 2016) may improve model accuracy. We did explore improving the model accuracy of cover data with quadratic polynomial models and found that they did not decrease the rRMSE by more than 1% consistently across the training and testing sets (Figure A1.6 and Table A1.16). Combining remotely sensed datasets such as Landsat and Sentinel-2, which has a global median average revisit time of less than three days (Li and Roy, 2017), would allow for further improvement of near real-time multitemporal monitoring of vegetation at management scales. Other options would be to use fusion algorithms relying on MODIS data, such as the spatial and temporal adaptive reflectance fusion model, StarFM (Gao et al., 2006), or the spatial temporal adaptive algorithm for mapping reflectance change (STAARCH) (Hilker et al., 2009). Remote sensing science and availability of data products in GEE will continue to improve, making it increasingly realistic to deliver accurate data in near real-time to decision-makers.

To date, one of the biggest obstacles facing rangeland ecologists is consistently sharing information derived from remotely sensed analysis with managers and ranchers. We are utilizing GEE by leveraging the ClimateEngine (Huntington et al., 2017) to distribute these modeled cover and biomass vegetation products to stakeholders in a timely, cost-effective, and automated way. One of the initial goals of this research was to provide accessible, timely, and zero-cost estimates of vegetation amounts across the grazing season to enable adaptive management and monitoring at the pasture, ranch, and landscape scale. A landscape-wide vegetation dataset such as this one can provide consistent unbiased data for making comparisons and sharing successful management strategies across property lines over time. As climate change continues to amplify the annual and interannual variability in rangeland ecosystems (Joyce et al., 2013), sharing successful adaptation and management strategies between ranchers and researchers will become increasingly necessary (Knapp and Fernandez-Gimenez, 2009). The analyses undertaken here support tool development by (1) testing the sensitivity of models across sensors and across the grazing season (2) and by empirically identifying a threshold for phenologically aligned model application.

## 5.0 Conclusions

Near real-time estimates of vegetation cover and biomass are critical to adaptive rangeland management. NDVI has been widely used for rangeland monitoring tools and can provide a rough proxy of vegetation production and phenology, but is less accurate when vegetation contains high proportions of standing dead or senescent vegetation. Developing phenology-driven predictive models specific to each Landsat 7 and 8 CDR product yielded consistent and nonbiased estimates of total vegetation cover and above-ground biomass across the grazing season. Applying these models in Google Earth Engine provides a platform for land managers and ranchers to utilize timely, cost-effective, and unbiased information to meet objectives and improve outcomes. We suggest that future ecological applications of remote sensing products that are developed with Google Earth Engine or other platforms should also seek to incorporate seasonality into product development and conduct sensitivity analyses, and validate the models with field data to ensure accurate performance under short- and long-term dynamic vegetation conditions.

**Supplementary Materials in Appendix 1:**, Figure S1: Sampling site plot layout, Table S1. Paired Landsat 7 and Landsat 8 scenes used in model building (including timing of in-field vegetation sampling) and for sensor model comparisons, Table S2. Candidate vegetation indices used in the best subset modeling step, Figure S2. Workflow diagram for final algorithm development, Table S3. The field, sensor and topographic variables used to correlate with residuals from the NDVI threshold algorithm, Table S4. Variable Selection using a bootstrapped best subset model approach for green (summer) biomass data, Table S5. Variable Selection using a bootstrapped best subset model approach for brown (fall) biomass data, Table S6. Variable Selection using a bootstrapped best subset model approach for All Year (Green + Brown) biomass data, Table S7. Variable Selection using a bootstrapped best subset model approach for green (summer) cover data, Table S8. Variable Selection using a bootstrapped best subset model approach for the fall (brown) cover data, Table S9. Variable Selection using a bootstrapped best subset model approach for the complete dataset (All Year) cover data, Table S10. Top candidate models for Cover, Table S11. Top candidate models for Biomass, Table S12. Paired Cover models, Table S13. Paired Biomass models, Figure S3.

Scatter plots between in-field estimates of cover and biomass with select vegetation indices (NDTI, NDII7, NDVI) using Landsat 7 data. Figure S4. Scatter plots between in-field estimates of cover and biomass with select vegetation indices (NDTI, NDII7, NDVI) using Landsat 8 data. Figure S5. Scatter plots between in-field estimates of cover and biomass with select vegetation indices (NDTI, NDII7, NDVI) using Landsat 7 and Landsat 8 data. Table S14. Table of Median and Mean pixel differences in Biomass across scene pairs across all model combinations and the associated vegetation index (NDII7 for Green, NDTI for Brown), Table S15. Table of Median and Mean differences in Cover between scene pairs across all model combinations and the associated vegetation index (NDII7 for Green, NDTI for Brown), Figure S6. Scatter plots of simple and polynomial linear regressions using the summer, fall, and all-year cover data for both Landsat 7 and Landsat 8, Figure S16. Model fit statistics for simple and polynomial linear regressions using the summer and fall cover data.

**References**

Asner, G. P., Elmore, A. J., Olander, L. P., Martin, R. E., & Harris, T. A. (2004). Grazing Systems, Ecosystem Responses, and Global Change. Annual Review of Environment and Resources, 29(1), 261–299. http://doi.org/10.1146/annurev.energy.29.062403.102142

Bestelmeyer, B. T., & Briske, D. D. (2012). Grand Challenges for Resilience-Based Management of Rangelands. Rangeland Ecology & Management, 65(November), 654–663. http://doi.org/10.2111/REM-D-12-00072.1

Breiman, L. (2001). Random Forests. Machine Learning, 45, 5–32.

Briske, D. D., Fuhlendorf, S. D., & Smeins, F. E. (2005). State-and-Transition Models, Thresholds, and Rangeland Health: A Synthesis of Ecological Concepts and Perspectives. Rangeland Ecology & Management, 58(1), 1–10. http://doi.org/10.2111/1551-5028

Briske, D. D., Washington-Allen, R. A., Johnson, C. R., & Lockwood, J. A. (2010). Catastrophic Thresholds: A Synthesis of Concepts, Perspectives, and Applications. Ecology and Society, 15(3).

Brunson, M. W., & Huntsinger, L. (2008). Ranching As A Conservation Strategy: Can Old Ranchers Save The New West? Rangeland Ecology & Management, 61(2), 137–147. http://doi.org/10.2111/07-063.1

Butterfield, H. S., & Malmström, C. M. (2009). The effects of phenology on indirect measures of aboveground biomass in annual grasses. International Journal of Remote Sensing, 30(12), 3133–3146. http://doi.org/10.1080/01431160802558774

Cramer, M. D., & Barger, N. N. (2014). Are mima-like mounds the consequence of long-term stability of vegetation spatial patterning? Palaeogeography, Palaeoclimatology, Palaeoecology, 409, 72–83. http://doi.org/10.1016/j.palaeo.2014.04.026

Crist, E. P. (1985). A TM Tasseled Cap equivalent transformation for reflectance factor data. Remote Sensing of Environment, 17, 301–306. http://doi.org/10.1016/0034-4257(85)90102-6

Crowley, P. H. (1992). Resampling methods for computation-intensive data analysis in ecology and evolution. Annual Review of Ecology and Systematics, 23, 405–447. http://doi.org/10.2307/2097295

Daughtry, C. S. T. (2001). Agroclimatology: Discriminating crop residues from soil by shortwave infrared reflectance. Agronomy Journal, 93(1), 125–131. http://doi.org/10.2134/agronj2001.931125x

Daughtry, C. S. T., & Hunt, E. R. (2008). Mitigating the effects of soil and residue water contents on remotely sensed estimates of crop residue cover. Remote Sensing of Environment, 112, 1647–1657. http://doi.org/10.1016/j.rse.2007.08.006

Daughtry, C. S. T., Hunt, E. R., Doraiswamy, P. C., & McMurtrey, J. E. (2005). Remote Sensing the Spatial Distribution of Crop Residues. Agronomy Journal, 97(3), 864. http://doi.org/10.2134/agronj2003.0291

Elvidge, C. (1990). Visible and near infrared reflectance characteristics of dry plant materials. International Journal of Remote Sensing, 11(10), 1775–1795.

Fleishchner, T. L. (1994). Ecological Costs of Livestock Grazing in Western North America. Society for Conservation Biology, 8(3), 629–644.

Friedel, M. H., & Bastin, G. N. (1988). Photographic standards for estimating compariative yield in arid rangelands. Australian Rangeland Journal, 10(1), 34–38.

Gao, F., Masek, J., Schwaller, M., & Hall, F. (2006). On the blending of the Landsat and MODIS surface reflectance: predicting daily Landsat surface reflectance. IEEE Transactions on Geoscience and Remote Sensing, 44(8), 2207–2218. http://doi.org/10.1109/TGRS.2006.872081

Gorelick, N., Hancher, M., Dixon, M., Ilyushchenko, S., Thau, D., & Moore, R. (2017). Google Earth Engine: Planetary-scale geospatial analysis for everyone. Remote Sensing of Environment, 202, 18–27. http://doi.org/10.1016/j.rse.2017.06.031

Graham, M. H. (2003). CONFRONTING MULTICOLLINEARITY IN ECOLOGICAL Multiple Regression. Ecology, 84(11), 2809–2815.

Guerschman, J. P., Hill, M. J., Renzullo, L. J., Barrett, D. J., Marks, A. S., & Botha, E. J. (2009). Estimating fractional cover of photosynthetic vegetation, non-photosynthetic vegetation and bare soil in the Australian tropical savanna region upscaling the EO-1 Hyperion and MODIS sensors. Remote Sensing of Environment, 113(5), 928–945. http://doi.org/10.1016/j.rse.2009.01.006

Guerschman, J. P., Scarth, P. F., Mcvicar, T. R., Renzullo, L. J., Malthus, T. J., Stewart, J. B., … Trevithick, R. (2015). Remote Sensing of Environment Assessing the effects of site heterogeneity and soil properties when unmixing photosynthetic vegetation , non-photosynthetic vegetation and bare soil fractions from Landsat and MODIS data. Remote Sensing of Environment, 161, 12–26. http://doi.org/10.1016/j.rse.2015.01.021

Hagen, S. C., Heilman, P., Marsett, R., Torbick, N., Salas, W., van Ravensway, J., & Qi, J. (2012). Mapping Total Vegetation Cover Across Western Rangelands With Moderate-Resolution Imaging Spectroradiometer Data. Rangeland Ecology & Management, 65(5), 456–467. http://doi.org/10.2111/REM-D-11-00188.1

Hansen, M. C., Potapov, P. V, Moore, R., Hancher, M., Turubanova, S. A., Tyukavina, A., … Townshend, J. R. G. (2013). High-Resolution Global Maps of 21st-Century Forest Cover Change. Science, 342(November), 850–854. http://doi.org/10.1126/science.1244693

Herrick, J. E., Lessard, V. C., Spaeth, K. E., Shaver, P. L., Dayton, R. S., Pyke, D. A., … Goebel, J. J. (2010). National ecosystem assessments supported by scientific and local knowledge. Frontiers in Ecology and the Environment, 8(8), 403–408. http://doi.org/10.1890/100017

Herrick, J. E., Zee, J. W. Van, Havstad, K. M., Burkett, L. M., Whitford, W. G., Pyke, D. A., … Shaver, P. L. (2005). Monitoring Manual for grassland, shrubland and savanna ecosystems. Las Cruces, NM, USA: USDA-ARS Jornada Experimental Range., 236.

Hilker, T., Wulder, M. a., Coops, N. C., Linke, J., McDermid, G., Masek, J. G., … White, J. C. (2009). A new data fusion model for high spatial- and temporal-resolution mapping of forest disturbance based on Landsat and MODIS. Remote Sensing of Environment, 113(8), 1613–1627. http://doi.org/10.1016/j.rse.2009.03.007

Holden, C. E., & Woodcock, C. E. (2016). An analysis of Landsat 7 and Landsat 8 under fl ight data and the implications for time series investigations. Remote Sensing of Environment. http://doi.org/10.1016/j.rse.2016.02.052

Hudak, A. T., Crookston, N. L., Evans, J. S., Falkowski, M. J., Smith, A. M. S., Gessler, P. E., & Morgan, P. (2006). Regression modeling and mapping of coniferous forest basal area and tree density from discrete-return lidar and multispectral satellite data. Canadian Journal of Remote Sensing, 32(2), 126–138. http://doi.org/10.5589/m06-007

Huete, A. R., & Jackson, R. D. (1987). Suitability of spectral indices for evaluating vegetation characteristics on arid rangelands. Remote Sensing Environment, 23(2), 213–218.

Huntington, J. L., Hegewisch, K. C., Daudert, B., Morton, C. G., Abatzoglou, J. T., McEvoy, D. J., & Erickson, T. (2017). Climate engine: Cloud computing and visualization of climate and remote sensing data for advanced natural resource monitoring and process understanding. Bulletin of the American Meteorological Society, 98(11), 2397–2409. http://doi.org/10.1175/BAMS-D-15-00324.1

Huntsinger, B. L., & Sayre, N. F. (2007). Introduction : The Working Landscapes Special Issue. Rangelands, 29(3), 3–4.

Ikeda, H., Okamoto, K., & Fukuhara, M. (1999). Estimation of aboveground grassland phytomass with a growth model using Landsat TM and climate data. International Journal of Remote Sensing, 20(11), 2283–2294. Retrieved from http://www.tandfonline.com/doi/abs/10.1080/014311699212254

Jacques, D. C., Kergoat, L., Hiernaux, P., Mougin, E., & Defourny, P. (2014). Monitoring dry vegetation masses in semi-arid areas with MODIS SWIR bands. Remote Sensing of Environment, 153, 40–49. http://doi.org/10.1016/j.rse.2014.07.027

Jansen, V. S., Kolden, C. A., Taylor, R. V., & A. Newingham, B. (2016). Quantifying livestock effects on bunchgrass vegetation with Landsat ETM+ data across a single growing season. International Journal of Remote Sensing, 37(1), 150–175. http://doi.org/10.1080/01431161.2015.1117681

Joyce, L. A., Briske, D. D., Brown, J. R., Polley, W. H., McCarl, B. A., & Bailey, D. W. (2013). Climate Change and North American Rangelands: Assessment of Mitigation and Adaptation Strategies. Rangeland Ecology and Management, 66(5), 512–528. http://doi.org/10.2111/REM-D-12-00142.1

Kagan, J., Ohmann, J., Gregory, M., Tobalske, C., Hak, J., & Fried, J. (2006). Final Report on Land Cover Mapping Methods : Map Zones 8 and 9, PNW ReGAP. Institute for Natural Resouces, Oregon State University,.

Kauth, R. J., & Thomas, G. S. (1976). The Tasselled Cap--A Graphic Description of the Spectral-Temporal Development of Agricultural Crops as Seen by LANDSAT. LARS Symposia. Retrieved from http://docs.lib.purdue.edu/cgi/viewcontent.cgi?article=1160&context=lars_symp

Knapp, C. N., & Fernandez-Gimenez, M. E. (2009). Knowledge in Practice: Documenting Rancher Local Knowledge in Northwest Colorado. Rangeland Ecology & Management, 62(6), 500–509. http://doi.org/10.2307/40495279

Knipling, E. (1970). Physical and physiological basis for the reflectance of visible and near-infrared radiation from vegetation. Remote Sensing of Environment, 1(3), 155–159.

Li, J., & Roy, D. P. (2017). A Global Analysis of Sentinel-2A , Sentinel-2B and Landsat-8 Data Revisit Intervals and Implications for Terrestrial Monitoring. Remote Sensing, 9(902), 1–17. http://doi.org/10.3390/rs9090902

Lilliefors, H. (1967). On the Kolmogorov-Smirnov test for normality with mean and variance unknown. Journal of the American Statistical Association, 62(318), 399–402. Retrieved from http://amstat.tandfonline.com/doi/abs/10.1080/01621459.1967.10482916

Malmstrom, C. M., Butterfield, H. S., Barber, C., Dieter, B., Harrison, R., Qi, J., … Wirka, J. (2009). Using Remote Sensing to Evaluate the Influence of Grassland Restoration Activities on Ecosystem Forage Provisioning Services. Restoration Ecology, 17(4), 526–538. http://doi.org/10.1111/j.1526-100X.2008.00411.x

Marsett, R. C., Qi, J., Heilman, P., Biedenbender, S. H., Watson, M. C., Amer, S., … Marsett, R. (2006). Remote Sensing for Grassland Management in the Arid Southwest. Rangeland Ecology & Management, 59(5), 530–540.

Masek, J. G., Vermote, E. F., Saleous, N. E., Wolfe, R., Hall, F. G., Huemmrich, K. F., … Lim, T. (2006). A Landsat Surface Reflectance Dataset. IEEE Geoscience and Remote Sensing Letters, 3(1), 68–72.

Mckeon, G., Day, K., Howden, S., Mott, J., Orr, D., Scattini, W., & Weston, E. (1990). Australian savannas : management for pastoral production. Journal of Biogeography, 17(4/5), 355–372.

McNairn, H., & Protz, R. (1993). Mapping Corn Residue Cover on Agricultural Fields in Oxford County, Ontario, Using Thematic Mapper. Canadian Journal of Remote Sensing, 19(2), 152–159.

Parsons, C. T., Momont, P. A., Delcurto, T., Mcinnis, M., Porath, L., & Marni, L. (2003). Cattle distribution patterns and vegetation use in mountain riparian areas. Journal Of Range Management, 56(4), 334–341.

Pineiro, G., Perelman, S., Guerschman, J. P., & Jose, P. M. (2008). How to evaluate models: Observed vs. predicted or predicted vs. observed? Ecological Modelling, 216, 316–322. http://doi.org/10.1016/j.ecolmodel.2008.05.006

Pyke, D., Herrick, J., Shaver, P., & Pellant, M. (2002). Rangeland health attributes and indicators for qualitative assessment. Journal of Range Management, 55(6), 584–597. http://doi.org/10.2307/4004002

R Development Core Team. (2016). R: A Language and Environment for Statistical Computing. R Foundation for Statistical Computing Vienna Austria, 0, {ISBN} 3-900051-07-0. http://doi.org/10.1038/sj.hdy.6800737

Renier, C., Waldner, F., Jacques, D. C., Babah Ebbe, M. A., Cressman, K., & Defourny, P. (2015). A dynamic vegetation senescence indicator for near-real-time desert locust habitat monitoring with MODIS. Remote Sensing, 7(6), 7545–7570. http://doi.org/10.3390/rs70607545

Roberts, D. A., Smith, M. O., & Adams, J. B. (1993). Green vegetation, nonphotosynthetic vegetation, and soils in AVIRIS data. Remote Sensing of Environment, 44(2–3), 255–269. http://doi.org/10.1016/0034-4257(93)90020-X

Rodríguez-caballero, E., Knerr, T., & Weber, B. (2015). Remote Sensing of Environment Importance of biocrusts in dryland monitoring using spectral indices. Remote Sensing of Environment, 170, 32–39. http://doi.org/10.1016/j.rse.2015.08.034

Roy D. P., Kovalskyy, V., Zhang, H. K., Vermote, E. F., Yan, L., Kumar, S. S., & Egorov, A. (2015). Characterization of Landsat-7 to Landsat-8 reflective wavelength and normalized difference vegetation index continuity. Remote Sensing of Environment, 0–13. http://doi.org/10.1016/j.rse.2015.12.024

Sayre, N. F., deBuys, W., Bestelmeyer, B. T., & Havstad, K. M. (2012). "The Range Problem" After a Century of Rangeland Science: New Research Themes for Altered Landscapes. Rangeland Ecology and Management, 65(6), 545–552. http://doi.org/10.2111/REM-D-11-00113.1

Sayre, N. F., McAllister, R. R., Bestelmeyer, B. T., Moritz, M., & Turner, M. D. (2013). Earth Stewardship of rangelands: Coping with ecological, economic, and political marginality. Frontiers in Ecology and the Environment, 11(7), 348–354. http://doi.org/10.1890/120333

Schmalz, H. (2011). Soil Spatial Heterogeneity and Measured Soil Responses: Factors in an Ecological Grazing Experiment on a Bunchgrass Prairie.

Stafford Smith, D. M., McKeon, G. M., Watson, I. W., Henry, B. K., Stone, G. S., Hall, W. B., & Howden, S. M. (2007). Learning from episodes of degradation and recovery in variable Australian rangelands. Proceedings of the National Academy of Sciences of the United States of America, 104(52), 20690–20695. http://doi.org/10.1073/pnas.0704837104

Sullins, M. J., Theobald, D. T., Jones, J. R., Burgess., L. M., Knight, R. L., Gilgert, W. C., & Marston, E. (2002). Lay of the Land: In Ranching west of the 100th meridian: culture, ecology, and economics. Washington, DC : Island Press,.

Svoray, T., Perevolotsky, A., & Atkinson, P. M. (2013). Ecological sustainability in rangelands: the contribution of remote sensing. International Journal of Remote Sensing, 34(17), 6216–6242. http://doi.org/10.1080/01431161.2013.793867

Thomas, L. (2017). R package. "Leaps": Regression Subset Selection., 8.

Todd, S. W., Hoffer, R. M., & Milchunas, D. G. (1998). Biomass estimation on grazed and ungrazed rangelands using spectral indices. International Journal of Remote Sensing, 19(3), 427–438. Retrieved from http://www.tandfonline.com/doi/abs/10.1080/014311698216071

Tucker, C. (1980). Remote sensing of leaf water content in the near infrared. Remote Sensing of Environment, 10(1), 23–32. Retrieved from http://www.sciencedirect.com/science/article/pii/0034425780900966

Van Leeuwen, W. J. D., & Huete, A. R. (1996). Effects of standing litter on the biophysical interpretation of plant canopies with spectral indices. Remote Sensing of Environment, 55(2), 123–138. http://doi.org/10.1016/0034-4257(95)00198-0

Vermote, E., Justice, C., Claverie, M., & Franch, B. (2016). Preliminary analysis of the performance of the Landsat 8/OLI land surface reflectance product. Remote Sensing of Environment. http://doi.org/10.1016/j.rse.2016.04.008

Vescovo, L., & Gianelle, D. (2008). Using the MIR bands in vegetation indices for the estimation of grassland biophysical parameters from satellite remote sensing in the Alps region of Trentino (Italy). Advances in Space Research, 41(11), 1764–1772. http://doi.org/10.1016/j.asr.2007.07.043

Wang, L., Zhou, X., Zhu, X., Dong, Z., & Guo, W. (2016). Estimation of biomass in wheat using random forest regression algorithm and remote sensing data. The Crop Journal, 4(3), 212–219. http://doi.org/10.1016/j.cj.2016.01.008

Washington-Allen, R. A., West, N. E., Ramsey, R. D., & Efroymson, R. A. (2006). A Protocol for Retrospective Remote Sensing – Based Ecological Monitoring of. Rangeland Ecology & Management, 59(1), 19–29.

Weltz, M. A., Dunn, G., Reeder, J., & Frasier, G. (2003). Ecological Sustainability of Rangelands. Arid Land Research and Management, 369–388. http://doi.org/10.1080/15324980390229292

West, N. E. (2003). History of Rangeland Monitoring in the U . S . A . Arid Land Research and Management, 17(4), 495–545. http://doi.org/10.1080/15324980390225584

Xu, D., Guo, X., Li, Z., Yang, X., & Yin, H. (2014). Measuring the dead component of mixed grassland with Landsat imagery. Remote Sensing of Environment, 142, 33–43. http://doi.org/10.1016/j.rse.2013.11.017

Yang, S., Feng, Q., Liang, T., Liu, B., Zhang, W., & Xie, H. (2018). Modeling grassland above-ground biomass based on artificial neural network and remote sensing in the Three-River Headwaters Region. Remote Sensing of Environment, 204, 448–455. http://doi.org/10.1016/j.rse.2017.10.011

Zheng, B., Campbell, J. B., Serbin, G., & Daughtry, C. S. T. (2013). Multitemporal remote sensing of crop residue cover and tillage practices: A validation of the minNDTI strategy in the United States. Journal of Soil and Water Conservation, 68(2), 120–131. http://doi.org/10.2489/jswc.68.2.120

Zhu, Z., & Woodcock, C. E. (2012). Object-based cloud and cloud shadow detection in Landsat imagery. Remote Sensing of Environment, 118, 83–94. http://doi.org/10.1016/j.rse.2011.10.028

# Chapter 3. Using airborne lidar to estimate above-ground grassland biomass and the effects of grazing and pixel size on spatial heterogeneity in a native bunchgrass ecosystem


## Abstract

The ability to quantify and monitor spatial heterogeneity in grasslands at landscape scales is necessary to identify and promote processes that increase habitat- and bio- diversity. However, quantifying above ground biomass over large areas at high spatial resolutions in short-statured grassland systems is challenging. In this study we use airborne lidar to create high resolution maps of aboveground biomass in a bunchgrass prairie. We then analyze these maps to determine how grazing impacts semivariogram-derived measures of spatial heterogeneity across 23 pasture areas. We also explore how these measures of heterogeneity change with increasing grid cell size to determine suitable resolutions for monitoring the impact of grazing on vegetation heterogeneity over time. Using lidar-derived data, we trained a Random Forest model to predict grassland aboveground biomass across our study area at a spatial resolution of 1.0668 m (3.5ft) (pseudo $R^2$=0.59, RMSD=139.4 g/$m^{-2}$). When aggregating this biomass data to coarser cell sizes, we observed that semivariogram models produced statistically different measures of heterogeneity at an alpha level of 0.05. The range statistic (a proxy for patch size) was the only pasture-level semivariogram metric sensitive to grazing, and this relationship was only significant when using high-resolution data (1m to 8m cell size). This study demonstrates the applicability of lidar data for quantifying short-statured grassland biomass. This research also successfully quantifies spatial heterogeneity at management scales and determines that within this Pacific Northwest bunchgrass prairie, grazing at low to moderate rates decreases spatial heterogeneity of vegetation biomass.


## 1.0 Introduction

Natural grassland ecosystems are subject to drivers of environmental change such as grazing and drought, which impact the conservation of critical species (Fleischner, 1994), annual forage production (Augustine & Mcnaughton, 1998), proper ecosystem function (Allen-Diaz, Chapin, Diaz, M. Howden, & Smith, 1995), and carbon storage (McSherry & Ritchie, 2013). However, relationships and feedbacks between drivers and outcomes of interest are relatively poorly understood (Herrick et al., 2010). Scientists and stakeholders

interested in monitoring how grassland system respond to environmental drivers have called for more research to study vegetation patterns and processes at larger spatial and temporal scales that align with land management practices (Bestelmeyer & Briske, 2012; Sayre, deBuys, Bestelmeyer, & Havstad, 2012; Sayre, McAllister, Bestelmeyer, Moritz, & Turner, 2013). This is due, in part, to the increasing need to quantify and monitor ecosystem services beyond livestock forage, and promote processes that increase vegetation heterogeneity given its positive link to biological diversity (Adler, Raff, & Lauenroth, 2001; Fuhlendorf & Engle, David, 2001; Fuhlendorf, Engle, Elmore, Limb, & Bidwell, 2012). Management practices such as grazing can have positive or negative impacts on various parameters of vegetation heterogeneity such as species composition, structure and biomass (Adler et al., 2001; Fuhlendorf & Engle, David, 2001), but few grassland studies quantify the effect of grazing on vegetation heterogeneity spatially (Adler et al., 2001; Bestelmeyer & Briske, 2012) and fewer still, quantify vegetation heterogeneity spatially using remotely sensed data (Virk & Mitchell, 2015).

We focus on quantifying the spatial heterogeneity of above ground biomass, because it can be monitored with remotely sensed data (e.g. Jansen et al., 2018, 2016; Todd et al., 1998) and it is correlated to measures of vegetation structure in grassland systems (e.g. Heady, 1957; Robel et al., 1970). To quantify spatial heterogeneity of vegetation biomass and how this pattern is impacted by grazing, two issues need to be addressed initially: 1) quantifying biomass accurately across the landscape and 2) determining the spatial resolution at which to quantify heterogeneity. Using field plot measures to accurately assess grassland vegetation metrics at landscape scales has proven difficult. The cost, time, and observer bias associated with field data collection and the need to monitor vegetation across large areas has led researchers to turn to remotely sensed data to provide estimates of grassland metrics such as cover or biomass (Booth & Tueller, 2003; Guerschman et al., 2015). While a variety of remotely sensed datasets and analysis methodologies have produced accurate measures of grassland vegetation that can be used for monitoring (Jacques, Kergoat, Hiernaux, Mougin, & Defourny, 2014; Jansen et al., 2018; Marsett et al., 2006) providing heterogeneity measures with gridded remotely sensed data is challenging due to the interaction between the scale of the imagery with the underlying physical or biologic pattern in question (Karl & Maurer, 2010). The ability to quantify patterns that are used to infer how an ecological process is

impacting the landscape is tied to the grain size (i.e. the grid cell size or pixel size) and extent of the study (Wiens, 1989). These relationships in turn impact the choice of resolution (or sensor) to use for analysis, as well as the analysis results (Lechner, Stein, Jones, & Ferwerda, 2009; Woodcock & Strahler, 1987).

Similarly, there is a need to identify what metric of spatial heterogeneity is appropriate to the ecological process of interest. Spatial heterogeneity can be quantified using a variety of metrics, including non-spatially dependent measures like the coefficient of variation, which provides a measure of variability over an area or distance (Adler et al., 2001), and spatially dependent measures produced using categorical maps, such as fractals, contagion, evenness, and patchiness (Li & Reynolds, 1994). Geo- or spatial- statistics provide another way to quantify spatial heterogeneity in continuous numerical data, producing measures of spatial dependence and spatial pattern (Adler et al., 2001). Spatial statistics such as Moran's I (Moran, 1950), the Getis-Ord general G statistic (Getis & Ord, 1992), semivariograms (Cohen, Spies, & Bradshaw, 1990; Matheron, 1971) and correlograms have all been used to provide spatial metrics of gridded remotely sensed data and explore how grazing affects vegetation heterogeneity (e.g., Sankey, Sankey, Weber, & Montagne, 2009; Virk & Mitchell, 2015). In this study, we focus on measures of spatial heterogeneity that quantify spatial patterns of continuous numerical data on above ground biomass.

Landscape-scale studies using remotely sensed data to quantify grassland spatial heterogeneity in relation to grazing have been conducted primarily with moderate-resolution passive sensors, including 10 m Sentinel-2 data (Scarth and Trevithick, 2017), 30m Landsat data (Virk & Mitchell 2015), and 20m data from Satellite Pour I'Observation de la Terre (SPOT) (Sankey et al., 2009). These previous studies provide spatial heterogeneity metrics for their respective ecosystems, but they do not explore the sensitivity of the reported spatial heterogeneity to the spatial resolution of the remotely sensed data. They are also limited by the use of passive sensors, which lack the ability to directly quantify vegetation structure or height. In contrast to passive sensors, active sensors such as lidar can more accurately assess vegetation structure, types, and biomass by providing 3-dimensional data as well as return intensity data on vegetation and surfaces (Eitel, Höfle, et al., 2016; Hudak, Evans, & Smith, 2009). Lidar is commonly used to map forested ecosystems and is increasingly being used to map small-statured vegetation communities such as arctic tundra (Greaves et al., 2016), salt

marsh habitat (Kulawardhana, Popescu, & Feagin, 2014), and the sage-brush steppe (Glenn et al., 2015; Li et al., 2017) yet research to-date in grassland systems is limited. This is potentially due to known limitations of lidar when estimating small-statured vegetation metrics, such as the negative impact of dense vegetation on lidar pulse penetration to the soil surface (Kulawardhana et al., 2014), or missing the highest portion of the plant material due to the sampling density of the lidar point cloud (Greaves et al., 2016).

Recent research suggests that despite these limitations, structural vegetation metrics such as biomass and height can be reliably measured with lidar in low-stature ecosystems (Greaves et al., 2015, 2016; Kulawardhana et al., 2014). Within grassland systems, vegetation metrics at plot scales have been quantified using ground based terrestrial laser scanners (TLS) (Cooper, Roy, Schaaf, & Paynter, 2017; Eitel, Magney, Vierling, Brown, & Huggins, 2014) or vehicle-mounted lidar systems (Radtke, Boland, & Scaglia, 2010; Schaefer & Lamb, 2016). Discrete return lidar collected with an unmanned aerial vehicle (UAV) has also demonstrated statistically significant relationships between lidar metrics and field estimates of canopy heights, cover and biomass in grasslands (Wang et al., 2017). Full waveform lidar collected during leaf-on and leaf-off dates has been used to classify grassland habitat (Zlinszky et al., 2014), as well as to provide variables for conservation objectives (Zlinszky, Deák, Kania, Schroiff, & Pfeifer, 2015), but rarely has airborne lidar collected with a plane been used to quantify biomass and vertical structure in natural grassland systems.

Because lidar can provide accurate fine-scale measures of vegetation biomass or structure, it can also facilitate an exploration of how grain (i.e. pixel or grid cell) size impacts the quantification of vegetation heterogeneity, as the raw point cloud data can be aggregated to increasingly coarser grid cell sizes (Eitel, Magney, Vierling, Greaves, & Zheng, 2016). It is ideal for remote sensing and ecological studies to quantify phenomena across varying grain sizes and spatial extents to provide a more complete understanding of how the process and pattern is impacted by the scales chosen for inquiry (e.g. Woodcock and Strahler, 1987), but cost, logistics and technology are often real-world barriers. The selection of remotely sensed data for analysis should be based on a knowledge of the system (i.e., the scene model; Woodcock and Strahler, 1987), cost, the objectives of the study, and the scale at which subsequent management action happens (Phinn, Stow, Franklin, Mertes, & Michaelsen, 2003; Wiens et al., 2009). The underlying assumption in selecting one cell size or sensor to quantify

spatial heterogeneity is that the resolution of the spectral data is higher than or equal to the scale of the heterogeneity of the ecological object or pattern in question; however, in most cases the ideal spatial resolution is unknown (Johansen, Coops, Gergel, & Stange, 2007). While costly airborne lidar data is impractical for monitoring grassland biomass or heterogeneity with repeat acquisitions, it can be used to assess at what spatial scale critical patterns of spatial heterogeneity are no longer detectable, thus answering the question of whether more affordable (but coarser-resolution) passive reflectance sensors can accurately quantify patterns of spatial heterogeneity in grassland biomes.

Our research objectives for this study were to 1) accurately model bunchgrass vegetation biomass from airborne lidar data using vegetation canopy, intensity and topographic metrics, 2) determine the impact increasing spatial resolution has on measures of spatial heterogeneity and 3) identify the measures of spatial heterogeneity most sensitive to grazing intensity and how this sensitivity changes with increasing spatial resolution of remotely sensed data.

## 2.0 Methods

### 2.1 Study area:

The Zumwalt Prairie is a Pacific Northwest Bunchgrass Prairie (PNWBP) habitat located in northeast Oregon (Figure 3.1). The PNWBP is a highly threatened and understudied temperate grassland ecosystem (Kimoto, DeBano, & Thorp, 2012; Tisdale, 1982) dominated by C3 bunchgrass species, including Idaho fescue (*Festuca idahoensis* Elmer), bluebunch wheatgrass (*Pseudoroegneria spicata* (Pursh) A. Love) and Sandberg's bluegrass (*Poa secunda* J Presl) which may be especially vulnerable to harmful effects of poorly managed grazing compared to other grassland systems (Adler, Milchunas, Lauenroth, Sala, & Burke, 2004; Mack, 1983; McLean & Tisdale, 1972). Elevations across the study area range from 1000 meters to 1600 meters. Average summer (June – August) temperatures range from 11.8 – 17.5˚C, with average annual precipitation of 348.3 mm (2006-2012 Zumwalt Weather Station).

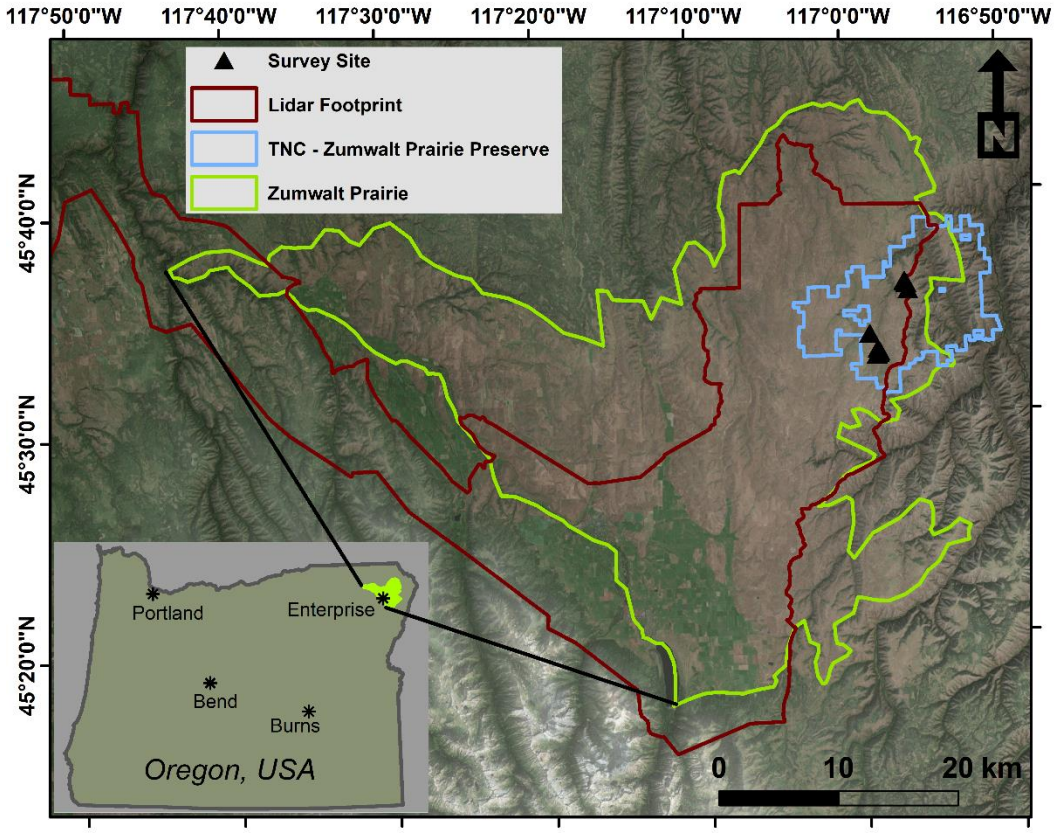


Figure 3.1. The Zumwalt Prairie study area showing the intersection between the lidar footprint of the Zumwalt Prairie Grassland habitat, and the Zumwalt Prairie Preserve. The locations of where in-field data were collected are also shown with black triangles.

## 2.2 Data

### 2.2.1. Field data

We collected data on above ground vegetation biomass, height, and foliar cover within 65 1m$^2$-quadrats on The Nature Conservancy's Zumwalt Prairie Preserve property on July 10$^{th}$ through the 14$^{th}$, directly after the lidar flight. This sampling period was selected to correspond with peak biomass and a time when the majority of the perennial grasses and forbs are still photosynthetically active. Quadrats were selected subjectively in the field to represent a gradient of vegetation amounts (e.g., Greaves et al., 2016). Vegetation cover and height data were estimated across 36 evenly distributed points within each 1 m$^2$-quadrat using a grid-point intercept approach following Godínez-Alvarez, Herrick, Mattocks, Toledo, & Van Zee, 2009. Above ground biomass data were collected by harvesting all standing vegetation within the quadrat. All clipped vegetation was bagged in the field and oven dried at 60° C to obtain a

dry weight for analysis. The center XY location of each quadrat was obtained using a TopCon GR-3 survey grade GPS system (nominal horizontal accuracy ~4 cm) running in Real Time Kinematic (RTK) mode using the same vertical and horizontal datum as the airborne lidar data.

Stocking rate data were calculated by pasture based on records provided by the land managers across the study area. Stocking rates are expressed as Animal Unit Months per hectare (AUM $ha^{-1}$). Adjustments in the stocking rates (AUM $ha^{-1}$) were calculated using animal use equivalencies (AUE) for the different type of livestock type (e.g. bulls had 1.2 AUE, yearlings 0.75 AUE, and cow-calf pairs 1.0 AUE).

2.2.2. Lidar data

Airborne lidar data were collected by Quantum Spatial on July 4$^{th}$ - July 10$^{th}$, 2015 using a Leica ALS70. Flying at an average altitude of 1400m, discrete return lidar data were acquired averaging 9.29 points per square meter with a fundamental non-vegetated vertical accuracy of 7.3 cm (average vertical accuracy = -1.3 cm), a horizontal accuracy of less than 5.5 cm, and an average pulse footprint diameter of 32 cm (Quantum Spatial Technical Report). The vendor provided point cloud and laser return intensity (1064 nm wavelength) raster data in the Oregon Statewide Lambert projection with a horizontal datum of NAD83 (2011) and a vertical datum NAVD88 (Geoid12A). We processed the lidar data in its native projection to match the vendor data and end user needs. There was high variability in pulse densities at the 1m scale across the study area which biased the data (Figure A2.1); therefore, we resampled the point cloud to create an even point density for biomass mapping using CloudCompare software (CloudCompare v2.6.2 2017). To do this, we fit a Delaunay 2.5D best fitting plane to the vendor provided point data, then sampled this plane to the chosen density of 0.85 points per square foot (9.15 points per square meter). This step was performed because initial analysis using the raw lidar point clouds produced maps with notable striping (see discussion for more detail, and Figure A2.1).

**2.3 Variable creation from lidar data**

2.3.1 Lidar-derived volume metric

Following Greaves et al., (2015) and (2016), we created a canopy volume raster using an optimization algorithm that produces a set of gridded ground and canopy surfaces based on

user-defined parameters (Eitel et al., 2014; Greaves et al., 2015). The ground rasters are built using double pass filter selecting the lowest lidar return within the specified grid cell on the first pass, and is further refined by searching a neighborhood for a lower surrounding point, if found, that grid cell gets the new lowest point value (i.e. the height (z) value) (Greaves et al., 2016). The canopy rasters are built by selecting the highest laser return in each grid cell for each of the specified raster resolutions. The optimization parameters are based on the grid cell size of the ground and canopy surfaces, the nearest neighbor search radius, as well as the grid cell size for the final calculation (See Greaves et al., 2015 for a detailed explanation). For this study, we created and searched a set of grids with cell sizes ranging from 15.24 cm (0.5 ft) to 121.94 cm (4 ft) at an increasing 15.24 cm (0.5 feet) interval for the ground, canopy, and final raster resolution. The nearest neighbor search parameter ranged from 4 to 20 neighbors and increased by increments of 4. In total we searched 2,560 possible parameter combinations and selected the grid set and neighborhood size that minimized the root mean square error using leave-one-out cross validation (LOOCV) with the training dataset (N=45) following (Greaves et al., 2016). We further evaluated the model with a test set (N=20) to verify the strength of the relationship. We then aggregated the canopy volume raster data to 1.0668 m (3.5 ft) grid cell size to best match the size of the field plots (1 m).

### 2.3.2. Canopy lidar metrics

Using the ground points generated during creation of the canopy volume metric, we normalized the point cloud to compute a set of common lidar metrics at the 1.0668 m (3.5 ft) scale. Using all the points greater than 2 cm height we computed the minimum, maximum, mean, standard deviation, and 25th and 75th percentiles of heights. We also computed total return and canopy density (Table 3.1).

### 2.3.3. Intensity data

Zonal means of the vendor-provided 0.3048 m (1ft) intensity data were computed for each $1m^2$ field vegetation quadrat. We computed the mean and max intensity for each of the 65 quadrats (Table 3.1, dataset: Intensity). The vendor performed minimal normalization accounting for the pulse distance, angle and channel-balancing using a propriety approach (pers. Com. with Quantum Spatial).

2.3.4. Lidar derived topographic metrics

Using the ground surface rasters obtained from the canopy volume creation, we created several topographic metrics at the 1.0668 m scale, including slope, aspect, curvature and the SAGA wetness index (Boehner et al., 2002) (Table 3.1). These variables, associated with topography, were included due to their potential influence on soil moisture, vegetation production (Gessler, Chadwick, Chamran, Althouse, & Holmes, 2000) and vegetation type (Fu, Liu, Ma, & Zhu, 2004) (Table 3.1, dataset: Topographic).

Table 3.1. Lidar-derived variables used to model aboveground biomass.

| Data Type | Variable | Details |
|---|---|---|
| Canopy | Vol | Canopy volume (Greaves et al., 2015, 2016) |
| Canopy | H_Mean | Average height |
| Canopy | H_Std | Standard deviation of height |
| Canopy | H_Max | Max height |
| Canopy | Tot_Returns | Number of all lidar returns |
| Canopy | Canopy_Dns | Points above 2 cm divided by all returns |
| Intensity | Int_Mean | Mean of vendor 0.3048 cm (1 ft) intensity raster |
| Intensity | Int_Max | Max of vendor 0.3048 cm (1 ft) intensity raster |
| Topographic | SWI | Saga Wetness Index SAGA GIS |
| Topographic | Slope | ArcMap Spatial Analyst Package |
| Topographic | Aspect | ArcMap Spatial Analyst Package |
| Topographic | Curve | ArcMap Spatial Analyst Package |

## 2.3 Model creation using Random Forests

Following methods described in Greaves et. al, 2016, we used Random Forests (Breiman, 2001) implemented in the randomForest package (Liaw & Wiener, 2002) in R (R Development Core Team, 2016) to determine what predictors most accurately estimated biomass. When run in regression mode, Random Forest provides model estimates by averaging the predictions across many decision trees, which are constructed based on a

random selection of the input data, as well as a random selection of the predictor variable used at each splitting node (Breiman, 2001). We tested seven different predictor sets to model biomass: 1) canopy, 2) topographic (topo), 3) intensity, 4) canopy + topo, 5) canopy + intensity, 6) intensity + topo, and 7) canopy + intensity + topo. To reduce the possibility of overfitting the models, for each predictor set we removed the highly correlated predictor variables (Spearman's rank $r > 0.90$). To further limit the predictor variables within each of the seven sets of predictor sets, we ran the model selection tool in the rfutilities package (Murphy, Evans, & Storfer, 2010) 1000 times and only included the variables which were selected in the majority (i.e. greater than 500) of model runs for subsequent Random Forest modelling. The best Random Forest models generated from each predictor set were then compared using the Random Forest pseudo $R^2$ , as well as the r-squared values between the predicted and observed estimates and the associated root mean squared difference (RMSD) metrics (Pineiro, Perelman, Guerschman, & Jose, 2008).

**2.4 Biomass mapping and summary statistics at the pasture scale**

Using the Random Forest model that minimized the RMSD, we employed the AsciiGridPredict Tool in the R package 'yaImpute' (Crookston & Finley, 2008) to predict biomass at 1.0668m scale across the study area. To analyze how grazing affects vegetation aboveground biomass, we then selected pastures within the study area that consisted primarily of upland prairie grassland habitat and were grazed before the lidar flight or were un-grazed for more than two years prior to the lidar acquisition. This selection criteria produced 23 unique pastures with an average size of 125 hectares (ha) (min=40 ha, max=745 ha) for further analysis, 8 of which had no recorded livestock grazing and 15 that had an average stocking rate of 0.80 Animal Unit Months (AUMs) per hectare (ha), with a minimum stocking rate of 0.39 AUMs/ha and a maximum stocking rate of 1.718 AUMs/ha. To remove the impact of non-grassland habitat and other objects on our results, we masked out the non-grassland habitat, human made structures, and stock ponds, and buffered all fences and roads across the analyzed pastures. Next, we computed summary statistics on the estimated biomass within each pasture, including the mean, the $10^{th}$, $25^{th}$, $50^{th}$, $75^{th}$, and $90^{th}$ percentiles, the standard deviation, and the coefficient of variation (CV).

## 2.5 Variogram modeling at different spatial resolutions

2.5.1 Upscaling the biomass raster to coarser scales:

To provide biomass estimates at varying resolutions, we aggregated the 1.0668 m masked biomass rasters for each pasture area to coarser spatial resolutions (i.e., grid cell sizes): 3 m, 5 m, 8 m, 20 m, and 30 m. We kept the geographic extent of the analysis areas fixed and consistent with the pasture areas, as this is the size related to grazing management. To do this, we re-projected the 1.0668 m biomass data from the NAD1983 2011 Oregon Statewide Lambert International Feet to WGS1984 UTM Zone 11. Next, we resampled the 1.0668 m data to 1 m using the bilinear approach and then aggregated by averaging the 1m data to the five coarser spatial scales. The coarser-scale spatial resolutions were selected to align with currently available short-wave infrared data from sensors such as WorldView-3 (4 to 8 m), Sentinel-2 (20 m), and Landsat (30 m) that have been shown to be useful in quantifying grassland vegetation in this system (V. Jansen et al., 2018; V. S. Jansen et al., 2016).

2.5.2 Semivariogram stats

The above ground biomass raster data for each pasture and scale were used to compute semivariograms to explore spatial measures of heterogeneity. The computation of the semivariogram takes the form:

$$\gamma(h) = \frac{1}{2n}\sum_{i=1}^{n} |z(s_i) - z(s_{i+h})|^2$$

Where $\gamma(h)$ is the semivariance for the distance bin h, z is the value of the biomass variable at two locations $s_i$ and $s_{i+h}$, with h signifying the distance between each pair and n is the number of pairs of sampling locations across each lag (or bin) h. For each pasture area we fit theoretical models consisting of the exponential, spherical, and linear form to the empirical semivariogram using the GSTAT package (Pebesma, 2004). We used the output from the exponential models for subsequent analysis, as these decreased error across the majority of pastures and resolutions. From the theoretical semivariograms the sill, nugget and range were computed. The sill refers to the point at which the variance no longer gets larger with increasing lag distances (variance beyond the range); the range is a measure of spatial dependence across distance, signifying the distance at which the variable in question is no

longer autocorrelated and provides an indicator of patch size (Townsend & Fuhlendorf, 2010). The nugget is the intercept along the y-axis representing variability or sampling error within the zero lag distance (Sadoti et al., 2014; Townsend and Fuhlendorf, 2010; Western et al., 1998; Fortin and Dale 2005). From the sill, nugget and range metrics we calculated the magnitude of spatial heterogeneity (MSH) (Lane & BassiriRad, 2005; Lin et al., 2010). The MSH is calculated by dividing the spatially structured variation (the sill minus the nugget) by the total sample variation (the sill) (Lane & BassiriRad, 2005). The MSH ranges in values from 0 to 1, with zero indicating no spatially structured heterogeneity and 1 indicating highly structured heterogeneity (Virk & Mitchell, 2015). We also calculated the nugget to sill ratio (nugget semivariance/total semivariance)*100 (Cambardella et al., 1994).

### 2.5.3 The effect of spatial resolution on measures of heterogeneity

To visualize how varying resolutions (grid cell size) influenced the measures of spatial heterogeneity (i.e. sill, nugget, range, etc.), we created boxplots for each semivariogram-derived metric by spatial resolution. To test which resolutions produced significantly different measures of heterogeneity, we computed pairwise Mann-Whitney U rank-sum tests between all possible pairs of grid cell sizes. We selected a non-parametric test because some of the semivariogram metrics at the varying grid sizes did not fit a gaussian distribution. We only performed the multiple comparison Mann-Whitney U tests when the semivariogram derived metric met the assumption of homogeneity of variance across all groups as tested with the Fligner-Killeen test. Statistically significant p-values were adjusted using the Bonferroni correction.

### 2.5.4 The effect of grazing on biomass statistics and measures of heterogeneity across varying resolutions

We explored the effect of grazing on pasture summary statistics and semivariogram-derived measures of heterogeneity using Spearman rank correlations, simple linear models and quadratic models. Because some initial linear models did not have normally distributed residuals, we transformed our predictor variables with log, reciprocal and square root transformations to determine whether these transformations helped in meeting the assumptions of a linear model. The effect of grazing was tested across each of the six resolutions separately and considered significant at the alpha level of 0.05.

## 3.0 Results

### 3.1 Field measured above ground biomass and vegetation height data

Across the 65 1m$^2$ quadrats sampled in 2015, the average field biomass was 268.9 g/m$^2$ with a range of 0 g/m$^2$ to 1213.9 g/m$^2$ (Table 3.2). The average mean height was 12.9 cm with a mean height range of 0 cm to 45.5 cm. The average max height across the 65 quadrats was 29.5 cm and ranged from 0 cm to 91 cm. Spearman rank correlations between biomass and the measures of vegetation structure (height mean and height max) were significant and strongly related (r-values greater than 0.80), with coefficients of determination ($r^2$) values greater than 0.70 (Figure 3.2).

Table 3.2. Summary statistics for field biomass and vegetation height data (N=65).

| Field Metric | Mean | Min | Max | 10th percentile | 90th percentile | SD |
|---|---|---|---|---|---|---|
| Above Ground Biomass | 268.9 | 0.0 | 1213.9 | 24.7 | 467.5 | 262.3 |
| Mean Height | 12.9 | 0.0 | 45.5 | 3.1 | 20. 8 | 9.6 |
| Max Height | 29.5 | 0.0 | 91.0 | 6.0 | 45.4 | 20.3 |

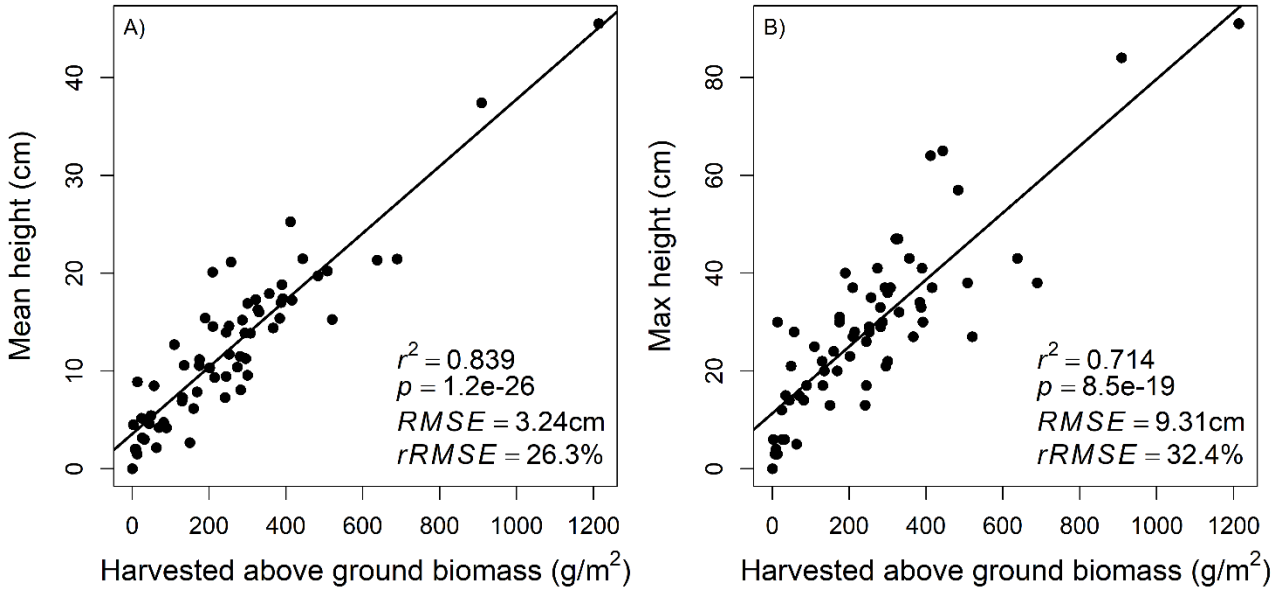


Figure 3.2. Linear relationships between harvest above ground biomass and mean vegetation height (a) and, harvested above ground field biomass and max field height (b) across the 65 one-meter field plots. The linear model coefficient of determination ($r^2$), p-value (p), root mean square error (RMSE) and relative root mean square error (rRMSE) are shown for each relationship.

## 3.2 Modeling grassland biomass with lidar data

### 3.2.1 Volume variable creation

Searching across all possible parameter combinations used to create the canopy volume metric (i.e., ground, canopy and output grid sizes and the nearest neighbor search windows) the optimal parameter set resulted in a 0.3048 m (1 ft) output grid size, a 0.4572 m (1.5 ft) canopy grid size, and a 0.4572 m (1.5 ft) ground grid size, using a 12 nearest neighborhood search window. The canopy volume metric was significantly related to the field biomass with the training data resulting in an $r^2$ of 0.67 and a RMSE of 116.6 g $m^{-2}$ (Figure 3.3A). We found similar results when predicting biomass with the testing set, which had an $r^2$ of 0.55 and a RMSD of 175.1 g $m^{-2}$ (Figure 3.3b). When dropping the quadrat that had an estimated aboveground biomass value over 1000 g/$m^2$ the relationship was still significant and RMSE remained similar (117.89 g/$m^2$) but the coefficient of determination value and p-value were reduced ($r^2$ = 0.29, p = 0.00012) compared to the original model. We elected to leave the in the large (> 1000 g/$m^2$) harvested above ground biomass sample although it inflates our $r^2$ value with the volume metric, due to it being a valid sample of an ecologically important grass species, basin wildrye (*Leymus cinereus (Scribn. & Merr. A. Love*), which provides important structure and forage for wildlife and livestock.

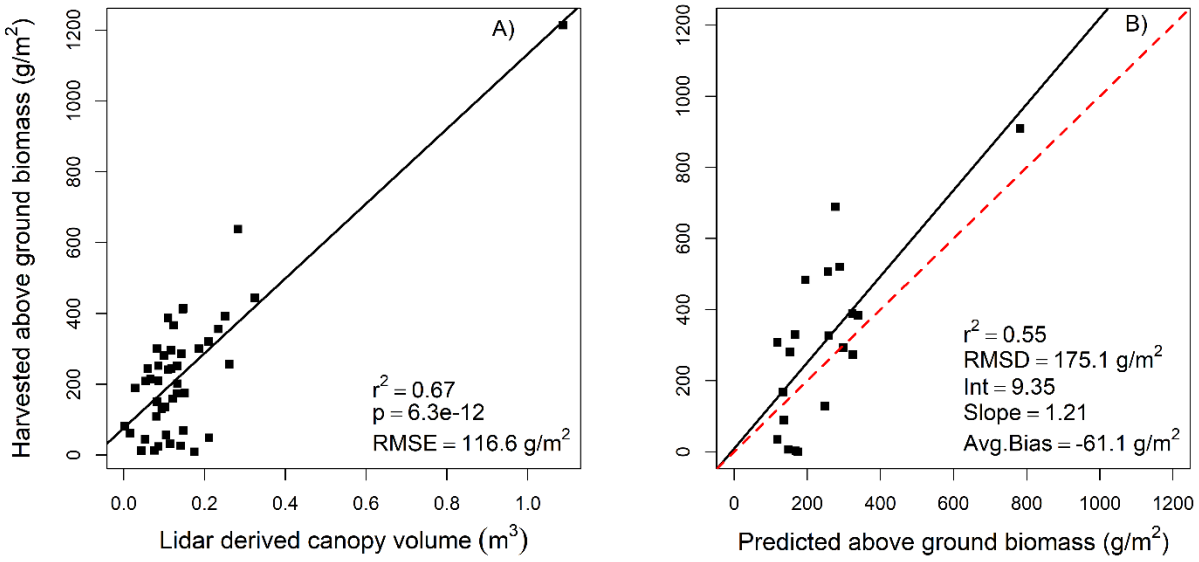


Figure 3.3. Grassland biomass canopy volume metric creation from airborne lidar A) Model for predicting in-field biomass from optimized lidar-derived canopy volume (training data) and B) Harvested biomass predicted from lidar-derived canopy volume (test data).

3.2.2 Random Forest modeling for above ground biomass estimates

Using the rfutilites model selection tool to determine what predictors in each predictor set were important (i.e., selected more than 50% of the time across the 1000 runs) revealed that only four of the seven final predictor sets had a unique set of selected variables (Table 3.3). For example, the Canopy + Intensity had the same selected variables as the Canopy + Topo + Intensity which included the variables: volume, max height and mean intensity. The selected predictors from the canopy only predictor set included the canopy volume metric, max height and canopy density. Slope was the only variable selected in the majority of model runs from the topographic predictor set. For the intensity predictor set, the mean and max intensity metrics were significantly correlated (spearman rank $r > 0.90$), therefore we included only the mean intensity metric for variable selection.

Table 3.3. Variable selection for Random Forest models. The numbers indicate how many times each variable was selected across 1000 Random Forest model runs using the model selection tool in the 'rfUtilities' package. Dashes represent variables not included in the model selection when testing each predictor set. The final Random Forest model for each predictor set only included predictors selected across more than 500 of the model runs. The bolded predictor sets are plotted in Figure 3.4.

| Variable | ***Canopy*** | ***Topo*** | ***Intensity*** | Canopy + Topo | ***Canopy* + *Intensity*** | Intensity + Topo | Canopy + Topo + Intensity |
|---|---|---|---|---|---|---|---|
| Vol | **1000** | - | - | 1000 | **1000** | - | 1000 |
| Tot_Returns | 0 | - | - | 0 | 0 | - | 0 |
| H_Max | **1000** | - | - | 1000 | **912** | - | 1000 |
| Canopy_Dns | **969** | - | - | 998 | 0 | - | 0 |
| SWI | - | 92 | - | 0 | - | 0 | 0 |
| Aspect | - | 0 | - | 0 | - | 0 | 0 |
| Slope | - | **1000** | - | 284 | - | 100 | 0 |
| Curve | - | 0 | - | 0 | - | 0 | 0 |
| Int_Mean | - | - | **1000** | - | **1000** | **1000** | 1000 |

When running Random Forest models across each unique predictor set, the Canopy + Intensity model outperformed all other predictor sets tested (Figure. 3.4). The pseudo $R^2$ was 0.59 with an observed versus predicted $R^2$ of 0.64, a RMSD of 139.4 $g/m^{-2}$, and a bias of -9.7 $g/m^{-2}$. The Canopy + Intensity model minimized the RMSD errors compared to the Canopy Only model by 34.8 $g/m^{-2}$ and by more than 80.0 $g/m^{-2}$ when compared to the Topo or Intensity only models. The Topo and Intensity models performed very poorly, having RMSD errors over 220 $g/m^2$.

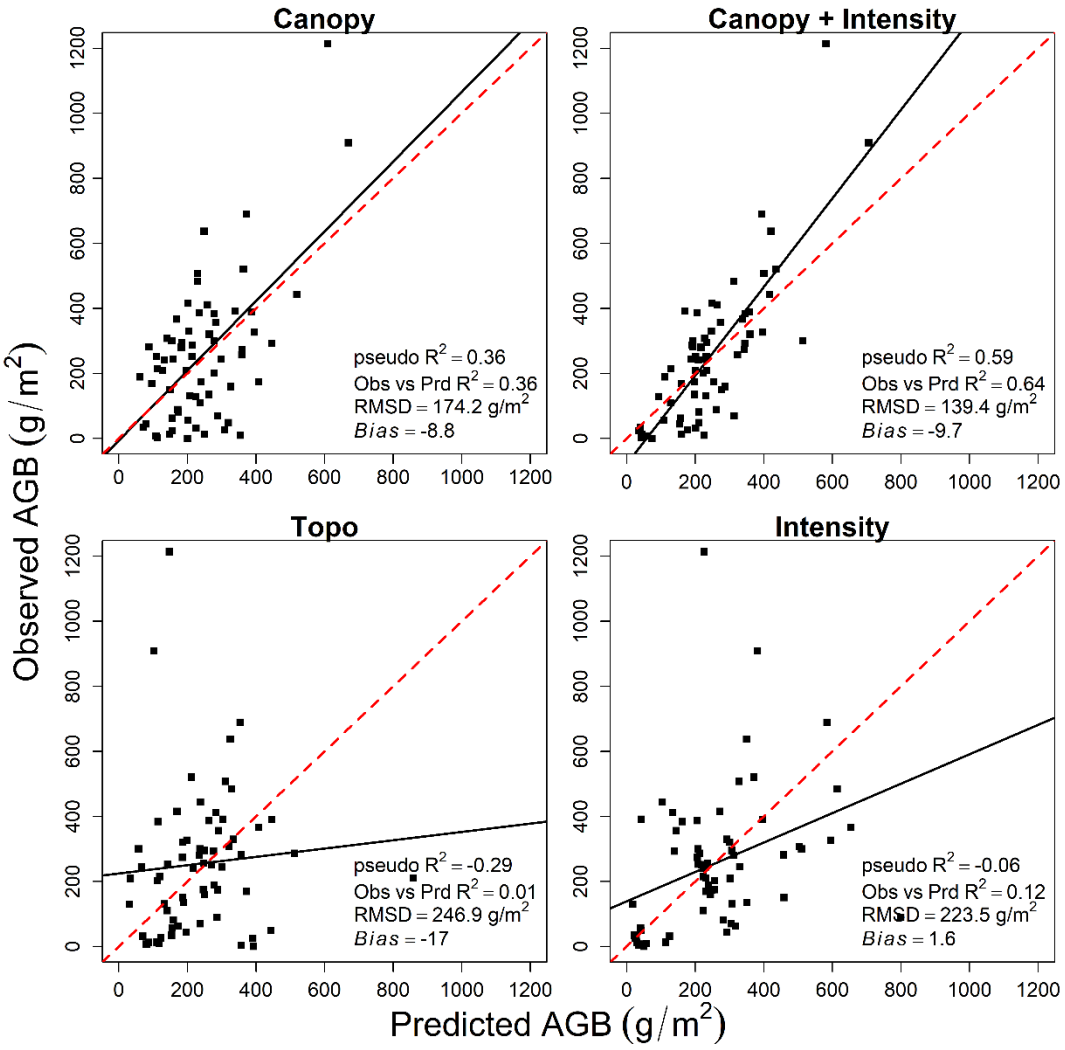


Figure 3.4. Random Forest model results across the four datasets that produced a unique set of predictor variables. See Table 3.3 for predictors used. The black lines represent the best fit line, while the dotted red line represents the one to one line.

### 3.2.3 Lidar-derived biomass maps

The biomass maps produced using the Canopy + Intensity model visually to correspond with landscape features and vegetation amounts across the study area, with shallow soil areas having low predicted biomass, and deeper soils and riparian areas having higher predicted biomass (Figure 3.5). For each pasture area (N=23), the average estimated biomass was 172.97 g/m$^{-2}$ and ranged from 117.40 g/m$^{-2}$ to 233.27 g/m$^{-2}$. The average 10$^{th}$ and 90$^{th}$ percentiles across all pasture areas varied with increasing cell size, with the finest resolution (1.0668m) data having the largest range between these two percentiles, and the coarsest resolution (30m) having the smallest range (Table 3.4).

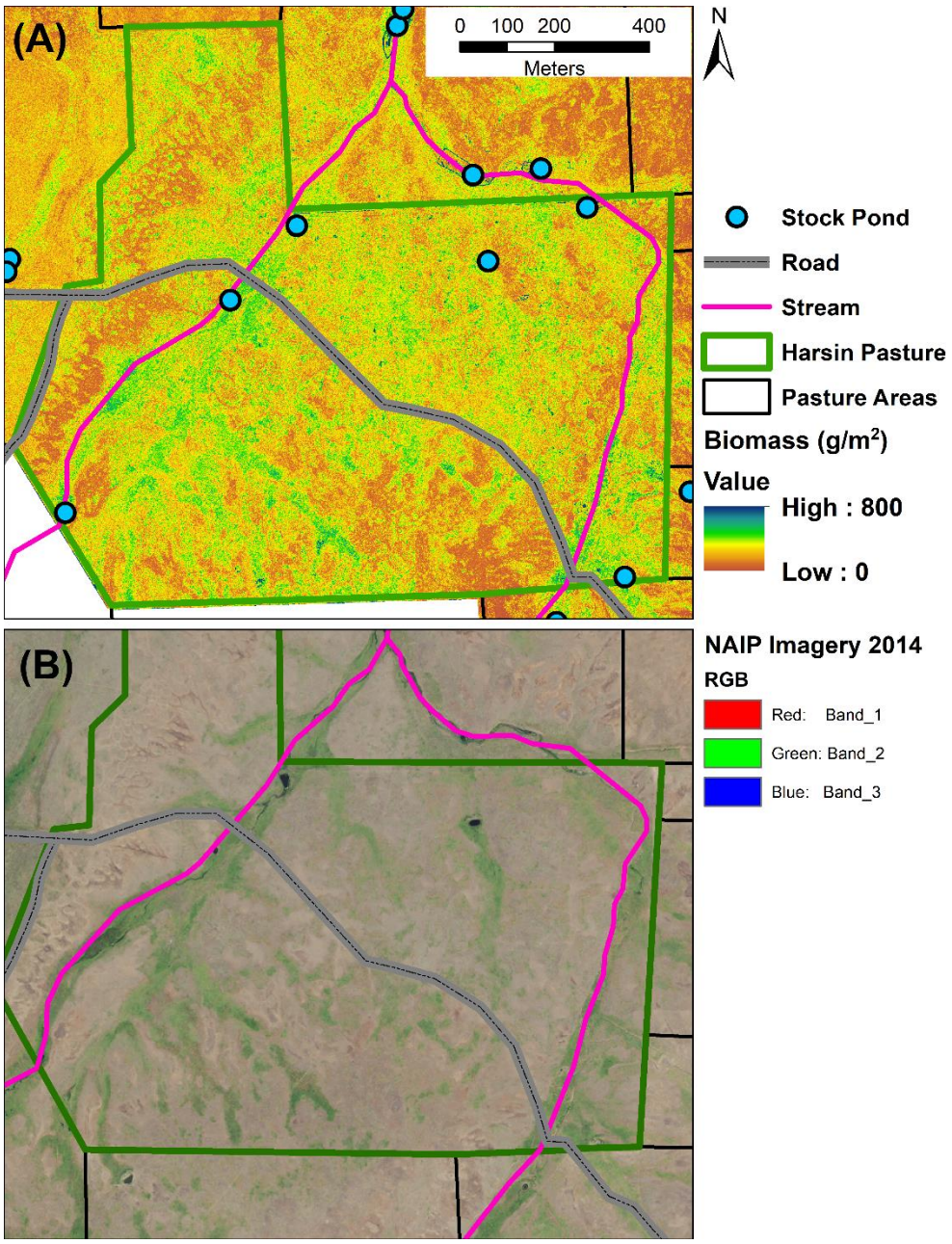


Figure 3.5. Lidar derived biomass map at the 1.0668m scale for the Harsin Pasture (A) along with 2014 NAIP imagery (B).

Table 3.4. Pasture-level modeled biomass summary statistics (N=23) across the varying grid cell sizes.

| Cell Size | Mean | Min | Max | 10th percentile | 90th percentile | CV |
|---|---|---|---|---|---|---|
| 1.0668 | 173.70 | 117.20 | 233.08 | 66.82 | 288.54 | 0.51 |
| 3 | 173.75 | 117.18 | 233.21 | 95.62 | 254.23 | 0.37 |
| 5 | 173.82 | 117.23 | 233.24 | 100.54 | 247.96 | 0.34 |
| 8 | 173.94 | 117.38 | 233.46 | 104.50 | 243.20 | 0.32 |
| 20 | 174.22 | 117.76 | 233.75 | 112.63 | 234.87 | 0.28 |
| 30 | 174.21 | 117.67 | 234.01 | 115.71 | 231.50 | 0.27 |

### 3.3 The effect of cell size on measures of spatial heterogeneity

The boxplots created for each of the semivariogram-derived metrics show observably different measures across the 6 grid cell sizes analyzed (Figure 3.6). Only the range and the sill met the assumption of homogeneity of variance needed for Mann-Whitney U rank-sum tests. Using the Mann-Whitney U test to compare the distributions of the range statistic between each grid cell size revealed that the 1.0668 m data was different from all other grid cell sizes. Significant differences were found across all other pairs except between the 3 m and 5 m, the 5 m and 8 m, and the 20 m and 30 m grid cell sizes (Figure 3.6, Table A2.3). The 1.0668 m sill metric was also statistically different from all other grid cell sizes. The sill metric at 3 m, 5 m and 8 m grid cell size were similar (i.e., no significant difference between these pairs) as were the 8m, 20m, and 30m grid cells sizes (Figure 3.6, Table A2.4).

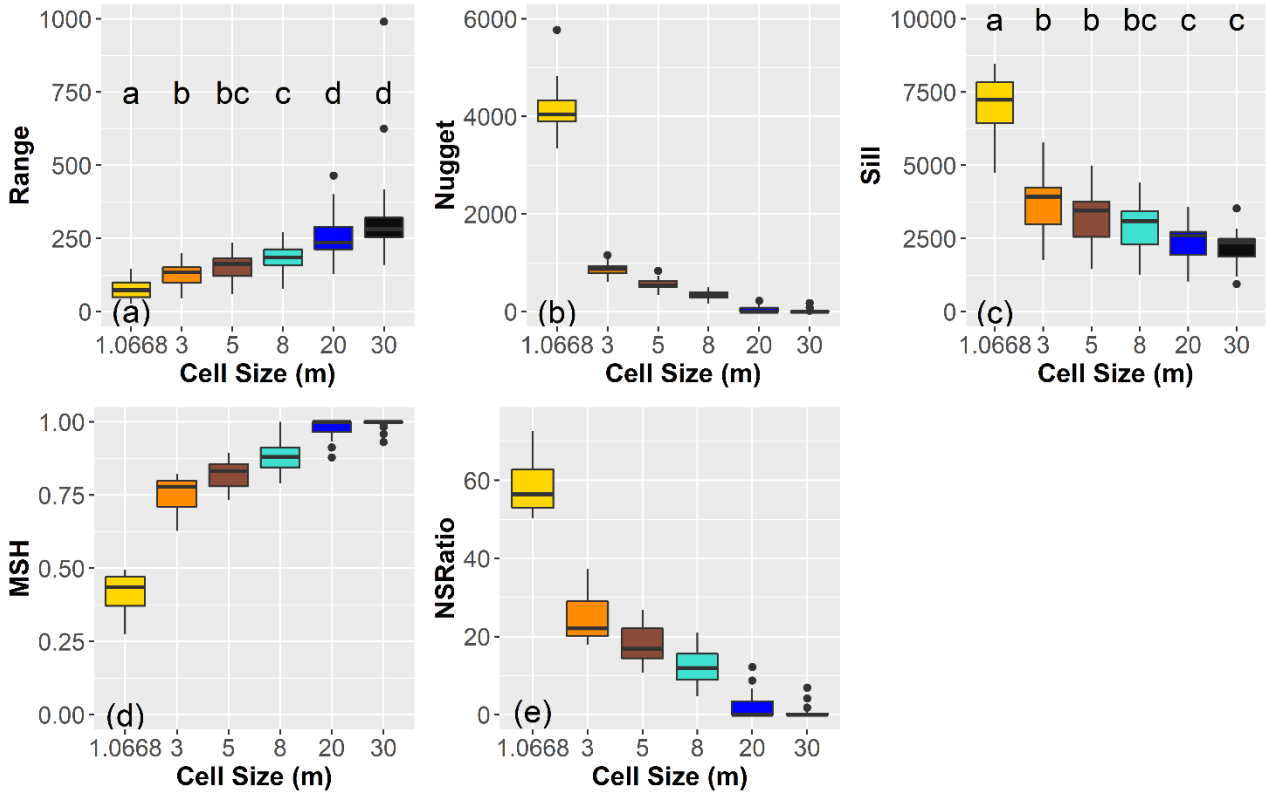


Figure 3.6. Boxplots of pasture-scale semivariogram metrics by cell size. The bold black lines in the middle of each colored box represent the median value (50$^{th}$ percentile), with the lower and upper limits of the box representing the 25$^{th}$ and 75$^{th}$ percentile respectively. The whiskers extend to the smallest and largest values falling within 1.5 times the associated value (lower value = 25$^{th}$ percentile, upper value = 75$^{th}$ percentile) of the interquartile range. The black dots represent outliers. Significant differences found between the cell sizes using the Mann-Whitney/Wilcoxon test for each semivariogram statistic that met the assumption of homogeneity of variance (Range and Sill) are indicated with different letters. Statistic Abbreviations are as follows: MSH = magnitude of spatial heterogeneity and NSRatio = nugget to sill ratio.

**3.4 Assessing the effects of grazing on pasture-scale biomass with summary and spatial statistics across the varying resolutions (grid cell sizes).**

The summary statistics were more sensitive to grazing than the semivariogram statistics (Table 3.5 and Table S1 (Spearman rank results)) using Spearman rank correlations, linear and quadratic models. In fact, the only semivariogram statistic sensitive to grazing was the range statistic, and this significant relationship was exclusively observed across the 1.0668 m to 8 m resolutions, using spearman rank, linear and quadratic models (Table 3.5, Table S1) with the 3 m resolution data having the highest $r^2$ value. The 75$^{th}$ percentile of biomass was significantly related to grazing intensity across all resolutions except the 1.0668 (Table 3.5)

when all pastures were included (N=23), and significant across all resolutions when we dropped the pasture with the greatest stocking rate (P5) due to its heavy influence on the summary statistic linear models (N=22). The pasture mean biomass statistic was found to be significantly correlated to stocking rates using the quadratic model and, also when using a linear model if the P5 pasture was dropped. The coefficient of variation was unique in that the only significant relationships were found with the quadratic models, and none with the linear models.

Table 3.5. Regression model results between pasture level summary and spatial statistics and stocking rate. The coefficients of determination values ($r^2$) that are significant at the 0.05 p-value are shown in bold with boxes around them. The italicized underlined values are models that violated assumptions of linear models. Statistic Abbreviations are as follows: Per10 = 10th Percentile, Per25 = 25th Percentile, Per75=75 Percentile, Per90 = 90th Percentile, CV=Coefficient of Variation, MSH = Magnitude of Spatial Heterogeneity, NSR = Nugget to Sill Ratio. The transform abbreviations are as follows: Recip = OLS using a reciprocal transformation on the predictor variable, None-OLR = one outlier was removed with no transformation performed on the data; Quad = Quadratic model was used.

| | | Grid Cell Size | | | | | |
|---|---|---|---|---|---|---|---|
| **Statistic** | **Transform** | **1.07m** | **3m** | **5m** | **8m** | **20m** | **30m** |
| Per10 | Recip | 0.04 | 0.05 | 0.05 | 0.06 | 0.07 | 0.08 |
| Per10 | Quad | 0.23 | 0.23 | 0.24 | 0.24 | **0.27** | **0.29** |
| Per10 | None-OLR | 0.12 | 0.14 | 0.14 | *0.14* | 0.17 | 0.18 |
| Per25 | None | 0.08 | 0.07 | 0.07 | 0.08 | 0.09 | 0.09 |
| Per25 | Quad | **0.27** | **0.28** | **0.28** | **0.28** | **0.28** | **0.28** |
| Per25 | None-OLR | **0.18** | 0.17 | 0.17 | 0.17 | **0.19** | **0.19** |
| Mean | None | 0.13 | 0.13 | 0.13 | 0.13 | 0.13 | 0.13 |
| Mean | Quad | **0.30** | **0.29** | **0.30** | **0.30** | **0.30** | **0.29** |
| Mean | None-OLR | **0.29** | **0.29** | **0.29** | **0.29** | **0.30** | **0.29** |
| Per75 | None | 0.15 | **0.17** | **0.18** | **0.18** | **0.18** | **0.18** |
| Per75 | Quad | **0.26** | **0.29** | **0.29** | **0.29** | **0.30** | **0.29** |
| Per75 | None-OLR | **0.23** | **0.26** | **0.26** | **0.27** | **0.27** | **0.26** |
| Per90 | None | *0.17* | *0.20* | *0.20* | *0.19* | *0.18* | *0.17* |
| Per90 | Quad | 0.23 | **0.27** | *0.27* | **0.27** | **0.27** | 0.25 |
| Per90 | None-OLR | *0.23* | **0.28** | **0.28** | **0.28** | *0.27* | *0.26* |
| CV | None | 0.05 | 0.03 | 0.03 | 0.03 | 0.05 | 0.05 |
| CV | Quad | **0.28** | **0.26** | 0.26 | **0.26** | **0.27** | **0.29** |
| CV | None - OLR | 0.13 | 0.10 | 0.09 | 0.10 | 0.12 | 0.12 |
| Range | none | **0.23** | **0.40** | **0.37** | **0.25** | 0.01 | *0.02* |
| Range | Quadratic | **0.42** | **0.54** | **0.45** | **0.28** | *0.02* | *0.07* |
| Range | Recip - OLR | **0.19** | **0.29** | **0.27** | **0.26** | 0.139 | 0.099 |
| Sill | None | 0.03 | 0.01 | *0.01* | 0.00 | 0.00 | 0.01 |
| Sill | Quad | 0.07 | 0.10 | 0.10 | 0.10 | 0.09 | 0.07 |
| Nugget | None | 0.02 | 0.00 | 0.00 | 0.00 | *0.03* | *0.09* |
| Nugget | Quad | 0.02 | 0.09 | 0.09 | 0.02 | 0.14 | 0.12 |
| MSH | None | *0.02* | *0.03* | 0.01 | *0.00* | *0.03* | *0.09* |
| MSH | Quad | *0.12* | *0.07* | *0.03* | *0.07* | *0.15* | *0.12* |
| NSR | None | 0.02 | 0.03 | 0.01 | 0.00 | 0.03 | 0.09 |
| NSR | Quad | 0.12 | 0.07 | 0.03 | 0.05 | 0.15 | 0.12 |

## 4.0 Discussion

### 4.1 Modelling and mapping bunchgrass vegetation biomass using airborne Lidar

The variables most useful to accurately quantify grassland biomass in all of the predictor datasets were canopy volume, max height and mean intensity. Similar to Greaves et al., 2016, the inclusion of the canopy volume variable was important in the final Random Forest model. Volumetric measures have also proved useful for estimating vegetation biomass using ground-based lidar in an agricultural setting (Eitel et al., 2014), to assess fuel-bed characteristics (Loudermilk et al., 2009) and to quantify shrub biomass (Greaves et al., 2015). The return intensity variable also was important in the Random Forest model, likely due to the increased return intensity of the Leica ALS70 laser (i.e. the 1064 nm wavelength) when contacting green vegetation as compared to bare ground or rock (Eitel, Höfle, et al., 2016). Intensity data is increasingly being applied to quantify vegetation biochemistry (Eitel et al., 2014; Magney, Vierling, Eitel, Huggins, & Garrity, 2016) and leaf area (Béland, Baldocchi, Widlowski, Fournier, & Verstraete, 2014; Béland, Widlowski, Fournier, Côté, & Verstraete, 2011) and in this study, the intensity metric was selected 100% of the time when it was included in a predictor dataset. The max height metric was the other lidar derived metric selected across all model runs when available as a predictor variable. It improved Random Forest model results when compared to a model excluding it (In model: RMSD = 139.4 $g/m^2$, Left out of model: RMSD=148.56 $g/m^2$). In other studies, max height has been used to assess vegetation height and biomass in short-statured vegetation communities even though it typically underestimates the field measures (Kulawardhana et al., 2014). In this study, due to the close relationship between the field measures of both the mean and max vegetation height with biomass (Figure 3.2), it is logical that a max height lidar measure would be useful for modeling biomass. None of the topographic variables were selected more than 50% of the time when these variables were included with other variable datasets (Canopy or Intensity). We speculate that this could be due to the high degree of fine-scale topographic heterogeneity across this system and that the scale at which we computed topographic measures (1m) does not align well with the scales that drive the system.

Our most accurate Random Forest model (Canopy + Intensity) had a pseudo R-squared of 0.59 and a RMSD of 139.4 $g/m^2$. This is a slightly better fit than was achieved in Wang et al., 2017 ($R^2$ = 0.34), who estimated grassland biomass generated from discrete lidar

collected via an UAV, and Kulawardhana et al., 2014 ($R^2$ = 0.33 for total biomass) who used multiple linear regression to estimat salt marsh biomass based on discrete return lidar collected by airplane along with spectral data from NAIP imagery. The estimated above ground biomass at the pasture scale with an average of 174.74 g/$m^2$ and range of 117 g/$m^2$ to 233.27 g/$m^2$ are comparable to results from previous remote sensing studies in the Zumwalt Prairie that used Landsat data to assess pasture scale above biomass (Jansen et al., 2018; Jansen et al., 2016). The power of these lidar-derived maps is their ability to capture fine-scale heterogeneity, enabling the visualization and quantification of fine-scale topography- and management-related patterns of vegetation. Coarsening the initial 1.0668 m (3.5 ft) data to larger grid cell sizes demonstrates that fine-scale information is lost as the data are aggregated to coarser resolutions (Figure 3.7). Results from this study demonstrate that in short-statured vegetation communities, the canopy volume and Random Forest modeling approach outlined by Greaves et al., 2016 can be applied to other short-statured vegetation communities such as grassland systems.

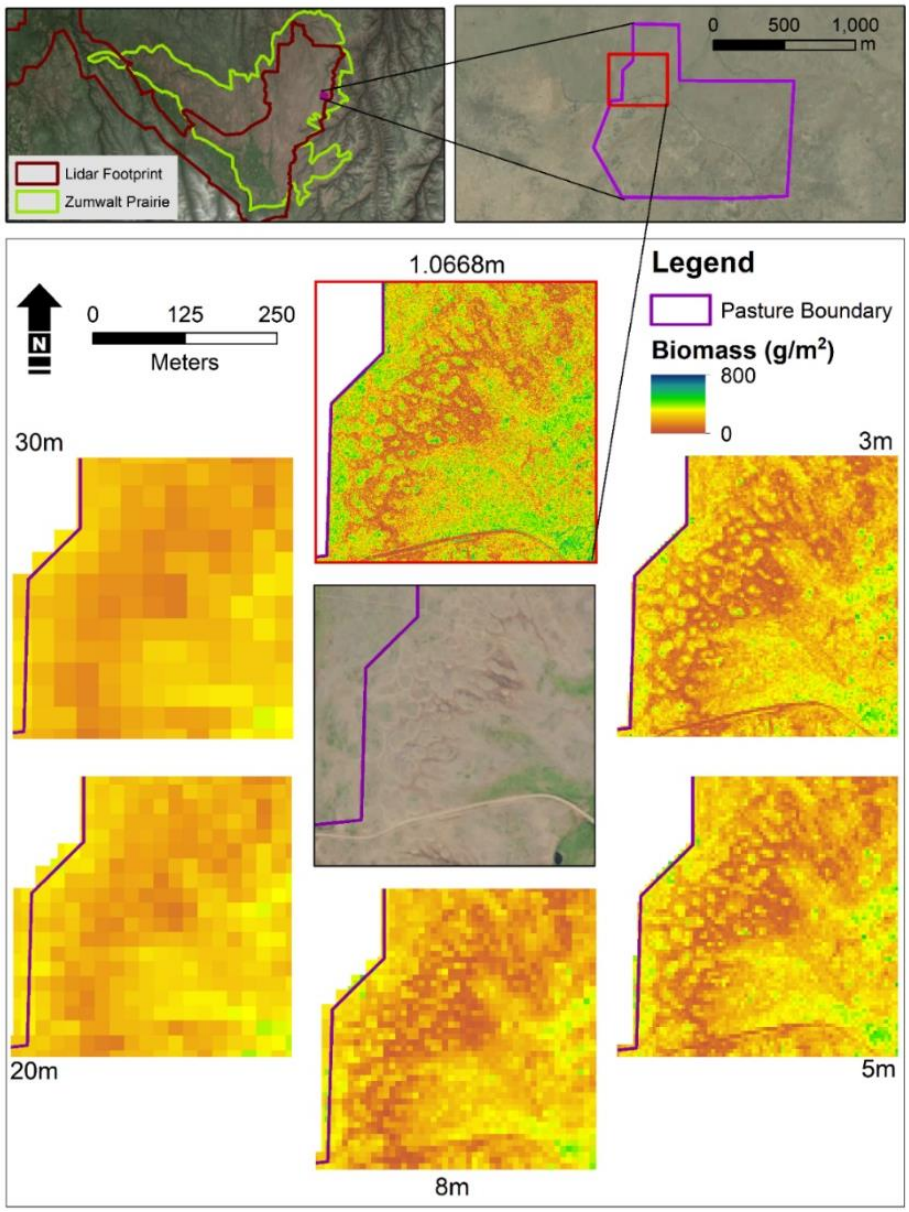


Figure 3.7. Grassland biomass at varying grid cell sizes (1.0668m, 3m, 5m, 8m, 20m, and 30m), produced by aggregating 1.0688m lidar derived biomass data for the Zumwalt Prairie in northeast Oregon.

To the authors' knowledge, this is one of the first studies using airplane-acquired lidar to estimate biomass across a short-statured grassland, and many improvements could be made. First, our models would have benefited from a field dataset with more high-biomass samples to enable greater confidence when predicting larger biomass values. Also, the lidar acquisition could be improved by acquiring a more uniform point cloud across the study area, with a

point density of greater than 9 points $m^{-2}$. This would have eliminated the need to normalize the point cloud density to reduce striping effects observed in the biomass (Figure A2.1). Furthermore, this would likely increase modeling accuracies. Our first analysis attempt with non-corrected point clouds had better accuracy (Figure A2.2) compared to the final models presented here, due to a higher average point density across the sample biomass quadrats. However, the lower point density in the remainder of the study area precluded extrapolation of these early models across the study area.

**4.2 The impact of spatial resolution on measures of spatial heterogeneity**

The aggregation of the fine-scale data to coarser scales revealed patterns similar to those described by Jupp et al., 1988; Wiens, 1989; Woodcock et al., 1988; Woodcock and Strahler, 1987, in that the overall variance (i.e., the sill) and fine scale variation (i.e., nugget) of the data were reduced, and the range increased (Figure 3.8). In testing the differences in the semivariogram measures across all grid cell sizes, the impact of aggregation is significant. This indicates that the semivariogram statistics provide different measures as the grid cell size changes. In selecting a plot size or spatial resolution to study a process and phenomena it is important to know how that decision impacts your findings (Wiens, 1989); here we see that biomass data quantified at the 1.0668 m scale provides statistically different spatial measures compared to the spatial measures when aggregated to larger grid cell sizes.

Following ideas in Strahler, Woodcock, & Smith, (1986) on the discrete scene model, when quantifying grassland vegetation with remotely sensed data, the resolution would be considered low when compared to a single leaf or single plant that is smaller than the size of the pixel but can be considered high if related to vegetation patches or pasture areas that are larger than the pixel being used for analysis. Using this rationale, our highest resolution data (i.e. 1.0668m) is not high-resolution data at the plant level. This is evident from the large average nugget and when plotting semivariograms for each resolution for a single pasture (Figure 3.8). The nugget can represent noise, sampling error, or the within pixel variation. In this study, we reason that the large nugget with the 1.0668m data is largely driven by within pixel variation between bunchgrass and soil. When we aggregate these data to coarser scales (3 m to 30 m), we smooth over the canopy gaps and reduce the variability in biomass, thus decreasing the nugget (semivariance) captured at fine scales.

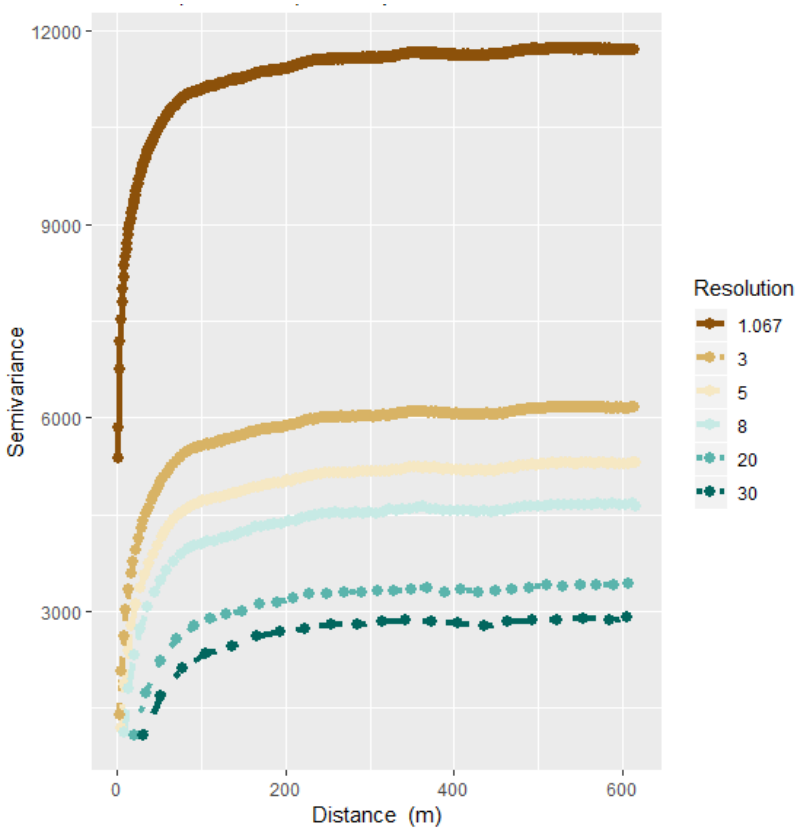


Figure 3.8. Empirical Semivariogram for the Harsin pasture using the six different increasing grid cell sizes.

Specifically exploring the range data at the finest scale (~1.0668 m), we obtained an average range of 78.8 m across all study pastures. This range value is similar to a previous study conducted in a mixed grassland in Saskatchewan, Canada which used a handheld spectroradiometer and found a range of 70 m using a leaf area index metric (He, Guo, Wilmshurst, & Si, 2006). In a study conducted within a Southern Californian chaparral and grassland, the semivariance within grassland sites using the Normalized Difference Vegetation Index (NDVI), and the Photochemical Reflectance Index (PRI) failed to produce clear range values across multiple years (Rahman, Gamon, Sims, & Schmidts, 2003). This was likely due to the small maximum lag interval of 20 m not being spatially large enough to capture the spatial dependence over a large area in the grassland sites. In both Rahman et al., 2003 and He et al., 2006, the authors point to sampling theories stating that in order to measure objects, one must sample at least at one-half the size of the object. Following this rationale, to effectively quantify biomass a pixel size less than 40 m would be suitable due to

our average range being 78.8 m. Interestingly, when we used coarser resolutions (20 m to 30 m) to quantify how spatial patterns correlate to grazing, these failed to produce significant relationships (See 4.3 below).

### 4.3 The impacts of spatial resolution on heterogeneity metrics used to quantify grazing effects

It is well documented that grazing can impact various aspects of vegetation heterogeneity from species composition, structure and biomass (Adler et al., 2001), yet the ability to quantify and monitor spatial heterogeneity of vegetation amount (i.e., biomass, cover, height) with remotely sensed data is dependent on the interaction between the spatial resolution of the data and the vegetation pattern on the ground. It is known that some resolutions will be too coarse to detect vegetation patterns (Wiens, 1989). In this study, testing the relationship between grazing intensity and the semivariogram-derived measures of heterogeneity across the various grid cell sizes revealed that the range statistic, which is related to patch size, was the only spatial statistic sensitive to grazing. We also observed that the sensitivity of this range statistic to grazing became weaker as the cell size increased, so much so that the 20 m and 30 m resolutions failed to provide significant relationships with grazing intensity. This is likely due to multiple patterns and processes working at different scales (Wu, 1999).

The results showing an increase in the patch size or range with higher grazing intensity are similar to Scarth & Trevithick, 2017, who observed increases in the range value with increased grazing using 10 m Sentinel-2 bare ground data in Australia. That the range value increased with grazing intensity contradicts Virk and Mitchell, 2015, who after two years found that grazing decreased the semivariogram range statistics. Virk and Mitchell 2015 also found that the MSH was sensitive to grazing and increased with grazing over the course of their study, whereas our results showed that this metric was not sensitive to grazing intensity at any scale. These differences are likely due to underlying differences in vegetation heterogeneity, grazing distribution and intensity (Adler et al., 2001), and the study length. Virk and Mitchell 2015 tracked vegetation across multiple years to monitor the change in heterogeneity with varying levels of grazing. Here we only use one year of data, which is not ideal, especially in grassland systems that can experience large year–to-year variations in production (Briske et al., 2015). Another influence could be that Virk and Mitchell 2015 modeled live biomass using NDVI, which can be impacted by standing dead vegetation and

litter in natural grassland systems (Jansen et al., 2018; Xu, Guo, Li, Yang, & Yin, 2014). Mapping the pattern of green vegetation signal (NDVI) only could potentially influence measures of heterogeneity.

Following Adler et al., 2001 there are two ways grazing decreases heterogeneity: 1) with selective grazing whereby grazing decreases contrast between vegetation types or 2) with patch or homogeneous grazing, whereby the grazing pattern is weaker than the vegetation pattern (Adler et al., 2001). From this study, we reason that selective grazing across the study area decreases the vegetation biomass, leading to reduced heterogeneity with greater stocking rates. That the range statistic was not significantly related to grazing at the 20 m and 30 m scale shows how the spatial scale used to study a pattern or process may influence the interpretation of results, and that these processes can be expressed differently depending on the scale at which they are studied (Townsend & Fuhlendorf, 2010). In other words, while the 30 m scale may be suitable to monitor vegetation biomass and a general change in quantity, this scale is not sensitive enough to detect changes in the spatial vegetation pattern (i.e. spatial heterogeneity measured with a spatial statistic) induced by grazing.

### 4.4 Implications for management and future analysis opportunities

The maps created using the Random Forest model provide the first landscape-scale maps of grassland biomass derived from airplane-gathered lidar in this grassland system and, to our knowledge, in any short-stature vegetation grassland. Fine-scale lidar datasets such as this one can provide needed spatially explicit information on vegetation such as structure or biomass which can be related to habitat needs for critical species (Greaves et al., 2016; Vierling, Vierling, Gould, Martinuzzi, & Clawges, 2008). They also provide data to better understand how management drivers impact vegetation biomass and structure at fine scales. For example, in this grassland system, grazing was associated with increasing patch size, suggesting a reduction in fine-scale biomass heterogeneity. This result can inform conservation and management actions which seek to increase habitat heterogeneity. Linking semivariogram-derived patch size metrics to other biological processes, such as erosion or weed invasion, as well as habitat requirements for wildlife species such as birds, would further reveal how this dataset and resulting spatial metrics could be used to monitor other conservation relevant indicators.

The result that the 20m and 30 m resolution data, equivalent to the resolution of Sentinel 2 or Landsat data, did not produce spatial heterogeneity metrics sensitive to grazing provides evidence that these sensors are not best suited to freely monitor how grazing impacts above ground biomass heterogeneity vegetation in this study area. Fortunately, higher resolution data are being made available (e.g., WorldView-3, Planet Labs, Inc., RapidEye) which could be used to monitor the effect of grazing on spatial heterogeneity over time. While the spatial heterogeneity metrics were not sensitive to grazing at coarser resolutions (i.e., 20m, 30m), the coefficient of variation (CV) metric was. This metric is often used as a non-spatial measure of heterogeneity (Adler et al., 2001) and was significantly related to grazing across all scales using a quadratic model. This finding is supported by Johnson et al., 2011, who modeled a significant quadratic effect of grazing on the structural heterogeneity across this same study area. In both studies, it was observed that coefficient of variation increased as grazing increased from no grazing to moderate grazing and decreased from moderate grazing to heavy grazing. This finding suggests that Landsat data at the 30 m scale can provide reliable estimates of this non-spatial heterogeneity measure.

Future studies investigating how grazing management impacts vegetation heterogeneity should explore additional spatial statistics at larger spatial extents and temporal scales. For example, spatial statistics such as Moran's I could be computed at the pasture and ranch scale over time, which would contribute to an improved understanding of the hierarchal and nested nature of this ecosystem, and how land management impacts heterogeneity at scales relevant to landscape processes and management (Fuhlendorf et al., 2012). It could also be informative to analyze the 1 m biomass data with an object-based approach for mapping vegetation patches as well as for habitat classification. Ideally, this approach segments spatial data based on meaningful ecological patterns, helping to overcome issues of information loss due to arbitrarily defined pixel areas (Karl & Maurer, 2010). Studying processes that interact with grazing to impact vegetation patterns, such as fire and soil characteristics, is another future area of interest.

## 5.0 Conclusion

Lidar processing and Random Forest modeling approaches developed to map and model shrub biomass in the Arctic Tundra also can provide significant relationships with

short-statured grassland biomass. The mapped output of these models provides landscape- and pasture-level estimates of biomass at fine (~1 m) resolutions. Aggregating the fine-scale biomass data to increasingly coarser grid sizes reveals how the spatial resolution of data (i.e. pixel size) from various remote sensing platforms impacts our ability to quantify spatial patterns of processes under question. This in turn informs the selection of the most appropriate sensor/spatial resolution to quantify or monitor a desired phenomenon or ecological process. For example, in this study when using semivariograms to study spatial heterogeneity high-resolution data, between 1 m and 8 m pixel size, is needed to monitor the effect of grazing on vegetation patchiness at peak biomass across this short-statured, highly heterogeneous grassland. Ecologically, we found evidence that grazing decreases vegetation heterogeneity within this grassland system, and we identified the spatial scales (1 m to 8 m) at which the process is most evident in gridded data. This is an important finding for future research and monitoring as well as current management practices which seek to increase heterogeneity in this and other similar grassland ecosystems.

**References**

Adler, P. B., Milchunas, D. G., Lauenroth, W. K., Sala, O. E., & Burke, I. C. (2004). Functional traits of graminoids in semi-arid steppes: A test of grazing histories. Journal of Applied Ecology, 41(4), 653–663. http://doi.org/10.1111/j.0021-8901.2004.00934.x

Adler, P., Raff, D., & Lauenroth, W. (2001). The effect of grazing on the spatial heterogeneity of vegetation. Oecologia, 128(4), 465–479. http://doi.org/10.1007/s004420100737

Allen-Diaz, B., Chapin, F. S., Diaz, S., M. Howden, J. P., & Smith, M. S. (1995). Rangelands in a Changing Climate: Impacts, Adaptations, and Mitigation. In: Climate Change 1995—Impacts, Adaptation and Mitigation, W. T. Watson, M. C. Zinyowera, R. H. Moss, and D. J. Dokken, (Eds.), Pp. 131–158.

Augustine, D. J., & Mcnaughton, S. J. (1998). Ungulate Effects on the Functional Species Composition of Plant Communities: Herbivore Selectivity and Plant Tolerance. Source: The Journal of Wildlife Management, 62(4), 1165–1183. http://doi.org/10.2307/3801981

Béland, M., Baldocchi, D. D., Widlowski, J. L., Fournier, R. A., & Verstraete, M. M. (2014). On seeing the wood from the leaves and the role of voxel size in determining leaf area distribution of forests with terrestrial LiDAR. Agricultural and Forest Meteorology, 184, 82–97. http://doi.org/10.1016/j.agrformet.2013.09.005

Béland, M., Widlowski, J. L., Fournier, R. A., Côté, J. F., & Verstraete, M. M. (2011). Estimating leaf area distribution in savanna trees from terrestrial LiDAR measurements. Agricultural and Forest Meteorology, 151(9), 1252–1266. http://doi.org/10.1016/j.agrformet.2011.05.004

Bestelmeyer, B. T., & Briske, D. D. (2012). Grand Challenges for Resilience-Based Management of Rangelands. Rangeland Ecology & Management, 65(November), 654–663. http://doi.org/10.2111/REM-D-12-00072.1

Boehner, J., Koethe, R., Conrad, O., Gross, J., Ringeler, A., & Selige, T. (2002). Soil Regionalisation by Means of Terrain Analysis and Process Parameterisation. Status and Prospect of Soil Information in South - Eastern Europe: Soil Databases, Projects and Applications, (May 2015), 1–4. http://doi.org/ISBN : 978-92-79-04972-9

Booth, D. T., & Tueller, P. T. (2003). Rangeland monitoring using remote sensing. Arid Land Research and Management, 17, 455–467. Retrieved from http://www.tandfonline.com/doi/abs/10.1080/713936105

Breiman, L. E. O. (2001). Random Forests. Machine Learning, 45, 5–32.

Briske, D. D., Joyce, L. a, Polley, H. W., Brown, J. R., Wolter, K., Morgan, J. a, … Bailey, D. W. (2015). Climate-change adaptation on rangelands: linking regional exposure with diverse adaptive capacity. Frontiers in Ecology and the Environment, 13(5), 249–256. http://doi.org/10.1890/140266

Cambardella, C. A., Moorman, T. B., Parkin, T. B., Karlen, D. L., Novak, J. M., Turco, R. F., & Konopka, A. E. (1994). Field-Scale Variability of Soil Properties in Central Iowa Soils. Soil Science Society of America Journal, 58(5), 1501. http://doi.org/10.2136/sssaj1994.03615995005800050033x

Cohen, W. B., Spies, T. A., & Bradshaw, G. A. (1990). Semivariograms of digital imagery for analysis of conifer canopy structure. Remote Sensing of Environment, 34(3), 167–178. http://doi.org/10.1016/0034-4257(90)90066-U

Cooper, S. D., Roy, D. P., Schaaf, C. B., & Paynter, I. (2017). Examination of the potential of terrestrial laser scanning and structure-from-motion photogrammetry for rapid nondestructive field measurement of grass biomass. Remote Sensing, 9(6). http://doi.org/10.3390/rs9060531

Crookston, N., & Finley, A. (2008). yaImpute: An R Package for kNN Imputation. Journal Of Statistical Software, 23(10). Retrieved from http://ddr.nal.usda.gov/handle/10113/16688

Eitel, J. U. H., Höfle, B., Vierling, L. A., Abellán, A., Asner, G. P., Deems, J. S., … Vierling, K. T. (2016). Beyond 3-D: The new spectrum of lidar applications for earth and ecological sciences. Remote Sensing of Environment, 186, 372–392. http://doi.org/10.1016/j.rse.2016.08.018

Eitel, J. U. H., Magney, T. S., Vierling, L. A., Brown, T. T., & Huggins, D. R. (2014). Field Crops Research LiDAR based biomass and crop nitrogen estimates for rapid , non-destructive assessment of wheat nitrogen status. Field Crops Research, 159, 21–32. http://doi.org/10.1016/j.fcr.2014.01.008

Eitel, J. U. H., Magney, T. S., Vierling, L. A., Greaves, H. E., & Zheng, G. (2016). An automated method to quantify crop height and calibrate satellite-derived biomass using hypertemporal lidar. Remote Sensing of Environment, 187, 414–422. http://doi.org/10.1016/j.rse.2016.10.044

Fleischner, T. L. (1994). Ecological Costs of Livestock Grazing in Western North America. Conservation Biology, 8(3), 629–644. http://doi.org/10.1046/j.1523-1739.1994.08030629.x

Fu, B. J., Liu, S. L., Ma, K. M., & Zhu, Y. G. (2004). Relationships between soil characteristics, topography and plant diversity in a heterogeneous deciduous broad-leaved forest near Beijing , China. Plant and Soil, 47–54.

Fuhlendorf, S. D., & Engle, David, M. (2001). Restoring Heterogeneity on Rangelands : Ecosystem Management Based on Evolutionary Grazing Patterns. BioScience, 51(8), 625–632.

Fuhlendorf, S. D., Engle, D. M., Elmore, R. D., Limb, R. F., & Bidwell, T. G. (2012). Conservation of Pattern and Process: Developing an Alternative Paradigm of Rangeland Management. Rangeland Ecology & Management, 65(6), 579–589. http://doi.org/10.2111/REM-D-11-00109.1

Gessler, P. E., Chadwick, O. A., Chamran, F., Althouse, L., & Holmes, K. (2000). Modeling Soil – Landscape and Ecosystem Properties Using Terrain Attributes. Soil Science Society of America Journal, 64(6), 2046–2056.

Getis, A., & Ord, J. K. (1992). The Analysis of Spatial Association, 24(3).

Glenn, N. F., Neuenschwander, A., Vierling, L. A., Spaete, L., Li, A., Shinneman, D. J., … Mcilroy, S. K. (2015). Remote Sensing of Environment Landsat 8 and ICESat-2 : Performance and potential synergies for quantifying dryland ecosystem vegetation cover and biomass ☆. Remote Sensing of Environment, (2015). http://doi.org/10.1016/j.rse.2016.02.039

Godínez-Alvarez, H., Herrick, J. E., Mattocks, M., Toledo, D., & Van Zee, J. (2009). Comparison of three vegetation monitoring methods: Their relative utility for ecological assessment and monitoring. Ecological Indicators, 9(5), 1001–1008. http://doi.org/10.1016/j.ecolind.2008.11.011

Greaves, H. E., Vierling, L. A., Eitel, J. U. H., Boelman, N. T., Magney, T. S., Prager, C. M., & Grif, K. L. (2016). High-resolution mapping of aboveground shrub biomass in Arctic tundra using airborne lidar and imagery. Remote Sensing of Environment, 184, 361–373.

Greaves, H. E., Vierling, L. a., Eitel, J. U. H., Boelman, N. T., Magney, T. S., Prager, C. M., & Griffin, K. L. (2015). Estimating aboveground biomass and leaf area of low-stature Arctic shrubs with terrestrial LiDAR. Remote Sensing of Environment, 164, 26–35. http://doi.org/10.1016/j.rse.2015.02.023

Guerschman, J. P., Scarth, P. F., Mcvicar, T. R., Renzullo, L. J., Malthus, T. J., Stewart, J. B., … Trevithick, R. (2015). Remote Sensing of Environment Assessing the effects of site heterogeneity and soil properties when unmixing photosynthetic vegetation , non-photosynthetic vegetation and bare soil fractions from Landsat and MODIS data. Remote Sensing of Environment, 161, 12–26. http://doi.org/10.1016/j.rse.2015.01.021

He, Y., Guo, X., Wilmshurst, J., & Si, B. C. (2006). Studying mixed grassland ecosystems II: Optimum pixel size. Canadian Journal of Remote Sensing, 32(2), 108–115. http://doi.org/10.5589/m06-018

Heady, H. F. (1957). The Measurement and Value of Plant Height in the Study of Herbaceous Vegetation. Ecology, 38(2), 313. http://doi.org/10.2307/1931691

Herrick, J. E., Lessard, V. C., Spaeth, K. E., Shaver, P. L., Dayton, R. S., Pyke, D. A., … Goebel, J. J. (2010). National ecosystem assessments supported by scientific and local knowledge. Frontiers in Ecology and the Environment, 8(8), 403–408. http://doi.org/10.1890/100017

Hudak, A. T., Evans, J. S., & Smith, A. M. S. (2009). LiDAR utility for natural resource managers. Remote Sensing, 1(4), 934–951. http://doi.org/10.3390/rs1040934

Jacques, D. C., Kergoat, L., Hiernaux, P., Mougin, E., & Defourny, P. (2014). Monitoring dry vegetation masses in semi-arid areas with MODIS SWIR bands. Remote Sensing of Environment, 153, 40–49. http://doi.org/10.1016/j.rse.2014.07.027

Jansen, V., Kolden, C., & Schmalz, H. (2018). The Development of Near Real-Time Biomass and Cover Estimates for Adaptive Rangeland Management Using Landsat 7 and Landsat 8 Surface Reflectance Products. Remote Sensing, 10(7), 1057. http://doi.org/10.3390/rs10071057

Jansen, V. S., Kolden, C. A., Taylor, R. V., & A. Newingham, B. (2016). Quantifying livestock effects on bunchgrass vegetation with Landsat ETM+ data across a single growing season. International Journal of Remote Sensing, 37(1), 150–175. http://doi.org/10.1080/01431161.2015.1117681

Johansen, K., Coops, N. C., Gergel, S. E., & Stange, Y. (2007). Application of high spatial resolution satellite imagery for riparian and forest ecosystem classification. Remote Sensing of Environment, 110(1), 29–44. http://doi.org/10.1016/j.rse.2007.02.014

Johnson, T. N., Kennedy, P. L., DelCurto, T., & Taylor, R. V. (2011). Bird community responses to cattle stocking rates in a Pacific Northwest bunchgrass prairie. Agriculture, Ecosystems & Environment, 144(1), 338–346. http://doi.org/10.1016/j.agee.2011.10.003

Jupp, D. L. B., Strahler, A. H., & Woodcock, C. E. (1988). Autocorrelation and Regularization in Digital Images I. Basic Theory. IEEE Transactions on Geoscience and Remote Sensing, 26(4), 463–473. http://doi.org/10.1109/36.3050

Karl, J. W., & Maurer, B. A. (2010). Multivariate correlations between imagery and field measurements across scales: Comparing pixel aggregation and image segmentation. Landscape Ecology, 25(4), 591–605. http://doi.org/10.1007/s10980-009-9439-4

Kimoto, C., DeBano, S., & Thorp, R. (2012). Investigating temporal patterns of a native bee community in a remnant North American bunchgrass prairie using blue vane traps. Journal of Insect Science, 12(108), 1–23. Retrieved from http://www.ncbi.nlm.nih.gov/pmc/articles/PMC3605028/

Kulawardhana, R. W., Popescu, S. C., & Feagin, R. a. (2014). Fusion of lidar and multispectral data to quantify salt marsh carbon stocks. Remote Sensing of Environment, 154, 345–357. http://doi.org/10.1016/j.rse.2013.10.036

Lane, D. R., & BassiriRad, H. (2005). Diminishing spatial heterogeneity in soil organic matter across a prairie restoration chronosequence. Restoration Ecology, 13(2), 403–412. http://doi.org/DOI 10.1111/j.1526-100X.2005.00050.x

Lechner, A. M., Stein, A., Jones, S. D., & Ferwerda, J. G. (2009). Remote sensing of small and linear features: Quantifying the effects of patch size and length, grid position and detectability on land cover mapping. Remote Sensing of Environment, 113(10), 2194–2204. http://doi.org/10.1016/j.rse.2009.06.002

Li, A., Dhakal, S., Glenn, N. F., Spaete, L. P., Shinneman, D. J., Pilliod, D. S., … McIlroy, S. K. (2017). Lidar aboveground vegetation biomass estimates in shrublands: Prediction, uncertainties and application to coarser scales. Remote Sensing, 9(9). http://doi.org/10.3390/rs9090903

Li, H., & Reynolds, J. F. (1994). A Simulation Experiment to Quantify Spatial Heterogeneity in Categorical Maps. Ecology, 75(8), 2446–2455.

Liaw, A., & Wiener, M. (2002). Classification and Regression by randomForest. R News, 2, 18–22.

Lin, Y., Hong, M., Han, G., Zhao, M., Bai, Y., & Chang, S. X. (2010). Grazing intensity affected spatial patterns of vegetation and soil fertility in a desert steppe. Agriculture, Ecosystems & Environment, 138(3–4), 282–292. http://doi.org/10.1016/j.agee.2010.05.013

Loudermilk, E. L., Hiers, J. K., O'Brien, J. J., Mitchell, R. J., Singhania, A., Fernandez, J. C., … Slatton, K. C. (2009). Ground-based LIDAR: A novel approach to quantify fine-scale fuelbed characteristics. International Journal of Wildland Fire, 18(6), 676–685. http://doi.org/10.1071/WF07138

Mack, R. N., & Pyke, D. A. (1983). THE DEMOGRAPHY OF BROMUS TECTORUM: VARIATION IN TIME AND SPACE. Journal of Ecology, 71, 69–93.

Magney, T. S., Vierling, L. A., Eitel, J. U. H., Huggins, D. R., & Garrity, S. R. (2016). Remote Sensing of Environment Response of high frequency Photochemical Re fl ectance Index ( PRI ) measurements to environmental conditions in wheat. Remote Sensing of Environment, 173, 84–97. http://doi.org/10.1016/j.rse.2015.11.013

Marsett, R. C., Qi, J., Heilman, P., Biedenbender, S. H., Watson, M. C., Amer, S., … Marsett, R. (2006). Remote Sensing for Grassland Management in the Arid Southwest. Rangeland Ecology & Management, 59(5), 530–540.

Matheron, G. (1971). The Theory of Regionalized Variables and it Applications, in Les Cahiers du Centre de Morphologie Mathgmatique de Fontainbleau, No 5. l~cole Nationale Sup~rieure des Mines de Paris.

McLean, A., & Tisdale, E. (1972). Recovery rate of depleted range sites under protection from grazing. Journal of Range Management, 178–184. Retrieved from http://www.jstor.org/stable/3897051

McSherry, M. E., & Ritchie, M. E. (2013). Effects of grazing on grassland soil carbon: a global review. Global Change Biology, 19(5), 1347–57. http://doi.org/10.1111/gcb.12144

Moran, P. (1950). Notes on continuous stochastic phenomena. Biometrika, 37(1), 17–23. Retrieved from http://www.jstor.org/stable/10.2307/2332142

Murphy, M. A., Evans, J. S., & Storfer, A. (2010). Quantifying Bufo boreas connectivity in Yellowstone National Park with landscape genetics Linked references are available on JSTOR for this article : Quantifying Bufo boreas connectivity in Yellowstone National Park with landscape genetics. Ecology, 91(1), 252–261.

Pebesma, E. J. (2004). Multivariable geostatistics in S: The gstat package. Computers and Geosciences, 30(7), 683–691. http://doi.org/10.1016/j.cageo.2004.03.012

Phinn, S. R., Stow, D. A., Franklin, J., Mertes, L. A. K., & Michaelsen, J. (2003). Remotely Sensed Data for Ecosystem Analyses : Combining Hierarchy Theory and Scene Models, 31(3), 429–441. http://doi.org/10.1007/s00267-002-2837-x

Pineiro, G., Perelman, S., Guerschman, J. P., & Jose, P. M. (2008). How to evaluate models: Observed vs. predicted or predicted vs. observed? Ecological Modelling, 216, 316–322. http://doi.org/10.1016/j.ecolmodel.2008.05.006

R Development Core Team. (2016). R: A Language and Environment for Statistical Computing. R Foundation for Statistical Computing Vienna Austria, 0, {ISBN} 3-900051-07-0. http://doi.org/10.1038/sj.hdy.6800737

Radtke, P. J., Boland, H. T., & Scaglia, G. (2010). An evaluation of overhead laser scanning to estimate herbage removals in pasture quadrats. Agricultural and Forest Meteorology, 150(12), 1523–1528. http://doi.org/10.1016/j.agrformet.2010.07.010

Rahman, A. F., Gamon, J. A., Sims, D. A., & Schmidts, M. (2003). Optimum pixel size for hyperspectral studies of ecosystem function in southern California chaparral and grassland. Remote Sensing of Environment, 84(2), 192–207. http://doi.org/10.1016/S0034-4257(02)00107-4

Robel, R. I., Briggs, J. N., Dayton, A. D., & Hulbert, L. C. (1970). Relationships between Visual Obstruction Measurements and Weight of Grassland Vegetation Relationships Between Visual Obstruction Measurements and Weight of Grassland Vegetation. Journal Of Range Management, 23(4), 295–297.

Sadoti, G., Pollock, M. G., Vierling, K. T., Albright, T. P., & Strand, E. K. (2014). Variogram models reveal habitat gradients predicting patterns of territory occupancy and nest survival among vesper sparrows. Wildlife Biology, 20(2), 97–107. http://doi.org/10.2981/wlb.13056

Sankey, T. T., Sankey, J. B., Weber, K. T., & Montagne, C. (2009). Geospatial Assessment of Grazing Regime Shifts and Sociopolitical Changes in a Mongolian Rangeland. Rangeland Ecology & Management, 62(6), 522–530. http://doi.org/10.2111/.1/REM-D-09-00014.1

Sayre, N. F., deBuys, W., Bestelmeyer, B. T., & Havstad, K. M. (2012). "The Range Problem" After a Century of Rangeland Science: New Research Themes for Altered Landscapes. Rangeland Ecology and Management, 65(6), 545–552. http://doi.org/10.2111/REM-D-11-00113.1

Sayre, N. F., McAllister, R. R., Bestelmeyer, B. T., Moritz, M., & Turner, M. D. (2013). Earth Stewardship of rangelands: Coping with ecological, economic, and political marginality. Frontiers in Ecology and the Environment, 11(7), 348–354. http://doi.org/10.1890/120333

Scarth, P., & Trevithick, R. (2017). Management effects on ground cover "Clumpiness": Scaling from field to Sentinel-2 cover estimates. International Archives of the Photogrammetry, Remote Sensing and Spatial Information Sciences - ISPRS Archives, 42(3W2), 183–188. http://doi.org/10.5194/isprs-archives-XLII-3-W2-183-2017

Schaefer, M. T., & Lamb, D. W. (2016). A Combination of Plant NDVI and LiDAR Measurements Improve the Estimation of Pasture Biomass in Tall Fescue ( Festuca arundinacea. http://doi.org/10.3390/rs8020109

Strahler, A. H., Woodcock, C. E., & Smith, J. a. (1986). On the nature of models in remote sensing. Remote Sensing of Environment, 20(2), 121–139. http://doi.org/10.1016/0034-4257(86)90018-0

Tisdale, E. W. (1982). Grasslands of Western North America: The Pacific Northwest Bunchgrass. p 232-245 in A.C. Nicholson, A. McLean, and T.E. Baker (eds.) Grassland ecology and classification (Symposium Proceedings). British Columbia Ministry of Forests, Kamloops, BC, Canada.

Todd, S. W., Hoffer, R. M., & Milchunas, D. G. (1998). Biomass estimation on grazed and ungrazed rangelands using spectral indices. International Journal of Remote Sensing, 19(3), 427–438. Retrieved from http://www.tandfonline.com/doi/abs/10.1080/014311698216071

Townsend, D. E., & Fuhlendorf, S. D. (2010). Evaluating Relationships between Spatial Heterogeneity and the Biotic and Abiotic Environments. The American Midland Naturalist, 163(2), 351–365. http://doi.org/10.1674/0003-0031-163.2.351

Vierling, K. T., Vierling, L. a, Gould, W. a, Martinuzzi, S., & Clawges, R. M. (2008). Lidar: shedding new light on habitat characterization and modeling. Frontiers in Ecology and the Environment, 6(2), 90–98. http://doi.org/10.1890/070001

Virk, R., & Mitchell, S. W. (2015). Effect of Different Grazing Intensities on the Spatial-Temporal Variability in Above-Ground Live Plant Biomass in North American Mixed Grasslands. Canadian Journal of Remote Sensing, 40(6), 423–439. http://doi.org/10.1080/07038992.2014.1009882

Wang, D., Xin, X., Shao, Q., Brolly, M., Zhu, Z., & Chen, J. (2017). Modeling aboveground biomass in Hulunber grassland ecosystem by using unmanned aerial vehicle discrete lidar. Sensors (Switzerland), 17(1), 1–19. http://doi.org/10.3390/s17010180

Western, A. W., Blöschl, G., & Grayson, R. B. (1998). Geostatistical characterisation of soil moisture patterns in the Tarrawarra catchment. Journal of Hydrology, 205(1–2), 20–37. http://doi.org/10.1016/S0022-1694(97)00142-X

Wiens, J. A. (1989). Spatial Scaling in Ecology. Functional Ecology, 3(4), 385–397.

Wiens, J., Sutter, R., Anderson, M., Blanchard, J., Barnett, A., Aguilar-Amuchastegui, N., … Laine, S. (2009). Selecting and conserving lands for biodiversity: The role of remote sensing. Remote Sensing of Environment, 113(7), 1370–1381. http://doi.org/10.1016/j.rse.2008.06.020

Woodcock, C. E., & Strahler, A. H. (1987). The Factor of Scale in Remote Sensing, 332, 311–332.

Woodcock, C. E., Strahler, A. H., & Jupp, D. L. (1988). The Use of Variograms in Remote Sensing : I . Scene Models and Simulated Images. Remote Sensing Environment, 25, 323–348. http://doi.org/10.1016/0034-4257(88)90108-3

Wu, J. (1999). Hierarchy and scaling: Extrapolating Information Along a Scaling Ladder. Canadian Journal of Remote Sensing, 25(4), 367–380.

Xu, D., Guo, X., Li, Z., Yang, X., & Yin, H. (2014). Measuring the dead component of mixed grassland with Landsat imagery. Remote Sensing of Environment, 142, 33–43. http://doi.org/10.1016/j.rse.2013.11.017

Zlinszky, A., Deák, B., Kania, A., Schroiff, A., & Pfeifer, N. (2015). Mapping natura 2000 habitat conservation status in a pannonic salt steppe with airborne laser scanning. Remote Sensing, 7(3), 2991–3019. http://doi.org/10.3390/rs70302991

Zlinszky, A., Schroiff, A., Kania, A., Deák, B., Mücke, W., Vári, Á., … Pfeifer, N. (2014). Categorizing grassland vegetation with full-waveform airborne laser scanning: A feasibility study for detecting natura 2000 habitat types. Remote Sensing, 6(9), 8056–8087. http://doi.org/10.3390/rs6098056

# Chapter 4: Short-term rangeland vegetation monitoring from space: Exploring the relationships between in-field stocking rates and end of year utilization with Landsat-derived biomass data for management and monitoring purposes

**Abstract**

Landscape scale data on vegetation amounts derived from remotely sensed data has the ability to improve the adaptive management cycle. In this paper we correlate biomass metrics produced from a previously developed Landsat model which estimates above ground biomass created for the Pacific Northwest bunchgrass prairie with short term monitoring data on stocking rate at the pasture scale and end of year utilization measures at the plot scale. Remotely sensed biomass metrics quantifying end of year residual biomass, and the relative difference in biomass between summer and fall were significantly correlated to short-term monitoring indicators at both the pasture and plot scales. Next, we created boxplots of our remotely sensed derived biomass metrics (Fall biomass, and the relative difference in biomass) by utilization class and selected the median values from the 13% and 50% graze class as classification threshold values. Displaying maps based on threshold values from the in-field utilization data highlight the year to year variability in end of season biomass due to climate variability, as well as areas that have greater amounts of change relative to other areas across the landscape. These results highlight the potential to integrate remote sensing tools into existing monitoring and management data to improve adaptive management and conservation outcomes on a grassland prairie.

## 1.0 Introduction

Temperate grassland ecosystems are threatened worldwide by conversion to crop agriculture (Hoekstra et al., 2005), livestock mismanagement (Alkemade et al., 2013), and woody plant encroachment (Van Auken, 2009). Over time, heavy stocking rates may reduce profitability and threaten the economic sustainability of ranching (Holechek, 1988; Holechek et al., 1999). Livestock can impact the structure and function of grassland ecosystems (Milchunas and Lauenroth, 1993) causing short-term effects such as reduced litter cover and compacted soils (Schmalz et al., 2013) as well as long-term effects, including reduced productivity and a shift from native perennial grasses to invasive annual grasses (Bartolome et

al., 1980; Reisner et al., 2013). Grazing has been used to increase heterogeneity of vegetation pattern in grasslands (Fuhlendorf and Engle, 2001; Fuhlendorf et al., 2012) which is a desired conservation outcome due to the link between habitat heterogeneity and biological diversity (Adler et al., 2001). In turn, wildlife such as birds, mammals, and insects have variable responses to grazing; some are sensitive to grazing, while other species benefit from grazing-induced changes in vegetation structure (Derner et al., 2009; Severson and Urness, 1994). Grazing on grassland systems is preferred land use over other land uses such as ex-urban development or cultivation (Brunson and Huntsinger, 2008). Therefore the continued existence of profitable ranches can help to decrease the threat of habitat loss by fragmentation and conversion to other land uses (Brunson and Huntsinger, 2008).

To avoid or mitigate the undesired effects of livestock grazing and to increase habitat diversity, many rangeland practitioners employ adaptive management strategies. Effective adaptive management relies upon monitoring the success or failure of implemented strategies (Joyce et al., 2013), distributing monitoring results that can be used for management action at relevant scales, and integrating stakeholder experiences into the scientific process (Bestelmeyer and Briske, 2012; Juntti et al., 2009). However, the ecological outcomes of grazing management decisions (e.g., setting stocking rates, animal species, or rotations) aimed at balancing economic profitability and long-term land productivity are difficult and expensive to measure adequately across large areas and across many years due to climatic variability and spatial heterogeneity. As a result, there is a significant lack of meaningful quantitative monitoring data collected at the landscape scale that can be accessed by land managers or ranchers for decision making (Bestelmeyer and Briske, 2012).

Research into remotely sensed approaches that provide estimates of commonly monitored rangeland attributes such as above ground biomass (e.g. Anderson et al., 1993; Jansen et al., 2018; Todd et al., 1998), vegetation fractional cover (e.g. Hagen et al., 2012; Marsett et al., 2006) or bare ground (e.g. Guerschman et al., 2009) has increased in recent years. Quantifying grazing-induced vegetation responses with remotely sensed data has been performed in a variety of ways, utilizing single year analysis to compare estimated vegetation amounts between pixels with different grazing levels (Jansen et al., 2016; Numata et al., 2007), or with timeseries analysis to track a vegetation index over time as a proxy for vegetation change to understand vegetation responses to drivers such as climate variability

and grazing management (Archer, 2004; Evans and Geerken, 2004; Washington-Allen et al., 2006; Wessels et al., 2012). Remote sensing research also continues to explore monitoring spatial heterogeneity with spatial statistics (Sankey et al., 2009; Scarth and Trevithick, 2017; Virk and Mitchell, 2015). While these studies highlight the ability of remotely sensed data to quantify vegetation amounts, characterize spatial heterogeneity and elucidate potential drivers of vegetation change, web-based platforms that easily display and analyzed vegetation monitoring data derived from remotely sensed data have only recently been created and made available to ranchers and or managers (e.g. RDMapper, Ford et al., 2017; https://vegmachine.net/; http://climateengine.org/ (Huntington et al., 2017); https://rangelands.app/ (Jones et al., 2018). Therefore the introduction of remotely sensed vegetation monitoring datasets into adaptive management frameworks is relatively new and their potential value is still being assessed.

To incorporate remotely sensed monitoring indicators into adaptive management of livestock grazing it is important to identify the types of indictors that are used in a decision-making context. Herrick et al., 2012 breaks down rangeland monitoring indicators into three groups 1) driving mechanisms (e.g. stocking rates, animal type, rotations) 2) short term responses (e.g. residual biomass or utilization), and 3) long term responses (e.g. species composition, soil stability). Short term indicators characterize direct impacts of drivers on ecosystem attributes and are used to adaptively manage in a timely manner and help interpret trends detected in long term indicators (Herrick et al., 2012). Long term indicators capture trends in ecosystem process and function and provide additional feedback about the influence of drivers (Herrick et al., 2012). This framework is helpful for defining monitoring objectives and clarifying the relationships between the short term monitoring indictors and the meaningful processes or phenomena in question (Herrick et al., 2012). As with field monitoring data, remotely sensed monitoring data should be tested and applied within existing adaptive management objectives and decision-making cycles.

In this paper we evaluate the utility of a remotely sensed biomass product created for a grassland in northeast Oregon (Jansen et al., 2018) to monitor short term vegetation responses to cattle grazing. Our two main objectives are 1) to determine which remotely sensed biomass metrics at the pasture scale have the strongest correlations to prescribed stocking rates, a driving mechanism indictor (also at the pasture scale), and 2) to determine which remotely

sensed biomass datasets are most correlated to in-field estimates of end of year utilization, a short-term response indicator used to monitor grazing at the plot scale. Using results from the second objective, we further explore a possible classification of biomass change and fall biomass raster datasets to demonstrate how the remote sensing vegetation data can be used as decision support for adaptive management.

## 2.0. Methods

### 2.1 Study area

This study took place on the Zumwalt Prairie in northeast Oregon which is a highly valued remnant of Pacific Northwest Bunchgrass Prairie (Figure 4.1). The Zumwalt Prairie is moderately productive (1200-1900 kg · $ha^{-1}$), privately owned and used primarily for cattle production. The Nature Conservancy, a private land owner within the study area, has been monitoring and adaptively managing livestock grazing to be compatible with conservation goals since 2006. Across the conservation area, residual vegetation and utilization have been measured annually to provide feedback to managers regarding livestock impacts. These measures, along with calculated indices of grazing response (GRI) (Reed et al., 1999) and managers' casual observations provide the "best available" information to interpret grazing effects and adjust timing and stocking rates for the following year's grazing rotation. Field and management data used in this study comes from two management units that have different grazing strategies. One unit (Unit 1) strives to keep stocking rates below a threshold of 0.7 animal unit months per hectare (AUM · $ha^{-1}$), based on research showing that stocking rates above that threshold had detrimental effects on invertebrates, songbird nesting and soil compaction (Johnson et al., 2011; Kimoto, 2012; Schmalz et al., 2013). The second unit (Unit 2) uses higher stocking rates with shorter durations and longer periods of rest for each pasture. Although the two management units have different management strategies, the long-term outcomes of sustaining productivity and preventing conversion to non-desirable vegetation are mutually desired.

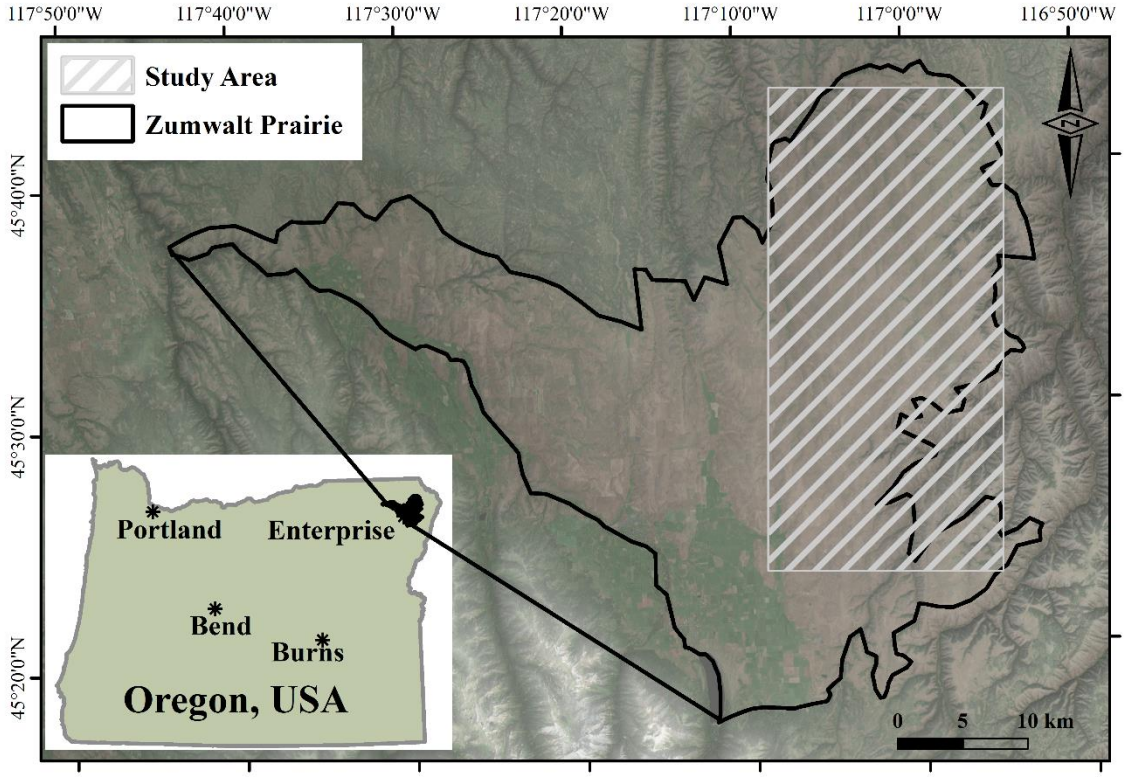


Figure 4.1. The Zumwalt Prairie, a pacific northwest bunchgrass prairie ecosystem located in northeastern Orgon. The field and management data came from two management units located on the eastern side of the larger grassland area.

## 2.2 Grazing Management and Monitoring Data

### 2.2.1 Pasture Stocking Rate Data

Across the three-year study period (2015 – 2017), stocking rates were calculated by pasture for each year based on records provided by managers including dates, number and type of grazing animal, and accessible hectares per pasture. Stocking rates are expressed as Animal Unit Months per hectare (AUM · $ha^{-1}$). Adjustments were made in animal use equivalencies (AUE) for different types of animals (e.g. bulls had 1.2 AUE, yearlings 0.75 AUE, and cow-calf pairs 1.0 AUE). Each stocking rate for each pasture in each year was categorized by season of use based on the grazing timing: Cool Summer (May 1 – June 30), Hot Summer (July 1 – September 15) and Fall (September 16 – November 30). When grazing dates overlapped two seasons, the season with the majority of grazing days was used. Average

stocking rates across the study period were 0.34 AUM · $ha^{-1}$ for Unit 1 and 0.73 AUM · $ha^{-1}$ for Unit 2.

2.2.2 Utilization data

Plot-scale utilization data were collected across the 2015-2017 field seasons using the Landscape Appearance Method (Coulloudon et al., 1999). In this rapid qualitative method, observers look for evidence of grazing on key forage plants and classify the plot into one of six categories corresponding to percent utilization. Monitoring plots were selected in a systematic random manner across the diversity of habitat types on the prairie including uplands, headwater swales and ephemeral stream reaches. We used utilization monitoring data from two different monitoring surveys, one from stubble height surveys (collected from 2015-2017) and the other from visual obstruction monitoring (collected only in 2015 and 2016). Plots were revisited in the field each year with a Garmin GPS unit but were not permanently marked. Plot selection was made without prior knowledge of typical patterns of livestock use within pastures; determination of "key areas" as are typically used for utilization estimates were considered. All utilization estimates were made at the end of the season (September – November) regardless of when cattle were moved out of pastures.

**2.3 Landsat Satellite Data Scene Selection**

To identify summer and fall Landsat scenes to be used for analysis, we used ClimateEngine (ClimateEngine.org) to calculate annual biomass curves based on biomass algorithms developed for this site (Jansen et al., 2018). Due to known differences in dominant plant phenology which impacts the timing of maximum summer biomass across the study area (Figure 4.2) we selected two different summer scenes corresponding to summer biomass for each year and one fall scene to compute fall or end of season residual biomass. (Table 4.1). The fall scene selected was the latest and clearest scene we could find for each year.

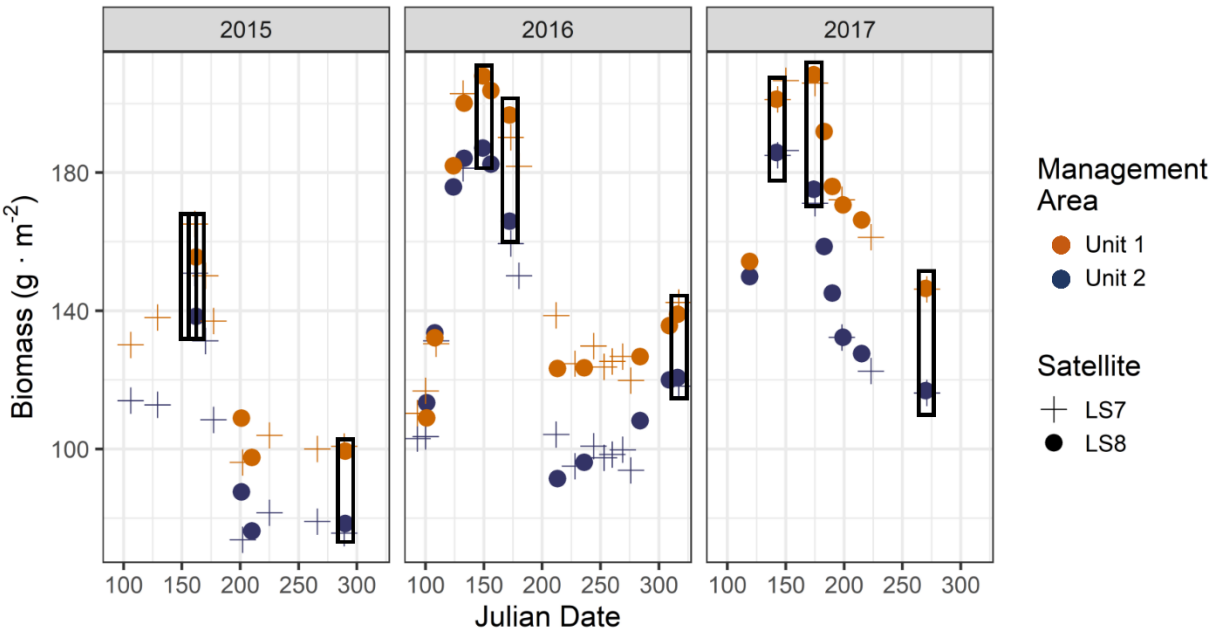


Figure 4.2. Scene selection for summer and fall biomass estimates across the Zumwalt Prairie, Oregon. Landsat 8 data (closed circles) were given preference to increase the available data used for pasture level statistics. Only in 2015 did we use a Landsat 7 summer scene to compare to the fall Landsat 8 scene. The scenes selected are boxed in with black rectangles.

We downloaded the climate data record (CDR) Collection1 Level 2 product for each of the scenes selected from the prior step off the USGS Earth Explorer (https//earthexplorer.usgs.gov/) website. These scenes are terrain-corrected and processed to at-surface reflectance. For each scene the pixel quality assurance band (pixel_qa) and aerosol band were used to mask clouds, cloud shadows, and smoke over the study site. We also masked out non-grassland vegetation as defined by the ReGap Ecological Systems data (Kagan et al., 2006) and manually masked any tree or shrub visible with the 2014 National Agriculture Inventory Program (NAIP) imagery that the ReGap Ecological Systems data mis-classified as tree or shrub habitat. With each masked scene, we computed above ground biomass for each pixel using the biomass algorithm developed for this study area (Jansen et al., 2018). This algorithm was observed to have a root mean squared difference (RMSD) of 34.6 $g \cdot m^{-2}$ and 32.2 $g \cdot m^{-2}$ using Landsat 7 and Landsat 8 CDR products respectively to predict above ground biomass across the growing season (Jansen et al., 2018). Once biomass raster data was computed for each scene (Early Summer, Late Summer, and Fall), we created relative difference biomass raster datasets for each year using following the equation:

((Fall Biomass Raster – Summer Biomass Raster) / Summer Biomass Raster)*100

For the summer period, we created two biomass raster datasets in each year, we created yearly pixel and pasture scale maximum biomass composites to capture the maximum values representing peak biomass production. The max summer pixel composites (Summer MaxPixel) were computed by selecting the maximum biomass value for each pixel value across the two summer biomass scenes. For the max summer pasture composites (Summer MaxPasture), the selection of raster data for the composite was guided by which scene produced the maximum average biomass across each pasture. We did not create fall composite images and instead elected to use the latest single fall scene for each year, that was cloud free, corresponding to end of year residual biomass. For the pasture scale analysis objective, we elected to only use the maximum pasture average in order to keep the biomass patterns true to one point in time and congruent with the scale of analysis for spatial statistics and interpretation purposes (Table 4.1). We then computed relative difference (RelDif) raster datasets using all the summer biomass rasters (early, late, maxpasture, maxpixel).

Table 4.1. Scenes selected for the analysis and associated biomass raster datasets used for the pasture and plot scale analysis.

| Year | Summer Scene Dates (Sensor) | Fall Scene Dates (Sensor) | Pasture Scale - Biomass Raster Datasets | Monitoring Plot Scale - Biomass Raster Datasets |
|---|---|---|---|---|
| 2015 | 6/10 (LS7), 6/11 (LS8) | 10/16 (LS8) | Summer Max Pasture<br>Fall<br>$RelDif_{maxpasture}$: Max Pasture to Fall | Early Summer<br>Late Summer<br>Fall<br>$RelDif_{maxpasture}$: Max Pasture to Fall<br>$RelDif_{maxpixel}$: Max Pixel to Fall<br>$RelDif_{EarlyScene}$: Early Summer to Fall<br>$RelDif_{LateScene}$: Late Summer to Fall |
| 2016 | 5/28 (LS8), 6/20 (LS8) | 11/11 (LS8) | | |
| 2017 | 5/22 (LS8), 6/23 (LS8) | 10/29 (LS8) | | |

**2.4. Computing pasture and ranch level biomass statistics**

For each pasture area that had a corresponding grazing record we used the biomass raster datasets from each year to compute a variety of summary and spatial statistics (Table 4.2). The general summary statistics calculated using the biomass raster data by pasture included the mean, the 10$^{th}$, 25$^{th}$, 50$^{th}$, 75$^{th}$, and 90$^{th}$ percentiles, as well as the standard deviation and coefficient of variation. To explore measures of spatial heterogeneity we computed the sill, nugget, range and magnitude of spatial heterogeneity (MSH) from theoretical variograms. Variograms provide measures of variance between all pairs of points across distances (i.e. bins). The computation of variograms takes the form:

$$\gamma(h) = \frac{1}{2n}\sum_{i=1}^{n} |z(s_i) - z(s_{i+h})|^2$$

Where $\gamma(h)$ is the semivariance for the distance bin h, z is the value of the biomass variable at two locations $s_i$ *and* $s_{i+h}$, with h signifying the distance between each pair and n is the number of pairs of sampling locations across each lag (or bin) h. For each pasture area we fit theoretical exponential and spherical models to the empirical variogram using the GSTAT package (Pebesma, 2004) in R version 3.3.3 (R Development Core Team, 2016) (http://www.r.project.org). The spherical model decreased model error across the majority of pasture areas tested, therefore we selected the output from this model to report statistics on. Using the theoretical spherical model, the sill, the range, and nugget were quantified. The sill is the leveling off point of the variance, where the variance of the data no longer increases (Bellehumeur and Legendre, 1998). The nugget is the y-axis intercept which represents sampling error, or within sampling unit variability (Townsend & Fuhlendorf, 2010; Western, Blöschl, & Grayson, 1998; Fortin and Dale, 2005). The range is a measure of the distance at which values are no longer correlated (Legendre and Fortin, 1989). This statistic is also thought as a measure of patch size (Townsend and Fuhlendorf, 2010). From the sill, nugget and range values we then calculated the magnitude of spatial heterogeneity (MSH) (Lane and BassiriRad, 2005; Lin et al., 2010). The MSH is calculated by dividing the spatially structured variation (the sill – the nugget) by the total sample variation (the sill) (Lane and BassiriRad, 2005). The MSH ranges in values from 0 to 1, with zero indicating no spatially structured heterogeneity and 1 indicating high structured heterogeneity (Virk and Mitchell, 2015). We

also calculated the Global Moran's I to explore how the spatial pattern of biomass relates to grazing management (e.g. Sankey et al., 2009).

Table 4.2. Pasture Statistic computed for each scene and year

| Statistic Type | Metric | Raster Datasets Analyzed | Computation Citation |
|---|---|---|---|
| Spatial heterogeneity | Variogram – Sill, Nugget, Range, MSH | Summer, Fall, Relative Diff | GStat (Pebesma, 2004) |
| Spatial heterogeneity | Global Moran's I | Summer, Fall, Relative Diff | Spdep (Bivand et al., 2013; Bivand and Piras, 2015) |
| Non-Spatial Heterogeneity | Coefficient of variation | Summer, Fall, Relative Diff | |
| Summary | Mean, Percentiles (10,25,50,75,90), Standard Deviation | Summer, Fall, Relative Diff | |

**2.5. Correlation to a driving indictor: Identifying the remotely sensed biomass metrics most sensitive to AUMs per hectare at the pasture scale**

To identify the biomass pasture metrics most sensitive to stocking rate at the pasture scale we calculated Spearman rank correlation coefficients between the pasture stocking rates ($AUM \cdot ha^{-1}$) and the biomass metrics listed in Table 4.2. Pastures used for statistical analysis had to meet the following conditions: 1) the pasture had to contain at least 20 valid pixels, 2) valid pixels had to account for more than 33% of all possible pixels within the pasture (i.e pastures that were mostly obscured by clouds were dropped), 3) the pasture had to be dominated by upland grassland vegetation (i.e. exclusion of canyon grassland pastures), 4) the period of grazing in the pasture had to occur between the selected summer and fall Landsat scenes, 5) pastures could not be used for supplemental feeding with hay. We also included ungrazed pastures that met criteria 1 – 3 and 5. The percentage of pastures that met the above criteria were 32.7% for 2015 (21% of pastures were removed due to clouds), 53.1% for 2016, and 59.0% for 2017. We performed this analysis for each year individually and all years

combined, as well as by season of use (Spring, Cool Summer, Hot Summer, Fall) using all years combined. Only significant (< 0.05 p-value) correlations are reported in this paper (see supplemental information for the complete list).

**2.6 Correlation to a short-term response indicator: Identifying the metrics most sensitive to end of year grazing utilization at the plot scale**

To identify the biomass raster datasets most sensitive to end of year grazing utilization, we computed Spearman rank correlations between in-field percent utilization with the mean and minimum biomass values extracted across a 2 x 2 pixel window intersecting each in-field monitoring plot. We did this for each of the raster datasets listed in Table 4.1 (monitoring plot scale analysis). For this plot-level analysis we again only used the in-field data from pastures that were grazed between the dates of the satellite overpasses or ungrazed across the entire year. We also limited the in-field dataset to only data collected in October and November to better match the timing of our remotely sensed fall data.

**2.7. Classifying biomass raster datasets to demonstrate the use of empirically-derived thresholds for monitoring and management interpretations.**

Using select raster datasets with significant relationships to the plot-level utilization estimates from the above step, we created boxplots and determined the median raster values associated with the in-field utilization classes aligned with the Landscape Appearance method (Table 4.4). We selected two breakpoints for a 3-class raster classification (low, medium and high) based on the median raster values corresponding to the midpoint of two utilization classes: 13% (midpoint of the 6 – 20% utilization class), and 50.5% (midpoint of the 41 – 60% utilization class). Thus the "Low" raster class represents the 0 – 5% utilization class; the "Med" raster class represents utilization classes between 6 and 40% and the "High" raster class represents utilization classes > 40%. The breakpoints selected here are based on prior research conducted in this habitat which established a 30 to 40% utilization guideline for bunchgrass vegetation to remain productive (Holechek, 1988; Skovlin et al., 1976) and that high stocking rates with utilization measures averaging above 35% across a pasture can be detrimental to grassland songbird nesting (Johnson et al., 2012). Large inter-annual variation in total production caused us to compute separate threshold values for the fall biomass raster dataset for 2015 (low annual production) and for 2016-2017 biomass raster data (high annual production; Figure A3.1). We did not separate the relative difference raster analysis based on

inter-annual variability, because in theory the relative difference equation should normalize the year to year variation in production. Using the biomass raster thresholds derived from their empirical relationship to in-field utilization, we mapped these categories across the study area to reveal patterns of end of year vegetation amounts and change in vegetation amounts between summer and fall.

## 3.0. Results

### 3.1. Biomass metrics most sensitive to stocking rate at the pasture scale

Spearman rank correlation coefficients between the pasture scale biomass metrics and pasture stocking rates revealed that the summary statistics were more consistently related to stocking rate compared to spatial statistics metrics derived from variogram models (Table A3.1). For each year of analysis (2015,2016,2017) using pasture scale biomass metrics, the estimated pasture area Fall biomass mean, and percentile metrics were negatively associated with higher stocking rates while coefficient of variation (CV) metric was also significantly correlated, but with a positive correlation to stocking rate (Table 4.3). With the pasture maximum relative difference raster, the 10th percentile was most strongly correlated to stocking rate across all years, with the mean, median and the 25th percentile also being significantly correlated. While these correlations are significant, none are above an absolute r value of 0.60, indicating a moderate to weak fit. Also, there was a decrease in the correlation coefficient when grouping data across the three years, for example the Fall mean biomass correlations for each single year had stronger negative correlations (< -0.50), compared to when all the data was grouped across all years (r = -0.28).

Table 4.3. Spearman rank correlations between stocking rate (AUM · $ha^{-1}$) and biomass raster statistics at the pasture scale. This table shows only the metrics that are significant across all years of data. For the complete table see appendix (Table A3.1).

| Raster Statistic | 2015 | | | 2016 | | | 2017 | | | All Years | | | 3-Yr Mean |
|---|---|---|---|---|---|---|---|---|---|---|---|---|---|
| | r | p-val | N | r | p-val | N | r | p-val | N | r | p-val | N | r |
| $Fall_{mean}$ | **-0.55** | **0.00** | 37 | **-0.56** | **0.00** | 60 | **-0.52** | **0.00** | 72 | **-0.28** | **0.00** | 169 | -0.54 |
| $Fall_{p10}$ | **-0.56** | **0.00** | 37 | **-0.59** | **0.00** | 60 | **-0.49** | **0.00** | 72 | **-0.24** | **0.00** | 169 | -0.55 |
| $Fall_{p25}$ | **-0.53** | **0.00** | 37 | **-0.57** | **0.00** | 60 | **-0.50** | **0.00** | 72 | **-0.26** | **0.00** | 169 | -0.53 |
| $Fall_{p50}$ | **-0.52** | **0.00** | 37 | **-0.54** | **0.00** | 60 | **-0.50** | **0.00** | 72 | **-0.27** | **0.00** | 169 | -0.52 |
| $Fall_{p75}$ | **-0.54** | **0.00** | 37 | **-0.51** | **0.00** | 60 | **-0.51** | **0.00** | 72 | **-0.29** | **0.00** | 169 | -0.52 |
| $Fall_{p90}$ | **-0.53** | **0.00** | 37 | **-0.49** | **0.00** | 60 | **-0.56** | **0.00** | 72 | **-0.30** | **0.00** | 169 | -0.53 |
| $Fall_{CV}$ | **0.50** | **0.00** | 37 | **0.51** | **0.00** | 60 | **0.32** | **0.01** | 72 | **0.16** | **0.04** | 169 | 0.44 |
| $RelDiff_{mean}$ | **-0.32** | **0.05** | 37 | **-0.33** | **0.01** | 60 | **-0.54** | **0.00** | 72 | **-0.30** | **0.00** | 169 | -0.40 |
| $RelDiff_{p10}$ | **-0.50** | **0.00** | 37 | **-0.52** | **0.00** | 60 | **-0.47** | **0.00** | 72 | **-0.38** | **0.00** | 169 | -0.50 |
| $RelDiff_{p25}$ | **-0.44** | **0.01** | 37 | **-0.47** | **0.00** | 60 | **-0.47** | **0.00** | 72 | **-0.34** | **0.00** | 169 | -0.46 |
| $RelDiff_{p50}$ | **-0.34** | **0.04** | 37 | **-0.33** | **0.01** | 60 | **-0.48** | **0.00** | 72 | **-0.27** | **0.00** | 169 | -0.38 |

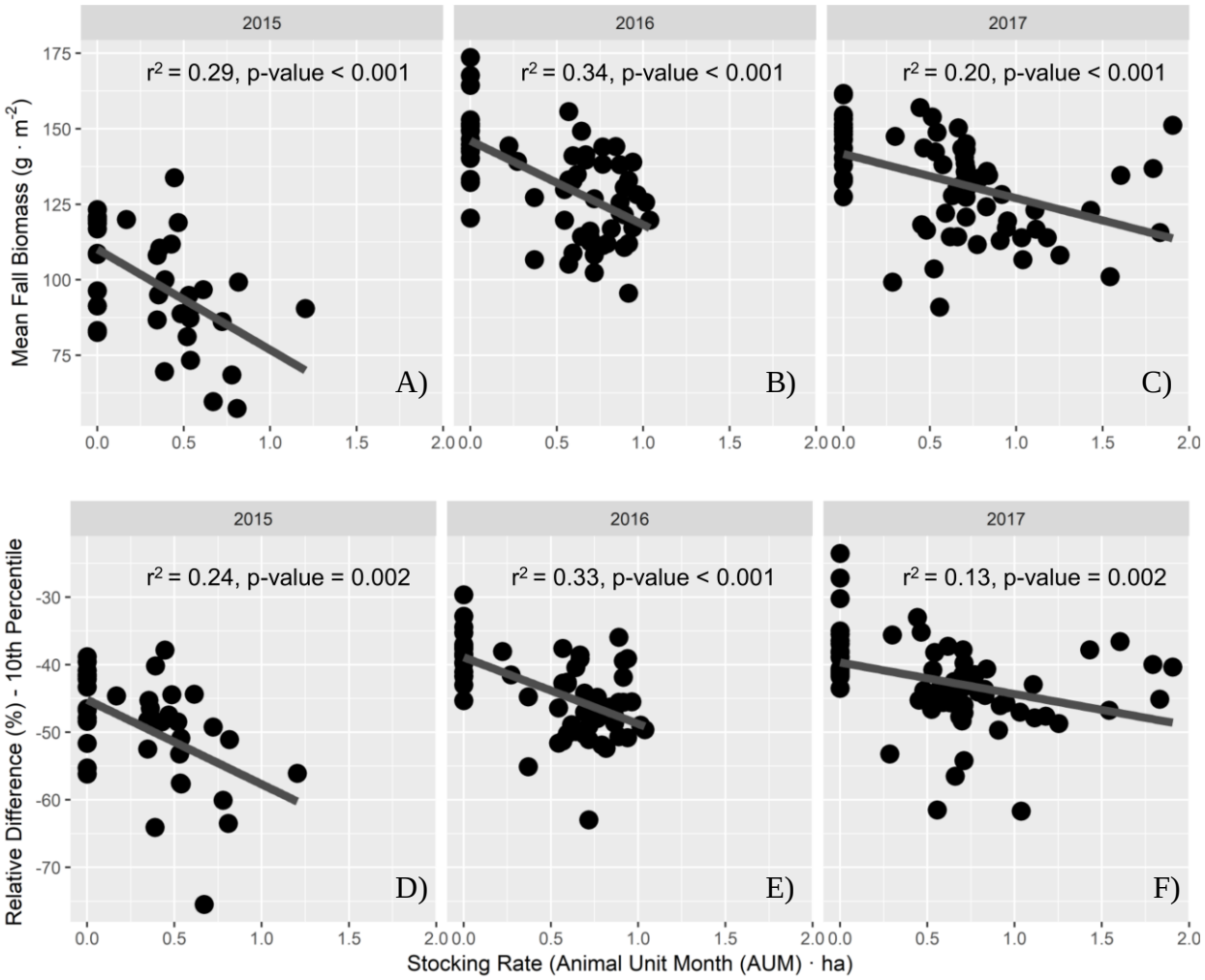


Figure 4.3. Relationships of select metrics, Mean Fall Biomass (A-C), and the Relative Difference 10th Percentile (D-F) for each year with stocking rate. The linear regression line for each plot is represented by the grey line, while each pasture is represented by a black dot.

### 3.2. Biomass raster data most sensitive to grazing utilization at the plot scale

Correlation coefficients between in-field utilization data collected at monitoring plots and the spatially corresponding biomass pixel values showed significant negative correlations. Similar to the pasture scale analysis results, the correlations were weak to moderately correlated, with all r values lower than an absolute value of 0.70. In all cases except for Fall biomass, the minimum pixel value in the 2 x 2 pixel window had stronger negative correlation compared to the average value across the 2 x 2 pixel window. The minimum pixel value from the relative difference raster, regardless of which summer scene or composite was used, were all significantly related to in-field utilization, with the Early Summer scene tending to have

the most significant correlations across the study period (Table 4.4), likely due to a reduced sample size that omitted outliers which were included in the other relative difference raster correlations.

Table 4.4. Spearman rank correlations between infield utilization measures and biomass raster data at the plot scale.

| Raster | 2x2 pixel window statistic | 2015 | | | 2016 | | | 2017 | | | All Years | | |
|---|---|---|---|---|---|---|---|---|---|---|---|---|---|
| | | r | p-val | N | r | p-val | N | r | p-val | N | r | p-val | N |
| Fall | Mean | **-0.33** | **0.00** | **197** | **-0.46** | **0.00** | **208** | **-0.47** | **0.00** | **114** | **-0.21** | **0.00** | **519** |
| $RelDif_{MaxPixel}$ | Mean | **-0.20** | **0.01** | **202** | **-0.44** | **0.00** | **214** | **-0.49** | **0.00** | **114** | **-0.38** | **0.00** | **530** |
| $RelDif_{MaxPasture}$ | Mean | -0.07 | 0.36 | **113** | **-0.32** | **0.00** | **208** | **-0.50** | **0.00** | **114** | **-0.26** | **0.00** | **435** |
| $RelDif_{EarlyScene}$ | Mean | **-0.39** | **0.00** | **96** | **-0.45** | **0.00** | **203** | **-0.69** | **0.00** | **114** | **-0.45** | **0.00** | **413** |
| $RelDif_{LateScene}$ | Mean | **-0.22** | **0.00** | **196** | **-0.14** | **0.04** | **208** | **-0.40** | **0.00** | **114** | **-0.24** | **0.00** | **518** |
| Fall | Min | **-0.31** | **0.00** | **197** | **-0.44** | **0.00** | **208** | **-0.47** | **0.00** | **114** | **-0.20** | **0.00** | **519** |
| $RelDif_{MaxPixel}$ | Min | **-0.26** | **0.00** | **202** | **-0.45** | **0.00** | **214** | **-0.53** | **0.00** | **114** | **-0.40** | **0.00** | **530** |
| $RelDif_{MaxPasture}$ | Min | **-0.29** | **0.00** | **113** | **-0.52** | **0.00** | **208** | **-0.63** | **0.00** | **113** | **-0.45** | **0.00** | **434** |
| $RelDif_{EarlyScene}$ | Min | **-0.35** | **0.00** | **84** | **-0.48** | **0.00** | **203** | **-0.69** | **0.00** | **114** | **-0.46** | **0.00** | **401** |
| $RelDif_{LateScene}$ | Min | **-0.29** | **0.00** | **196** | **-0.21** | **0.00** | **208** | **-0.44** | **0.00** | **114** | **-0.28** | **0.00** | **518** |

### 3.3 Classifying raster datasets based on empirically defined utilization thresholds.

The boxplots of the Fall and RelDif raster data grouped by each Landscape Appearance utilization grazing class, revealed overlapping distributions of data across groups with the median raster value decreasing with increased grazing utilization (Table 4.4). To classify the change in biomass across the year we elected to use the $RelDif_{MaxPixel}$ raster dataset, because it had the largest number of valid pixels (i.e. spatial coverage) providing the largest sample size across the study period (i.e. the least amount of missing data due to clouds) (Table 4.4). The relative difference boxplots median values grouped by utilization class, produced a small range in median values from -36% to -50%. This range is much smaller compared to the corresponding in-field utilization range, which extends from 0% to 94%, illustrating the differences between the remotely sensed and in-field short-term indicators. With the fall biomass data, there was around 20 $g \cdot m^{-2}$ difference separating the Medium from the High raster classes within both the low and high production years. The difference in raster values across production years (i.e. high year - low year for any graze class) was approximately 40 $g \cdot m^{-2}$. The increased difference observed between low and high

production years, as compared to the within year differences illustrates the importance of climate as a major influence on end of year residual biomass (Table 4.5).

Table 4.5. Defining biomass raster class thresholds using the median biomass pixel values grouped by in-field utilization classes. Bold values were used as breakpoints for raster classification.

| Grazing Utilization Range (%) | Graze Class Midpoint (%) | Relative Difference (%) | Fall Biomass High ($g/m^2$) | Fall Biomass Low ($g/m^2$) | Raster Class (degree of change) |
|---|---|---|---|---|---|
| 0 - 5 | 2.5 | -35.87 | 153.93 | 119.42 | Low |
| 6 - 20 | 13 | **-39.53** | **150.92** | **110.34** | Med |
| 21 - 40 | 30.5 | -41.77 | 135.94 | 93.45 | Med |
| 41 - 60 | 50.5 | **-42.63** | **129.70** | **90.13** | High |
| 61 - 80 | 70.5 | -47.16 | 122.39 | 63.60 | High |
| 81 - 94 | 87.8 | -50.17 | 128.98 | NA | High |

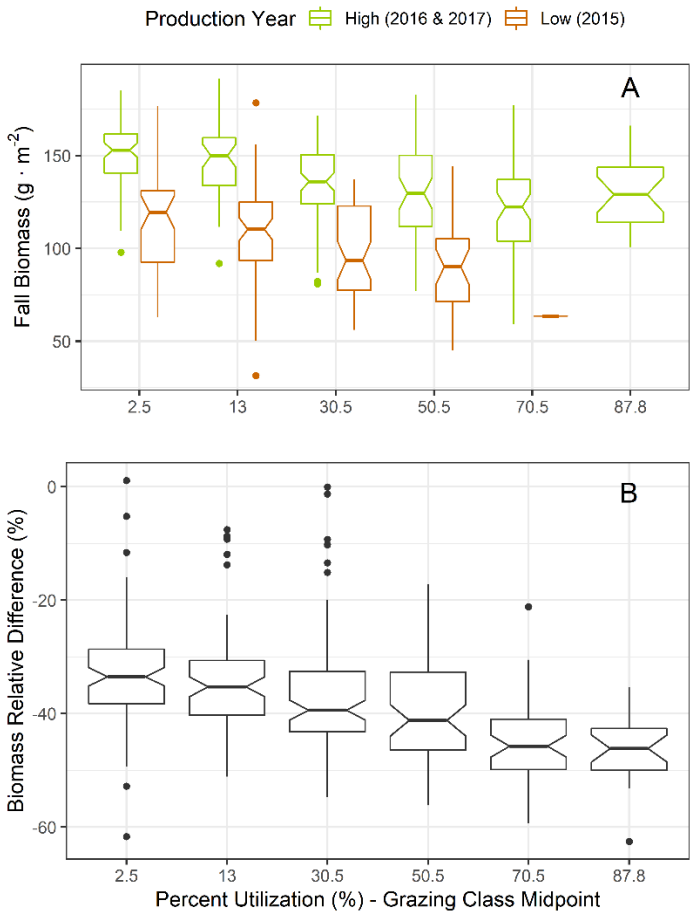


Figure 4.4. Boxplots of the (A) fall biomass and (B) relative difference raster at each of the utilization monitoring plots grouped by graze class. The fall biomass (A) data for 2015, a low production year, are shown in orange (N=197), while the high production year data are shown with green (N=322). The narrow boxplot for the 70.5 graze class in 2015 was due to only one recorded observation in the 70.5 graze class. The relative difference in biomass (B) obtained from the minimum value of the 2 x 2 pixel window when using the max summer pixel composite to compute the relative difference raster is represented by black boxplots (N=530).

## 4.0 Discussion

Biomass estimates derived from Landsat satellite data were significantly correlated to both a driving indicator (stocking rate) and a short-term response indicator (utilization), demonstrating the potential for remote sensing to inform adaptive rangeland management. The application of remote sensing to rangeland management is powerful because of its capacity to provide vegetation estimates continuously across landscape scales that are not feasible to evaluate with infield monitoring data. However, this source of information is

relatively new to most managers, and it is necessary to build evidence based on empirical relationships to begin relating common in-field monitoring metrics to remote sensing metrics.

Before investigating the potential to use remote sensing as a tool for monitoring short term responses, we first wanted to establish the strength of the relationship between remote sensing data and the fundamental management driver in rangelands: stocking rate. In our study, because stocking rates at the pasture scale had consistently strong correlations with the fall mean biomass, and the relative difference 10th percentile, we recommend using these metrics (See Figure 4.5) for monitoring applications in this system. While we explored the use of spatial heterogeneity metrics provided by variograms and the Moran's I, these metrics were not consistently sensitive to stocking rate across all years. This finding aligns with Jansen 2018 (Chapter 3) which showed that the 30 x 30m spatial resolution is too large to detect finer scale changes in vegetation patch size and heterogeneity that grazing induces on this already highly heterogeneous landscape (Chapter 3). Our biomass to stocking rate relationships were weaker than Jansen et al., 2016 who found an r-squared of 0.79 when experimentally controlling the timing and duration and Numata et al., 2007 who found an r-squared of 0.70 and focused on one grass species and had many pasture areas with higher stocking rates. We were not surprised to find weaker relationships in our study, which was observational and therefore did not control for historical land use and management effects, timing of grazing, stocking rate, or habitat types. Timing of grazing is particularly important; stocking rate as a driver is not expected to be strongly related to total change in biomass as calculated between the summer and fall scenes in pastures that were grazed early in the season and had an opportunity for re-growth before the summer drought period began (typically late July). Furthermore, stocking rate does not account for reductions in biomass incurred from other herbivores (trespass cattle, elk, ground squirrels, and insects) or from senescence, all of which affect our correlation results. For example, elk populations in northeast Oregon have been increasing since the 1990s, with recent estimates between 1000 – 2500 animals on the Zumwalt Prairie (ODFW, unpublished data). Their effects on vegetation are not accounted for in our study.

Relating the biomass raster data to in-field grazing utilization collected at the plot scale produced similar correlation coefficient values as compared to our analysis with stocking rates at the pasture scale. The differences in the Spearman rank correlation

coefficients between the early and late summer relative difference biomass data, reveals the effect that intra-year biomass variability (i.e. plant phenology) has on analysis results. Accounting for this within year variability in the timing of maximum biomass estimates is important for accurate and meaningful results (Evans and Geerken, 2004). Here we account for this variability by presenting results of the relative difference raster using the summer max pixel composite. We selected to present these results over the other relative difference raster datasets for two reasons: 1) the $RelDif_{maxpixel}$ dataset contained the most valid data (i.e. least obscured by clouds) which produced the largest sample size thus encompassing the full range of values in this complex landscape 2) we felt that the maximum pixel analysis procedure used to create the $RelDif_{maxpixel}$ data is more robust to year to year variability and more straightforward to calculate consistently in future years. The moderate to weak results between plot scale data and the biomass raster data was likely due to a variety of reasons. In-field utilization estimation is subjective and can have high observer variability (Smith et al., 2005). Also, geographic co-registration and the spatial scale of the field plot to the Landsat data can lead to spatial mismatches between the field plot and the Landsat pixels. Furthermore previous studies have shown that stratifying the landscape by habitat type improves statistical relationships (Kawamura et al., 2005) and in general is helpful when making inferences from sample data (Elzinga et al., 1998). Here we combined utilization data that were collected across sites with a variety of dominant species (i.e. rhizomatous grasses and bunchgrass species). We did this to produce a generalized end product that can be easily applied across the study area and interpreted for management decisions. We see this general grouping impact our final results observing a higher median value in the 87.8% utilization grass class compared to the 70.5% grass class using the high production fall biomass data. This is due to the utilization estimates in the 87.8% class only being collected during stubble height surveys in 2017 which were predominately collected within riparian sites. These riparian sites closer to water sources, typically have higher amounts of vegetation compared to upland sites. As with stocking rate, the timing of grazing relative to the opportunity for re-growth within the growing season contributes variability to the relationship between in-field utilization and biomass raster data.

Associating traditional management and field data used to monitor relevant abiotic or biotic indicators with remotely sensed data provides an important frame of reference that

increases the usefulness and application of satellite data for monitoring and management (e.g. Tsalyuk et al., 2015). Classification of the Fall and Relative Difference biomass raster datasets using threshold values derived from associating the raster data with a traditional utilization estimation method highlights areas with different amounts of vegetation change, locations of low and high residual biomass, as well as the inter-annual variability due to climate (Figure 4.4). In grassland systems variability in production driven by climate is well known (Briske et al., 2015), and an understanding of this inter-annual variation is important in both the management of these systems (Allen-Diaz et al., 1995; Joyce et al., 2013) as well as analysis procedures (e.g. Archer, 2004; Brinkmann et al., 2011; Evans and Geerken, 2004; Wessels et al., 2012). This is exemplified and easily visualized when applying thresholds derived during a low biomass year to a year with high biomass and visa-versa. For example, when we apply the low biomass classification to the 2016 Fall biomass data, the only places that appear to meet the "High" degree of change criteria are the patches that had received prescribed burns that year. In contrast, when applying the high production classification to the 2015 fall biomass the pixels with Low and Med degree of change fall mostly within old fields, pastures that have been rested for multiple years and areas close to stream channels—places that have the greatest productivity (Figure A3.2). Interpreting these results could lead to erroneous conclusions about livestock management, since the thresholds are not sensitive to the particular year in question. Calculating the relative difference in biomass between the summer and the fall helps to overcome the year to year variability as observed when mapping the fall residual biomass (Figure 4.4). Mapping the relative difference raster data across 2015-2017 shows a pattern aligned with management (grazing and fire) as well as past land use history such as cultivated fields. The small range (< 4%) between the Medium and High classification thresholds indicates weak sensitivity of this algorithm to quantifying moderate grazing at the 30m scale. Future research could seek to increase this range between the two classes by using more covariates within the statistical analysis (i.e. timing of grazing, summer rainfall etc.) or use a classification approach to attempt to map utilization into relevant classes and adjust in-field methods (i.e. plot size) to better align with the spatial resolution of Landsat data.

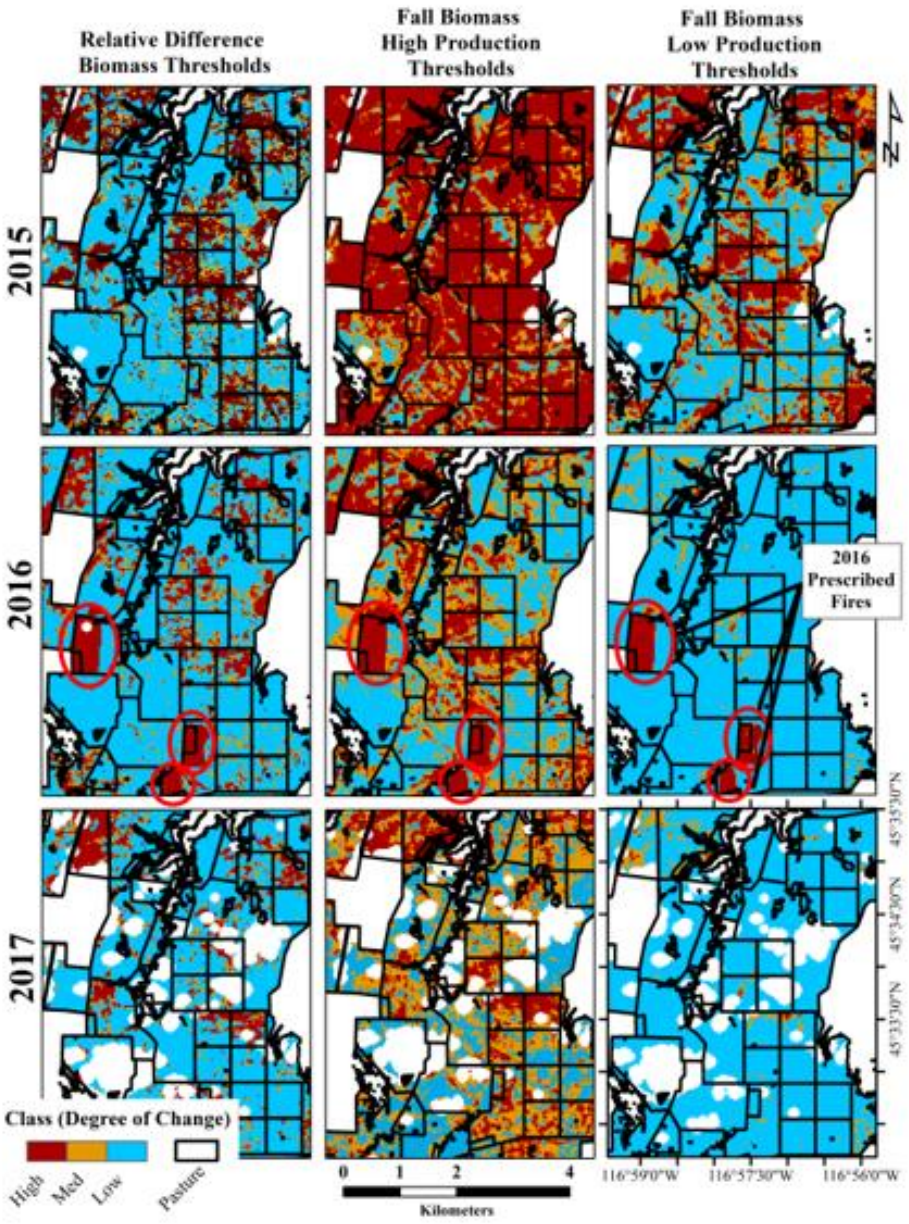


Figure 4.5. Classified relative difference and fall biomass maps using both low production and high production thresholds across 2015 to 2017. The 3 classes of change are high (red), medium (orange) and low (blue) with 2016 fires circled with red ovals.

## 5.0 Management and Monitoring Implications

In this observational study, we linked a primary driver (stocking rate) and common short-term response indicator (utilization) to satellite-derived biomass data, demonstrating the potential utility of satellite data in adaptive rangeland management. We purposely kept the input data and analysis as general as possible and acknowledge that the results showed

moderate to weak relationships between the remotely sensed biomass metrics and short-term grazing monitoring indicators. However, few relationships evaluated at management scales in rangelands are statistically robust, and we believe that more insight can be gleaned when plotting this data at the pasture scale and categorizing individual pastures by their management history and season of use (Figure 4.5). These plots allow for examination of outlier points that weaken statistical significance, and they highlight the utility of this data as an adaptive management or monitoring tool. For example, when plotting fall biomass across years at the pasture scale, several pastures with high stocking rates also had high fall biomass and showed less change between Summer and Fall, which was not expected. Further examination of these pastures revealed that they were grazed for 5 days each early in the season (late May to early June) during an above normal production year, and within high production pastures, allowing for significant re-growth by the time the fall scene was acquired. Plotting individual pastures in this way, combined with a manager's knowledge of the pastures' characteristics and grazing history, provides valuable feedback that can be integrated into adaptive management. In this example, the raster data improves a managers' confidence in the potential for re-growth under specific circumstances, which may lead to adjustments in timing or intensity of grazing in the subsequent year. At the other end of the stocking rate scale, plotting the 10th percentile of the relative difference by pasture revealed pastures that had abnormally large relative difference values. When reviewing this with the land manager, we learned that these two pastures had high use by trespass cattle, which was not accounted for in the manager's records. Highlighting areas with greater-than-desired changes in biomass could allow a manager to investigate reasons for the patterns, and if necessary reduce stocking rates, rest the pasture entirely for a year, or graze at a different time to ameliorate the conditions. The subsequent years' relative difference map and plots could then provide feedback about the management adjustments.

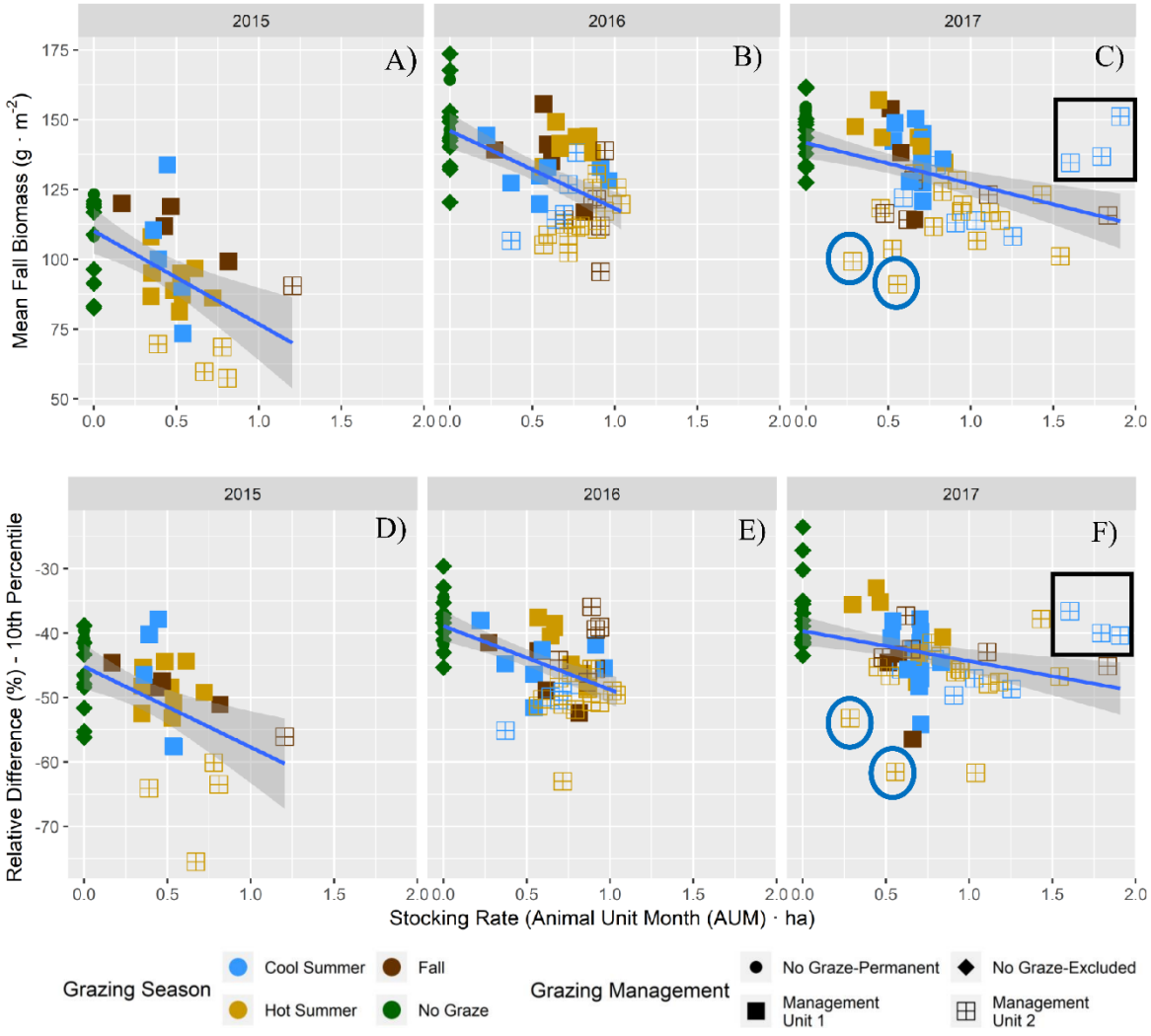


Figure 4.6. Relationships of select metrics, Mean Fall Biomass (A-C), and the Relative Difference 10th Percentile (D-F) for each year with stocking rate. The time of grazing (Grazing Season) is represented with color while the grazing management type are represented by different symbols. Three pastures grazed during the cool summer season are highlighted with the black box were grazed heavily for 5 days each from May 5/26 to 6/9 in 2017. Pastures with trespass cattle are highlighted with the blue circles.

Using threshold values to classify biomass maps is a straightforward way to display remote sensing data for quick interpretation. Applying thresholds to relative difference data reduces bias from inter-annual variability in production. Alternatively, managers can choose to derive thresholds from years with above average production to act as an indicator of areas which have the capacity to remain above ecologically relevant residual biomass thresholds even in low production years. Results such as these are important conservation tools which help to focus management on areas that have greater production or conservation potential (e.g.

Wiens et al., 2009), since the greatest difficulty may lie in maintaining the higher range of biomass quantity as climate variability is projected to increase with increasing concentrations of man-made greenhouse gases (IPCC 2012; Briske et al., 2015; Joyce et al., 2013). By mapping locations of biomass that in most years stays above important habitat thresholds, managers can try to ensure that the higher biomass component of their landscape remains intact, by removing management drivers that reduce vegetation amounts like fire or grazing, depending on the grassland system. We also propose that thresholds could be determined in other ways and guided by the rancher or manager. For example, managers who have spent time surveying pastures could choose a particular pasture to represent "moderate" use and that pasture could be used as the breakpoint for classification on a pasture scale.

Quantifying vegetation change between summer and fall, as well as residual biomass can provide an important base layer for improving sampling designs for in-field monitoring. For example, if the goal is to monitor grazing utilization efficiently and effectively, stratifying the landscape using the relative difference raster can potentially improve pasture or ranch wide estimates compared to a simple random sampling design. Also, the fall and relative difference maps could be used to identify critical and key areas to monitor for signs of overuse or trends in plant composition. The thresholds listed in this study should be continuously improved with new monitoring and research data and tested for applicability when land managers define new objectives. Ideally this remotely sensed data can advance the adaptive management cycle in an iterative process whereby the remotely sensed data improves in-field grazing monitoring efforts by providing better stratification for increased efficiency and in turn that yearly monitoring data would provide feedback to improve the remotely sensed classification of the fall and relative difference biomass monitoring products.

Lastly, we think it is also important to point out some considerations with how remotely sensed monitoring relates to current monitoring data and its interpretation for adaptive management. First, utilization and relative difference in biomass are estimates of two different things: utilization is an estimation of what percentage of forage plants have been removed, while relative difference in biomass is an estimate of the change in all vegetation, including losses due to senescence. These two indicators provide two frames of reference for the units regarding the estimation of vegetation change. The resulting differences in measurement units and associated ranges need to be investigated further to help managers

transition to using remote sensing indicators. At present, we do not consider relative difference to be a direct proxy for utilization. Second, because stocking rate does not account for reductions in biomass incurred from other herbivores (trespass cattle, elk, ground squirrels, and insects) or from senescence, we advise caution when interpreting patterns of total biomass change across a pasture; some of these changes were caused by livestock, but not all. For this reason, we refrain from interpreting relative difference maps strictly as indicators of livestock use patterns.

## 6.0 Conclusion

While many remote sensing studies seek to understand how stocking rate or grazing intensity change the above ground estimates of vegetation or vegetation indices (Jansen et al., 2016; Kawamura et al., 2005; Todd et al., 1998) few have related remotely sensed data to estimates of grazing utilization with a relative difference biomass raster data computed from pre and post grazing satellite scenes or estimates of end of season residual biomass. In performing the analysis in such a way, we hope that this technology will be more easily adopted and understood for short term monitoring and adaptive management. The ability to monitor large landscapes with satellite data is an important step in improving in-field data collection efforts, the adaptive management cycle and conservation outcomes at meaningful scales. In this study we attempted to move beyond the statistics of modeling of vegetation amounts with remotely sensed data and demonstrated how remotely sensed vegetation data can directly inform adaptive management.

## References

Adler, P., Raff, D., Lauenroth, W., 2001. The effect of grazing on the spatial heterogeneity of vegetation. Oecologia 128, 465–479. doi:10.1007/s004420100737

Alkemade, R., Reid, R.S., van den Berg, M., de Leeuw, J., Jeuken, M., 2013. Assessing the impacts of livestock production on biodiversity in rangeland ecosystems. Proc. Natl. Acad. Sci. 110, 20900–20905. doi:10.1073/pnas.1011013108

Allen-Diaz, B., Chapin, F.S., Diaz, S., M. Howden, J.P., Smith, M.S., 1995. Rangelands in a Changing Climate: Impacts, Adaptations, and Mitigation. Clim. Chang. 1995—Impacts, Adapt. Mitigation, W. T. Watson, M. C. Zinyowera, R. H. Moss, D. J. Dokken, (eds.), pp. 131–158.

Anderson, G.L., Hanson, J.D., Haas, R.H., 1993. Evaluating Landsat Thematic Mapper Derived Vegetation Indices for Estimating Above-Ground Biomass on Semiarid Ranglelands. Remote Sens. Environ. 45, 165–175.

Archer, E.R.M., 2004. Beyond the '" climate versus grazing "' impasse : using remote sensing to investigate the effects of grazing system choice on vegetation cover in the eastern Karoo 57, 381–408. doi:10.1016/S0140-1963(03)00107-1

Bartolome, J.W., Stroud, M.C., Heady, H.F., 1980. Influence of Natural Mulch on Forage Production on Differing California Annual Range Sites. J. Range Manag. 33, 4. doi:10.2307/3898219

Bellehumeur, C., Legendre, P., 1998. Multiscale sources of variation in ecological variables: Modeling spatial dispersion, elaborating sampling designs. Landsc. Ecol. 13, 15–25. doi:10.1023/A:1007903325977

Bestelmeyer, B.T., Briske, D.D., 2012. Grand Challenges for Resilience-Based Management of Rangelands. Rangel. Ecol. Manag. 65, 654–663. doi:10.2111/REM-D-12-00072.1

Bivand, R., Hauke, J., Kossowski, T., 2013. Computing the jacobian in gaussian spatial autoregressive models: An illustrated comparison of available methods. Geogr. Anal. 45, 150–179. doi:10.1111/gean.12008

Bivand, R., Piras, G., 2015. Comparing Implementations of Estimation Methods for Spatial Econometrics. J. Stat. Softw. 63. doi:10.18637/jss.v063.i18

Brinkmann, K., Dickhoefer, U., Schlecht, E., Buerkert, A., 2011. Quantification of aboveground rangeland productivity and anthropogenic degradation on the Arabian Peninsula using Landsat imagery and field inventory data. Remote Sens. Environ. 115, 465–474. doi:10.1016/j.rse.2010.09.016

Briske, D.D., Joyce, L. a, Polley, H.W., Brown, J.R., Wolter, K., Morgan, J. a, McCarl, B. a, Bailey, D.W., 2015. Climate-change adaptation on rangelands: linking regional exposure with diverse adaptive capacity. Front. Ecol. Environ. 13, 249–256. doi:10.1890/140266

Brunson, M.W., Huntsinger, L., 2008. Ranching As A Conservation Strategy: Can Old Ranchers Save The New West? Rangel. Ecol. Manag. 61, 137–147. doi:10.2111/07-063.1

Coulloudon, B., Eshelman, K., Gianola, J., Habich, N., Hughes, L., Johnson, C., Pellant, M., Podborny, P., Rasmussen, A., Robles, B., Shaver, P., Spehar, J., Willoughby, J., 1999. Landscape Appearance Method in Utilization Studies and Residual Measurements, Technical Reference 1734-3. Bureau of Land Management. 165 pp. 165.

Derner, J.D., Lauenroth, W.K., Stapp, P., Augustine, D.J., 2009. Society for Range Management Livestock as Ecosystem Engineers for Grassland Bird Habitat in the Western Great Plains of North America. Soc. Range Manag. 62, 111–118.

Elzinga, C., Salzer, D., Willoughby, J., 1998. Measuring and monitoring plant populations. BLM technical Reference 1730-1.

Evans, J., Geerken, R., 2004. Discrimination between climate and human-induced dryland degradation. J. Arid Environ. 57, 535–554. doi:10.1016/S0140-1963(03)00121-6

Ford, L.D., Butterfield, H.S., Van Hoorn, P.A., Allen, K.B., Inlander, E., Schloss, C., Schuetzenmeister, F., Tsalyuk, M., 2017. Testing a Remote Sensing-Based Interactive System for Monitoring Grazed Conservation Lands. Rangelands 39, 123–132. doi:10.1016/j.rala.2017.06.005

Fuhlendorf, S.D., Engle, David, M., 2001. Restoring Heterogeneity on Rangelands : Ecosystem Management Based on Evolutionary Grazing Patterns. Bioscience 51, 625–632.

Fuhlendorf, S.D., Engle, D.M., Elmore, R.D., Limb, R.F., Bidwell, T.G., 2012. Conservation of Pattern and Process: Developing an Alternative Paradigm of Rangeland Management. Rangel. Ecol. Manag. 65, 579–589. doi:10.2111/REM-D-11-00109.1

Guerschman, J.P., Hill, M.J., Renzullo, L.J., Barrett, D.J., Marks, A.S., Botha, E.J., 2009. Estimating fractional cover of photosynthetic vegetation, non-photosynthetic vegetation and bare soil in the Australian tropical savanna region upscaling the EO-1 Hyperion and MODIS sensors. Remote Sens. Environ. 113, 928–945. doi:10.1016/j.rse.2009.01.006

Hagen, S.C., Heilman, P., Marsett, R., Torbick, N., Salas, W., van Ravensway, J., Qi, J., 2012. Mapping Total Vegetation Cover Across Western Rangelands With Moderate-Resolution Imaging Spectroradiometer Data. Rangel. Ecol. Manag. 65, 456–467. doi:10.2111/REM-D-11-00188.1

Herrick, J.E., Duniway, M.C., Pyke, D. a., Bestelmeyer, B.T., Wills, S.A., Brown, J.R., Karl, J.W., Havstad, K.M., 2012. A holistic strategy for adaptive land management. Jounral Soil Water Conserv. 67, 105A–113A. doi:10.2489/jswc.67.4.105A

Hoekstra, J.M., Boucher, T.M., Ricketts, T.H., Roberts, C., 2005. Confronting a biome crisis: global disparities of habitat loss and protection. Ecol. Lett. 8, 23–29. doi:10.1111/j.1461-0248.2004.00686.x

Holechek, J., 1988. An approach for setting the stocking rate. Rangelands 10, 10–14.

Holechek, J., Gomez, H., Molinar, F., Galt, D., 1999. Grazing studies: what we've learned. Rangelands 21, 12–16.

Huntington, J.L., Hegewisch, K.C., Daudert, B., Morton, C.G., Abatzoglou, J.T., McEvoy, D.J., Erickson, T., 2017. Climate engine: Cloud computing and visualization of climate and remote sensing data for advanced natural resource monitoring and process understanding. Bull. Am. Meteorol. Soc. 98, 2397–2409. doi:10.1175/BAMS-D-15-00324.1

IPCC, 2012: Managing the Risks of Extreme Events and Disasters to Advance Climate Change Adaptation. A Special Report of Working Groups I and II of the Intergovernmental Panel on Climate Change. Field, C.B., Barros, V., Stocker, T.F., Qin, D., Dokken, D.J., Ebi, K.L., Mastrandrea, M.D., Mach, K.J., Plattner, G.-K., Allen, S.K., Tignor, M., Midgley, P.M., 2012. IPCC, 2012: Cambridge University Press, Cambridge, UK, and New York,. doi:10.1017/CBO9781139177245

Jansen, V., Kolden, C., Schmalz, H., 2018. The Development of Near Real-Time Biomass and Cover Estimates for Adaptive Rangeland Management Using Landsat 7 and Landsat 8 Surface Reflectance Products. Remote Sens. 10, 1057. doi:10.3390/rs10071057

Jansen, V.S., Kolden, C.A., Taylor, R. V., A. Newingham, B., 2016. Quantifying livestock effects on bunchgrass vegetation with Landsat ETM+ data across a single growing season. Int. J. Remote Sens. 37, 150–175. doi:10.1080/01431161.2015.1117681

Johnson, T.N., Kennedy, P.L., DelCurto, T., Taylor, R. V., 2011. Bird community responses to cattle stocking rates in a Pacific Northwest bunchgrass prairie. Agric. Ecosyst. Environ. 144, 338–346. doi:10.1016/j.agee.2011.10.003

Johnson, T.N., Kennedy, P.L., Etterson, M. a., 2012. Nest success and cause-specific nest failure of grassland passerines breeding in prairie grazed by livestock. J. Wildl. Manage. 76, 1607–1616. doi:10.1002/jwmg.437

Jones, M.O., Allred, B.W., Naugle, D.E., Maestas, J.D., Donnelly, P., Metz, L.J., Karl, J., Smith, R., Bestelmeyer, B., Boyd, C., Kerby, J.D., McIver, J.D., 2018. Innovation in rangeland monitoring: annual, 30 m, plant functional type percent cover maps for U.S. rangelands, 1984-2017. Ecosphere 9, e02430. doi:10.1002/ecs2.2430

Joyce, L.A., Briske, D.D., Brown, J.R., Polley, W.H., McCarl, B.A., Bailey, D.W., 2013. Climate Change and North American Rangelands: Assessment of Mitigation and Adaptation Strategies. Rangel. Ecol. Manag. 66, 512–528. doi:10.2111/REM-D-12-00142.1

Juntti, M., Russel, D., Turnpenny, J., 2009. Evidence , politics and power in public policy for the environment. Environ. Sci. Policy 12, 207–215. doi:10.1016/j.envsci.2008.12.007

Kagan, J., Ohmann, J., Gregory, M., Tobalske, C., Hak, J., Fried, J., 2006. Final Report on Land Cover Mapping Methods : Map Zones 8 and 9, PNW ReGAP, Institute for Natural Resouces, Oregon State University,.

Kawamura, K., Akiyama, T., Yokota, H., Tsutsumi, M., Yasuda, T., Watanabe, O., Wang, S., 2005. Quantifying grazing intensities using geographic information systems and satellite remote sensing in the Xilingol steppe region, Inner Mongolia, China. Agric. Ecosyst. Environ. 107, 83–93. doi:10.1016/j.agee.2004.09.008

Kimoto, C., DeBano, S., & Thorp, R. (2012). Investigating temporal patterns of a native bee community in a remnant North American bunchgrass prairie using blue vane traps. Journal of Insect Science, 12(108), 1–23.

Lane, D.R., BassiriRad, H., 2005. Diminishing spatial heterogeneity in soil organic matter across a prairie restoration chronosequence. Restor. Ecol. 13, 403–412. doi:DOI 10.1111/j.1526-100X.2005.00050.x

Legendre, P., Fortin, M.J., 1989. Spatial pattern and ecological analysis. Vegetatio 80, 107–138. doi:10.1007/BF00048036

Lin, Y., Hong, M., Han, G., Zhao, M., Bai, Y., Chang, S.X., 2010. Grazing intensity affected spatial patterns of vegetation and soil fertility in a desert steppe. Agric. Ecosyst. Environ. 138, 282–292. doi:10.1016/j.agee.2010.05.013

Marsett, R.C., Qi, J., Heilman, P., Biedenbender, S.H., Watson, M.C., Amer, S., Weltz, M., Goodrich, D., Marsett, R., 2006. Remote Sensing for Grassland Management in the Arid Southwest. Rangel. Ecol. Manag. 59, 530–540.

Milchunas, D., Lauenroth, W., 1993. Quantitative effects of grazing on vegetation and soils over a global range of environments. Ecol. Monogr. 63, 327–366.

Numata, I., Roberts, D.A., Chadwick, O.A., Schimel, J., Sampaio, F.R., Leonidas, F.C., Soares, J. V., 2007. Characterization of pasture biophysical properties and the impact of grazing intensity using remotely sensed data. Remote Sens. Environ. 109, 314–327. doi:10.1016/j.rse.2007.01.013

Pebesma, E.J., 2004. Multivariable geostatistics in S: The gstat package. Comput. Geosci. 30, 683–691. doi:10.1016/j.cageo.2004.03.012

R Development Core Team, 2016. R: A Language and Environment for Statistical Computing. R Found. Stat. Comput. Vienna Austria 0, {ISBN} 3-900051-07-0. doi:10.1038/sj.hdy.6800737

Reed, F., Roath, R., Bradford, D., 1999. The Grazing Response Index: A simple and effective method to evaluate grazing impacts. Rangelands 21, 3–6.

Reisner, M.D., Grace, J.B., Pyke, D.A., Doescher, P.S., 2013. Conditions favouring Bromus tectorum dominance of endangered sagebrush steppe ecosystems. J. Appl. Ecol. 50, 1039–1049. doi:10.1111/1365-2664.12097

Sankey, T.T., Sankey, J.B., Weber, K.T., Montagne, C., 2009. Geospatial Assessment of Grazing Regime Shifts and Sociopolitical Changes in a Mongolian Rangeland. Rangel. Ecol. Manag. 62, 522–530. doi:10.2111/.1/REM-D-09-00014.1

Scarth, P., Trevithick, R., 2017. Management effects on ground cover “Clumpiness”: Scaling from field to Sentinel-2 cover estimates. Int. Arch. Photogramm. Remote Sens. Spat. Inf. Sci. - ISPRS Arch. 42, 183–188. doi:10.5194/isprs-archives-XLII-3-W2-183-2017

Schmalz, H.J., Taylor, R. V., Johnson, T.N., Kennedy, P.L., DeBano, S.J., Newingham, B.A., McDaniel, P.A., 2013. Soil Morphologic Properties and Cattle Stocking Rate Affect Dynamic Soil Properties. Rangel. Ecol. Manag. 66, 445–453.

Severson, K.E., Urness, P.J., 1994. Livestock grazing: a tool to improve wildlife habitat, in: Vavra, M., Laylock, W.A., Pieper, R.D. (Eds.), Ecological Implications of Livestock Herbivory in the West. Society for Range Management, Denver, CO, USA, pp. 232–249.

Skovlin, J.M., Harris, R.W., Strickler, G.S., Garrison, G.A., 1976. Effects of cattle grazing methods on ponderosa pine-bunchgrass range in the Pacific Northwest.

Smith, L., Ruyle, G., Maynard, J., Barker, S., Meyer, W., Stewart, D., 2005. Principles of Obtaining and Interpreting Utilization Data on Rangelands.

Todd, S.W., Hoffer, R.M., Milchunas, D.G., 1998. Biomass estimation on grazed and ungrazed rangelands using spectral indices. Int. J. Remote Sens. 19, 427–438.

Townsend, D.E., Fuhlendorf, S.D., 2010. Evaluating Relationships between Spatial Heterogeneity and the Biotic and Abiotic Environments. Am. Midl. Nat. 163, 351–365. doi:10.1674/0003-0031-163.2.351

Tsalyuk, M., Kelly, M., Koy, K., Getz, W.M., Butterfield, H.S., 2015. Monitoring the Impact of Grazing on Rangeland Conservation Easements Using MODIS Vegetation Indices. Rangel. Ecol. Manag. 68, 173–185. doi:10.1016/j.rama.2015.01.006

Van Auken, O.W., 2009. Causes and consequences of woody plant encroachment into western North American grasslands. J. Environ. Manage. 90, 2931–2942. doi:10.1016/j.jenvman.2009.04.023

Virk, R., Mitchell, S.W., 2015. Effect of Different Grazing Intensities on the Spatial-Temporal Variability in Above-Ground Live Plant Biomass in North American Mixed Grasslands. Can. J. Remote Sens. 40, 423–439. doi:10.1080/07038992.2014.1009882

Washington-Allen, R.A., West, N.E., Ramsey, R.D., Efroymson, R.A., 2006. A Protocol for Retrospective Remote Sensing – Based Ecological Monitoring of. Rangel. Ecol. Manag. 59, 19–29.

Wessels, K.J., van den Bergh, F., Scholes, R.J., 2012. Limits to detectability of land degradation by trend analysis of vegetation index data. Remote Sens. Environ. 125, 10–22. doi:10.1016/j.rse.2012.06.022

Western, A.W., Blöschl, G., Grayson, R.B., 1998. Geostatistical characterisation of soil moisture patterns in the Tarrawarra catchment. J. Hydrol. 205, 20–37. doi:10.1016/S0022-1694(97)00142-X

Wiens, J., Sutter, R., Anderson, M., Blanchard, J., Barnett, A., Aguilar-Amuchastegui, N., Avery, C., Laine, S., 2009. Selecting and conserving lands for biodiversity: The role of remote sensing. Remote Sens. Environ. 113, 1370–1381. doi:10.1016/j.rse.2008.06.020

# Appendix 1. Supplemental Materials for Chapter 2.

Supplementary Materials: The development of near real-time biomass and cover estimates for adaptive rangeland management using Landsat surface reflectance products

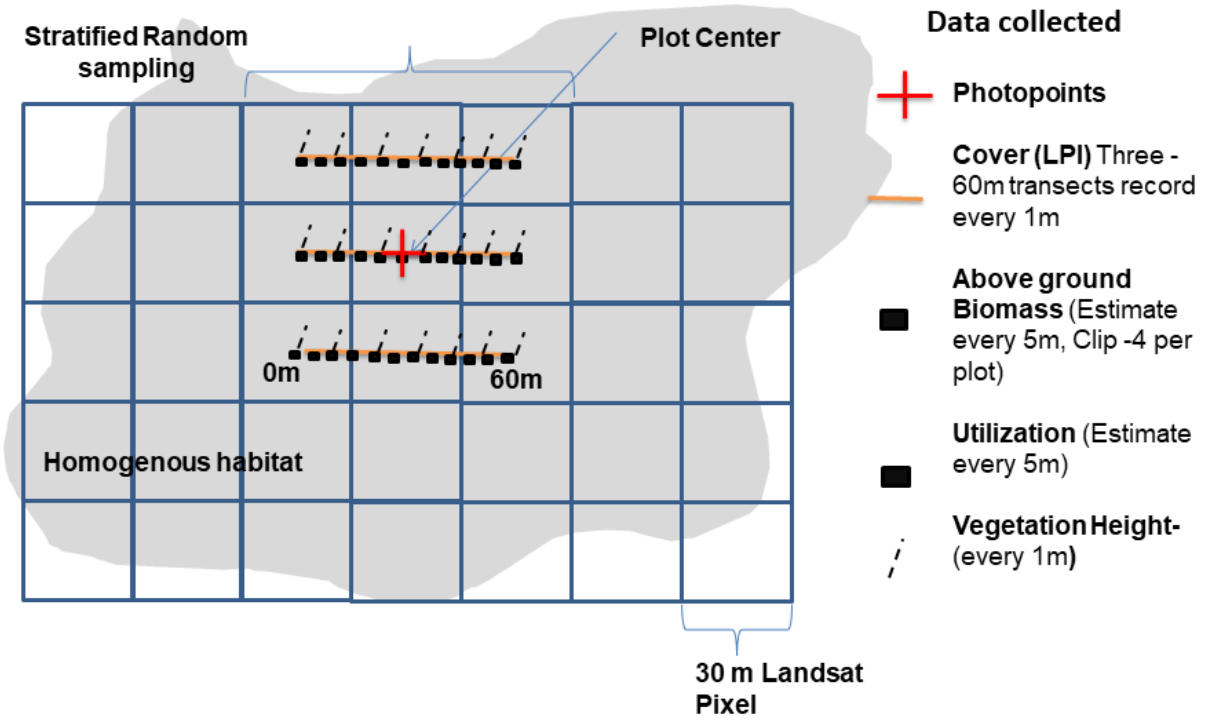


Figure A1.1**.** Sampling site plot layout.

Caption: Sample sites were selected using a stratified random sampling approach and homogeneity at the site was validated in the field. At each site, three 60m transects were established in an east-west direction and 30m apart in the north-south direction. Along each transect, cover, vegetation color and vegetation height of functional groups was collected at 1m intervals using line-point intercept. Above-ground biomass and utilization were estimated in 1 x 0.5m quadrats every 5m along each transect. All biomass was clipped in four quadrats: at 30m on the southern and northern transects and at 20m and 40m on the center transect.

Table A1.1. Paired Landsat 7 and Landsat 8 scenes used in model building (including timing of in-field vegetation sampling) and for sensor model comparisons.

| Year | Scene Date | Julian Date | Sensor | Path/Row | Scene used for Model Creation | In-field Sampling Dates |
|---|---|---|---|---|---|---|
| 2013 | 28 Jun | 179 | LS8 | P43/R28 | | |
| 2013 | 29 Jun | 180 | LS7 | P42/R28 | | |
| 2014 | 23 Jun | 174 | LS7 | P43/R28 | | |
| 2014 | 24 Jun | 175 | LS8 | P42/R28 | | |
| 2014 | 11 Sep | 254 | LS7 | P43/R28 | | |
| 2014 | 12 Sep | 255 | LS8 | P42/R28 | | |
| 2014 | 19 Sep | 262 | LS8 | P43/R28 | x | 19 - 28 Sep |
| 2014 | 20 Sep | 263 | LS7 | P42/R28 | x | 19 - 28 Sep |
| 2015 | 10 Jun | 161 | LS7 | P43/R28 | x | 1 – 25 Jun |
| 2015 | 11 Jun | 162 | LS8 | P42/R28 | x | 1 – 25 Jun |
| 2015 | 26 Jun | 177 | LS7 | P43/R28 | | |
| 2015 | 27 Jun | 178 | LS8 | P42/R28 | | |
| 2015 | 16 Oct | 289 | LS7 | P43/R28 | x | 21 Sep - 6 Oct |
| 2015 | 17 Oct | 290 | LS8 | P42/R28 | x | 21 Sep - 6 Oct |
| 2016 | 20 Jun | 172 | LS8 | P43/R28 | x | 2 – 15 Jun |
| 2016 | 21 Jun | 173 | LS7 | P42/R28 | x | 2 – 15 Jun |
| 2016 | 24 Sep | 268 | LS8 | P43/R28 | x | 26 Sept – 7 Oct |
| 2016 | 25 Sep | 269 | LS7 | P42/R28 | x | 26 Sept - 7 Oct |
| 2017 | 23 Jun | 174 | LS8 | P43/R28 | | |
| 2017 | 24 Jun | 175 | LS7 | P42/R28 | | |
| 2017 | 18 Aug | 230 | LS7 | P43/R28 | | |
| 2017 | 19 Aug | 231 | LS8 | P42/R28 | | |
| 2017 | 27 Sep | 270 | LS8 | P43/R28 | | |
| 2017 | 28 Sep | 271 | LS7 | P42/R28 | | |

Table A1.2. Candidate vegetation indices used in the best subset modeling step.

| Index and abbreviation | Formula | Reference |
|---|---|---|
| Normalized Difference Vegetation Index (NDVI) | $\frac{NIR - RED}{NIR + RED}$ | Tucker (1979) |
| Soil Adjusted Vegetation Index (SAVI) | $\frac{NIR-RED}{NIR+RED+0.5}*(1+0.5)$ | Huete (1988) |
| Renormalized Difference Vegetation Index (RDVI) | $\frac{NIR - RED}{\sqrt{(NIR + RED)}}$ | Ruejean and Breon (1995); Haboudane et al. (2004) |
| Modified Triangular Vegetation Index 1 (MTVI1) | $1.2[1.2(NIR-GREEN)-2.5(RED-GREEN)]$ | Haboudane et al. (2004) |
| Normalized Canopy Index (NCI) | $\frac{MIR - GREEN}{MIR + GREEN}$ | Vescovo & Gianelle (2008) |
| Normalized Difference Cover Index (NDCI) / Normalized Difference senescent vegetation index (NDSVI) | $\frac{MIR - RED}{MIR + RED}$ | Marsett et al. (2006) Zhang & Guo (2008) |
| Plant Senesce Reflectance Index (PSRI) | $\frac{RED - GREEN}{NIR}$ | Merzlyak et al. (1999) |
| Soil Adjusted Total Vegetation Index (SATVI) | $\frac{MIR-RED}{MIR+RED+0.5}$ *(1+0.5)-(SWIR2/2) | Marsett et al. (2006) |
| Normalized Burn Ratio or Normalized Difference Infrared Index 7 (NDII7) | $\frac{NIR - SWIR2}{NIR + SWIR2}$ | Hardisky et al. (1983); Key & Benson (2006) |
| Normalized Difference Water Index (NDWI) | $\frac{NIR - MIR}{NIR + MIR}$ | Hardisky et al. (1983); Gao (1996) |
| Enhanced Vegetation Index (EVI) | $(2.5)*\frac{NIR-RED}{NIR+6*RED-7.5*Blue+1}$ | Liu and Huete (1995) |
| Tasseled Cap Brightness index (BI) | $0.2043_{blue} + 0.4158_{green} + 0.5524_{red} + 0.5741_{NIR} + 0.3124_{MIR} + 0.2303_{SWIR2}$ | Crist (1985) |
| Tasseled Cap Greenness index (GVI) | $-0.1603_{blue} - 0.2819_{green} - 0.4934_{red} + 0.7940_{NIR} - 0.0002_{MIR} - 0.1446_{SWIR2}$ | Crist (1985) |
| Tasseled Cap Wetness index (WI) | $0.0315_{blue} + 0.2021_{green} + 0.3102_{red} + 0.1594_{NIR} - 0.6806_{MIR} - 0.6109_{SWIR2}$ | Crist (1985) |
| Normalized Difference Tillage Index (NDTI) | $\frac{MIR - SWIR2}{MIR + SWIR2}$ | Van Deventer et al., 1997 |

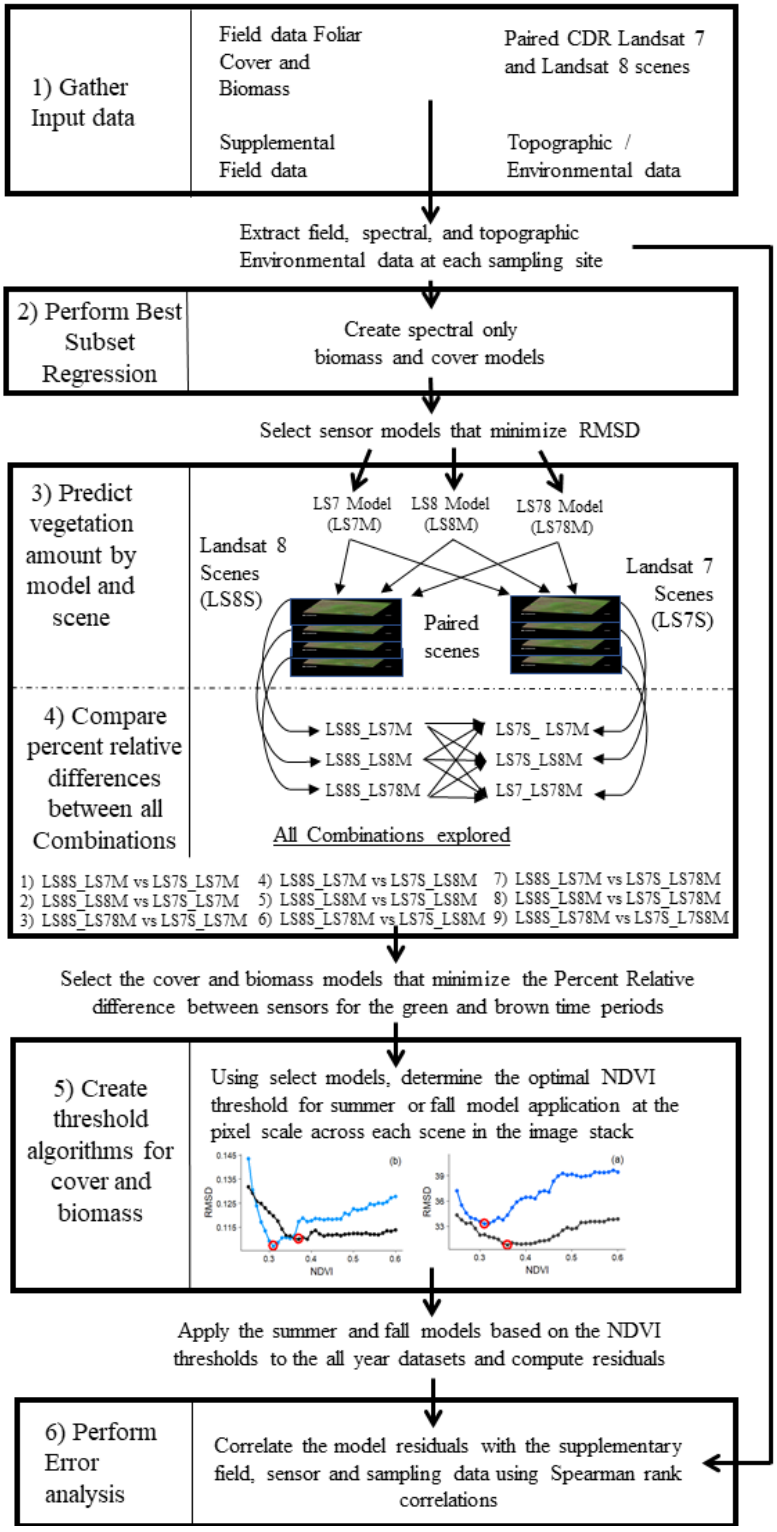


Figure A1.2. Workflow diagram for final algorithm development.

Table A1.3. The field, sensor and topographic variables used to correlate with residuals from the NDVI threshold algorithm. LPI is line-point intercept. NED is National Elevation Dataset. CDR is Climate Data Record

| Variable | Data Source |
|---|---|
| % Mean Utilization | Utilization |
| % Perennial Grass | LPI - Top Canopy |
| % Annual Grass | LPI - Top Canopy |
| % Perennial Forb | LPI - Top Canopy |
| % Annual Forb | LPI - Top Canopy |
| % Litter Cover | LPI - Top Canopy |
| % Green Color | LPI - Top Canopy |
| % Brown & SD Color | LPI - Top Canopy |
| % Soil Surface | LPI - Soil Surface |
| % Rock | LPI - Soil Surface |
| % Moss or Lichen | LPI - Soil Surface |
| Aspect | NED 30m DEM |
| Slope | NED 30m DEM |
| Sensor Date | Landsat CDR |
| Prior Rain Lag (days) | Landsat CDR/Zumwalt WX Station |
| Infield Sample Lag (Days) | Sensor/Field |
| Infield Sample Date | Field Data |

Table A1.4. Variable Selection using a bootstrapped best subset model approach for Green (Summer) Biomass data.

| Time | Sensor | Model Rank | Variable Count | NDVI | SAVI | RDVI | MTVII | NCI | NDCI | PSRI | SATVI | NDII7 | NDWI | EVI | TC-BRI | TC-GRE | TC-WET | NDTI |
|---|---|---|---|---|---|---|---|---|---|---|---|---|---|---|---|---|---|---|
| Green | LS7 | 1 | 1 | 0 | 0 | 0 | 0 | 0 | 0 | 0 | 0 | 73 | **927** | 0 | 0 | 0 | 0 | 0 |
| | LS7 | 2 | 1 | 0 | 0 | 0 | 0 | 0 | 0 | 0 | 0 | **918** | 73 | 0 | 0 | 8 | 1 | 0 |
| | LS8 | 1 | 1 | 0 | 0 | 0 | 0 | 0 | 0 | 0 | 28 | **853** | 97 | 0 | 0 | 0 | 22 | 0 |
| | LS8 | 2 | 1 | 0 | 0 | 0 | 0 | 0 | 0 | 0 | 59 | 120 | **784** | 0 | 0 | 0 | 37 | 0 |
| | LS7LS8 | 1 | 1 | 0 | 0 | 0 | 0 | 0 | 0 | 0 | 0 | **753** | 247 | 0 | 0 | 0 | 0 | 0 |
| | LS7LS8 | 2 | 1 | 0 | 0 | 0 | 0 | 0 | 0 | 0 | 0 | 247 | **753** | 0 | 0 | 0 | 0 | 0 |
| | LS7 | 1 | 2 | 5 | 20 | 24 | 61 | 1 | 61 | 184 | 3 | **647** | 258 | **681** | 3 | 43 | 7 | 2 |
| | LS7 | 2 | 2 | 24 | 23 | 20 | 58 | 7 | 116 | **454** | 6 | **543** | 362 | 340 | 6 | 33 | 6 | 2 |
| | LS8 | 1 | 2 | 3 | 1 | 2 | **333** | 0 | 0 | 2 | 55 | **848** | 81 | 176 | 188 | 17 | 242 | 52 |
| | LS8 | 2 | 2 | 4 | 3 | 56 | 162 | 0 | 0 | 10 | 130 | **785** | 136 | 78 | 254 | 68 | **276** | 38 |
| | LS7LS8 | 1 | 2 | 0 | 0 | 0 | 44 | 0 | 0 | 15 | 12 | **981** | 19 | **925** | 0 | 0 | 4 | 0 |
| | LS7LS8 | 2 | 2 | 0 | 0 | 0 | 350 | 0 | 7 | **465** | 73 | **899** | 100 | 64 | 7 | 0 | 35 | 0 |

Table A1.5. Variable Selection using a bootstrapped best subset model approach for Brown (Fall) Biomass data.

| Time | Sensor | Model Rank | Variable Count | NDVI | SAVI | RDVI | MTVII | NCI | NDCI | PSRI | SATVI | NDII7 | NDWI | EVI | TC-BRI | TC-GRE | TC-WET | NDTI |
|---|---|---|---|---|---|---|---|---|---|---|---|---|---|---|---|---|---|---|
| Brown | LS7 | 1 | 1 | 0 | 0 | 0 | 0 | 0 | 0 | 0 | 0 | 0 | 0 | 0 | 0 | 0 | 0 | **1000** |
| | LS7 | 2 | 1 | 0 | 0 | 0 | 0 | 0 | 0 | 0 | 0 | **852** | 0 | 0 | 0 | 148 | 0 | 0 |
| | LS8 | 1 | 1 | 0 | 0 | 0 | 0 | 0 | 0 | 0 | 0 | 0 | 0 | 0 | 0 | 0 | 0 | **1000** |
| | LS8 | 2 | 1 | 0 | 0 | 0 | 0 | 0 | 0 | 0 | 0 | **1000** | 0 | 0 | 0 | 0 | 0 | 0 |
| | LS7LS8 | 1 | 1 | 0 | 0 | 0 | 0 | 0 | 0 | 0 | 0 | 0 | 0 | 0 | 0 | 0 | 0 | **1000** |
| | LS7LS8 | 2 | 1 | 0 | 0 | 0 | 0 | 0 | 0 | 0 | 0 | **1000** | 0 | 0 | 0 | 0 | 0 | 0 |
| | LS7 | 1 | 2 | 28 | 5 | 4 | 39 | 190 | 14 | **256** | 2 | 217 | 217 | 50 | 94 | 85 | 16 | **783** |
| | LS7 | 2 | 2 | 40 | 45 | 39 | 100 | 117 | 95 | 116 | 54 | **191** | 176 | 70 | 47 | 33 | 24 | **853** |
| | LS8 | 1 | 2 | 0 | 0 | 5 | 2 | 134 | 9 | 256 | 4 | 183 | 182 | 10 | 64 | **328** | 4 | **819** |
| | LS8 | 2 | 2 | 4 | 10 | 167 | 18 | 116 | 51 | 123 | 14 | 96 | 157 | 29 | 85 | **197** | 26 | **907** |
| | LS7LS8 | 1 | 2 | 4 | 5 | 6 | 0 | 195 | 0 | 104 | 1 | 138 | 141 | 3 | 34 | **506** | 1 | **862** |
| | LS7LS8 | 2 | 2 | 10 | 29 | **302** | 6 | 121 | 66 | 72 | 10 | 134 | 127 | 11 | 47 | 187 | 2 | **876** |

Table A1.6. Variable Selection using a bootstrapped best subset model approach for All Year (Green + Brown) Biomass data.

| Time | Sensor | Model Rank | Variable Count | NDVI | SAVI | RDVI | MTVII | NCI | NDCI | PSRI | SATVI | NDII7 | NDWI | EVI | TC-BRI | TC-GRE | TC-WET | NDTI |
|---|---|---|---|---|---|---|---|---|---|---|---|---|---|---|---|---|---|---|
| All Year | LS7 | 1 | 1 | 0 | 0 | 0 | 0 | 0 | 0 | 0 | 0 | 196 | 0 | 0 | 0 | 0 | 0 | **804** |
| | LS7 | 2 | 1 | 0 | 0 | 0 | 0 | 0 | 0 | 0 | 0 | **804** | 0 | 0 | 0 | 7 | 0 | 189 |
| | LS8 | 1 | 1 | 0 | 0 | 0 | 0 | 0 | 0 | 0 | 0 | 258 | 0 | 0 | 0 | 0 | 0 | **742** |
| | LS8 | 2 | 1 | 0 | 0 | 0 | 0 | 0 | 0 | 0 | 0 | **742** | 0 | 0 | 0 | 0 | 0 | 258 |
| | LS7LS8 | 1 | 1 | 0 | 0 | 0 | 0 | 0 | 0 | 0 | 0 | 128 | 0 | 0 | 0 | 0 | 0 | **872** |
| | LS7LS8 | 2 | 1 | 0 | 0 | 0 | 0 | 0 | 0 | 0 | 0 | **872** | 0 | 0 | 0 | 0 | 0 | 128 |
| | LS7 | 1 | 2 | 1 | 0 | 0 | **642** | 6 | 0 | 131 | 0 | 333 | 41 | 148 | 0 | **646** | 2 | 50 |
| | LS7 | 2 | 2 | 2 | 3 | 0 | 108 | 4 | 0 | 534 | 4 | **817** | 79 | 170 | 1 | 127 | 3 | 148 |
| | LS8 | 1 | 2 | 27 | 0 | 0 | 10 | 0 | 0 | 2 | 13 | **955** | 671 | 2 | 1 | 0 | 3 | 316 |
| | LS8 | 2 | 2 | 23 | 27 | 0 | 16 | 1 | 0 | 0 | 18 | **787** | 266 | 6 | 5 | 1 | 5 | **845** |
| | LS7LS8 | 1 | 2 | 1 | 0 | 0 | 8 | 0 | 0 | 20 | 0 | **991** | 312 | 17 | 0 | 6 | 0 | **645** |
| | LS7LS8 | 2 | 2 | 1 | 1 | 0 | 6 | 0 | 0 | 16 | 0 | 542 | **634** | 22 | 0 | 5 | 0 | **773** |

Table A1.7. Variable Selection using a bootstrapped best subset model approach for Green (Summer) Cover data.

| Time | Sensor | Model Rank | Variable Count | NDVI | SAVI | RDVI | MTVII | NCI | NDCI | PSRI | SATVI | NDII7 | NDWI | EVI | TC-BRI | TC-GRE | TC-WET | NDTI |
|---|---|---|---|---|---|---|---|---|---|---|---|---|---|---|---|---|---|---|
| Green | LS7 | 1 | 1 | 0 | 0 | 0 | 0 | 0 | 0 | 0 | 0 | **952** | 48 | 0 | 0 | 0 | 0 | 0 |
| | LS7 | 2 | 1 | 0 | 1 | 10 | 0 | 0 | 0 | 0 | 0 | 48 | **928** | 0 | 0 | 1 | 0 | 12 |
| | LS8 | 1 | 1 | 0 | 0 | 0 | 0 | 0 | 0 | 0 | 0 | **995** | 0 | 0 | 0 | 0 | 0 | 5 |
| | LS8 | 2 | 1 | 114 | 59 | 1 | 0 | 0 | 0 | 2 | 0 | 5 | **547** | 0 | 0 | 0 | 0 | 272 |
| | LS7LS8 | 1 | 1 | 0 | 0 | 0 | 0 | 0 | 0 | 0 | 0 | **1000** | 0 | 0 | 0 | 0 | 0 | 0 |
| | LS7LS8 | 2 | 1 | 0 | 2 | 0 | 0 | 0 | 0 | 0 | 0 | 0 | **959** | 0 | 0 | 0 | 0 | 39 |
| | LS7 | 1 | 2 | 52 | 88 | 87 | 5 | 1 | **510** | 2 | 174 | **781** | 2 | 75 | 173 | 8 | 42 | 0 |
| | LS7 | 2 | 2 | 215 | 148 | 57 | 17 | 13 | **343** | 5 | 140 | **695** | 17 | 50 | 221 | 19 | 60 | 0 |
| | LS8 | 1 | 2 | 8 | 10 | 5 | 0 | 31 | 50 | 188 | 119 | **858** | **358** | 1 | 120 | 245 | 1 | 6 |
| | LS8 | 2 | 2 | 29 | 27 | 88 | 13 | 57 | 101 | 177 | 158 | **744** | **218** | 1 | 159 | 192 | 11 | 25 |
| | LS7LS8 | 1 | 2 | 20 | 22 | 0 | 0 | 42 | **619** | 17 | 63 | **916** | 64 | 12 | 104 | 110 | 11 | 0 |
| | LS7LS8 | 2 | 2 | **190** | 68 | 16 | 10 | 161 | 180 | 16 | 29 | **926** | 52 | 63 | 77 | 177 | 35 | 0 |

Table A1.8. Variable Selection using a bootstrapped best subset model approach for the Fall (Brown) Cover data.

| Time | Sensor | Model Rank | Variable Count | NDVI | SAVI | RDVI | MTVII | NCI | NDCI | PSRI | SATVI | NDII7 | NDWI | EVI | TC-BRI | TC-GRE | TC-WET | NDTI |
|---|---|---|---|---|---|---|---|---|---|---|---|---|---|---|---|---|---|---|
| Brown | LS7 | 1 | 1 | 0 | 0 | 0 | 0 | 0 | 0 | 0 | 0 | 0 | 0 | 0 | 0 | 0 | 0 | **1000** |
| | LS7 | 2 | 1 | 0 | 0 | 0 | 0 | 0 | 0 | 0 | 0 | **524** | 0 | 0 | 0 | 476 | 0 | 0 |
| | LS8 | 1 | 1 | 0 | 0 | 0 | 0 | 0 | 0 | 0 | 0 | 0 | 0 | 0 | 0 | 0 | 0 | **1000** |
| | LS8 | 2 | 1 | 0 | 0 | 0 | 0 | 0 | 0 | 0 | 0 | **997** | 0 | 0 | 0 | 3 | 0 | 0 |
| | LS7LS8 | 1 | 1 | 0 | 0 | 0 | 0 | 0 | 0 | 0 | 0 | 0 | 0 | 0 | 0 | 0 | 0 | **1000** |
| | LS7LS8 | 2 | 1 | 0 | 0 | 0 | 0 | 0 | 0 | 0 | 0 | **1000** | 0 | 0 | 0 | 0 | 0 | 0 |
| | LS7 | 1 | 2 | 0 | 0 | 6 | 2 | 5 | 2 | 43 | 202 | 14 | 12 | 42 | 221 | 9 | **454** | **988** |
| | LS7 | 2 | 2 | 2 | 1 | 9 | 0 | 13 | 4 | 16 | **636** | 14 | 22 | 23 | 86 | 2 | 186 | **986** |
| | LS8 | 1 | 2 | 1 | 1 | 109 | 0 | 21 | 1 | 65 | 35 | 4 | 3 | 0 | **633** | 84 | 47 | **996** |
| | LS8 | 2 | 2 | 3 | 3 | 186 | 0 | 23 | 4 | 36 | **300** | 9 | 8 | 2 | 123 | 151 | 160 | **992** |
| | LS7LS8 | 1 | 2 | 0 | 0 | 87 | 0 | 11 | 1 | 2 | 24 | 1 | 2 | 0 | **774** | 41 | 58 | **999** |
| | LS7LS8 | 2 | 2 | 0 | 0 | 155 | 3 | 2 | 1 | 2 | **492** | 2 | 2 | 0 | 72 | 93 | 177 | **999** |

Table A1.9. Variable Selection using a bootstrapped best subset model approach for the complete dataset (All Year) Cover data.

| Time | Sensor | Model Rank | Variable Count | NDVI | SAVI | RDVI | MTVII | NCI | NDCI | PSRI | SATVI | NDII7 | NDWI | EVI | TC-BRI | TC-GRE | TC-WET | NDTI |
|---|---|---|---|---|---|---|---|---|---|---|---|---|---|---|---|---|---|---|
| All Year | LS7 | 1 | 1 | 0 | 0 | 0 | 0 | 0 | 0 | 0 | 0 | 0 | 0 | 0 | 0 | 0 | 0 | **1000** |
| | LS7 | 2 | 1 | 0 | 0 | 0 | 0 | 0 | 0 | 0 | 0 | **1000** | 0 | 0 | 0 | 0 | 0 | 0 |
| | LS8 | 1 | 1 | 0 | 0 | 0 | 0 | 0 | 0 | 0 | 0 | 0 | 0 | 0 | 0 | 0 | 0 | **1000** |
| | LS8 | 2 | 1 | 0 | 0 | 0 | 0 | 0 | 0 | 0 | 0 | **1000** | 0 | 0 | 0 | 0 | 0 | 0 |
| | LS7LS8 | 1 | 1 | 0 | 0 | 0 | 0 | 0 | 0 | 0 | 0 | 0 | 0 | 0 | 0 | 0 | 0 | **1000** |
| | LS7LS8 | 2 | 1 | 0 | 0 | 0 | 0 | 0 | 0 | 0 | 0 | **1000** | 0 | 0 | 0 | 0 | 0 | 0 |
| | LS7 | 1 | 2 | 0 | 0 | 0 | 13 | 1 | 328 | 27 | 0 | **317** | 310 | 236 | 65 | 12 | 20 | **671** |
| | LS7 | 2 | 2 | 0 | 0 | 0 | 20 | 1 | 213 | 115 | 21 | 150 | 133 | **411** | 58 | 6 | 28 | **844** |
| | LS8 | 1 | 2 | 0 | 0 | 0 | 0 | 0 | 0 | 0 | 0 | **1000** | **1000** | 0 | **0** | 0 | 0 | 0 |
| | LS8 | 2 | 2 | 0 | 0 | 0 | 211 | 23 | 455 | 0 | **1** | 0 | 3 | 13 | 161 | 0 | 134 | **999** |
| | LS7LS8 | 1 | 2 | 0 | 0 | 0 | 0 | 0 | 2 | 0 | 0 | **994** | **994** | 0 | **4** | 0 | 0 | 6 |
| | LS7LS8 | 2 | 2 | 0 | 0 | 0 | 6 | 3 | 538 | 2 | **0** | 6 | 6 | 179 | 215 | 0 | 51 | **994** |

Table A1.10. Top candidate models for Cover

| Time | Sensor | Predictor Var | VIF | Train-N | r2 | rRMSE | RMSD | Test-N | r2 | rRMSE | RMSD |
|---|---|---|---|---|---|---|---|---|---|---|---|
| Green | LS7 | NDII7 | NA | 60 | 0.70 | 16.89 | 0.11 | 20 | 0.70 | 17.39 | 0.11 |
| | LS7 | NDWI | NA | 60 | 0.67 | 17.64 | 0.11 | 20 | 0.70 | 17.49 | 0.11 |
| | LS7 | NDII7, NDCI | 1.61 | 60 | 0.74 | 15.63 | 0.10 | 20 | 0.68 | 17.98 | 0.11 |
| | LS7 | NDII7, NDCI | 1.60 | 60 | 0.74 | 15.63 | 0.10 | 20 | 0.67 | 18.00 | 0.11 |
| | LS8 | NDII7 | NA | 93 | 0.78 | 16.07 | 0.10 | 30 | 0.75 | 13.00 | 0.08 |
| | LS8 | NDWI | NA | 93 | 0.75 | 17.26 | 0.10 | 30 | 0.70 | 14.39 | 0.09 |
| | LS8 | NDII7, NDWI | 54.33 | 93 | 0.79 | 15.84 | 0.10 | 30 | 0.77 | 12.35 | 0.08 |
| | LS8 | NDII7, NDWI | 53.87 | 93 | 0.79 | 15.84 | 0.10 | 30 | 0.77 | 12.37 | 0.08 |
| | LS78 | NDII7 | NA | 153 | 0.75 | 16.44 | 0.10 | 50 | 0.72 | 14.85 | 0.09 |
| | LS78 | NDWI | NA | 153 | 0.71 | 17.62 | 0.11 | 50 | 0.69 | 15.74 | 0.10 |
| | LS78 | NDII7, NDCI | 1.77 | 153 | 0.77 | 15.80 | 0.10 | 50 | 0.70 | 15.53 | 0.10 |
| | LS78 | NDII7, TCGRE | 15.77 | 153 | 0.76 | 15.96 | 0.10 | 50 | 0.69 | 15.41 | 0.10 |
| Brown | LS7 | NDTI | NA | 78 | 0.78 | 19.87 | 0.10 | 26 | 0.81 | 17.07 | 0.09 |
| | LS7 | NDII7 | NA | 78 | 0.63 | 25.70 | 0.14 | 26 | 0.68 | 22.52 | 0.12 |
| | LS7 | NDTI, TCWET | 1.15 | 78 | 0.80 | 19.21 | 0.10 | 26 | 0.81 | 17.04 | 0.09 |
| | LS7 | NDTI, SATVI | 1.67 | 78 | 0.80 | 19.21 | 0.10 | 26 | 0.81 | 17.03 | 0.09 |
| | LS8 | NDTI | NA | 99 | 0.72 | 21.73 | 0.11 | 32 | 0.72 | 22.71 | 0.13 |
| | LS8 | NDII7 | NA | 99 | 0.62 | 25.12 | 0.13 | 32 | 0.59 | 27.81 | 0.15 |
| | LS8 | NDTI, TCBRI | 1.02 | 99 | 0.73 | 21.34 | 0.11 | 32 | 0.74 | 21.84 | 0.12 |
| | LS8 | NDTI, SATVI | 1.18 | 99 | 0.73 | 21.46 | 0.11 | 32 | 0.73 | 22.05 | 0.12 |
| | LS78 | NDTI | NA | 177 | 0.75 | 20.92 | 0.11 | 58 | 0.73 | 20.69 | 0.11 |
| | LS78 | NDII7 | NA | 177 | 0.59 | 26.82 | 0.14 | 58 | 0.62 | 25.49 | 0.14 |
| | LS78 | NDTI, TCBRI | 1.01 | 177 | 0.76 | 20.51 | 0.11 | 58 | 0.74 | 19.97 | 0.11 |
| | LS78 | NDTI, SATVI | 1.28 | 177 | 0.76 | 20.57 | 0.11 | 58 | 0.74 | 20.17 | 0.11 |
| All Year | LS7 | NDTI | NA | 120 | 0.65 | 22.85 | 0.13 | 40 | 0.72 | 21.00 | 0.12 |
| | LS7 | NDII7 | NA | 120 | 0.48 | 27.57 | 0.15 | 40 | 0.57 | 25.70 | 0.15 |
| | LS7 | NDTI, NDII7 | 4.84 | 120 | 0.65 | 22.79 | 0.13 | 40 | 0.72 | 20.82 | 0.12 |
| | LS7 | NDTI, EVI | 2.32 | 120 | 0.66 | 22.28 | 0.12 | 40 | 0.74 | 20.23 | 0.12 |
| | LS8 | NDTI | NA | 184 | 0.69 | 20.55 | 0.12 | 62 | 0.70 | 21.02 | 0.12 |
| | LS8 | NDII7 | NA | 184 | 0.58 | 23.93 | 0.14 | 62 | 0.51 | 26.82 | 0.15 |
| | LS8 | NDII7, NDWI | 29.58 | 184 | 0.72 | 19.53 | 0.11 | 62 | 0.72 | 19.58 | 0.11 |
| | LS8 | NDTI, NDCI | 1.54 | 184 | 0.70 | 20.21 | 0.11 | 62 | 0.69 | 21.44 | 0.12 |
| | LS78 | NDTI | NA | 304 | 0.67 | 21.71 | 0.12 | 102 | 0.70 | 20.74 | 0.12 |
| | LS78 | NDII7 | NA | 304 | 0.54 | 25.47 | 0.14 | 102 | 0.53 | 26.23 | 0.15 |
| | LS78 | NDII7, NDWI | 24.47 | 304 | 0.69 | 20.94 | 0.12 | 102 | 0.73 | 19.59 | 0.11 |
| | LS78 | NDTI, NDCI | 1.61 | 304 | 0.67 | 21.41 | 0.12 | 102 | 0.70 | 20.75 | 0.12 |

Table A1.11. Top candidate models for Biomass

| | | | | Train- | | | | Test | | | |
|---|---|---|---|---|---|---|---|---|---|---|---|
| Time | Sensor | Predictor Var | VIF | N | r2 | rRMSE | RMSD | -N | r2 | rRMSE | RMSD |
| Green | LS7 | NDWI | NA | 60 | 0.72 | 21.70 | 37.32 | 20 | 0.78 | 22.52 | 36.96 |
| | LS7 | NDII7 | NA | 60 | 0.69 | 22.84 | 39.27 | 20 | 0.81 | 21.25 | 34.87 |
| | LS7 | EVI, NDII7 | 6.98 | 60 | 0.75 | 20.57 | 35.36 | 20 | 0.78 | 22.96 | 37.69 |
| | LS7 | NDII7, PSRI | 4.97 | 60 | 0.73 | 21.08 | 36.25 | 20 | 0.78 | 22.59 | 37.08 |
| | LS8 | NDII7 | NA | 93 | 0.80 | 20.07 | 32.08 | 30 | 0.81 | 16.86 | 28.96 |
| | LS8 | NDWI | NA | 93 | 0.79 | 20.88 | 33.37 | 30 | 0.83 | 15.87 | 27.26 |
| | LS8 | NDII7, MTVII | 12.26 | 93 | 0.84 | 18.28 | 29.22 | 30 | 0.79 | 17.28 | 29.69 |
| | LS8 | NDII7+TCBRI | 1.00 | 93 | 0.83 | 18.47 | 29.53 | 30 | 0.81 | 16.68 | 28.66 |
| | LS78 | NDII7 | NA | 153 | 0.76 | 21.38 | 35.07 | 50 | 0.81 | 18.50 | 30.89 |
| | LS78 | NDWI | NA | 153 | 0.75 | 21.68 | 35.56 | 50 | 0.81 | 18.47 | 30.84 |
| | LS78 | NDII7, EVI | 8.13 | 153 | 0.79 | 19.87 | 32.60 | 50 | 0.82 | 18.22 | 30.42 |
| | LS78 | NDII7, PSRI | 5.02 | 153 | 0.78 | 20.62 | 33.82 | 50 | 0.83 | 17.57 | 29.34 |
| Brown | LS7 | NDTI | NA | 78 | 0.71 | 30.46 | 32.67 | 25 | 0.77 | 24.19 | 26.43 |
| | LS7 | NDII7 | NA | 78 | 0.56 | 37.61 | 40.35 | 25 | 0.75 | 25.19 | 27.52 |
| | LS7 | NDTI, NCI | 1.45 | 78 | 0.72 | 30.04 | 32.23 | 25 | 0.76 | 24.85 | 27.15 |
| | LS7 | NDTI, NDCI | 1.16 | 78 | 0.72 | 30.27 | 32.47 | 25 | 0.77 | 24.57 | 26.84 |
| | LS8 | NDTI | NA | 99 | 0.67 | 30.88 | 31.20 | 32 | 0.70 | 26.69 | 32.02 |
| | LS8 | NDII7 | NA | 99 | 0.51 | 37.79 | 38.18 | 32 | 0.65 | 29.04 | 34.83 |
| | LS8 | NDTI, TCGRE | 1.94 | 99 | 0.67 | 30.78 | 31.11 | 32 | 0.72 | 26.25 | 31.48 |
| | LS8 | NDTI, NDWI | 1.07 | 99 | 0.68 | 30.53 | 30.85 | 32 | 0.71 | 26.52 | 31.81 |
| | LS78 | NDTI | NA | 177 | 0.69 | 30.73 | 31.80 | 57 | 0.73 | 25.86 | 29.54 |
| | LS78 | NDII7 | NA | 177 | 0.50 | 39.07 | 40.44 | 57 | 0.65 | 29.51 | 33.71 |
| | LS78 | NDTI, NCI | 1.17 | 177 | 0.70 | 30.39 | 31.45 | 57 | 0.73 | 25.90 | 29.59 |
| | LS78 | NDTI, NDCI | 1.05 | 177 | 0.70 | 30.49 | 31.55 | 57 | 0.72 | 26.08 | 29.79 |
| All Year | LS7 | NDTI | NA | 120 | 0.67 | 29.32 | 40.52 | 40 | 0.76 | 25.94 | 37.26 |
| | LS7 | NDII7 | NA | 120 | 0.63 | 30.97 | 42.80 | 40 | 0.72 | 28.55 | 41.02 |
| | LS7 | NDII7, TCGRE | 25.76 | 120 | 0.63 | 30.82 | 42.60 | 40 | 0.73 | 27.67 | 39.76 |
| | LS7 | NDII7, NDTI | 5.25 | 120 | 0.68 | 28.57 | 39.49 | 40 | 0.79 | 24.43 | 35.09 |
| | LS8 | NDTI | NA | 184 | 0.74 | 26.34 | 35.38 | 62 | 0.77 | 27.22 | 35.32 |
| | LS8 | NDII7 | NA | 184 | 0.74 | 26.13 | 35.10 | 62 | 0.72 | 29.17 | 37.84 |
| | LS8 | NDII7. NDWI | 22.60 | 184 | 0.78 | 24.13 | 32.42 | 62 | 0.76 | 27.00 | 35.02 |
| | LS8 | NDTI, NDII7 | 5.43 | 184 | 0.78 | 24.17 | 32.47 | 62 | 0.77 | 27.17 | 35.24 |
| | LS78 | NDTI | NA | 304 | 0.70 | 27.88 | 37.82 | 102 | 0.76 | 26.10 | 35.11 |
| | LS78 | NDII7 | NA | 304 | 0.69 | 28.43 | 38.57 | 102 | 0.70 | 29.19 | 39.26 |
| | LS78 | NDII7, NDTI | 4.88 | 304 | 0.74 | 26.19 | 35.53 | 102 | 0.77 | 25.55 | 34.37 |
| | LS78 | NDTI, NDWI | 2.57 | 304 | 0.74 | 26.22 | 35.57 | 102 | 0.77 | 25.76 | 34.65 |

Table A1.12. Paired Cover models

| VIFm | Time | Sensor | var | int | beta1 | beta2 | N - Train | r2 | aRMSE | rRMSE | RMSD | N - Test | r2 | aRMSE | rRMSE |
|---|---|---|---|---|---|---|---|---|---|---|---|---|---|---|---|
| NA | Summer | LS7 | NDII7 | 0.44 | 0.95 | NA | 60 | 0.70 | 0.11 | 16.89 | 0.11 | 20 | 0.7 | 0.11 | 17.39 |
| NA | Summer | LS7 | NDWI | 0.64 | 1.31 | NA | 60 | 0.67 | 0.11 | 17.64 | 0.11 | 20 | 0.7 | 0.11 | 17.49 |
| 1.61 | Summer | LS7 | NDII7, NDCI | 0.97 | 1.13 | -1.11 | 60 | 0.74 | 0.1 | 15.63 | 0.1 | 20 | 0.68 | 0.11 | 17.98 |
| 1.6 | Summer | LS7 | NDII7, NDCI | 0.98 | 1.13 | -1.13 | 60 | 0.74 | 0.1 | 15.63 | 0.1 | 20 | 0.67 | 0.11 | 18 |
| NA | Summer | LS8 | NDII7 | 0.44 | 0.92 | NA | 60 | 0.74 | 0.1 | 15.62 | 0.1 | 20 | 0.7 | 0.11 | 17.45 |
| NA | Summer | LS8 | NDWI | 0.61 | 1.2 | NA | 60 | 0.70 | 0.11 | 16.96 | 0.11 | 20 | 0.7 | 0.11 | 17.52 |
| 1.91 | Summer | LS8 | NDII7, NDCI | 0.82 | 1.05 | -0.77 | 60 | 0.76 | 0.09 | 15.05 | 0.09 | 20 | 0.7 | 0.11 | 17.25 |
| 1.91 | Summer | LS8 | NDII7, NDCI | 0.83 | 1.05 | -0.79 | 60 | 0.76 | 0.09 | 15.05 | 0.09 | 20 | 0.7 | 0.11 | 17.24 |
| NA | Summer | LS78 | NDII7 | 0.44 | 0.93 | NA | 120 | 0.72 | 0.1 | 16.28 | 0.1 | 40 | 0.7 | 0.11 | 17.42 |
| NA | Summer | LS78 | NDWI | 0.62 | 1.24 | NA | 120 | 0.68 | 0.11 | 17.47 | 0.11 | 40 | 0.69 | 0.11 | 17.54 |
| 1.66 | Summer | LS78 | NDII7, NDCI | 0.87 | 1.08 | -0.9 | 120 | 0.75 | 0.1 | 15.4 | 0.1 | 40 | 0.69 | 0.11 | 17.58 |
| 1.66 | Summer | LS78 | NDII7, NDCI | 0.88 | 1.09 | -0.92 | 120 | 0.75 | 0.1 | 15.4 | 0.1 | 40 | 0.69 | 0.11 | 17.6 |
| NA | Fall | LS7 | NDTI | -0.09 | 3.83 | NA | 71 | 0.73 | 0.11 | 21.39 | 0.11 | 23 | 0.86 | 0.08 | 15.45 |
| NA | Fall | LS7 | NDII7 | 0.63 | 1.93 | NA | 71 | 0.53 | 0.14 | 28.02 | 0.14 | 23 | 0.8 | 0.1 | 19.16 |
| 1.08 | Fall | LS7 | NDTI, TCWET | -0.32 | 3.99 | 0 | 71 | 0.74 | 0.1 | 20.68 | 0.1 | 23 | 0.84 | 0.08 | 15.85 |
| 1.44 | Fall | LS7 | NDTI, SATVI | -0.37 | 4.22 | 0 | 71 | 0.74 | 0.1 | 20.68 | 0.1 | 23 | 0.84 | 0.08 | 15.93 |
| NA | Fall | LS8 | NDTI | -0.15 | 4.39 | NA | 71 | 0.71 | 0.11 | 22.18 | 0.11 | 23 | 0.83 | 0.09 | 16.23 |
| NA | Fall | LS8 | NDII7 | 0.56 | 2.02 | NA | 71 | 0.53 | 0.14 | 27.87 | 0.14 | 23 | 0.73 | 0.11 | 20.74 |
| 1.04 | Fall | LS8 | NDTI, SATVI | -0.36 | 4.53 | 0 | 71 | 0.73 | 0.11 | 21.17 | 0.11 | 23 | 0.79 | 0.1 | 18.22 |
| 1.04 | Fall | LS8 | NDTI, SATVI | -0.36 | 4.53 | 0 | 71 | 0.73 | 0.11 | 21.17 | 0.11 | 23 | 0.79 | 0.1 | 18.29 |
| NA | Fall | LS78 | NDTI | -0.11 | 4.05 | NA | 142 | 0.71 | 0.11 | 22.06 | 0.11 | 46 | 0.84 | 0.08 | 15.99 |
| NA | Fall | LS78 | NDII7 | 0.59 | 1.84 | NA | 142 | 0.50 | 0.15 | 28.97 | 0.15 | 46 | 0.71 | 0.12 | 21.96 |
| 1.03 | Fall | LS78 | NDTI, TCBRI | -0.32 | 3.93 | 0 | 142 | 0.73 | 0.11 | 21.15 | 0.11 | 46 | 0.8 | 0.09 | 17.7 |
| 1.14 | Fall | LS78 | NDTI, SATVI | -0.35 | 4.31 | 0 | 142 | 0.73 | 0.11 | 21.18 | 0.11 | 46 | 0.81 | 0.09 | 17.38 |
| NA | All-year | LS7 | NDTI | 0.02 | 2.94 | NA | 121 | 0.67 | 0.12 | 21.8 | 0.12 | 40 | 0.74 | 0.12 | 20.28 |
| NA | All-year | LS7 | NDII7 | 0.5 | 0.85 | NA | 121 | 0.48 | 0.15 | 27.32 | 0.15 | 40 | 0.64 | 0.13 | 22.62 |
| 4.71 | All-year | LS7 | NDTI, NDII7 | -0.06 | 3.43 | -0.19 | 121 | 0.67 | 0.12 | 21.62 | 0.12 | 40 | 0.73 | 0.12 | 20.63 |
| 1.98 | All-year | LS7 | NDTI, EVI | 0 | 3.5 | -0.11 | 121 | 0.69 | 0.12 | 20.93 | 0.12 | 40 | 0.72 | 0.12 | 20.81 |
| NA | All-year | LS8 | NDTI | 0 | 3.23 | NA | 121 | 0.7 | 0.12 | 20.82 | 0.12 | 40 | 0.71 | 0.13 | 21.37 |
| NA | All-year | LS8 | NDII7 | 0.48 | 0.93 | NA | 121 | 0.54 | 0.14 | 25.71 | 0.14 | 40 | 0.62 | 0.14 | 23.26 |
| 25.56 | All-year | LS8 | NDII7, NDWI | -0.05 | 3.6 | -3.63 | 121 | 0.72 | 0.11 | 19.95 | 0.11 | 40 | 0.77 | 0.11 | 18.35 |
| 1.49 | All-year | LS8 | NDTI, NDCI | 0.13 | 3.51 | -0.38 | 121 | 0.71 | 0.11 | 20.42 | 0.11 | 40 | 0.7 | 0.13 | 21.44 |
| NA | All-year | LS78 | NDTI | 0.02 | 3.04 | NA | 242 | 0.67 | 0.12 | 21.57 | 0.12 | 80 | 0.72 | 0.12 | 20.66 |
| NA | All-year | LS78 | NDII7 | 0.49 | 0.88 | NA | 242 | 0.5 | 0.15 | 26.6 | 0.15 | 80 | 0.63 | 0.13 | 22.93 |
| 21.06 | All-year | LS78 | NDII7, NDWI | -0.01 | 3.25 | -3.26 | 242 | 0.69 | 0.12 | 21.13 | 0.12 | 80 | 0.78 | 0.11 | 18.59 |
| 1.47 | All-year | LS78 | NDTI, NDCI | 0.16 | 3.3 | -0.4 | 242 | 0.69 | 0.12 | 21.18 | 0.12 | 80 | 0.71 | 0.12 | 20.61 |

Table A1.13. Paired Biomass models

| VIFm | Time | Sensor | var | int | beta1 | beta2 | N - Train | r2 | aRMSE | rRMSE | RMSD | N - Test | r2 | aRMSE | rRMSE |
|---|---|---|---|---|---|---|---|---|---|---|---|---|---|---|---|
| NA | Summer | LS7 | NDII7 | 0.44 | 0.95 | NA | 60 | 0.70 | 0.11 | 16.89 | 0.11 | 20 | 0.7 | 0.11 | 17.39 |
| NA | Summer | LS7 | NDWI | 0.64 | 1.31 | NA | 60 | 0.67 | 0.11 | 17.64 | 0.11 | 20 | 0.7 | 0.11 | 17.49 |
| 1.61 | Summer | LS7 | NDII7, NDCI | 0.97 | 1.13 | -1.11 | 60 | 0.74 | 0.1 | 15.63 | 0.1 | 20 | 0.68 | 0.11 | 17.98 |
| 1.6 | Summer | LS7 | NDII7, NDCI | 0.98 | 1.13 | -1.13 | 60 | 0.74 | 0.1 | 15.63 | 0.1 | 20 | 0.67 | 0.11 | 18 |
| NA | Summer | LS8 | NDII7 | 0.44 | 0.92 | NA | 60 | 0.74 | 0.1 | 15.62 | 0.1 | 20 | 0.7 | 0.11 | 17.45 |
| NA | Summer | LS8 | NDWI | 0.61 | 1.2 | NA | 60 | 0.70 | 0.11 | 16.96 | 0.11 | 20 | 0.7 | 0.11 | 17.52 |
| 1.91 | Summer | LS8 | NDII7, NDCI | 0.82 | 1.05 | -0.77 | 60 | 0.76 | 0.09 | 15.05 | 0.09 | 20 | 0.7 | 0.11 | 17.25 |
| 1.91 | Summer | LS8 | NDII7, NDCI | 0.83 | 1.05 | -0.79 | 60 | 0.76 | 0.09 | 15.05 | 0.09 | 20 | 0.7 | 0.11 | 17.24 |
| NA | Summer | LS78 | NDII7 | 0.44 | 0.93 | NA | 120 | 0.72 | 0.1 | 16.28 | 0.1 | 40 | 0.7 | 0.11 | 17.42 |
| NA | Summer | LS78 | NDWI | 0.62 | 1.24 | NA | 120 | 0.68 | 0.11 | 17.47 | 0.11 | 40 | 0.69 | 0.11 | 17.54 |
| 1.66 | Summer | LS78 | NDII7, NDCI | 0.87 | 1.08 | -0.9 | 120 | 0.75 | 0.1 | 15.4 | 0.1 | 40 | 0.69 | 0.11 | 17.58 |
| 1.66 | Summer | LS78 | NDII7, NDCI | 0.88 | 1.09 | -0.92 | 120 | 0.75 | 0.1 | 15.4 | 0.1 | 40 | 0.69 | 0.11 | 17.6 |
| NA | Fall | LS7 | NDTI | -0.09 | 3.83 | NA | 71 | 0.73 | 0.11 | 21.39 | 0.11 | 23 | 0.86 | 0.08 | 15.45 |
| NA | Fall | LS7 | NDII7 | 0.63 | 1.93 | NA | 71 | 0.53 | 0.14 | 28.02 | 0.14 | 23 | 0.8 | 0.1 | 19.16 |
| 1.08 | Fall | LS7 | NDTI, TCWET | -0.32 | 3.99 | 0 | 71 | 0.74 | 0.1 | 20.68 | 0.1 | 23 | 0.84 | 0.08 | 15.85 |
| 1.44 | Fall | LS7 | NDTI, SATVI | -0.37 | 4.22 | 0 | 71 | 0.74 | 0.1 | 20.68 | 0.1 | 23 | 0.84 | 0.08 | 15.93 |
| NA | Fall | LS8 | NDTI | -0.15 | 4.39 | NA | 71 | 0.71 | 0.11 | 22.18 | 0.11 | 23 | 0.83 | 0.09 | 16.23 |
| NA | Fall | LS8 | NDII7 | 0.56 | 2.02 | NA | 71 | 0.53 | 0.14 | 27.87 | 0.14 | 23 | 0.73 | 0.11 | 20.74 |
| 1.04 | Fall | LS8 | NDTI, SATVI | -0.36 | 4.53 | 0 | 71 | 0.73 | 0.11 | 21.17 | 0.11 | 23 | 0.79 | 0.1 | 18.22 |
| 1.04 | Fall | LS8 | NDTI, SATVI | -0.36 | 4.53 | 0 | 71 | 0.73 | 0.11 | 21.17 | 0.11 | 23 | 0.79 | 0.1 | 18.29 |
| NA | Fall | LS78 | NDTI | -0.11 | 4.05 | NA | 142 | 0.71 | 0.11 | 22.06 | 0.11 | 46 | 0.84 | 0.08 | 15.99 |
| NA | Fall | LS78 | NDII7 | 0.59 | 1.84 | NA | 142 | 0.50 | 0.15 | 28.97 | 0.15 | 46 | 0.71 | 0.12 | 21.96 |
| 1.03 | Fall | LS78 | NDTI, TCBRI | -0.32 | 3.93 | 0 | 142 | 0.73 | 0.11 | 21.15 | 0.11 | 46 | 0.8 | 0.09 | 17.7 |
| 1.14 | Fall | LS78 | NDTI, SATVI | -0.35 | 4.31 | 0 | 142 | 0.73 | 0.11 | 21.18 | 0.11 | 46 | 0.81 | 0.09 | 17.38 |
| NA | All-year | LS7 | NDTI | 0.02 | 2.94 | NA | 121 | 0.67 | 0.12 | 21.8 | 0.12 | 40 | 0.74 | 0.12 | 20.28 |
| NA | All-year | LS7 | NDII7 | 0.5 | 0.85 | NA | 121 | 0.48 | 0.15 | 27.32 | 0.15 | 40 | 0.64 | 0.13 | 22.62 |
| 4.71 | All-year | LS7 | NDTI, NDII7 | -0.06 | 3.43 | -0.19 | 121 | 0.67 | 0.12 | 21.62 | 0.12 | 40 | 0.73 | 0.12 | 20.63 |
| 1.98 | All-year | LS7 | NDTI, EVI | 0 | 3.5 | -0.11 | 121 | 0.69 | 0.12 | 20.93 | 0.12 | 40 | 0.72 | 0.12 | 20.81 |
| NA | All-year | LS8 | NDTI | 0 | 3.23 | NA | 121 | 0.7 | 0.12 | 20.82 | 0.12 | 40 | 0.71 | 0.13 | 21.37 |
| NA | All-year | LS8 | NDII7 | 0.48 | 0.93 | NA | 121 | 0.54 | 0.14 | 25.71 | 0.14 | 40 | 0.62 | 0.14 | 23.26 |
| 25.56 | All-year | LS8 | NDII7, NDWI | -0.05 | 3.6 | -3.63 | 121 | 0.72 | 0.11 | 19.95 | 0.11 | 40 | 0.77 | 0.11 | 18.35 |
| 1.49 | All-year | LS8 | NDTI, NDCI | 0.13 | 3.51 | -0.38 | 121 | 0.71 | 0.11 | 20.42 | 0.11 | 40 | 0.7 | 0.13 | 21.44 |
| NA | All-year | LS78 | NDTI | 0.02 | 3.04 | NA | 242 | 0.67 | 0.12 | 21.57 | 0.12 | 80 | 0.72 | 0.12 | 20.66 |
| NA | All-year | LS78 | NDII7 | 0.49 | 0.88 | NA | 242 | 0.5 | 0.15 | 26.6 | 0.15 | 80 | 0.63 | 0.13 | 22.93 |
| 21.06 | All-year | LS78 | NDII7, NDWI | -0.01 | 3.25 | -3.26 | 242 | 0.69 | 0.12 | 21.13 | 0.12 | 80 | 0.78 | 0.11 | 18.59 |
| 1.47 | All-year | LS78 | NDTI, NDCI | 0.16 | 3.3 | -0.4 | 242 | 0.69 | 0.12 | 21.18 | 0.12 | 80 | 0.71 | 0.12 | 20.61 |

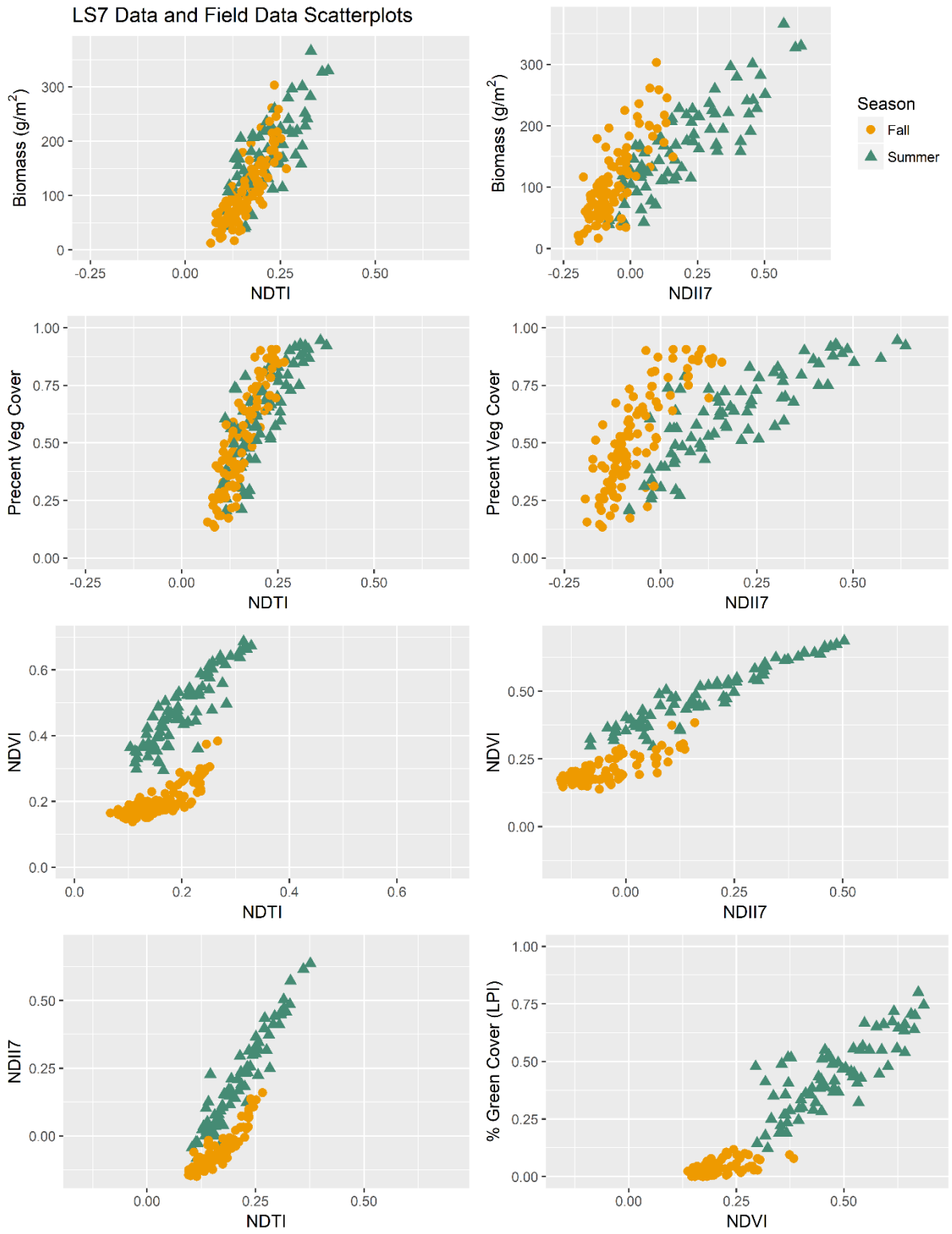


Figure A1.3. Scatter plots between in-field estimates of cover and biomass with select vegetation indices (NDTI, NDII7, NDVI) using Landsat 7 data

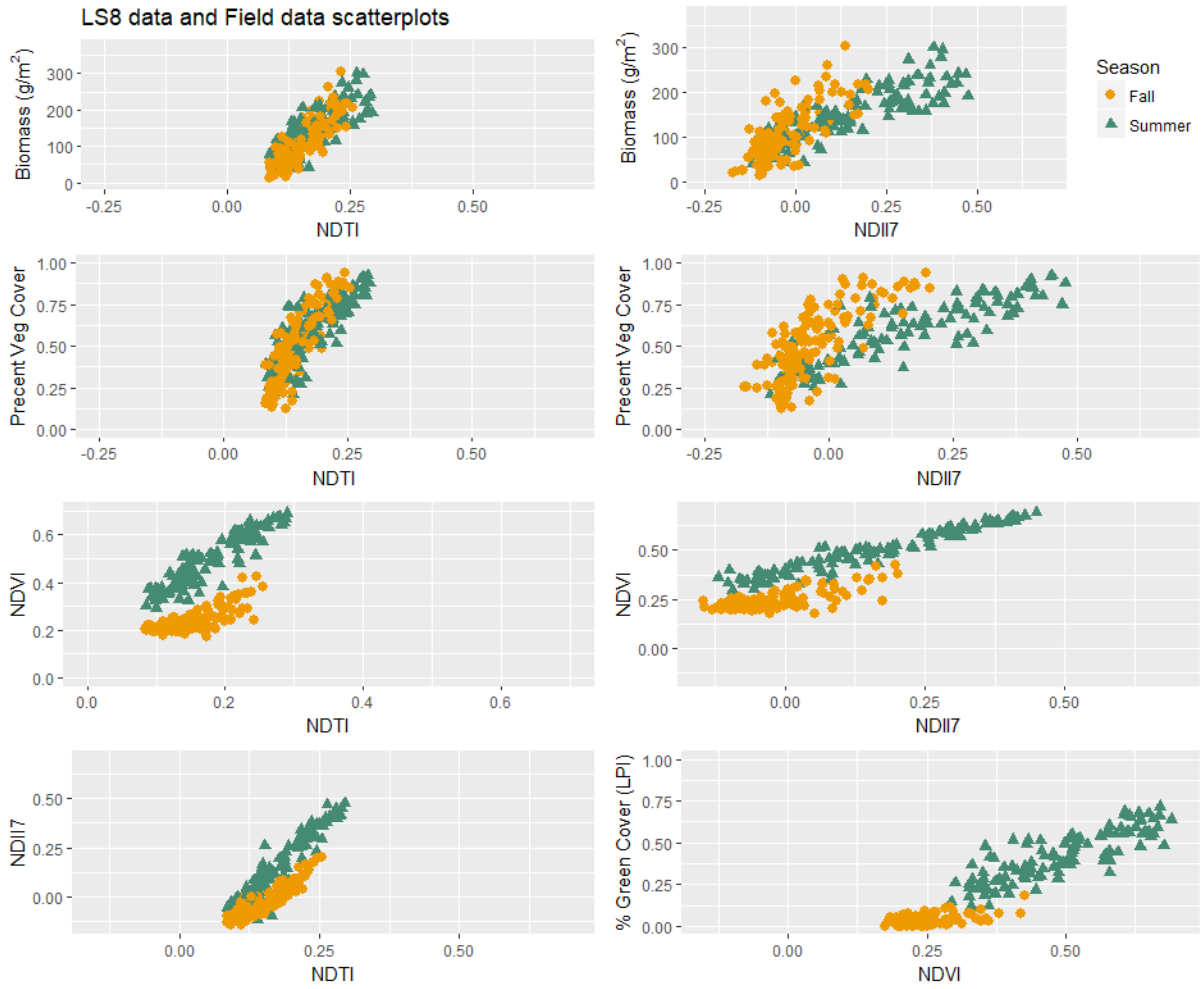


Figure A1.4. Scatter plots between in-field estimates of cover and biomass with select vegetation indices (NDTI, NDII7, NDVI) using Landsat 8 data

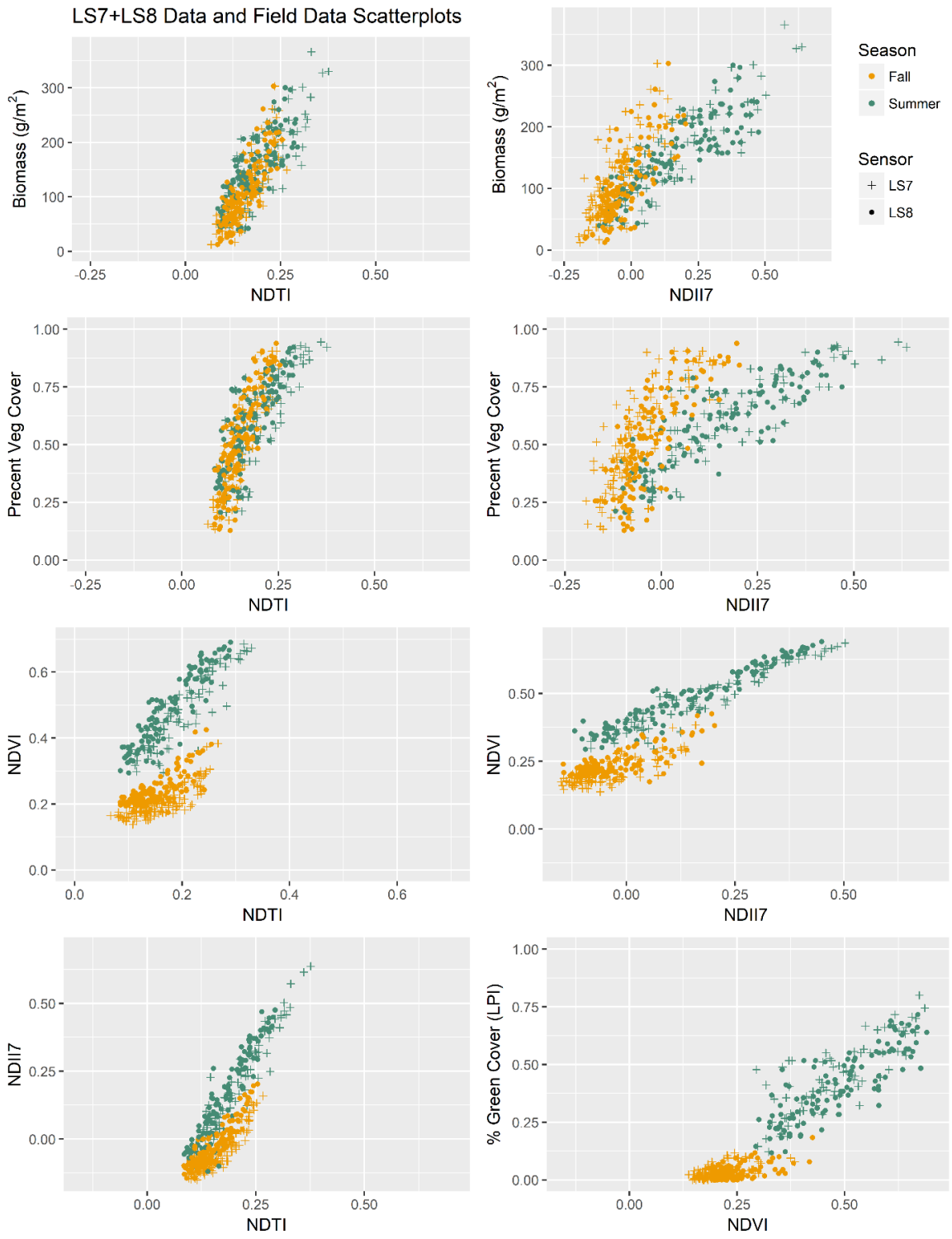


Figure A1.5. Scatter plots between in-field estimates of cover and biomass with select vegetation indices (NDTI, NDII7, NDVI) using Landsat 7 and Landsat 8 data.

Table A1.14. Table of Median and Mean pixel differences in Biomass across scene pairs across all model combinations and the associated vegetation index (NDII7 for Green, NDTI for Brown).

| Time | Scenes Compared | Statistic | LS8SLS7M LS7SLS7M | LS8SLS8M LS7SLS7M | LS8SLS78M LS7SLS7M | LS8SLS7M LS7SLS8M | LS8SLS8M LS7SLS8M | LS8SLS78M LS7SLS8M | LS8SLS7M LS7SLS78M | LS8SLS8M LS7SLS78M | LS8SLS78M LS7SLS78M |
|---|---|---|---|---|---|---|---|---|---|---|---|
| Green | Jun. 28-29 2013 | Median | 2.31 | 0.78 | 1.35 | 3.82 | 2.29 | 2.87 | 3.26 | 1.73 | 2.31 |
| | | Mean | 2.59 | 1.14 | 0.89 | 4.06 | 2.61 | -6.33 | 3.51 | 2.04 | 2.55 |
| | Jun. 23-24 2014 | Median | 1.26 | -0.35 | 0.29 | 2.87 | 1.26 | 1.90 | 2.23 | 0.62 | 1.26 |
| | | Mean | 0.93 | -0.64 | -0.03 | 2.50 | 0.93 | 1.54 | 1.89 | 0.32 | 0.93 |
| | Jun. 10-11 2015 | Median | -1.13 | -2.73 | -2.09 | 0.48 | -1.12 | -0.49 | -0.16 | -1.76 | -1.12 |
| | | Mean | -1.91 | -3.59 | -2.80 | -0.31 | -1.88 | -1.22 | -0.68 | -2.47 | -1.87 |
| | Jun. 26-27 2015 | Median | 4.14 | 2.63 | 3.19 | 5.62 | 4.11 | 4.67 | 5.08 | 3.57 | 4.14 |
| | | Mean | 4.27 | 2.77 | 3.32 | 5.73 | 4.23 | 4.78 | 5.21 | 3.70 | 4.26 |
| | Jun. 20-21 2016 | Median | 2.91 | 1.29 | 1.94 | 4.51 | 2.89 | 3.54 | 3.87 | 2.26 | 2.90 |
| | | Mean | 3.00 | 1.39 | 2.03 | 4.58 | 2.98 | 3.62 | 3.96 | 2.35 | 2.99 |
| | Jun. 23-24 2017 | Median | 1.99 | 0.34 | 1.01 | 3.63 | 1.98 | 2.66 | 2.97 | 1.31 | 1.99 |
| | | Mean | 2.14 | 0.51 | 1.17 | 3.76 | 2.13 | 2.79 | 3.11 | 1.48 | 2.14 |
| | All Scene Averages | Avg Median | 1.91 | 0.33 | 0.95 | 3.49 | 1.90 | 2.52 | 2.88 | 1.29 | 1.91 |
| | | Std Median | 1.62 | 1.65 | 1.63 | 1.59 | 1.61 | 1.59 | 1.61 | 1.64 | 1.62 |
| | | Avg Mean | 1.84 | 0.26 | 0.76 | 3.39 | 1.83 | 0.86 | 2.83 | 1.06 | 1.57 |
| | | Std Mean | 1.95 | 2.00 | 1.90 | 1.91 | 1.93 | 3.72 | 1.86 | 1.94 | 1.93 |
| Brown | Sep. 11-12 2014 | Median | -6.68 | -4.54 | -5.09 | -8.01 | -5.88 | -6.43 | -7.39 | -5.25 | -5.80 |
| | | Mean | -6.55 | -3.55 | -4.79 | -8.18 | -5.56 | -6.32 | -6.26 | -5.11 | -5.73 |
| | Sep. 19-20 2014 | Median | 1.19 | 3.20 | 2.53 | -0.15 | 1.86 | 1.19 | 0.51 | 2.52 | 1.84 |
| | | Means | 1.93 | 3.55 | 3.01 | 0.47 | 2.06 | 2.59 | 0.83 | 2.72 | 2.62 |
| | Oct. 16-17 2015 | Median | -2.88 | -0.67 | -1.16 | -4.21 | -2.00 | -2.49 | -3.70 | -1.47 | -1.97 |
| | | Mean | -2.10 | 0.21 | 0.15 | -3.35 | -0.63 | -1.93 | -3.25 | -0.54 | -1.08 |
| | Sep. 24-25 2016 | Median | -3.35 | -1.30 | -1.93 | -4.69 | -2.64 | -3.27 | -4.02 | -1.97 | -2.61 |
| | | Mean | -3.10 | -0.57 | -1.22 | -3.91 | -1.70 | -2.61 | -3.46 | -1.25 | -1.83 |
| | Aug. 18-19 2017 | Median | -1.20 | 0.71 | -0.05 | -2.54 | -0.63 | -1.39 | -1.77 | 0.14 | -0.62 |
| | | Mean | -2.19 | 1.66 | -0.01 | 2.01 | -0.49 | -0.81 | -1.32 | 0.70 | -0.60 |
| | Sep. 27-28 2017 | Median | -2.08 | -0.13 | -0.85 | -3.42 | -1.47 | -2.19 | -2.68 | -0.73 | -1.45 |
| | | Mean | -1.63 | 0.29 | -0.38 | -6.72 | -0.94 | -1.65 | -2.27 | 3.74 | -1.17 |
| | All Scene Averages | Avg Median | -2.50 | -0.45 | -1.09 | -3.84 | -1.79 | -2.43 | -3.18 | -1.13 | -1.77 |
| | | Std Median | 2.38 | 2.32 | 2.27 | 2.37 | 2.32 | 2.27 | 2.40 | 2.34 | 2.29 |
| | | Avg Mean | -2.28 | 0.26 | -0.54 | -3.28 | -1.21 | -1.79 | -2.62 | 0.04 | -1.30 |
| | | Std Mean | 2.49 | 2.16 | 2.31 | 3.61 | 2.26 | 2.63 | 2.16 | 2.88 | 2.45 |

Table A1.15. Table of Median and Mean differences in Cover between scene pairs across all model combinations and the associated vegetation index (NDII7 for Green, NDTI for Brown).

| Time | Scenes Compared | Stat | LS8SLS7M LS7SLS7M | LS8SLS8M LS7SLS7M | LS8SLS78M LS7SLS7M | LS8SLS7M LS7SLS8M | LS8SLS8M LS7SLS8M | LS8SLS78M LS7SLS8M | LS8SLS7M LS7SLS78M | LS8SLS8M LS7SLS78M | LS8SLS78M LS7SLS78M | LS8VI-LS7VI |
|---|---|---|---|---|---|---|---|---|---|---|---|---|
| Green | Jun. 28-29 2013 | Median | 0.87 | 0.79 | 1.04 | 1.68 | 1.60 | 1.85 | 1.43 | 1.35 | 1.60 | 0.61 |
| | | Mean | 0.91 | 0.84 | 1.09 | 1.73 | 1.66 | 1.91 | 1.48 | 1.41 | 1.66 | 3.09 |
| | Jun. 23-24 2014 | Median | 0.34 | 0.16 | 0.41 | 1.12 | 0.94 | 1.20 | 0.86 | 0.69 | 0.94 | 2.5 |
| | | Mean | 0.04 | -0.10 | 0.15 | 0.83 | 0.69 | 0.94 | 0.58 | 0.43 | 0.69 | 8.25 |
| | Jun. 10-11 2015 | Median | -1.46 | -1.62 | -1.36 | -0.67 | -0.84 | -0.58 | -0.93 | -1.09 | -0.84 | -1.6 |
| | | Mean | -1.89 | -2.04 | -1.79 | -1.11 | -1.26 | -1.00 | -1.36 | -1.51 | -1.26 | 1.09 |
| | Jun. 26-27 2015 | Median | 2.06 | 2.00 | 2.25 | 2.88 | 2.82 | 3.07 | 2.64 | 2.57 | 2.82 | 1.99 |
| | | Mean | 2.00 | 1.93 | 2.18 | 2.82 | 2.75 | 3.00 | 2.57 | 2.50 | 2.75 | -25.25 |
| | Jun. 20-21 2016 | Median | 1.57 | 1.38 | 1.64 | 2.35 | 2.17 | 2.42 | 2.10 | 1.91 | 2.17 | 5.87 |
| | | Mean | 1.58 | 1.40 | 1.66 | 2.37 | 2.19 | 2.44 | 2.11 | 1.93 | 2.19 | 5.45 |
| | Jun. 23-24 2017 | Median | 0.99 | 0.76 | 1.02 | 1.76 | 1.53 | 1.79 | 1.50 | 1.27 | 1.53 | 3.95 |
| | | Mean | 1.02 | 0.81 | 1.07 | 1.80 | 1.59 | 1.84 | 1.54 | 1.33 | 1.59 | 7.71 |
| | All Scene Averages | Avg Median | 0.62 | 0.49 | 0.71 | 1.30 | 1.17 | 1.39 | 1.09 | 0.96 | 1.17 | 2.22 |
| | | Std Median | 1.07 | 1.07 | 1.09 | 1.17 | 1.16 | 1.20 | 1.13 | 1.13 | 1.16 | 2.59 |
| | | Avg Mean | 0.52 | 0.40 | 0.62 | 1.21 | 1.09 | 1.30 | 0.99 | 0.87 | 1.09 | 0.06 |
| | | Std Mean | 1.20 | 1.20 | 1.21 | 1.28 | 1.27 | 1.31 | 1.25 | 1.25 | 1.27 | 12.69 |
| Brown | Sep. 11-12 2014 | Median | -5.18 | -3.87 | -4.13 | -5.87 | -4.56 | -4.82 | -5.57 | -4.26 | -4.52 | -3.8 |
| | | Mean | -4.28 | -3.87 | -4.09 | -6.11 | -3.96 | -4.02 | -6.59 | -9.75 | -4.51 | -3.67 |
| | Sep. 19-20 2014 | Median | 0.93 | 2.21 | 1.88 | 0.22 | 1.51 | 1.18 | 0.54 | 1.82 | 1.49 | 1.28 |
| | | Mean | 1.64 | 2.90 | 2.46 | 0.62 | 2.13 | 1.61 | 1.00 | 2.16 | 2.28 | 1.57 |
| | Oct. 16-17 2015 | Median | -2.20 | -0.86 | -1.09 | -2.84 | -1.50 | -1.73 | -2.59 | -1.26 | -1.49 | -1.23 |
| | | Mean | -1.81 | -0.47 | -0.68 | -2.42 | -1.08 | -1.29 | -2.21 | -0.87 | -1.08 | -0.99 |
| | Sep. 24-25 2016 | Median | -2.67 | -1.38 | -1.68 | -3.38 | -2.09 | -2.39 | -3.06 | -1.76 | -2.07 | -1.76 |
| | | Mean | -1.98 | -0.83 | -1.28 | -2.89 | -1.48 | -1.76 | -2.17 | -1.26 | -2.11 | -1.28 |
| | Aug. 18-19 2017 | Median | -1.00 | 0.26 | -0.12 | -1.76 | -0.50 | -0.89 | -1.38 | -0.12 | -0.50 | -0.44 |
| | | Mean | -0.74 | 1.23 | 0.51 | -1.43 | -0.35 | -0.72 | -1.03 | -0.45 | -0.15 | -0.25 |
| | Sep. 27-28 2017 | Median | -1.71 | -0.44 | -0.80 | -2.46 | -1.19 | -1.55 | -2.09 | -0.82 | -1.18 | -1.02 |
| | | Mean | -1.30 | -0.07 | -0.66 | -2.19 | -0.84 | -1.26 | -1.86 | -0.51 | -0.71 | -0.84 |
| | All Scene Averages | Avg Median | -1.69 | -0.58 | -0.85 | -2.30 | -1.19 | -1.46 | -2.02 | -0.91 | -1.18 | -1.16 |
| | | Std Median | 1.84 | 1.71 | 1.70 | 1.93 | 1.75 | 1.76 | 1.89 | 1.73 | 1.73 | 1.66 |
| | | Avg Mean | -1.21 | -0.16 | -0.54 | -2.06 | -0.80 | -1.06 | -1.84 | -1.53 | -0.90 | -0.91 |
| | | Std Mean | 1.70 | 1.91 | 1.84 | 2.04 | 1.69 | 1.59 | 2.23 | 3.51 | 1.93 | 1.69 |

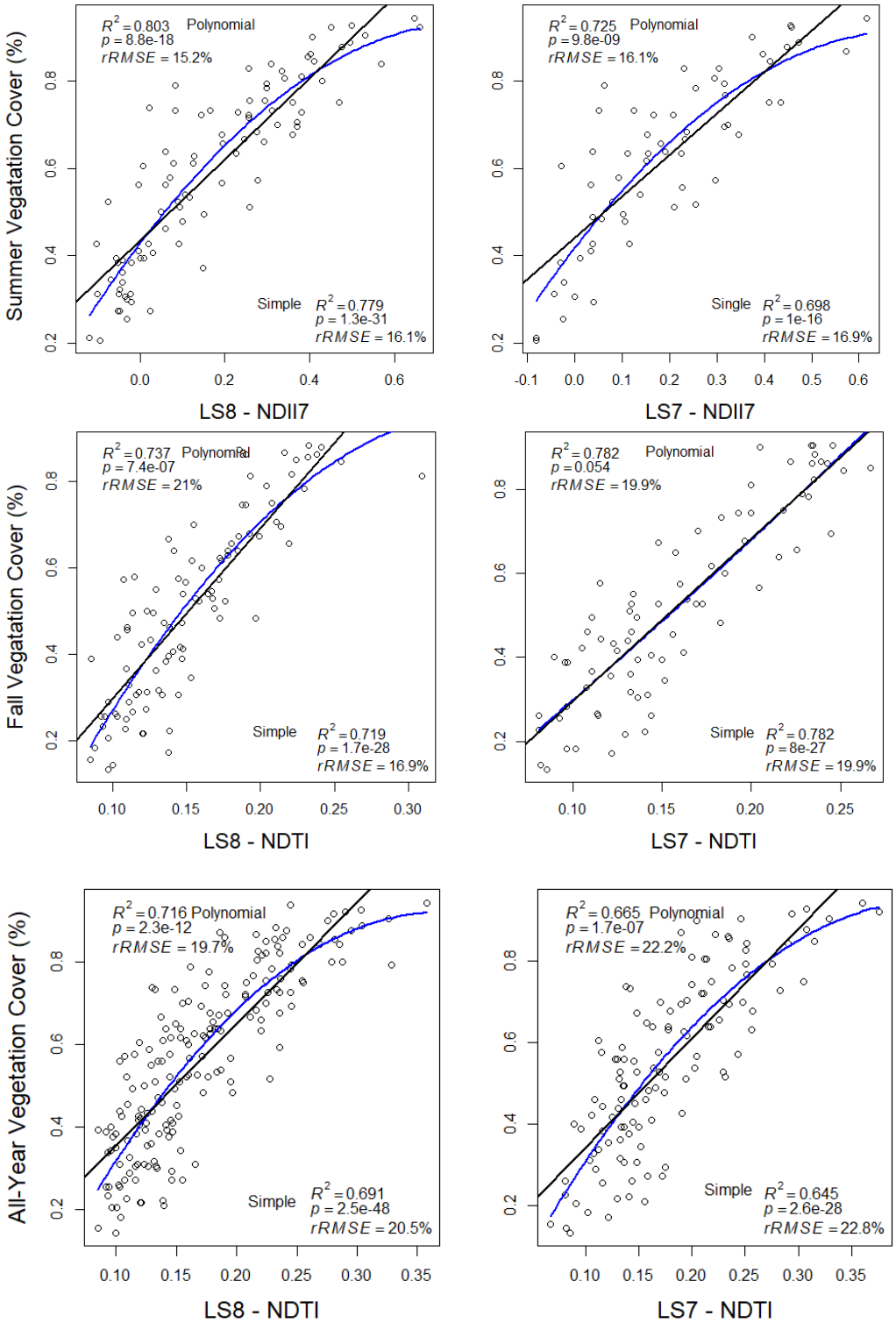


Figure A1.6. Scatter plots of simple and polynomial linear regressions using the summer, fall, and all-year cover data for both Landsat7 and Landsat 8.

Table A1.16. Model fit statistics for simple and polynomial linear regressions using the summer and fall cover data

| Metric | Time | Sensor | Model | Veg Index | Training | | | | Lillie-test | Testing | | | |
|---|---|---|---|---|---|---|---|---|---|---|---|---|---|
| | | | | | N | $R^2$ | rRMSE | RMSD | | N | $R^2$ | rRMSE | RMSD |
| Cover | Summer | LS7 | Simple | NDII7 | 60 | 0.70 | 16.89 | 0.106 | 0.89 | 20 | 0.70 | 17.39 | 0.111 |
| | Summer | LS7 | Polynomial | NDII7 | 60 | 0.72 | 16.12 | 0.101 | 0.47 | 20 | 0.70 | 17.03 | 0.108 |
| | Summer | LS8 | Simple | NDII7 | 93 | 0.78 | 16.07 | 0.097 | 0.60 | 30 | 0.75 | 13.00 | 0.085 |
| | Summer | LS8 | Polynomial | NDII7 | 60 | 0.80 | 15.20 | 0.091 | 0.48 | 30 | 0.77 | 11.97 | 0.078 |
| | Fall | LS7 | Simple | NDTI | 78 | 0.78 | 19.87 | 0.104 | 0.48 | 26 | 0.81 | 17.07 | 0.090 |
| | Fall | LS7 | Polynomial | NDTI | 78 | 0.78 | 19.85 | 0.104 | 0.48 | 26 | 0.81 | 17.15 | 0.091 |
| | Fall | LS8 | Simple | NDTI | 99 | 0.72 | 21.73 | 0.110 | 0.51 | 32 | 0.72 | 22.71 | 0.125 |
| | Fall | LS8 | Polynomial | NDTI | 99 | 0.74 | 21.02 | 0.106 | 0.84 | 32 | 0.72 | 22.16 | 0.122 |
| | All-Year | LS7 | Simple | NDTI | 120 | 0.65 | 22.84 | 0.12 | 0.64 | 40 | 0.72 | 21.00 | 0.121 |
| | All-Year | LS7 | Polynomial | NDTI | 120 | 0.67 | 22.18 | 0.12 | 0.93 | 40 | 0.75 | 20.50 | 0.118 |
| | All-Year | LS8 | Simple | NDTI | 184 | 0.69 | 20.55 | 0.12 | 0.61 | 62 | 0.70 | 21.02 | 0.115 |
| | All-Year | LS8 | Polynomial | NDTI | 184 | 0.72 | 19.70 | 0.11 | 0.89 | 62 | 0.74 | 18.97 | 0.104 |

# Appendix 2. Supplemental Materials for Chapter 3.

Table A2.1. Spearman Rank correlations between Stocking rate and biomass spatial and summary statistics (N=23). Correlations significant at the 0.05 p-valule are bolded.

| Stat | Scale | sill | range | nugget | MSH | NSRatio | mean | p10 | p25 | p50 | p75 | p90 | SD | CV |
|---|---|---|---|---|---|---|---|---|---|---|---|---|---|---|
| r | 1 | -0.02 | **0.60** | -0.12 | 0.00 | 0.00 | **-0.43** | -0.39 | **-0.44** | **-0.43** | **-0.43** | **-0.49** | -0.07 | 0.34 |
| p-val | 1 | 0.94 | **0.00** | 0.59 | 0.98 | 0.98 | **0.04** | 0.06 | **0.04** | **0.04** | **0.04** | **0.02** | 0.74 | 0.11 |
| r | 3 | 0.02 | **0.78** | 0.07 | -0.12 | 0.12 | **-0.43** | **-0.44** | **-0.42** | **-0.41** | **-0.47** | **-0.51** | 0.00 | 0.28 |
| p-val | 3 | 0.92 | **0.00** | 0.74 | 0.59 | 0.59 | **0.04** | **0.03** | **0.05** | **0.05** | **0.02** | **0.01** | 0.99 | 0.19 |
| r | 5 | 0.00 | **0.75** | 0.02 | -0.05 | 0.05 | **-0.42** | **-0.41** | **-0.42** | **-0.41** | **-0.47** | **-0.52** | 0.02 | 0.30 |
| p-val | 5 | 0.99 | **0.00** | 0.92 | 0.80 | 0.80 | **0.05** | **0.05** | **0.05** | **0.05** | **0.02** | **0.01** | 0.92 | 0.16 |
| r | 8 | 0.00 | **0.55** | 0.05 | 0.00 | 0.05 | **-0.42** | **-0.42** | **-0.42** | **-0.41** | **-0.46** | **-0.51** | 0.06 | 0.32 |
| p-val | 8 | 0.99 | **0.01** | 0.81 | 0.99 | 0.81 | **0.05** | **0.05** | **0.05** | **0.05** | **0.03** | **0.01** | 0.77 | 0.14 |
| r | 20 | 0.11 | 0.25 | -0.17 | 0.15 | -0.15 | **-0.44** | **-0.44** | **-0.44** | **-0.43** | **-0.49** | **-0.51** | 0.13 | 0.35 |
| p-val | 20 | 0.61 | 0.24 | 0.43 | 0.48 | 0.48 | **0.03** | **0.03** | **0.03** | **0.04** | **0.02** | **0.01** | 0.54 | 0.10 |
| r | 30 | 0.01 | 0.23 | -0.19 | 0.19 | -0.19 | **-0.46** | **-0.44** | **-0.44** | **-0.44** | **-0.46** | **-0.49** | 0.13 | 0.36 |
| p-val | 30 | 0.95 | 0.28 | 0.38 | 0.40 | 0.40 | **0.03** | **0.04** | **0.03** | **0.04** | **0.03** | **0.02** | 0.54 | 0.09 |

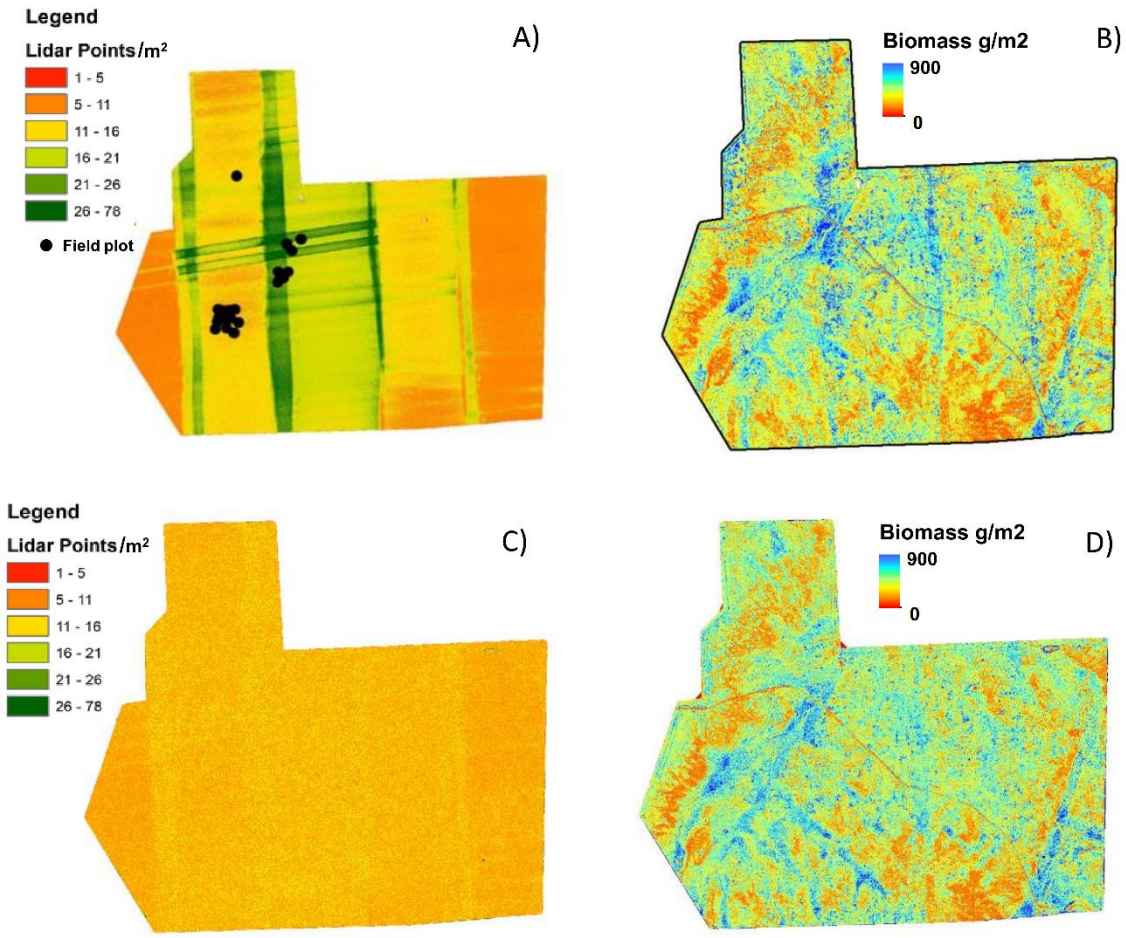


Figure A2.1. Raw vendor point clouds (A), with associated biomass map (B), the post processed density point cloud (C), and after CloudCompare processing at 9.15 points per square meter as well as the resulting biomass map (D).

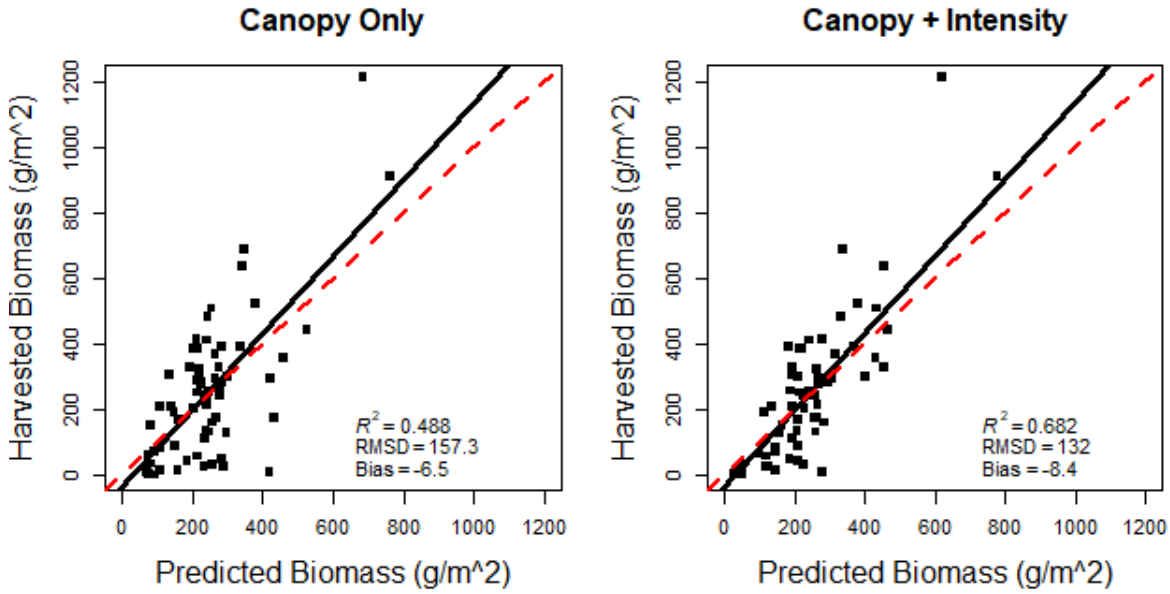


Figure A2.2. Applying the random forest modeling approach to the non-corrected lidar point clouds.

Table. A2.2 Linear and Quadratic models for the pasture scale summary Stats (N=23). $r^2$ values significant at the 0.05 p-val are in boxes and bold. The symbol ** denotes that these models violate the assumption of normally distributed residuals using the Lillie test (italicized).

| Statistic | Transformation | 1.0668m | 2m | 5m | 8m | 20m | 30m |
|---|---|---|---|---|---|---|---|
| P10 | Recip | 0.04 | 0.05 | 0.05 | 0.06 | 0.07 | 0.08 |
| P10 | Quadratic | 0.23 | 0.23 | 0.24 | 0.24 | **0.27** | **0.29** |
| P25 | none | 0.08 | 0.07 | 0.07 | 0.08 | 0.09 | 0.09 |
| P25 | Quadratic | **0.27** | **0.28** | **0.28** | **0.28** | **0.28** | **0.28** |
| Mean | none | 0.13 | 0.13 | 0.13 | 0.13 | 0.13 | 0.13 |
| Mean | Quadratic | **0.30** | **0.29** | **0.30** | **0.30** | **0.30** | **0.29** |
| P75 | none | 0.15 | **0.17** | **0.18** | **0.18** | **0.18** | **0.18** |
| P75 | Quadratic | **0.26** | **0.29** | **0.29** | **0.29** | **0.30** | **0.29** |
| P90 | none** | *0.17* | *0.20* | *0.20* | *0.19* | *0.18* | *0.17* |
| P90 | Quadratic** | 0.23 | **0.27** | *0.27* | **0.27** | **0.27** | 0.25 |
| CV | none | 0.05 | 0.03 | 0.03 | 0.03 | 0.05 | 0.05 |
| CV | Quadratic | **0.28** | **0.26** | 0.26 | **0.26** | **0.27** | **0.29** |

Table A2.3. Pairwise comparisons of pasture Range metric between different cell sizes using the Mann-Whitney U Wilcoxon rank sum test. The p-values were adjusted with the Bonferroni correction.

| Grid Size | 1.0668 | 3 | 5 | 8 | 20 |
|---|---|---|---|---|---|
| 3 | **0.00** | | | | |
| 5 | **0.00** | 0.25 | | | |
| 8 | **0.00** | **0.00** | 0.54 | | |
| 20 | **0.00** | **0.00** | **0.00** | **0.01** | |
| 30 | **0.00** | **0.00** | **0.00** | **0.00** | 1.00 |

Table A2.4. Pairwise comparisons of pasture Sill metric between different cell sizes using the Mann-Whitney U Wilcoxon rank sum test. The p-values were adjusted with the Bonferroni correction.

| Grid Size | 1.0668 | 3 | 5 | 8 | 20 |
|---|---|---|---|---|---|
| 3 | **0.00** | | | | |
| 5 | **0.00** | 0.92 | | | |
| 8 | **0.00** | 0.12 | 1.00 | | |
| 20 | **0.00** | **0.00** | **0.02** | 0.48 | |
| 30 | **0.00** | **0.00** | **0.00** | 0.17 | 1.00 |

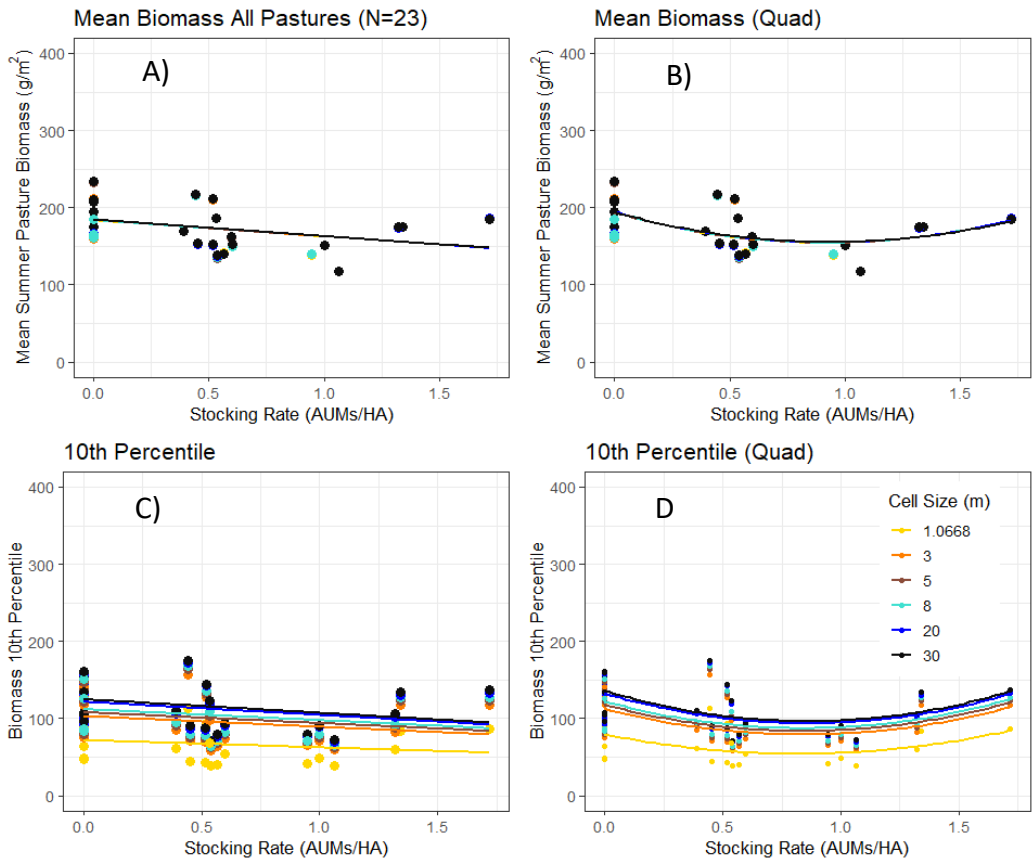


Figure A2.3. Linear (A,C) and quadratic ((Quad) B,D) models for the mean and 10$^{th}$ percentiles across all cell sizes (N=23).

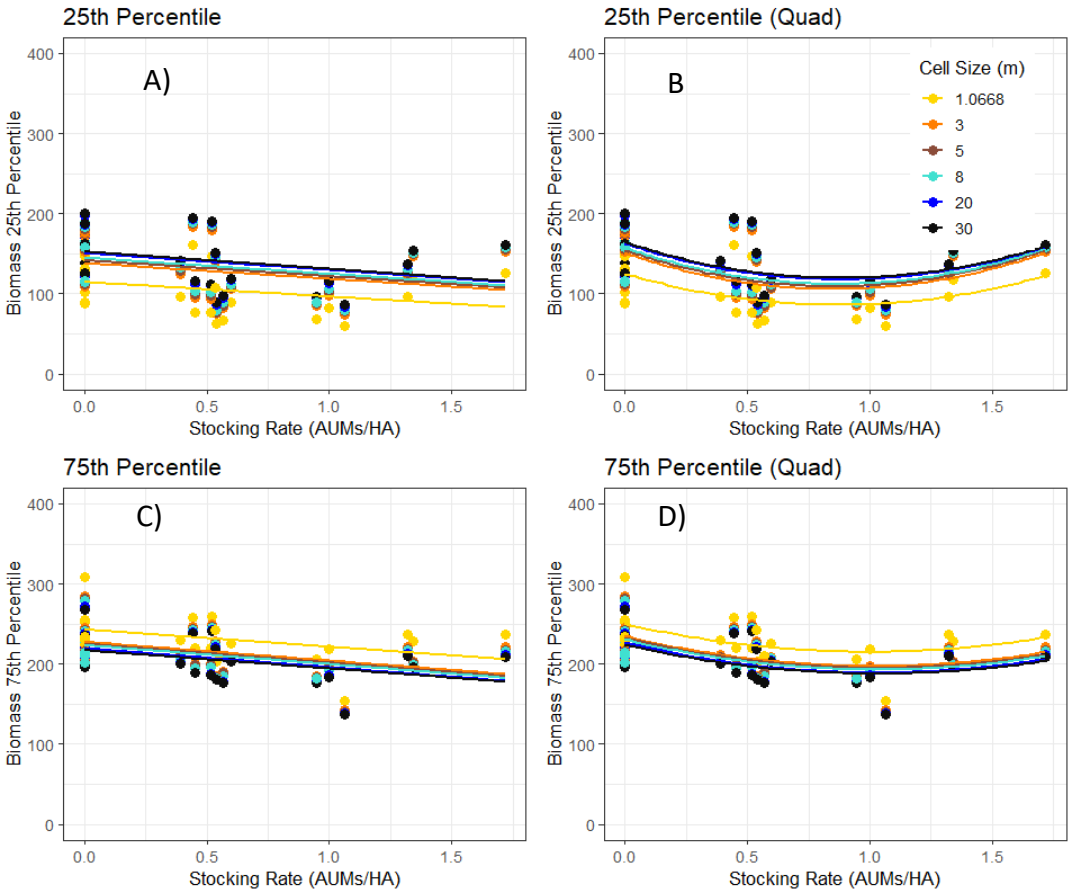


Figure A2.4. Linear (A,C) and quadratic ((Quad) B,D) models for the 25$^{th}$ and 75$^{th}$ percentiles across all cell sizes (N=23).

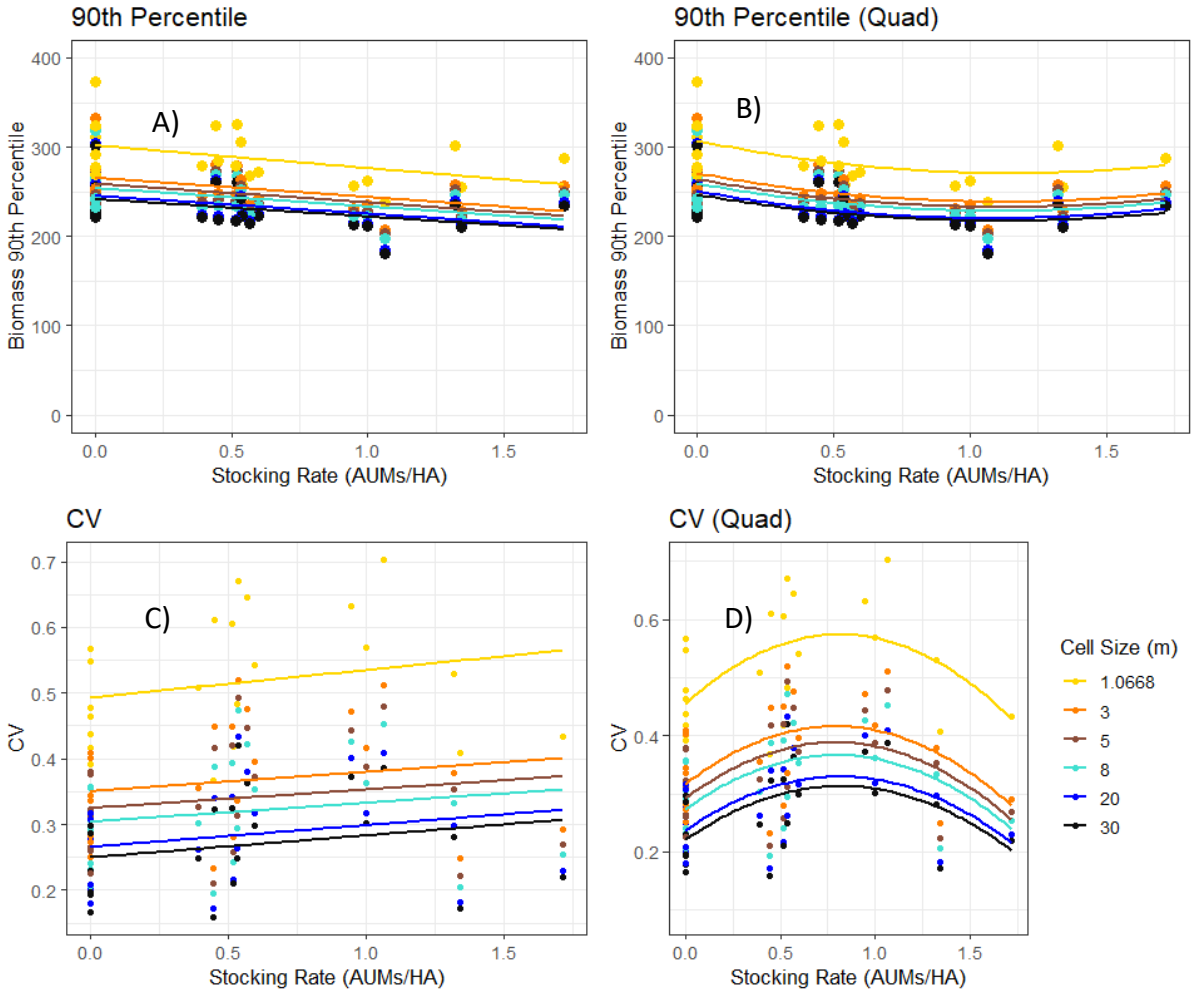


Figure A2.5. Linear (A,C) and quadratic ((Quad) B,D) models for the 90th and coefficient of variation across all cell sizes (N=23).

Table A2.5. Linear and Quadratic models for the pasture scale summary Stats with 1 outlier (P5) removed (N=22). r2 values significant at the 0.05 p-val are in boxes and bold. The symbol ** denotes that these models violate the assumption of normally distributed residuals using the Lillie test (italicized).

| Statistic | Transformation | 1.0668m | 2m | 5m | 8m | 20m | 30m |
|---|---|---|---|---|---|---|---|
| P10 | none | 0.12 | 0.14 | 0.14 | *0.14* | 0.17 | 0.18 |
| P10 | Quadratic | 0.20 | 0.21 | 0.22 | 0.22 | 0.26 | **0.27** |
| P25 | none | **0.18** | 0.17 | 0.17 | 0.17 | **0.19** | **0.19** |
| P25 | Quadratic | 0.26 | 0.26 | 0.26 | 0.26 | **0.27** | **0.27** |
| Mean | none | **0.29** | **0.29** | **0.29** | **0.29** | **0.30** | **0.29** |
| Mean | Quadratic | **0.23** | **0.23** | **0.23** | **0.23** | **0.23** | **0.23** |
| P75 | none | **0.23** | **0.26** | **0.26** | **0.27** | **0.27** | **0.26** |
| P75 | Quadratic | 0.26 | **0.29** | **0.29** | **0.30** | **0.31** | **0.29** |
| P90 | none** | *0.23* | **0.28** | **0.28** | **0.28** | *0.27* | *0.26* |
| P90 | Quadratic** | 0.24 | *0.29* | *0.29* | *0.29* | *0.29* | *0.26* |
| CV | none | 0.13 | 0.10 | 0.09 | 0.10 | 0.12 | 0.12 |
| CV | Quadratic | 0.26 | 0.24 | 0.24 | 0.24 | 0.26 | **0.28** |

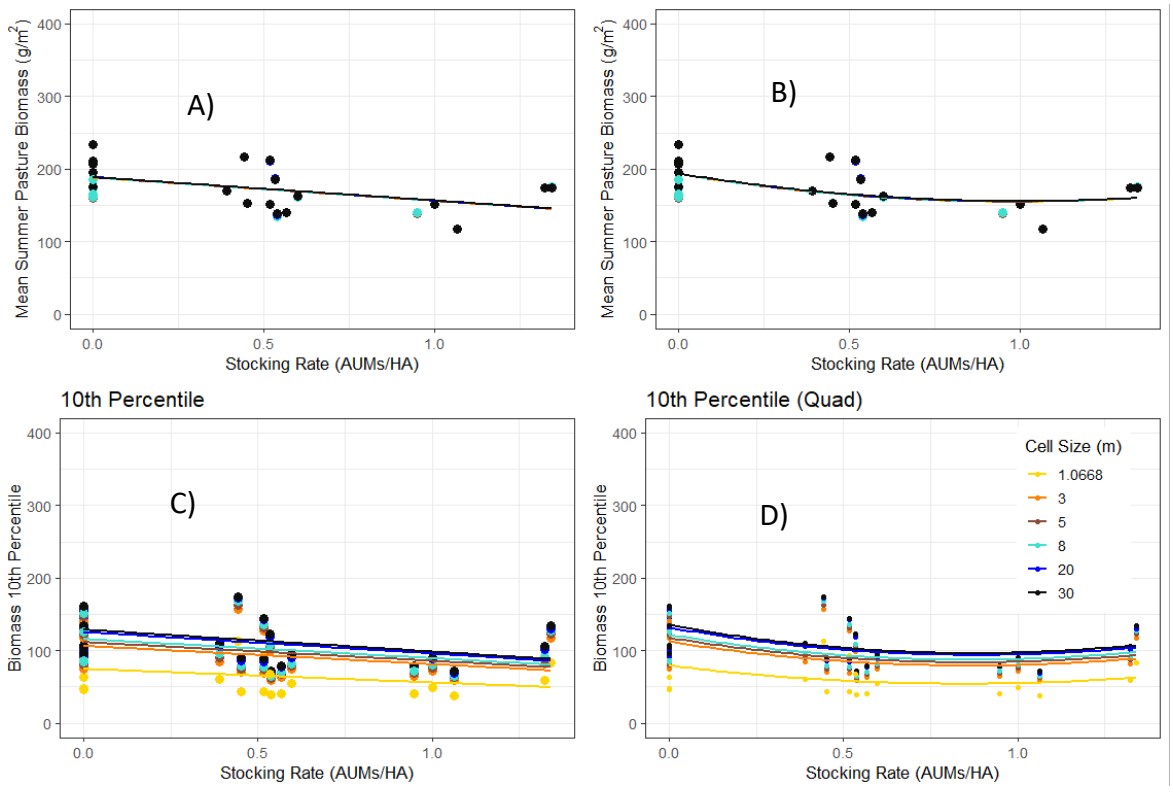


Figure A2.6. Linear (A,C) and quadratic ((Quad) B,D) models for the mean and 10th percentiles across all cell sizes (N=22).

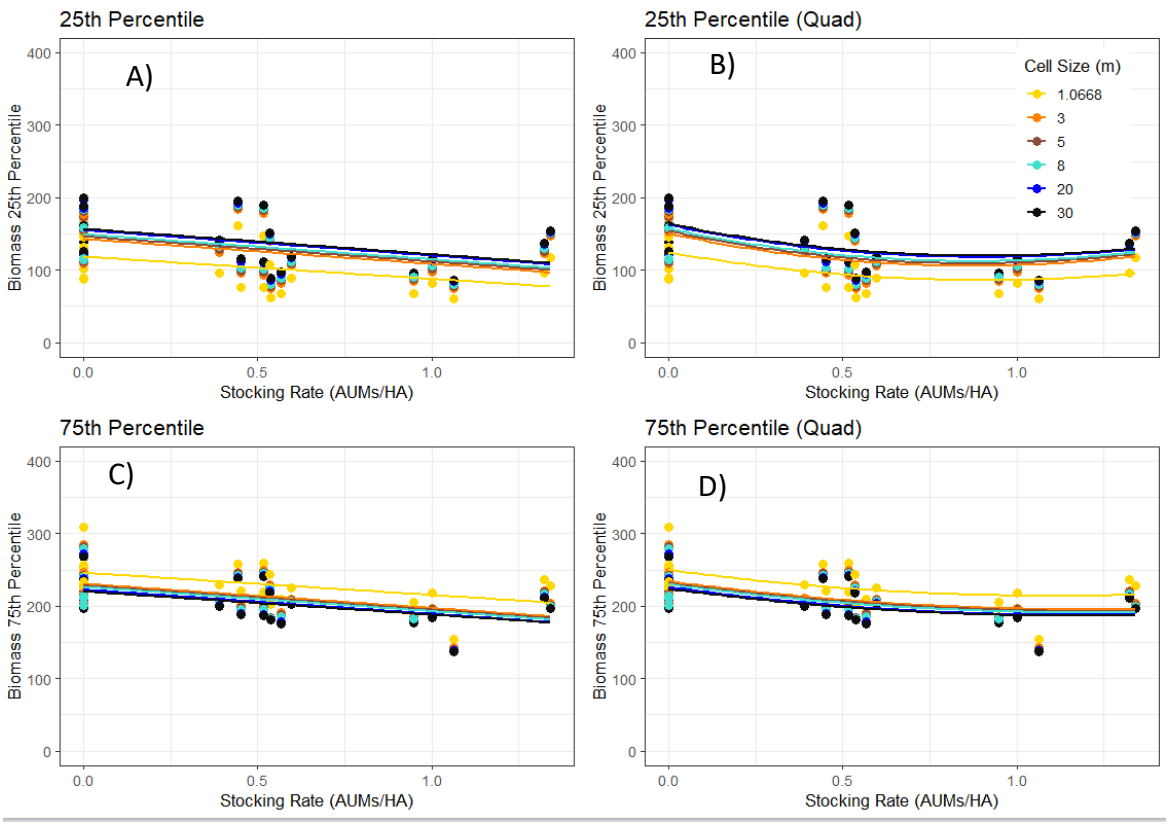


Figure A2.7. Linear (A,C) and quadratic ((Quad) B,D) models for the 25$^{th}$ and 75$^{th}$ percentiles across all cell sizes (N=23).

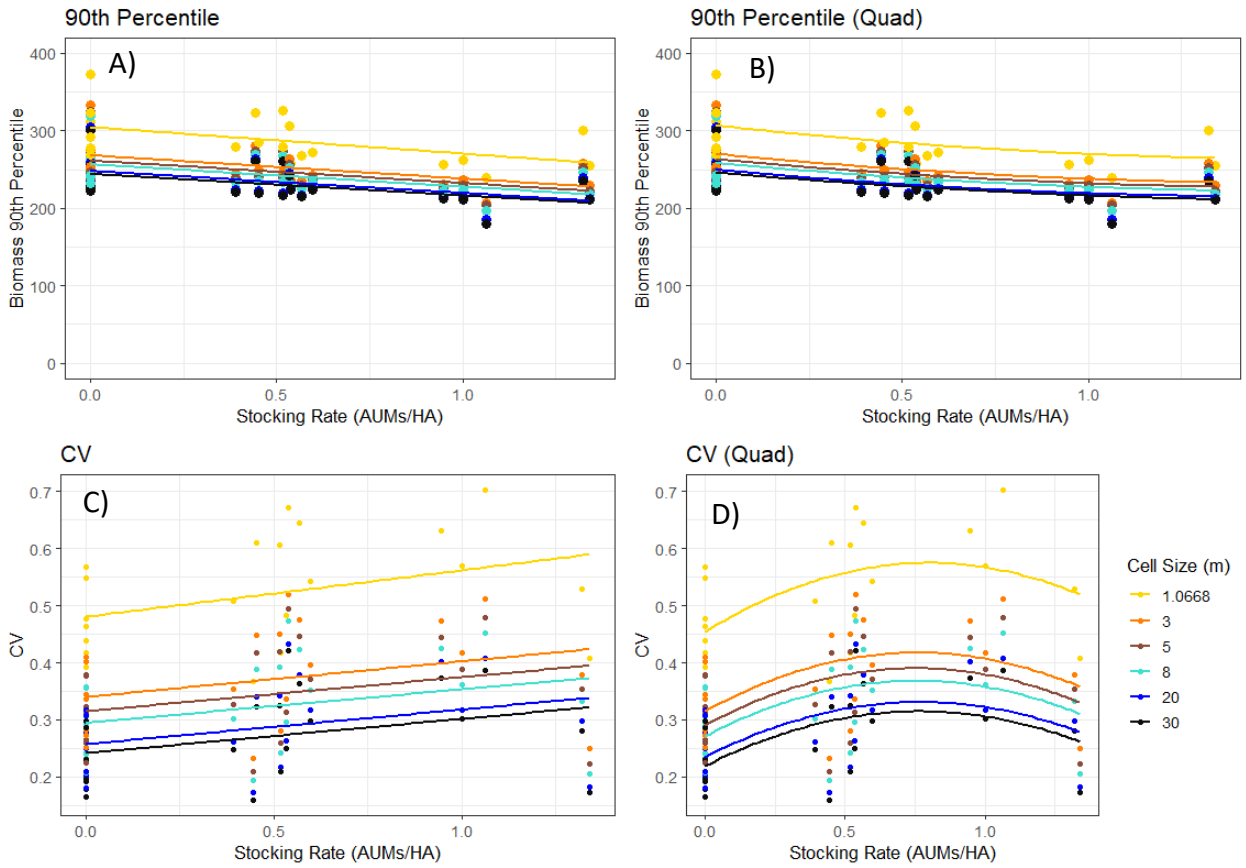


Figure A2.8. Linear (A,C) and quadratic ((Quad) B,D) models for the 90$^{th}$ and coefficient of variation across all cell sizes (N=22).

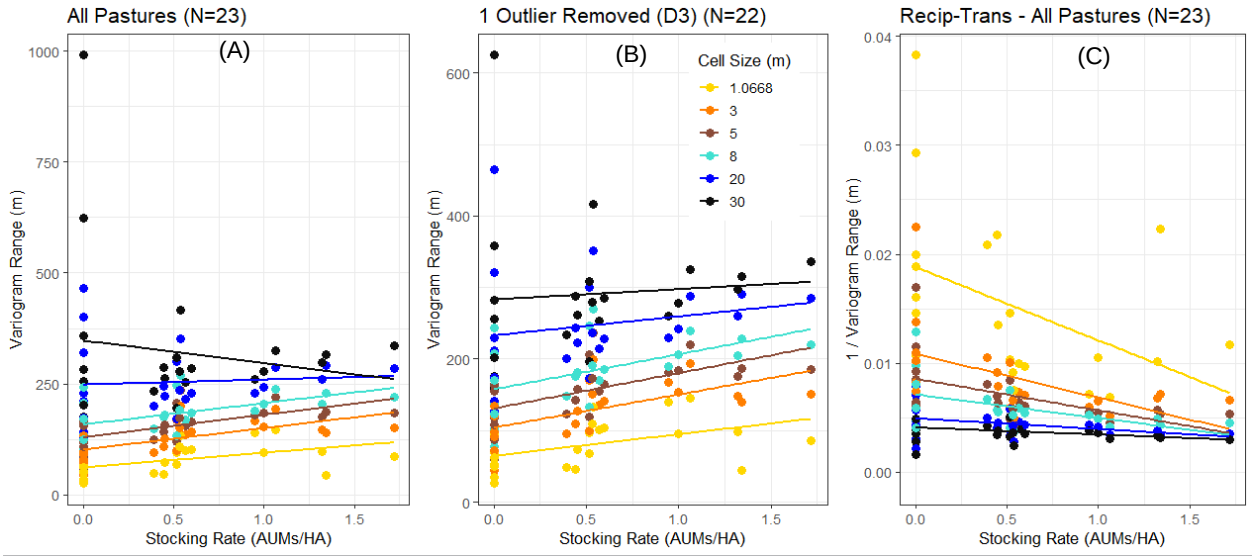


Figure A2.9. Linear models for the range statistic across all cell sizes, for the complete data set (A), when one outlier was removed (B), and using the reciprocal transformation (C).

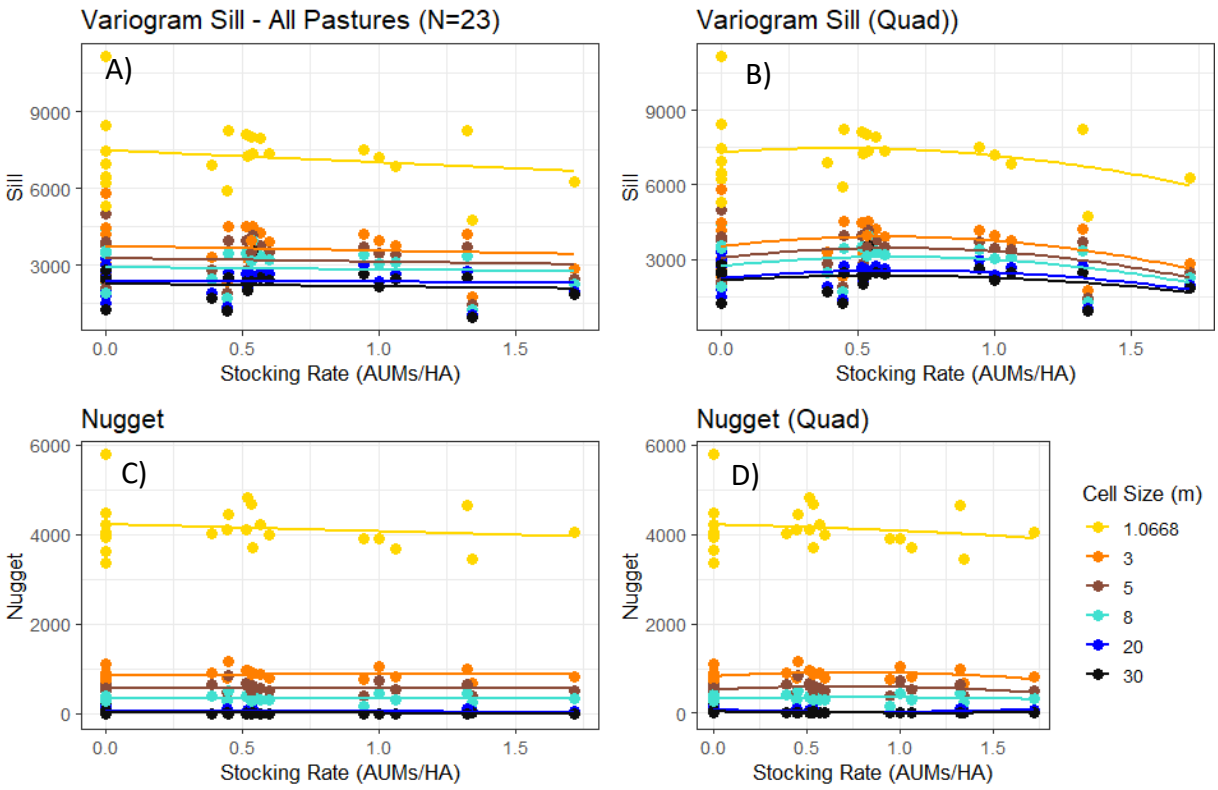


Figure A2.10. Linear (A,C) and quadratic ((Quad) B,D) models for the range statistic all cell sizes.

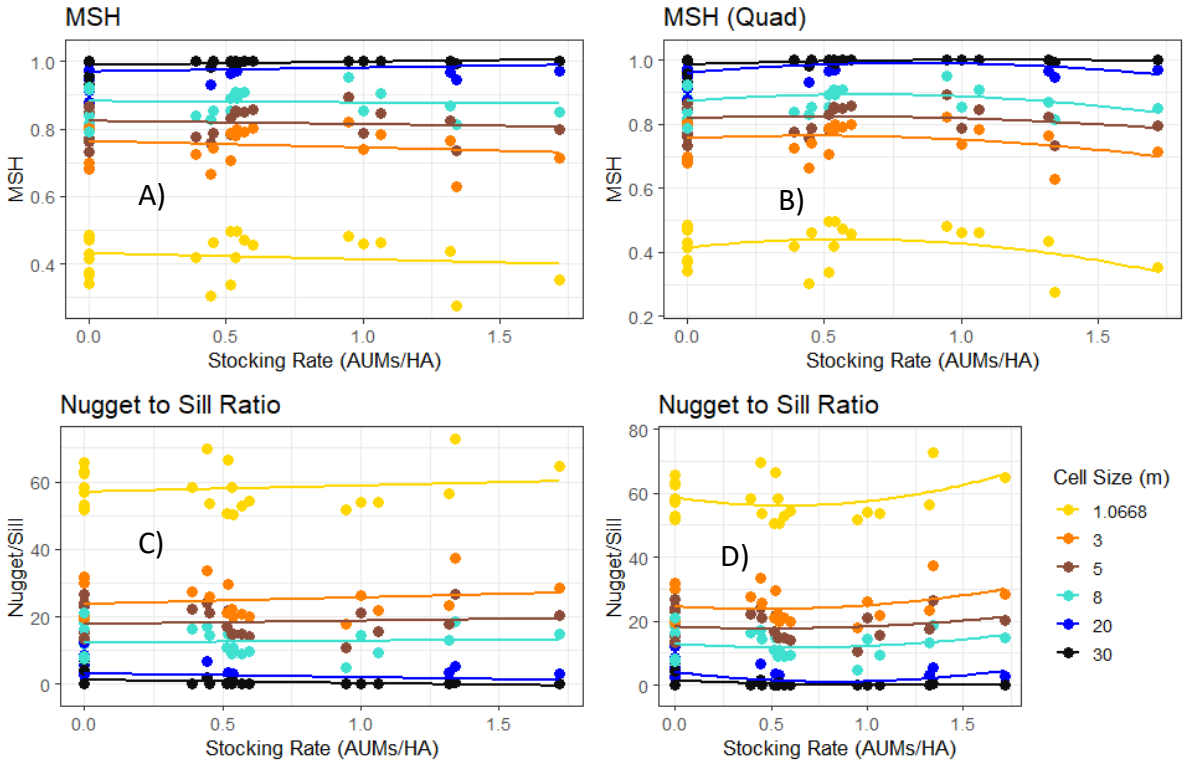


Figure A2.11. Linear (A,C) and quadratic ((Quad) B,D) models for the range statistic all cell sizes.

# Appendix 3. Supplemental Materials for Chapter 4.

Table A3.1. Complete Table of spearman rank correlations between pasture level metrics and stocking rate.

| | 2015 | | | 2016 | | | 2017 | | | All Years | | | 3 Year Mean |
|---|---|---|---|---|---|---|---|---|---|---|---|---|---|
| Pasture Metric | r | p-val | N | r | p-val | N | r | p-val | N | r | p-val | N | r |
| Summer_sill | 0.04 | 0.80 | 37 | 0.17 | 0.20 | 60 | **-0.24** | **0.04** | 72 | **-0.16** | **0.04** | 169 | -0.01 |
| Summer_range | 0.17 | 0.33 | 37 | 0.24 | 0.06 | 60 | -0.05 | 0.68 | 72 | 0.08 | 0.32 | 169 | 0.12 |
| Summer_nugget | 0.07 | 0.69 | 37 | 0.08 | 0.52 | 60 | 0.01 | 0.90 | 72 | 0.03 | 0.67 | 169 | 0.06 |
| Summer_MSH | -0.08 | 0.65 | 37 | -0.10 | 0.45 | 60 | -0.04 | 0.76 | 72 | -0.06 | 0.46 | 169 | -0.07 |
| Summer_mean | **-0.52** | **0.00** | 37 | **-0.26** | **0.05** | 60 | -0.18 | 0.13 | 72 | -0.07 | 0.36 | 169 | -0.32 |
| Summer_p10. | **-0.51** | **0.00** | 37 | **-0.27** | **0.04** | 60 | 0.04 | 0.72 | 72 | 0.04 | 0.64 | 169 | -0.25 |
| Summer_p25. | **-0.49** | **0.00** | 37 | **-0.26** | **0.04** | 60 | -0.07 | 0.55 | 72 | -0.01 | 0.86 | 169 | -0.27 |
| Summer_p50. | **-0.51** | **0.00** | 37 | **-0.32** | **0.01** | 60 | -0.18 | 0.13 | 72 | -0.09 | 0.24 | 169 | -0.34 |
| Summer_p75. | **-0.51** | **0.00** | 37 | -0.23 | 0.08 | 60 | **-0.25** | **0.04** | 72 | -0.12 | 0.13 | 169 | -0.33 |
| Summer_p90. | **-0.45** | **0.00** | 37 | -0.12 | 0.38 | 60 | **-0.26** | **0.03** | 72 | -0.11 | 0.14 | 169 | -0.28 |
| Summer_sd | 0.03 | 0.85 | 37 | 0.17 | 0.18 | 60 | **-0.28** | **0.02** | 72 | **-0.17** | **0.03** | 169 | -0.02 |
| Summer_CV | **0.45** | **0.00** | 37 | **0.28** | **0.03** | 60 | **-0.27** | **0.02** | 72 | -0.11 | 0.16 | 169 | 0.15 |
| Summer_Moran_I | **-0.38** | **0.02** | 37 | **-0.32** | **0.01** | 60 | -0.12 | 0.30 | 72 | **-0.26** | **0.00** | 169 | -0.28 |
| Fall_sill | 0.09 | 0.59 | 37 | 0.31 | **0.02** | 60 | 0.10 | 0.39 | 72 | 0.01 | 0.89 | 169 | 0.17 |
| Fall_range | 0.09 | 0.60 | 37 | 0.21 | 0.11 | 60 | -0.13 | 0.28 | 72 | 0.03 | 0.72 | 169 | 0.06 |
| Fall_nugget | 0.21 | 0.20 | 37 | -0.06 | 0.64 | 60 | -0.18 | 0.14 | 72 | -0.04 | 0.57 | 169 | -0.01 |
| Fall_MSH | -0.20 | 0.24 | 37 | 0.06 | 0.67 | 60 | 0.19 | 0.10 | 72 | 0.05 | 0.54 | 169 | 0.02 |
| Fall_mean | **-0.55** | **0.00** | 37 | **-0.56** | **0.00** | 60 | **-0.52** | **0.00** | 72 | **-0.28** | **0.00** | 169 | -0.54 |
| Fall_p10. | **-0.56** | **0.00** | 37 | **-0.59** | **0.00** | 60 | **-0.49** | **0.00** | 72 | **-0.24** | **0.00** | 169 | -0.55 |
| Fall_p25. | **-0.53** | **0.00** | 37 | **-0.57** | **0.00** | 60 | **-0.50** | **0.00** | 72 | **-0.26** | **0.00** | 169 | -0.53 |
| Fall_p50. | **-0.52** | **0.00** | 37 | **-0.54** | **0.00** | 60 | **-0.50** | **0.00** | 72 | **-0.27** | **0.00** | 169 | -0.52 |
| Fall_p75. | **-0.54** | **0.00** | 37 | **-0.51** | **0.00** | 60 | **-0.51** | **0.00** | 72 | **-0.29** | **0.00** | 169 | -0.52 |
| Fall_p90. | **-0.53** | **0.00** | 37 | **-0.49** | **0.00** | 60 | **-0.56** | **0.00** | 72 | **-0.30** | **0.00** | 169 | -0.53 |
| Fall_sd | 0.06 | 0.71 | 37 | **0.38** | **0.00** | 60 | 0.16 | 0.18 | 72 | 0.05 | 0.50 | 169 | 0.20 |
| Fall_CV | **0.50** | **0.00** | 37 | **0.51** | **0.00** | 60 | **0.32** | **0.01** | 72 | **0.16** | **0.04** | 169 | 0.44 |
| Fall_Moran_I | **-0.49** | **0.00** | 37 | **-0.33** | **0.01** | 60 | -0.22 | 0.06 | 72 | **-0.32** | **0.00** | 169 | -0.35 |
| RelDif_sill | 0.44 | **0.01** | 37 | 0.18 | 0.17 | 60 | -0.20 | 0.09 | 72 | 0.04 | 0.64 | 169 | 0.14 |
| RelDif_range | 0.41 | **0.01** | 37 | 0.19 | 0.15 | 60 | 0.08 | 0.50 | 72 | **0.16** | **0.04** | 169 | 0.23 |
| RelDif_nugget | 0.28 | 0.09 | 37 | 0.12 | 0.36 | 60 | 0.04 | 0.72 | 72 | 0.06 | 0.45 | 169 | 0.15 |
| RelDif_MSH | 0.00 | 0.98 | 37 | 0.02 | 0.86 | 60 | -0.07 | 0.58 | 72 | 0.04 | 0.62 | 169 | -0.02 |
| RelDif_mean | -0.32 | 0.05 | 37 | **-0.33** | **0.01** | 60 | **-0.54** | **0.00** | 72 | **-0.30** | **0.00** | 169 | -0.40 |
| RelDiff_p10. | **-0.50** | **0.00** | 37 | **-0.52** | **0.00** | 60 | **-0.47** | **0.00** | 72 | **-0.38** | **0.00** | 169 | -0.50 |
| RelDiff_p25. | **-0.44** | **0.01** | 37 | **-0.47** | **0.00** | 60 | **-0.47** | **0.00** | 72 | **-0.34** | **0.00** | 169 | -0.46 |
| RelDiff_p50. | **-0.34** | **0.04** | 37 | **-0.33** | **0.01** | 60 | **-0.48** | **0.00** | 72 | **-0.27** | **0.00** | 169 | -0.38 |
| RelDiff_p75. | -0.20 | 0.24 | 37 | -0.24 | 0.07 | 60 | **-0.52** | **0.00** | 72 | **-0.25** | **0.00** | 169 | -0.32 |
| Diff_p90. | -0.10 | 0.58 | 37 | -0.20 | 0.12 | 60 | **-0.55** | **0.00** | 72 | **-0.27** | **0.00** | 169 | -0.28 |
| RelDif_sd | 0.41 | **0.01** | 37 | 0.21 | 0.10 | 60 | -0.21 | 0.07 | 72 | 0.04 | 0.65 | 169 | 0.14 |
| RelDif_CV | -0.18 | 0.27 | 37 | 0.00 | 0.99 | 60 | **0.49** | **0.00** | 72 | 0.14 | 0.06 | 169 | 0.10 |
| RelDif_Moran_I | -0.17 | 0.31 | 37 | -0.23 | 0.07 | 60 | -0.03 | 0.78 | 72 | -0.14 | 0.06 | 169 | -0.15 |
| RelDif_DeltaRanged | -0.14 | 0.39 | 37 | 0.13 | 0.31 | 60 | -0.02 | 0.85 | 72 | 0.06 | 0.47 | 169 | -0.01 |
| RelDif_DeltaSill | -0.03 | 0.88 | 37 | -0.20 | 0.13 | 60 | 0.18 | 0.13 | 72 | 0.12 | 0.11 | 169 | -0.01 |
| RelDif_DeltaNugget | 0.00 | 0.99 | 37 | -0.17 | 0.18 | 60 | -0.13 | 0.28 | 72 | -0.08 | 0.33 | 169 | -0.10 |
| RelDif_DeltaMorans | -0.26 | 0.12 | 37 | 0.15 | 0.25 | 60 | -0.15 | 0.20 | 72 | -0.03 | 0.69 | 169 | -0.09 |
| RelDif_DeltaCV | 0.21 | 0.22 | 37 | 0.18 | 0.17 | 60 | **0.46** | **0.00** | 72 | **0.27** | **0.00** | 169 | 0.28 |

Table A3.2. Spearman rank correlations between pasture level metrics and stocking rate, grouped by season of use. Shown are statistics that were significant in at least two out of three seasons at the 0.05 p-value.

| Raster | Cool Summer | | | Hot Summer | | | Fall | | | All season |
|---|---|---|---|---|---|---|---|---|---|---|
| Statistic | r | p-val | N | r | p-val | N | r | p-val | N | Mean |
| $Fall_{mean}$ | -0.21 | **0.05** | 91 | -0.40 | **0.00** | 103 | -0.38 | **0.00** | 73 | -0.33 |
| $Fall_{p10}$ | -0.19 | 0.08 | 91 | -0.37 | **0.00** | 103 | -0.36 | **0.00** | 73 | -0.31 |
| $Fall_{p25}$ | -0.18 | 0.09 | 91 | -0.39 | **0.00** | 103 | -0.38 | **0.00** | 73 | -0.31 |
| $Fall_{p50}$ | -0.19 | 0.07 | 91 | -0.39 | **0.00** | 103 | -0.40 | **0.00** | 73 | -0.33 |
| $Fall_{p75}$ | -0.22 | **0.03** | 91 | -0.41 | **0.00** | 103 | -0.38 | **0.00** | 73 | -0.34 |
| $Fall_{p90}$ | -0.27 | **0.01** | 91 | -0.43 | **0.00** | 103 | -0.33 | **0.00** | 73 | -0.35 |
| $Fall_{CV}$ | 0.04 | 0.71 | 91 | 0.27 | **0.01** | 103 | 0.33 | **0.00** | 73 | 0.22 |
| $Fall_{Moran's\_I}$ | -0.13 | 0.23 | 91 | -0.46 | **0.00** | 103 | -0.34 | **0.00** | 73 | -0.31 |
| $RelDif_{mean}$ | -0.38 | **0.00** | 91 | -0.42 | **0.00** | 103 | -0.28 | **0.02** | 73 | -0.36 |
| $RelDif_{p10}$ | -0.39 | **0.00** | 91 | -0.52 | **0.00** | 103 | -0.42 | **0.00** | 73 | -0.44 |
| $RelDif_{p25}$ | -0.36 | **0.00** | 91 | -0.48 | **0.00** | 103 | -0.37 | **0.00** | 73 | -0.40 |
| $RelDif_{p50}$ | -0.34 | **0.00** | 91 | -0.39 | **0.00** | 103 | -0.29 | **0.01** | 73 | -0.34 |
| $RelDif_{p75}$ | -0.36 | **0.00** | 91 | -0.34 | **0.00** | 103 | -0.24 | **0.04** | 73 | -0.31 |
| $RelDif_{p90}$ | -0.37 | **0.00** | 91 | -0.34 | **0.00** | 103 | -0.21 | 0.07 | 73 | -0.30 |
| $\Delta RelDif_{CV}$ | 0.43 | **0.00** | 91 | 0.23 | **0.02** | 103 | 0.20 | 0.09 | 73 | 0.29 |

Table A3.3. Complete statistics between plot-level utilization estimates and the biomass rasters.

| **Raster** | **2x2 pixel window stat** | **2015** | | | **2016** | | | **2017** | | |
|---|---|---|---|---|---|---|---|---|---|---|
| | | **r** | **p-val** | **N** | **r** | **p-val** | **N** | **r** | **p-val** | **N** |
| $Summer_{Early}$ | Mean | -0.12 | 0.23 | 110 | -0.08 | 0.27 | 194 | 0.22 | 0.01 | 139 |
| $Summer_{Late}$ | Mean | -0.17 | 0.01 | 247 | -0.19 | 0.01 | 211 | -0.12 | 0.17 | 139 |
| $Summer_{MaxPix}$ | Mean | -0.17 | 0.01 | 250 | -0.11 | 0.09 | 215 | -0.08 | 0.36 | 139 |
| Fall | Mean | -0.33 | 0.00 | 197 | -0.46 | 0.00 | 208 | -0.47 | 0.00 | 114 |
| $RelDif_{MaxPixel}$ | Mean | -0.20 | 0.01 | 202 | -0.44 | 0.00 | 214 | -0.49 | 0.00 | 114 |
| $RelDif_{MaxPasture}$ | Mean | -0.09 | 0.36 | 113 | -0.32 | 0.00 | 208 | -0.50 | 0.00 | 114 |
| $RelDif_{EarlyScene}$ | Mean | -0.39 | 0.00 | 96 | -0.45 | 0.00 | 203 | -0.69 | 0.00 | 114 |
| $RelDif_{LateScene}$ | Mean | -0.22 | 0.00 | 196 | -0.14 | 0.04 | 208 | -0.40 | 0.00 | 114 |
| $Summer_{Early}$ | Min | -0.14 | 0.15 | 110 | -0.13 | 0.08 | 194 | 0.15 | 0.07 | 139 |
| $Summer_{Late}$ | Min | -0.21 | 0.00 | 247 | -0.22 | 0.00 | 211 | -0.12 | 0.15 | 139 |
| $Summer_{MaxPix}$ | Min | -0.21 | 0.00 | 250 | -0.15 | 0.03 | 215 | -0.08 | 0.33 | 139 |
| Fall | Min | -0.31 | 0.00 | 197 | -0.44 | 0.00 | 208 | -0.47 | 0.00 | 114 |
| $RelDif_{MaxPixel}$ | Min | -0.26 | 0.00 | 202 | -0.45 | 0.00 | 214 | -0.53 | 0.00 | 114 |
| $RelDif_{MaxPasture}$ | Min | -0.29 | 0.00 | 113 | -0.52 | 0.00 | 208 | -0.64 | 0.00 | 113 |
| $RelDif_{EarlyScene}$ | Min | -0.35 | 0.00 | 84 | -0.48 | 0.00 | 203 | -0.69 | 0.00 | 114 |
| $RelDif_{LateScene}$ | Min | -0.29 | 0.00 | 196 | -0.21 | 0.00 | 208 | -0.44 | 0.00 | 114 |

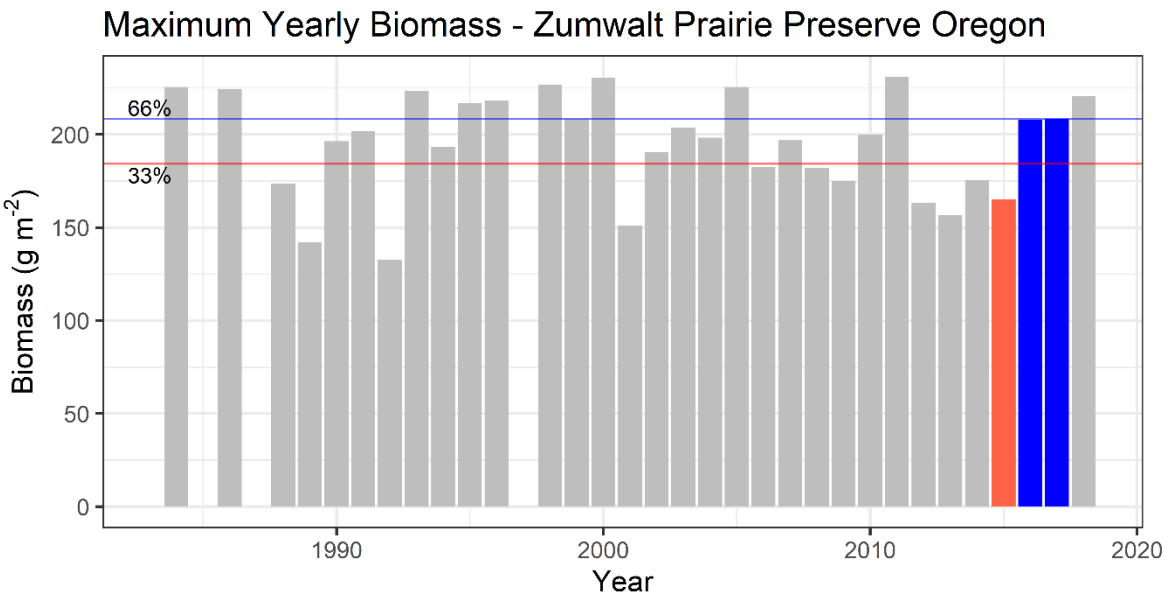


Figure A3.1. Maximum yearly biomass across the Zumwalt prairie preserve. The highlighted blue bars are the 2016 and 2017 growing season and the red bar is the 2015 growing season. The horizontal colored lines represent the 33 percentile (red) and the 66 percentile (blue) of maximum yearly production.

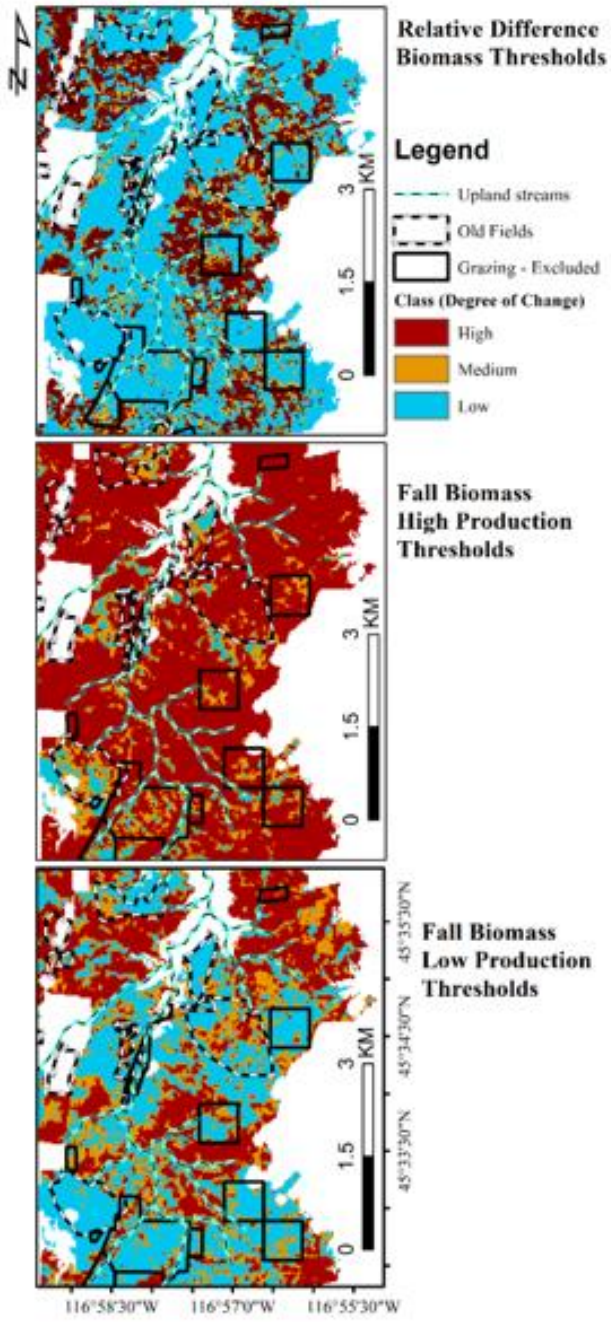


Figure A3.2. Biomass raster data mapped for 2015. The old fields are outlined with black and white lines, with pasture that have been rested from livestock grazing shown with a black outline. The upland stream areas are colored with turquoise and black stripping.

Table A3.4. Rainfall accumulation and lag time correlations with max summer biomass between May, June or July. The values in bold had significant spearman rank correlations. The green highlighted correlation is plotted (figure 2).

| | Accumulation period --->>>> ----->>>> | | | | | | | | | | | |
|---|---|---|---|---|---|---|---|---|---|---|---|---|
| Month | 1 | 2 | 3 | 4 | 5 | 6 | 7 | 8 | 9 | 10 | 11 | 12 |
| 6 | 0.02 | - | - | - | - | - | - | - | - | - | - | - |
| 5 | **0.49** | **0.37** | - | - | - | - | - | - | - | - | - | - |
| 4 | 0.19 | **0.51** | **0.41** | - | - | - | - | - | - | - | - | - |
| 3 | 0.18 | 0.21 | **0.53** | **0.47** | - | - | - | - | - | - | - | - |
| 2 | 0.25 | 0.29 | 0.30 | **0.62** | **0.60** | - | - | - | - | - | - | - |
| 1 | 0.11 | 0.27 | 0.26 | 0.32 | **0.57** | **0.56** | - | - | - | - | - | - |
| 12 | 0.19 | 0.20 | 0.34 | 0.29 | 0.33 | **0.53** | **0.55** | - | - | - | - | - |
| 11 | 0.05 | 0.07 | 0.15 | 0.23 | 0.27 | **0.38** | **0.61** | **0.55** | - | - | - | - |
| 10 | 0.17 | 0.05 | 0.19 | 0.21 | 0.32 | 0.34 | **0.39** | **0.62** | **0.62** | - | - | - |
| 9 | 0.24 | 0.30 | 0.16 | 0.25 | 0.29 | 0.31 | **0.36** | **0.40** | **0.65** | **0.69** | - | - |
| 8 | **0.47** | **0.39** | **0.47** | **0.39** | **0.43** | **0.46** | **0.49** | **0.47** | **0.51** | **0.69** | **0.69** | - |
| 7 | **0.37** | **0.52** | **0.42** | **0.52** | **0.52** | **0.60** | **0.61** | **0.67** | **0.63** | **0.64** | **0.77** | **0.76** |
| 6 | 0.12 | 0.23 | **0.43** | **0.35** | **0.45** | **0.47** | **0.56** | **0.55** | **0.59** | **0.59** | **0.61** | **0.71** |

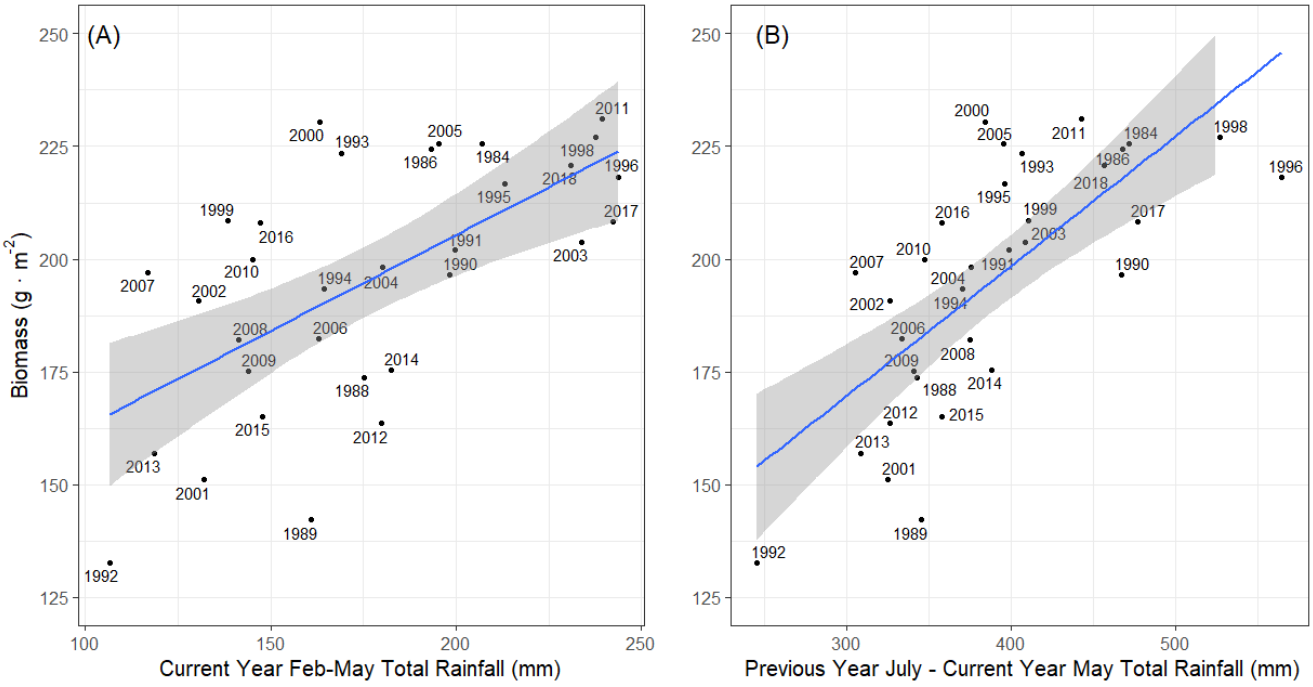


Figure A3.2. Maximum yearly biomass plotted against the previous rain fall accumulation periods (A) current year rainfall accumulation totals between February through May, and (B) is the accumulation period starting in July of the previous year and running until May of the current year. The 11 month July-May accumulation period had the highest spearman rank correlation co-efficient with maximum biomass (table 4).

Table A3.5. Potential water deficit (Precipitation - potential evapotranspiration) accumulation and lag time period correlations with max biomass between May, June or July. The values in bold had significant Spearmans rank correlations.

| | Accumulation period --->>>> | | | | | | | | | | | |
|---|---|---|---|---|---|---|---|---|---|---|---|---|
| Month | 1 | 2 | 3 | 4 | 5 | 6 | 7 | 8 | 9 | 10 | 11 | 12 |
| 6 | 0.09 | - | - | - | - | - | - | - | - | - | - | - |
| 5 | **0.52** | **0.45** | - | - | - | - | - | - | - | - | - | - |
| 4 | 0.31 | **0.54** | **0.43** | - | - | - | - | - | - | - | - | - |
| 3 | 0.17 | 0.28 | **0.53** | **0.48** | - | - | - | - | - | - | - | - |
| 2 | 0.25 | 0.31 | 0.35 | **0.66** | **0.59** | - | - | - | - | - | - | - |
| 1 | 0.13 | 0.32 | 0.32 | **0.38** | **0.64** | **0.59** | - | - | - | - | - | - |
| 12 | 0.17 | 0.26 | **0.40** | **0.37** | **0.37** | **0.62** | **0.56** | - | - | - | - | - |
| 11 | 0.07 | 0.07 | 0.14 | 0.29 | 0.33 | **0.38** | **0.61** | **0.60** | - | - | - | - |
| 10 | 0.20 | 0.09 | 0.18 | 0.28 | **0.37** | **0.39** | **0.44** | **0.65** | **0.61** | - | - | - |
| 9 | 0.33 | **0.40** | 0.31 | 0.30 | **0.37** | **0.41** | **0.38** | **0.40** | **0.63** | **0.64** | - | - |
| 8 | **0.42** | **0.39** | **0.46** | **0.41** | **0.44** | **0.49** | **0.50** | **0.51** | **0.54** | **0.67** | **0.69** | - |
| 7 | 0.32 | **0.43** | **0.44** | **0.52** | **0.49** | **0.54** | **0.57** | **0.57** | **0.60** | **0.59** | **0.71** | **0.69** |
| 6 | 0.13 | 0.21 | **0.38** | **0.42** | **0.51** | **0.44** | **0.51** | **0.57** | **0.56** | **0.62** | **0.61** | **0.69** |

Table A3.6. Correlations coefficient improvement with potential evapotranspiration. Positive (highlighted with green values) indicated higher correlation coefficients with Potential water deficit versus precipitation with maximum above ground biomass. The cells that are within boxes were significantly correlations with maximum above ground biomass using both precipitation and potential water deficit.

| Month | 1 | 2 | 3 | 4 | 5 | 6 | 7 | 8 | 9 | 10 | 11 | 12 |
|---|---|---|---|---|---|---|---|---|---|---|---|---|
| 6 | 0.07 | - | - | - | - | - | - | - | - | - | - | - |
| 5 | **0.03** | **0.08** | - | - | - | - | - | - | - | - | - | - |
| 4 | 0.12 | **0.03** | **0.02** | - | - | - | - | - | - | - | - | - |
| 3 | -0.01 | 0.07 | **0.00** | **0.01** | - | - | - | - | - | - | - | - |
| 2 | 0.00 | 0.02 | 0.05 | **0.04** | **-0.01** | - | - | - | - | - | - | - |
| 1 | 0.02 | 0.05 | 0.06 | 0.06 | **0.07** | **0.03** | - | - | - | - | - | - |
| 12 | -0.02 | 0.06 | 0.06 | 0.08 | 0.04 | **0.09** | **0.01** | - | - | - | - | - |
| 11 | 0.02 | 0.00 | -0.01 | 0.06 | 0.06 | 0.00 | **0.00** | **0.05** | - | - | - | - |
| 10 | 0.03 | 0.04 | -0.01 | 0.07 | 0.05 | 0.05 | **0.05** | **0.03** | **-0.01** | - | - | - |
| 9 | 0.09 | **0.10** | 0.15 | 0.05 | 0.08 | 0.10 | **0.02** | **0.00** | **-0.02** | **-0.05** | - | - |
| 8 | **-0.05** | **0.00** | **-0.01** | **0.02** | **0.01** | **0.03** | **0.01** | **0.04** | **0.03** | **-0.02** | **0.00** | - |
| 7 | -0.05 | **-0.09** | **0.02** | **0.00** | **-0.03** | **-0.06** | **-0.04** | **-0.10** | **-0.03** | **-0.05** | **-0.06** | **-0.07** |
| 6 | 0.01 | -0.02 | **-0.05** | **0.07** | **0.06** | **-0.03** | **-0.05** | **0.02** | **-0.03** | **0.03** | **0.00** | **-0.02** |

Table A3.8. Monthly Precipitation accumulation and lag time period correlations with max fall biomass between September, October or November. The values in bold had most significant Spearmans rank correlations between accumulated rainfall to max fall biomass. The green highlighted correlation is plotted (figure 3).

| Month | 1 | 2 | 3 | 4 | 5 | 6 | 7 | 8 | 9 | 10 | 11 | 12 |
|---|---|---|---|---|---|---|---|---|---|---|---|---|
| 11 | 0.25 | - | - | - | - | - | - | - | - | - | - | - |
| 10 | **0.42** | **0.38** | - | - | - | - | - | - | - | - | - | - |
| 9 | 0.13 | **0.46** | **0.47** | - | - | - | - | - | - | - | - | - |
| 8 | -0.07 | 0.12 | 0.31 | **0.34** | - | - | - | - | - | - | - | - |
| 7 | 0.03 | -0.06 | 0.03 | 0.23 | 0.32 | - | - | - | - | - | - | - |
| 6 | 0.25 | 0.20 | 0.12 | 0.19 | 0.33 | **0.40** | - | - | - | - | - | - |
| 5 | **0.45** | **0.44** | **0.41** | 0.33 | 0.34 | **0.48** | **0.53** | - | - | - | - | - |
| 4 | 0.20 | **0.48** | **0.46** | **0.41** | **0.36** | **0.41** | **0.50** | **0.54** | - | - | - | - |
| 3 | 0.03 | 0.14 | 0.43 | **0.43** | **0.39** | 0.34 | **0.44** | **0.52** | **0.52** | - | - | - |
| 2 | 0.01 | 0.04 | 0.15 | **0.44** | **0.50** | **0.42** | **0.39** | **0.44** | **0.51** | **0.54** | - | - |
| 1 | -0.11 | -0.01 | 0.02 | 0.11 | 0.36 | **0.43** | **0.38** | **0.35** | **0.38** | **0.47** | **0.51** | - |
| 12 | -0.05 | -0.14 | -0.02 | -0.03 | 0.05 | 0.27 | **0.39** | **0.36** | 0.33 | **0.36** | **0.44** | **0.48** |
| 11 | -0.10 | -0.14 | -0.18 | -0.09 | -0.08 | 0.02 | 0.28 | 0.32 | 0.29 | 0.26 | 0.32 | **0.42** |

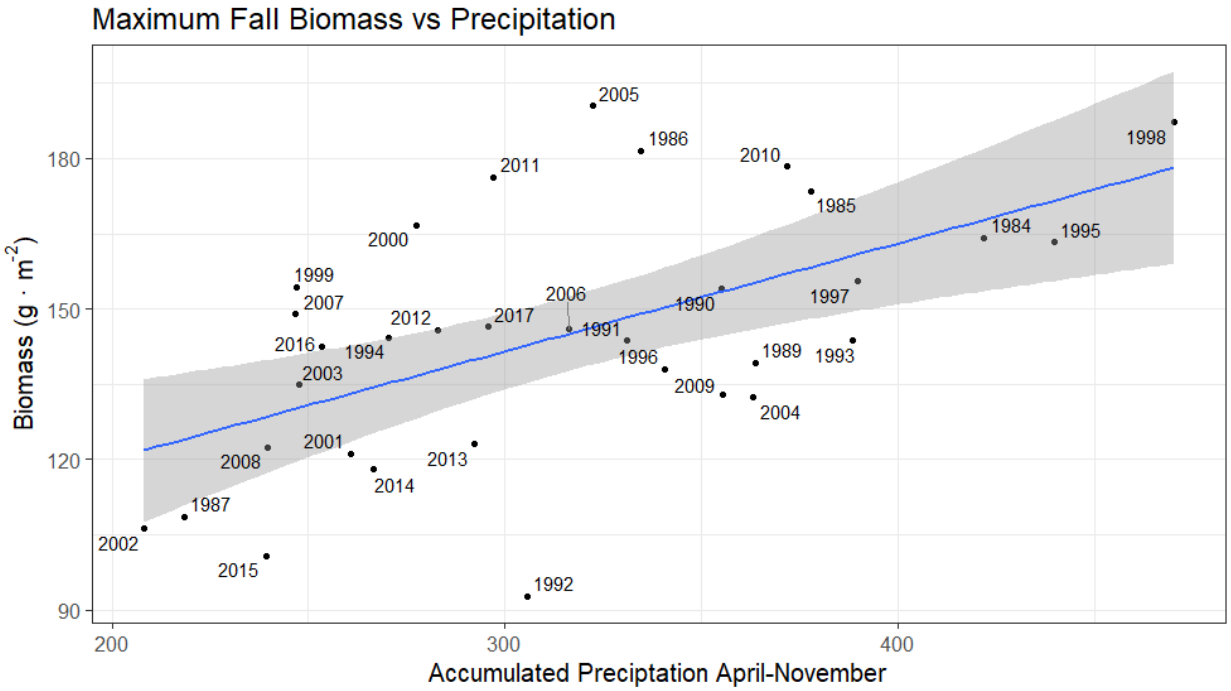


Figure A3.3. Maximum fall biomass plotted against the accumulated precipitation from April through November for the Zumwalt Prairie Preserve.

Table A3.8. Potential water deficit (Precipitation - potential evapotranspiration) accumulation and lag time period correlations with max fall biomass between September, October or November. The values in bold had significant Spearmans rank correlations. The green highlighted correlation is plotted (figure 4).

| Month | 1 | 2 | 3 | 4 | 5 | 6 | 7 | 8 | 9 | 10 | 11 | 12 |
|---|---|---|---|---|---|---|---|---|---|---|---|---|
| 11 | 0.24 | - | - | - | - | - | - | - | - | - | - | - |
| 10 | **0.46** | **0.57** | - | - | - | - | - | - | - | - | - | - |
| 9 | 0.20 | **0.44** | **0.44** | - | - | - | - | - | - | - | - | - |
| 8 | -0.03 | 0.21 | 0.32 | **0.37** | - | - | - | - | - | - | - | - |
| 7 | 0.12 | -0.02 | 0.08 | 0.22 | 0.31 | - | - | - | - | - | - | - |
| 6 | 0.28 | 0.20 | 0.10 | 0.23 | **0.35** | **0.41** | - | - | - | - | - | - |
| 5 | **0.45** | **0.52** | **0.42** | 0.33 | **0.41** | **0.52** | **0.55** | - | - | - | - | - |
| 4 | 0.24 | **0.48** | **0.45** | **0.39** | **0.37** | **0.45** | **0.51** | **0.53** | - | - | - | - |
| 3 | 0.04 | 0.16 | **0.41** | **0.43** | 0.34 | **0.36** | **0.42** | **0.49** | **0.52** | - | - | - |
| 2 | 0.09 | 0.12 | 0.21 | **0.50** | **0.50** | **0.42** | **0.40** | **0.46** | **0.57** | **0.56** | - | - |
| 1 | -0.11 | 0.05 | 0.10 | 0.18 | **0.41** | **0.45** | **0.41** | **0.36** | **0.42** | **0.49** | **0.53** | - |
| 12 | -0.11 | -0.12 | 0.03 | 0.04 | 0.09 | 0.34 | **0.37** | **0.40** | **0.35** | **0.42** | **0.41** | **0.49** |
| 11 | -0.13 | -0.15 | -0.17 | -0.04 | 0.02 | 0.06 | 0.31 | **0.39** | **0.36** | 0.29 | **0.40** | **0.44** |

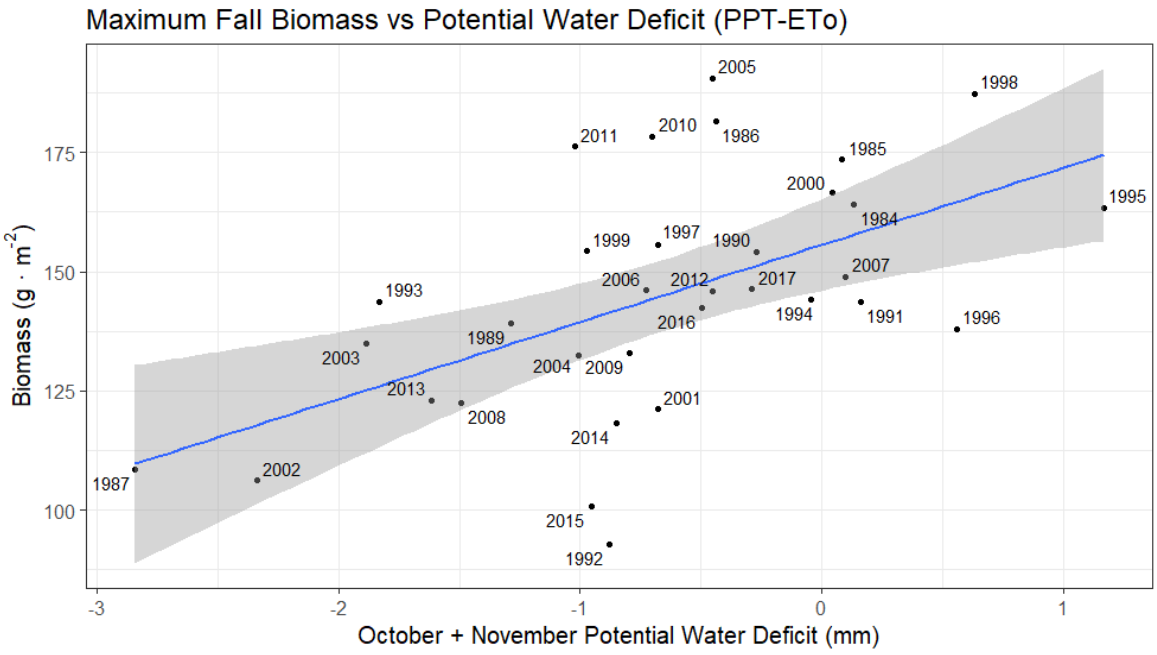


Figure A3.4. Maximum fall biomass plotted against the accumulated Potential Water Deficit (PPT-ETo) from October through November for the Zumwalt Prairie Preserve.

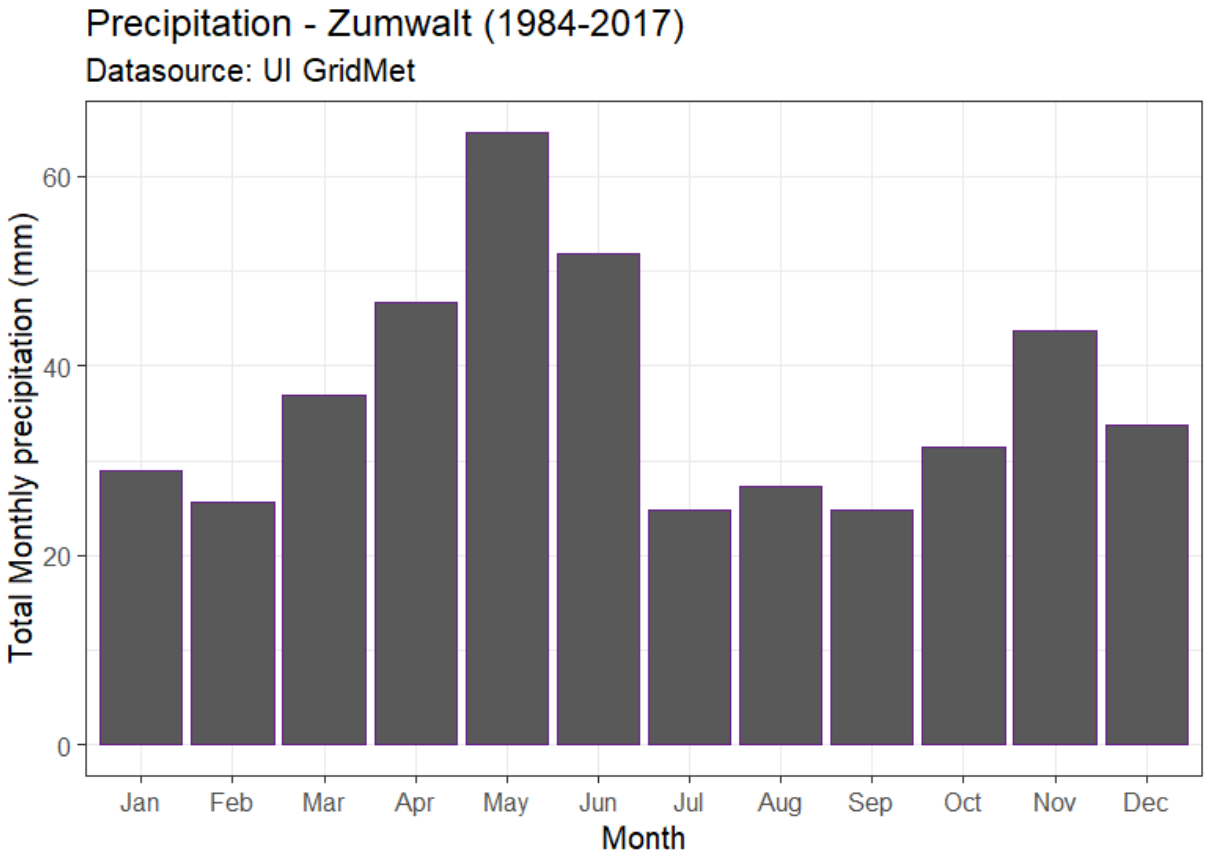


Figure A3.5. Average monthly preciptation totals for the Zumwalt Prairie Preserve from 1984 to 2017 using GridMet Climate data (Abatzoglou, 2013).

Reference:
Abatzoglou, J. T., 2013: Development of gridded surface meteorological data for ecological applications and modelling. Int. J. Climatol., 33, 121–131, doi:10.1002 /joc.3413.

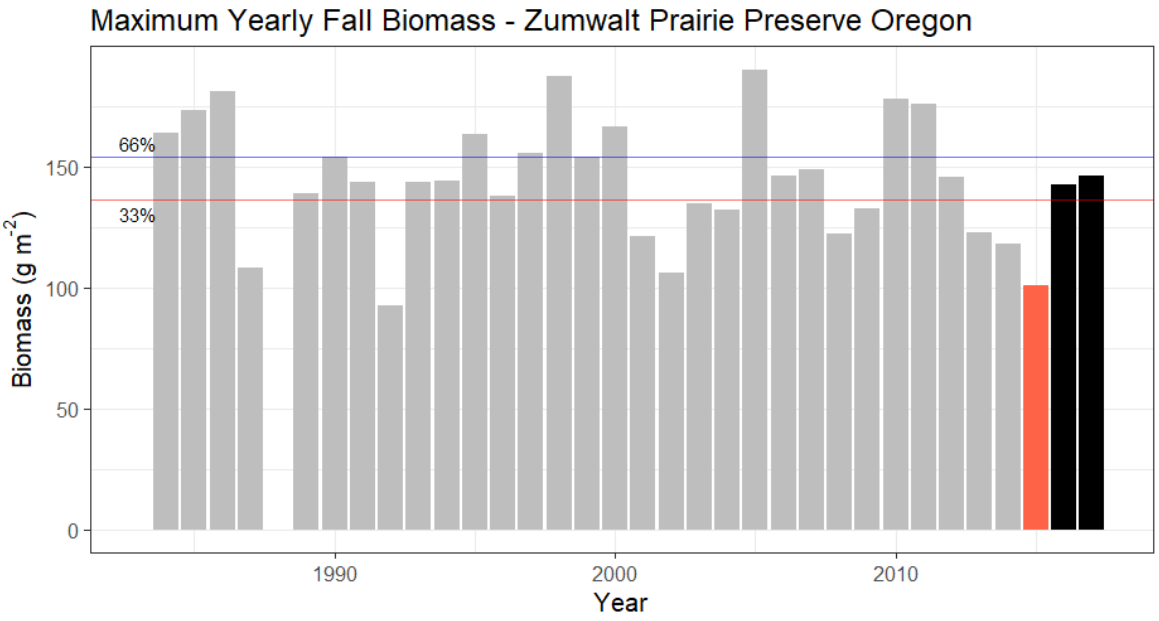


Figure A3.6. The maximum fall biomass average for each year across the Zumwalt Prairie preserve from 1984 to 2017 using the biomass algrothim developed for this habitat type (Jansen et al., 2018).

## Appendix 4. MDPI Open Access Information and Policy

**All articles published by MDPI are made immediately available worldwide under an open access license. This means:**

- everyone has free and unlimited access to the full-text of ***all*** articles published in MDPI journals;
- everyone is free to re-use the published material if proper accreditation/citation of the original publication is given;
- open access publication is supported by the authors' institutes or research funding agencies by payment of a comparatively low Article Processing Charge (APC) for accepted articles.